STRINGQFT

String-Theoretic Construction
of Quantum Field Theory

VOLUME VIII

M2-Brane Probes and 3d SCFTs

Xingyang Yu

StringQFT v1.0

Drafted with AI assistance under the supervision of the author.
Manuscript free to read. All rights reserved.

Contents

VIII.1 M2-branes and near-horizon geometry **1**
VIII.1.1 A membrane and its transverse fields 1
VIII.1.2 Canonical fluctuations and the Green function 3
VIII.1.3 Why several membranes demand a new theory 5
VIII.1.4 The harmonic M2 solution and its throat 8
VIII.1.5 Electric charge fixes the radius 10
VIII.1.6 The Hopf circle and type IIA units 12
VIII.1.7 Controlled regimes and physical comparisons 13
VIII.1.8 Exercises 16
Status and sources 17

VIII.2 From BLG to ABJM **20**
VIII.2.1 The three-bracket and its gauge algebra 20
VIII.2.2 The BLG action and the two SU(2) factors 22
VIII.2.3 A circular brane route to arbitrary rank 26
VIII.2.4 The torus period becomes a complex quotient 30
VIII.2.5 The ABJM fields and quartic interaction 34
VIII.2.6 The compact abelian quotient and its scope 38
VIII.2.7 Exercises 42
Status and sources 44

VIII.3 ABJM moduli spaces and monopole operators **47**
VIII.3.1 The separated positions and their finite identifications 47
VIII.3.2 A primitive flux and its electric charge 50
VIII.3.3 Bare energy, low dressings and the scalar families 51
VIII.3.4 When scalar states imply extra currents 53
VIII.3.5 Global form in the rank-two BLG comparison 55
VIII.3.6 Protected comparisons beyond the quotient 56
VIII.3.7 Exercises 58
Status and sources 59

VIII.4 ABJ theory and fractional M2-branes **63**
VIII.4.1 One circle, two ranks 63
VIII.4.2 Which charge does a rank measure? 66
VIII.4.3 A rational example and a change of representative 69

VIII.4.4 A wrapped wall and the accuracy of the comparison 71
VIII.4.5 Historical variables and the remaining QFT question 73
VIII.4.6 Exercises 75
Status and sources 76

VIII.5 From Calabi–Yau fourfolds to Chern–Simons theories 78
VIII.5.1 What does a membrane circle leave behind? 78
VIII.5.2 The circle remembers a two-form 81
VIII.5.3 Why RR flux writes a Chern–Simons level 83
VIII.5.4 From FI slope to the missing circle coordinate 86
VIII.5.5 The conifold calculation returns ABJM 89
VIII.5.6 Two curve periods test the construction 92
Status and sources 97

VIII.6 Vacuum geometry of Chern–Simons quivers 99
VIII.6.1 Which vacuum remembers a membrane? 99
VIII.6.2 Auxiliary fields select the geometric branch 100
VIII.6.3 A circle survives the gauge quotient 103
VIII.6.4 The integer lattice fixes the finite quotient 106
VIII.6.5 When does the quotient have complex dimension four? 109
VIII.6.6 Fields, monopoles and several branes 113
VIII.6.7 Where the construction changes 116
Status and sources 118

VIII.7 Toric fourfolds from Chern–Simons tilings 121
VIII.7.1 From a threefold tiling to a fourfold question 121
VIII.7.2 Perfect matchings solve the F equations 123
VIII.7.3 The compact gauge lattice determines the quotient 124
VIII.7.4 Edge flows lift the Kasteleyn polynomial 127
VIII.7.5 Reading and counting the toric fourfold 129
VIII.7.6 Crystals and the boundary of the dictionary 132
Status and sources 135

VIII.8 Flavors, monopoles, and quantum geometry 137
VIII.8.1 Where the reduction circle ends 137
VIII.8.2 The flavored quiver and its parity choice 140
VIII.8.3 What opposite monopoles know 142
VIII.8.4 From monopoles to six toric variables 144
VIII.8.5 Eight coordinates and the Segre cone 145
VIII.8.6 Two fixed components and what the conifold misses 148
Status and sources 150

VIII.9 Higgsing and mass deformations of membrane quivers 152
VIII.9.1 Two deformations, two questions 152
VIII.9.2 How a bifundamental vacuum joins gauge nodes 153
VIII.9.3 The five-field parent and its selected quotient 154

VIII.9.4 Two Higgs routes from one parent . . . 158
VIII.9.5 The component mass and the rank-one control . . . 161
VIII.9.6 Square blocks, bilinears and classical limits . . . 163
VIII.9.7 Exercises . . . 166
Status and sources . . . 167

VIII.10 M2-branes at non-toric cones 169
VIII.10.1 The question posed by a quadric . . . 169
VIII.10.2 From the source quiver to one-brane positions . . . 170
VIII.10.3 Why the compact gauge fields leave a finite quotient . . . 174
VIII.10.4 Counting functions, and what they count . . . 175
VIII.10.5 The thickened apex and the quantum question . . . 178
VIII.10.6 Geometry and the edge of the method . . . 180
VIII.10.7 Exercises . . . 181
Status and sources . . . 182

VIII.11 Localization and the physical R charge 184
VIII.11.1 A supersymmetric deformation of the sphere integral . . . 184
VIII.11.2 The determinant fixes an absolute normalization . . . 186
VIII.11.3 One membrane and the regulated Fourier integral . . . 187
VIII.11.4 A trial R charge is a measurable variable . . . 189
VIII.11.5 Extremizing physical charges in ABJM . . . 190
VIII.11.6 Squashing with its supersymmetric background . . . 191
VIII.11.7 Exercises . . . 194
Status and sources . . . 195

VIII.12 Large-N free energy and geometric volume 197
VIII.12.1 A continuum of ABJM eigenvalues . . . 197
VIII.12.2 Counting fermion states instead . . . 199
VIII.12.3 The gravity coefficient and its normalization . . . 201
VIII.12.4 A flavored Q111 saddle . . . 202
VIII.12.5 Volume from holomorphic functions . . . 204
VIII.12.6 Extrema and the reach of the comparison . . . 206
VIII.12.7 Exercises . . . 208
Status and sources . . . 209

VIII.13 An atlas of M2-brane constructions 212
VIII.13.1 From a question to a construction . . . 212
VIII.13.2 Compact groups and probe geometries . . . 213
VIII.13.3 Choosing a circle and a toric description . . . 215
VIII.13.4 Changing a vacuum or changing a theory . . . 216
VIII.13.5 Observables and what agreement tests . . . 218
VIII.13.6 Beyond brane probes . . . 220
VIII.13.7 Exercises . . . 220
Status and sources . . . 221

Chapter VIII.1

M2-branes and near-horizon geometry

A string's worldsheet gives a useful perturbative starting point. An M2-brane instead fills a $(2+1)$-dimensional worldvolume. Its simplest observable is its transverse displacement, and the first calculation is the propagation of that displacement on one flat membrane. When many membranes meet, the single-brane action no longer determines their interacting theory. A second, classical description becomes available: their electric charge produces a throat whose size and circle geometry can be calculated. We will follow these two sides of the same object without assuming that one calculation proves the complete quantum duality.

VIII.1.1 A membrane and its transverse fields

Take one planar M2 along x^0, x^1, x^2. The remaining coordinates describe its position. A displacement in the first transverse direction, $X^3 = v$, moves the whole membrane without changing its shape. A varying $X^3(x)$ describes a bend. The distinction between the constant v and the fluctuation about it will matter when we compute a two-point function. Figure VIII.1.1 follows one membrane through that distinction.

The figure holds the same membrane fixed while changing which aspect is measured. We now make the energy of the bend quantitative. In static gauge $x^\mu = \xi^\mu$, $\mu = 0, 1, 2$, the embedding coordinates are the eight functions $X^I(\xi)$, $I = 3, \ldots, 10$. In flat spacetime with a vanishing pullback of the background three-form, the bosonic area action is the relevant term. A nonzero three-form adds a Wess–Zumino coupling but does not enter the present flat fluctuation calculation.

If only X^3 varies, pulling back the flat metric gives

$$g_{\mu\nu} = \eta_{\mu\nu} + \partial_\mu X^3 \partial_\nu X^3, \qquad \eta_{\mu\nu} = \mathrm{diag}(-1, 1, 1). \tag{VIII.1.1}$$

Thus a bend changes the induced metric even though the ambient metric has not changed. For all eight displacements, the last term becomes a sum over I.

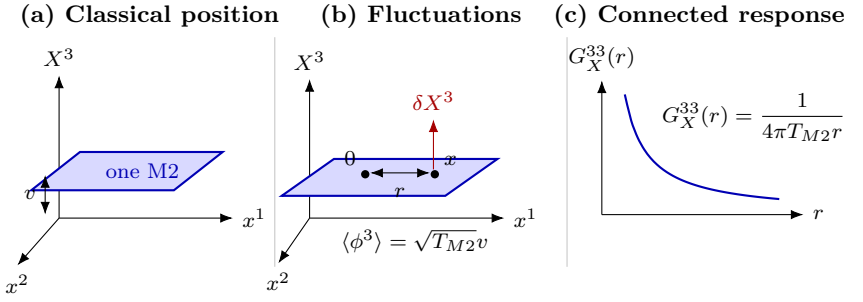


Figure VIII.1.1: The same single M2 in all three panels, with x^0 common and suppressed. The plane spans x^1, x^2; X^3 is transverse. Panel (a) places it at the constant displacement v, measured from the coordinate origin, not from another brane. Panel (b) marks two points a worldvolume distance r apart in a chosen vacuum and a small local fluctuation. Panel (c) shows their connected Gaussian correlator at $r > 0$. The membrane charge and positive tension T_{M2} are held fixed; the correlator measures fluctuations, not the classical displacement v.

With the constant background three-form absent, the area term is

$$S_{\text{area}} = -T_{M2} \int d^3x \, \sqrt{-\det g_{\mu\nu}}, \qquad g_{\mu\nu} = \eta_{\mu\nu} + \sum_{I=3}^{10} \partial_\mu X^I \partial_\nu X^I. \tag{VIII.1.2}$$

This is the bosonic limit of the supermembrane action. It is an input about the physical object, while the following expansion is a consequence of that input. Write $M^\mu{}_\nu = \sum_I \partial^\mu X^I \partial_\nu X^I$. Since M is already quadratic in gradients,

$$\sqrt{-\det g} = \sqrt{\det(\mathbf{1} + M)} = 1 + \frac{1}{2} \operatorname{tr} M + O\big((\partial X)^4\big) = 1 + \frac{1}{2} \sum_I \partial_\mu X^I \partial^\mu X^I + O\big((\partial X)^4\big). \tag{VIII.1.3}$$

Here $\det \eta = -1$ supplies the first equality. Removing the constant membrane rest energy leaves

$$S^{(2)} = -\frac{T_{M2}}{2} \int d^3x \sum_{I=3}^{10} \partial_\mu X^I \partial^\mu X^I. \tag{VIII.1.4}$$

For X^3 alone, the integrand is $T_{M2}(\partial_0 X^3)^2/2 - T_{M2}|\boldsymbol{\nabla} X^3|^2/2$. The sign of the time term therefore gives positive kinetic energy. The gradient expansion asks for small slopes, not a small constant displacement. For one nonzero transverse field the determinant lemma gives an exact check of the next term. If $s = \partial_\mu X^3 \partial^\mu X^3$, then $\det(\mathbf{1} + M) = 1 + s$ because M has rank one. Hence

$$\sqrt{-\det g} = \sqrt{1+s} = 1 + \frac{s}{2} - \frac{s^2}{8} + O(s^3). \tag{VIII.1.5}$$

The quartic term changes the dynamics of a bent single membrane at larger slopes. It still depends on the same one embedding field, so it cannot supply the missing degrees of freedom of a coincident stack.

The coordinate X^3 has length units. To compare it with a canonically normalized field, set

$$\phi^I = \sqrt{T_{M2}}\, X^I, \qquad S^{(2)} = -\frac{1}{2}\int d^3x \sum_I \partial_\mu \phi^I \partial^\mu \phi^I. \tag{VIII.1.6}$$

In units $\hbar = c = 1$, a dimensionless action and a three-dimensional measure give

$$[d^3x] = M^{-3}, \qquad [T_{M2}] = M^3, \qquad [X^I] = M^{-1}, \qquad [\phi^I] = M^{1/2}. \tag{VIII.1.7}$$

These are engineering dimensions of the free field in this vacuum. They do not assign an anomalous dimension to fields of an interacting membrane stack.

A concrete bend makes the expansion parameter visible. At a fixed time, put $X^3 = v + a\cos(qx^1)$ and set the other transverse coordinates constant. The maximum slope is $|aq|$, while the value of v is unrestricted by the gradient expansion. The extra static energy per unit x^2 length and per period $2\pi/q$ is

$$\frac{\Delta E}{L_2} = \frac{T_{M2}}{2}\int_0^{2\pi/q} dx^1\, a^2 q^2 \sin^2(qx^1) = \frac{\pi T_{M2} a^2 q}{2}, \qquad |aq| \ll 1. \tag{VIII.1.8}$$

The same integral is zero for a uniform translation, $q = 0$ at fixed position. The quadratic theory therefore describes a massless displacement mode; it does not confine the membrane to the coordinate origin. We will now normalize that mode so its propagator is directly comparable with the standard scalar Green function.

VIII.1.2 Canonical fluctuations and the Green function

How can a local measurement distinguish the membrane's chosen position from a quantum fluctuation about it? The canonical field in (VIII.1.6) has a standard Gaussian kinetic operator. It also fixes the complex chart used later. Pair the eight real coordinates into four fields,

$$C^A = \sqrt{\frac{T_{M2}}{2}}(X^{2A+1} + iX^{2A+2}), \qquad \sum_A \partial_\mu C^A \partial^\mu \overline{C}_A = \frac{T_{M2}}{2}\sum_{I=3}^{10} \partial_\mu X^I \partial^\mu X^I. \tag{VIII.1.9}$$

This is a normalization identity for one abelian membrane, not an identification of its fields with gauge-invariant local operators in an interacting stack.

Now choose the translational vacuum $X^3 = v + \delta X^3$ and set the other expectation values to zero. This choice fixes the shift zero mode so that a Gaussian inverse kinetic operator is meaningful on the infinite Euclidean worldvolume. After Wick rotation, require the Green function to decay at spatial infinity and consider $r = |x| > 0$. The connected subtraction removes the constant vacuum contribution:

$$\begin{aligned} G_X^{33}(x) &= \langle X^3(x) X^3(0)\rangle - \langle X^3\rangle^2 = \langle \delta X^3(x)\delta X^3(0)\rangle, \\ G_X^{IJ}(x) &= \frac{\delta^{IJ}}{T_{M2}}\int \frac{d^3p}{(2\pi)^3}\frac{e^{ip\cdot x}}{p^2}. \end{aligned} \tag{VIII.1.10}$$

The inverse p^2 follows from the canonical quadratic action, with one factor T_{M2}^{-1} when we return to the position coordinate. The Fourier integral is radial. Align the polar axis of momentum space with x; the angular integral is

$$\int_{S^2} d\Omega_p \, e^{ipr\cos\vartheta} = 2\pi \int_{-1}^{1} du \, e^{ipru} = \frac{4\pi \sin(pr)}{pr}. \tag{VIII.1.11}$$

This exposes the $1/r$ factor before the remaining radial integral. The latter needs a regulator before it is evaluated. With $e^{-\epsilon p}$ and $\epsilon > 0$, it becomes

$$\begin{aligned} G_{\phi,\epsilon}(r) &= \frac{1}{2\pi^2 r} \int_0^\infty dp \, e^{-\epsilon p} \frac{\sin(pr)}{p} \\ &= \frac{1}{2\pi^2 r} \arctan\Big(\frac{r}{\epsilon}\Big) \xrightarrow[\epsilon\to 0^+]{} \frac{1}{4\pi r}. \end{aligned} \tag{VIII.1.12}$$

The arctangent follows by differentiating the regulated integral with respect to r, integrating $(\epsilon^2 + r^2)^{-1}\epsilon$, and fixing its value to zero at $r = 0$. This calculation fixes the coefficient away from contact points. An independent normalization check treats the answer as the Green function of $-\nabla^2$ in three Euclidean dimensions. For $G_\phi(r) = A/r$, the flux through a sphere is

$$\int_{S_r^2} (-\boldsymbol{\nabla} G_\phi) \cdot d\mathbf{S} = 4\pi r^2 \frac{A}{r^2} = 4\pi A = 1, \qquad A = \frac{1}{4\pi}. \tag{VIII.1.13}$$

The unit source condition and decay at infinity choose the Green function up to contact conventions. Combining the two calculations yields the position-field result

$$\boxed{G_X^{IJ}(r) = \frac{\delta^{IJ}}{4\pi T_{M2} r}, \qquad r > 0.} \tag{VIII.1.14}$$

For $I = J = 3$, v is absent. The same coefficient and Kronecker delta now cover the eight independent transverse fluctuations of one membrane.

The object in (VIII.1.14) is a correlator of a gauge-fixed displacement field in a flat background and a chosen worldvolume vacuum. It is not an intrinsic relational bulk observable, and the calculation has specified no gravity-decoupling limit. At an orbifold, a coordinate on the covering space is identified with its images. In a nonabelian stack, a matrix entry or a casually selected eigenvalue changes under gauge transformations. Neither is automatically a local gauge-invariant observable. A comparison with a gauge theory must therefore specify whether it concerns a vacuum position, an invariant local operator, or a correlator in a fixed state.

For example, keep a constant vacuum v and compare points at distances r and $2r$. The connected correlator gives

$$\langle X^3(x) X^3(0)\rangle = v^2 + \frac{1}{4\pi T_{M2} r}, \qquad G_X^{33}(2r) = \frac{1}{2} G_X^{33}(r). \tag{VIII.1.15}$$

Only the connected term changes with separation. The v^2 term is the product of one-point functions and must disappear when we ask about a propagating fluctuation. This distinction will recur when we compare a position on a vacuum branch with an invariant operator.

VIII.1.3 Why several membranes demand a new theory

The quadratic action answers a sharp question about one membrane. It has no label distinguishing two coincident membranes. The higher-gradient terms of the same embedding still depend on only eight transverse coordinates; they do not prescribe a nonabelian field algebra. We therefore need symmetry, duality and geometry to identify a candidate theory for a stack.

One algebraic answer is the Bagger–Lambert construction. It supplies a three-dimensional action with eight transverse scalars, fermions and a nonpropagating gauge field, with 16 supersymmetries closing on shell under its three-algebra hypotheses. This is a concrete interacting candidate, not a formula for arbitrary N coincident membranes. Chapter 2 studies the algebra, physical realization and global questions. A different route uses Chern–Simons matter, where the gauge field can enter without a continuous dimensionful gauge coupling.

We can see the latter attraction before writing an interacting action. Use $D_\mu = \partial_\mu + iA_\mu$. Every term in this operator must have the same mass dimension, and the field strength is its commutator:

$$[\partial_\mu] = M, \qquad [A_\mu] = M, \qquad F_{\mu\nu} = \frac{1}{i}[D_\mu, D_\nu], \qquad [F_{\mu\nu}] = M^2. \tag{VIII.1.16}$$

For the dimensional comparison, write the Yang–Mills term with its mostly-plus Lorentzian sign and indicate only the field content of the Chern–Simons term:

$$S_{\mathrm{YM}} = -\frac{1}{2g_{\mathrm{YM}}^2}\int d^3x\ \mathrm{Tr}_f\, F_{\mu\nu}F^{\mu\nu}, \qquad S_{\mathrm{CS}} \sim k\int \mathrm{Tr}(A\wedge dA + \text{terms cubic in } A)\,. \tag{VIII.1.17}$$

The trace obeys $\mathrm{Tr}_f(T^aT^b) = \delta^{ab}/2$, so the Yang–Mills coefficient is $-F^a_{\mu\nu}F^{a\mu\nu}/(4g^2_{\mathrm{YM}})$. The Chern–Simons expression records dimensions only. Its coefficients, factors of i and signs depend on the gauge-field and orientation conventions and are left unspecified here; it is not a complete action. Because $[d^3x] = M^{-3}$, the two densities have distinct units:

$$[\mathrm{Tr}_f\, F_{\mu\nu}F^{\mu\nu}] = M^4, \qquad [\mathrm{Tr}(A_\mu\partial_\nu A_\rho)] = M^3. \tag{VIII.1.18}$$

Action dimensionlessness therefore requires

$$[g^2_{\mathrm{YM}}] = M, \qquad [k] = M^0. \tag{VIII.1.19}$$

The discrete level k is compatible with a scale-free fixed-point candidate, whereas a Yang–Mills description carries a mass scale. Large-gauge consistency supplies quantization of k under a specified compact gauge group; dimension counting alone does not. Neither the existence of a fixed point nor its identification with a membrane theory follows from (VIII.1.19). The ABJM construction provides the additional supersymmetry and matter input in Chapter 2.

To identify a candidate theory for N membranes at $\mathbb{C}^4/\mathbb{Z}_k$, one can start with branes in a different duality frame or with the proposed transverse target. The two routes answer different questions. Figure VIII.1.2 names every change of description. Here $N, k > 0$ throughout, and k has the same meaning in both routes.

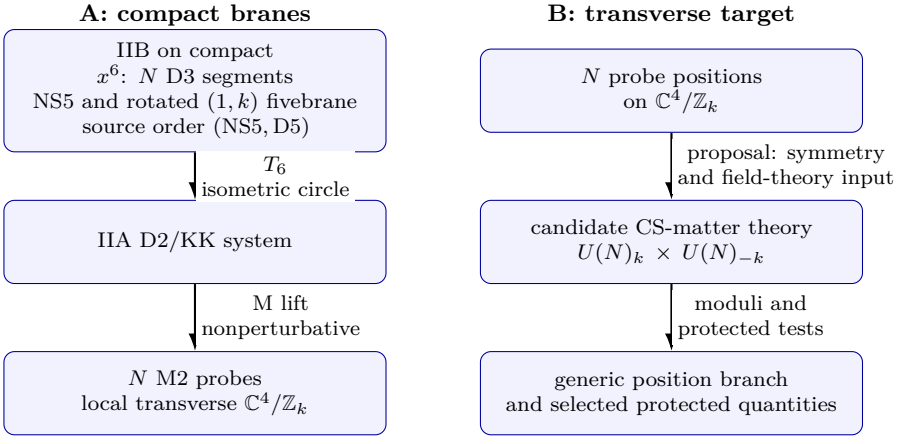


Figure VIII.1.2: Two routes with the same N and k. In A, the D3 segments share compact x^6 and the NS5 has directions 012345; the rotated fivebrane is the one specified in the text. Source charge order is $(\mathrm{NS5}, \mathrm{D5}) = (1, k)$, while the book's $(\mathrm{D5}, \mathrm{NS5})$ order is $(k, 1)$. The T_6 arrow requires an isometric circle and its zero-mode description; the M lift is nonperturbative. In B, the arrow from geometry to a candidate action includes independent field-theory input. The lower box in B compares a branch of vacua, and the protected test samples only a sector. Neither arrow by itself establishes complete infrared dynamics.

The compact-brane route

In route A, N D3-branes wrap segments of a compact x^6 circle between an NS5 along 012345 and a rotated fivebrane. The latter spans $012[3,7]_\theta[4,8]_\theta[5,9]_\theta$, where each bracket means a line in the indicated coordinate plane. The source orders its fivebrane charges as $(\mathrm{NS5}, \mathrm{D5}) = (1, k)$; in the book's $(\mathrm{D5}, \mathrm{NS5})$ order the same charges are $(k, 1)$. This is only a permutation of the recorded pair, not a duality transformation.

For the standard six-supercharge ultraviolet construction used here, fix $C_0 = 0$, $k > 0$, finite $g_s^{\mathrm{B}} > 0$, and $0 < \theta < \pi/2$ with $\tan\theta = k g_s^{\mathrm{B}}$. The two intervals carry a three-dimensional Yang–Mills–Chern–Simons matter description. The angle and opposite levels belong to this specified brane orientation:

$$\tan\theta = k g_s^{\mathrm{B}}, \qquad (k_1, k_2) = (k, -k). \tag{VIII.1.20}$$

Their gauge couplings depend on their respective lengths L_i as

$$g_{3,i}^2 = \frac{4\pi g_s^{\mathrm{B}}}{L_i}, \qquad (k_1, k_2) = (k, -k). \tag{VIII.1.21}$$

The ordering of the bare levels follows the chosen orientation of the two intervals. It is not determined by the dimensional argument of the previous section. A special axion modulus can change the ultraviolet supercharge count, so the six-supercharge description is tied to the zero-axion conditions just stated. It is also separate from the proposed infrared supersymmetry and from any quantum enhancement.

Now T-dualize the isometric compact x^6 direction, retaining the sector described by its zero modes. The D3 segments become D2-branes in IIA, and the fivebranes contribute KK and flux data. The IIA configuration is then lifted nonperturbatively to M-theory. In the corresponding local geometric description, the N branes probe an orbifold with transverse position space $\mathbb{C}^4/\mathbb{Z}_k$. This gives a route to identifying the infrared membrane target. Its use of the IIB charge-frame transformation and the M lift remains an explicit condition of the duality chain; neither operation is a perturbative consequence of the D3 segment drawing. The primitive-cycle geometry and complete action are developed in Chapter 2.

The transverse-target route

Route B begins by positing N M2 probes of $\mathbb{C}^4/\mathbb{Z}_k$, with the orbifold acting by a common phase on four complex transverse coordinates. For one abelian membrane the chart (VIII.1.9) makes the common-phase action concrete:

$$C^A \longmapsto e^{2\pi i/k} C^A, \qquad (C^1, \ldots, C^4) \sim (e^{2\pi i/k} C^1, \ldots, e^{2\pi i/k} C^4). \tag{VIII.1.22}$$

In the ABJM $SU(4)$-covariant scalar chart, the four fields are written $(A_1, A_2, B_1^\dagger, B_2^\dagger)$ and have the same residual phase weight. That is distinct from treating all four as holomorphic chiral coordinates. The quotient and its gauge origin are derived in Chapters 2 and 3.

The proposed interacting theory has full compact gauge group $U(N)_k \times U(N)_{-k}$ and bifundamental matter. Supersymmetry, Chern–Simons structure and field-theory consistency specify its action. The bare quotient geometry alone does not uniquely determine that action or its global line-operator data. For example, the simplest invariant of one complex component under the common phase is its kth power:

$$(C^A)^k \longmapsto e^{2\pi i} (C^A)^k = (C^A)^k. \tag{VIII.1.23}$$

This geometric invariant illustrates the quotient; it does not by itself construct a local ABJM operator before gauge invariance and magnetic flux are addressed. On a generic diagonal branch, the candidate's vacuum positions can be compared with the unordered positions of N probes, represented by

$$\mathrm{Sym}^N\big(\mathbb{C}^4/\mathbb{Z}_k\big). \tag{VIII.1.24}$$

The expression is a target for the comparison, not a derivation of every branch of the quantum theory. For $N = 1$ and $k > 1$, the nontrivial common-phase quotient prevents a covering-space coordinate C^A from descending to an invariant local coordinate. At $k = 1$ the quotient is trivial and the flat-target coordinate does descend. This geometric statement is distinct from gauge invariance of the bare ABJM matter field before gauge fixing or dual-photon dressing. For $N > 1$, diagonal entries make sense as positions in a chosen generic-branch gauge, while local operators must pass the gauge-invariance test.

At $k = 1$ a covering coordinate descends geometrically, but a bare bifundamental field of the candidate gauge theory still requires a specified gauge-invariant construction to become a local operator. At $k = 2$, the points C^A and $-C^A$ represent the same

orbifold position; a linear covering coordinate cannot distinguish them on the quotient. This small example separates a target-space coordinate from a field in a chosen gauge. Chapters 2 and 3 will derive the candidate action, position branch and magnetic dressing that the picture anticipates.

VIII.1.4 The harmonic M2 solution and its throat

A stack changes a different object: the eleven-dimensional fields around it. We take the sourced, purely electric classical M2 solution as a physical input. Its radial dependence can nevertheless be derived from the exterior Laplace equation, and its near-source metric can be reduced to a recognizable geometry. This calculation uses coincident sources at the tip of the common-phase $\mathbb{C}^4/\mathbb{Z}_k$ cone, $k > 0$, with zero discrete torsion and leading equal-rank charge.

Place coincident M2-branes along x^0, x^1, x^2, and write $\eta_{\mu\nu} = \mathrm{diag}(-1, 1, 1)$ for their flat worldvolume metric, where $\mu, \nu = 0, 1, 2$. The eight transverse coordinates form $\mathbb{C}^4/\mathbb{Z}_k$, with positive integer k. On the four complex coordinates z^A, $A = 1, \ldots, 4$, the generator acts by $z^A \mapsto e^{2\pi i/k} z^A$. Its angular section at radius $r > 0$ is $Y_7 = S^7/\mathbb{Z}_k$, with unit metric $d\Omega^2_{7,k}$. The radius r and the length L below have dimensions of length. We consider the common-phase quotient, equal-rank leading charge, and zero discrete torsion.

The radial power follows from the transverse space before any charge normalization is imposed. For a radial function $H(r)$ on this flat eight-dimensional cone, the source-free Laplace equation is

$$\nabla^2_8 H = \frac{1}{r^7}\frac{d}{dr}\left(r^7 \frac{dH}{dr}\right) = 0 \qquad (r > 0). \tag{VIII.1.25}$$

Integrating twice gives $H = h_0 + q/r^6$. The constant is $h_0 = 1$ when the metric approaches the flat transverse cone at large r. We write $q = L^6$; then H is dimensionless. The explicit wrong-power comparison below shows why a six-transverse-dimensional falloff cannot be imported.

The standard classical, purely electric M2 solution supplies the remaining physical input. With $\mathrm{vol}_{012} = dx^0 \wedge dx^1 \wedge dx^2$ and $G_4 = dC_3$, it reads

$$\begin{aligned} ds^2_{11} &= H^{-2/3}\eta_{\mu\nu}dx^\mu dx^\nu + H^{1/3}\big(dr^2 + r^2 d\Omega^2_{7,k}\big), \\ G_4 &= \mathrm{vol}_{012} \wedge d(H^{-1}), \qquad H = 1 + \frac{L^6}{r^6}. \end{aligned} \tag{VIII.1.26}$$

We use this sourced supergravity solution; the radial Laplace calculation checks one exterior consequence and does not by itself derive the full field equations. The unequal warp powers have a direct effect. Along the membrane, proper lengths carry $H^{-1/3}$; transverse proper lengths carry $H^{1/6}$. Thus the same charge both redshifts motion parallel to the source and expands its transverse angular section relative to the coordinate metric. The normalization of L is still unknown until we measure the electric flux.

The power of r is a useful diagnostic. If we borrowed the r^{-4} falloff of a source with six transverse directions, then

$$\nabla_8^2(r^{-4}) = r^{-7}\frac{d}{dr}\big(-4r^2\big) = -8r^{-6} \neq 0 \qquad (r>0). \tag{VIII.1.27}$$

By contrast $r^7\partial_r(r^{-6}) = -6$ is constant. The quotient changes the angular identification but not this local radial differential operator away from the tip. At $k=1$ the angular section is S^7; at $k=2$ its points are paired by a common sign, while the local form of the metric and radial exponent remain the same.

Near the source, $r \ll L$ makes $H \simeq L^6/r^6$. Substitution in (VIII.1.26) gives

$$ds_{11}^2 \simeq \frac{r^4}{L^4}\eta_{\mu\nu}dx^\mu dx^\nu + \frac{L^2}{r^2}dr^2 + L^2 d\Omega_{7,k}^2. \tag{VIII.1.28}$$

The angular section already has constant physical radius L. To recognize the other factor, set $\rho = 2r^2/L^3$, an inverse-length coordinate. Since $dr/r = d\rho/(2\rho)$ and $r^4/L^4 = L^2\rho^2/4$, the metric becomes

$$ds_{11}^2 = \frac{L^2}{4}\left(\rho^2\eta_{\mu\nu}dx^\mu dx^\nu + \frac{d\rho^2}{\rho^2}\right) + L^2 d\Omega_{7,k}^2. \tag{VIII.1.29}$$

The parentheses are the Poincaré metric of unit-radius AdS_4. Consequently $R_{\mathrm{AdS}_4} = L/2$ and $R_{Y_7} = L$. The factor of two follows from the radial change of variable, not from a convention for drawing the throat. Substituting $d\rho = 4r\,dr/L^3$ back into the radial term recovers L^2dr^2/r^2, a quick check of both radii.

The geometry also gives a precise sense in which the source lies down a throat. At fixed x^μ and fixed angular coordinates, the near-source proper radial distance between r_1 and r_2 is

$$s(r_1,r_2) = \int_{r_1}^{r_2}\sqrt{g_{rr}}\,dr = L\int_{r_1}^{r_2}\frac{dr}{r} = L\log\frac{r_2}{r_1}. \tag{VIII.1.30}$$

It diverges as $r_1 \to 0$ in the ideal classical solution. The same metric redshifts a local clock at fixed r. Along a static worldline $ds^2 = -H^{-2/3}dt^2$, so

$$d\tau = H^{-1/3}dt \simeq \frac{r^2}{L^2}dt, \qquad E_{\text{coordinate}} = H^{-1/3}E_{\text{local}}. \tag{VIII.1.31}$$

The radial distance and redshift follow from the same warp factor that produced the AdS metric. They explain why dropping the asymptotically flat part of H isolates a different energy region. The classical metric alone does not identify its exact interacting boundary theory.

The near-horizon operation also has a decoupling interpretation. Let ℓ_p be the eleven-dimensional Planck length and hold

$$U = \frac{r^2}{\ell_p^3} \tag{VIII.1.32}$$

fixed as $\ell_p \to 0$, with the source count and k fixed. The flux calculation below will give $L \propto \ell_p$ at fixed charges. Hence $r/L \propto \ell_p^{1/2} \to 0$, and the additive 1 in H disappears. This limit selects the throat; it leaves L/ℓ_p finite. Weakly curved gravity therefore requires a separate large-charge expansion.

Figure VIII.1.3 collects the geometric scales without identifying the small Hopf circle with the radius of the whole sphere.

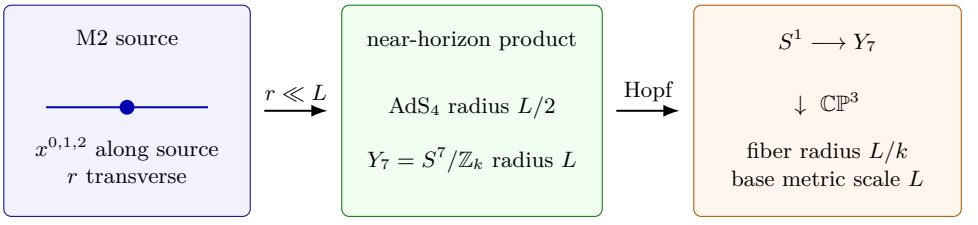


Figure VIII.1.3: One stack of positive-charge M2 sources at the tip of $\mathbb{C}^4/\mathbb{Z}_k$. The worldvolume is $x^{0,1,2}$ and r points outward in the transverse cone. The panels describe the same N, k and L, with $L^6 = 32\pi^2 k N \ell_p^6$ at leading classical order. The first arrow takes $r \ll L$; the second displays the Hopf decomposition of that same throat. Radii are proper metric scales, while r is a coordinate. The picture does not vary k or identify a finite-charge radius.

The limit in the preceding equation is particularly transparent after putting $r = \ell_p^{3/2}\sqrt{U}$ and $L = (32\pi^2 k N)^{1/6}\ell_p$. Holding N, k, U fixed gives

$$\frac{r}{L} = \frac{\sqrt{U\ell_p}}{(32\pi^2 k N)^{1/6}} \longrightarrow 0, \qquad \frac{L}{\ell_p} = (32\pi^2 k N)^{1/6}. \tag{VIII.1.33}$$

The first expression removes the asymptotic 1 from H, but the second stays finite at fixed charge. This is why selecting the throat and using weakly curved gravity are separate operations. To know when the latter is possible, we first have to determine L from electric charge.

VIII.1.5 Electric charge fixes the radius

The harmonic equation leaves one positive length L undetermined. The membrane couples electrically to the three-form, so an outward flux through the angular seven-manifold measures its classical charge. The relative orientation matters: use mostly-plus signature, outward angular orientation, and $\mathrm{vol}_{11} = -\alpha \wedge \beta$ as in the stated membrane convention. Then a positive electric source has positive outward $*G_4$.

To turn L into a charge, the flux sign and the membrane unit must both be fixed. Use mostly-plus signature and the orthonormal coframe

$$e^\mu = H^{-1/3} dx^\mu, \qquad e^r = H^{1/6} dr, \qquad E^a = H^{1/6} r\, \widehat{E}^a \quad (a = 1, \ldots, 7), \tag{VIII.1.34}$$

where $\widehat{E}^a$ is an outward-oriented orthonormal coframe for the unit Y_7. Define the physical forms $\alpha = e^0 \wedge e^1 \wedge e^2 \wedge e^r$ and $\beta = E^1 \wedge \cdots \wedge E^7$. Declare the eleven-dimensional

orientation $\mathrm{vol}_{11} = -\alpha \wedge \beta$. The Lorentzian inner product gives $\langle \alpha, \alpha \rangle = -1$, so the defining relation $\alpha \wedge *\alpha = \langle \alpha, \alpha \rangle \mathrm{vol}_{11}$ implies

$$\alpha \wedge *\alpha = -\mathrm{vol}_{11} = \alpha \wedge \beta, \qquad *\alpha = +\beta. \tag{VIII.1.35}$$

This orientation assigns positive outward flux to the electric branch in (VIII.1.26).

Differentiating H^{-1} and converting to that frame gives

$$\frac{dH^{-1}}{dr} = \frac{6L^6}{r^7 H^2}, \qquad G_4 = \frac{6L^6}{r^7 H^{7/6}} \alpha, \qquad *G_4 = 6L^6 \, \widehat{\mathrm{vol}}_{Y_7}, \tag{VIII.1.36}$$

where $\widehat{\mathrm{vol}}_{Y_7}$ is the outward unit-metric volume form. In the last equality, the factor $H^{7/6} r^7$ in β cancels the radial factor in G_4. The electric flux is therefore independent of which sphere at $r > 0$ surrounds the source. In the near-horizon physical volume forms v_4 and v_7, the same branch is $G_4 = (6/L) v_4 = (3L^3/8) \widehat{v}_4$ and $*G_4 = 6L^6 \widehat{v}_7$, with $\widehat{v}_4$ the oriented unit-radius AdS_4 form. Reversing the ambient orientation reverses the written flux sign.

In our length convention the gravitational coupling and positive membrane tension are

$$2\kappa_{11}^2 = (2\pi)^8 \ell_p^9, \qquad T_{M2} = \frac{1}{(2\pi)^2 \ell_p^3}, \qquad 2\kappa_{11}^2 T_{M2} = (2\pi)^6 \ell_p^6. \tag{VIII.1.37}$$

The tension is a physical input. A unit seven-sphere has volume $2\pi^4/\Gamma(4) = \pi^4/3$. The common-phase $\mathbb{Z}_k$ action is free on that sphere: if a nonidentity phase fixed a point, all four coordinates would vanish, which is impossible on S^7. Each generic orbit has k points, so

$$\mathrm{Vol}(Y_7) = \frac{1}{k} \mathrm{Vol}(S^7) = \frac{\pi^4}{3k}. \tag{VIII.1.38}$$

The orbifold tip is where the membranes sit; it does not introduce fixed points on the surrounding angular section.

Let N denote the leading classical charge measured on the quotient. The electric flux integral now yields

$$\begin{aligned} N &= \frac{1}{2\kappa_{11}^2 T_{M2}} \int_{Y_7} *G_4 = \frac{6L^6}{(2\pi)^6 \ell_p^6} \frac{\pi^4}{3k} = \frac{L^6}{32\pi^2 k \ell_p^6}, \\ L^6 &= 32\pi^2 k N \ell_p^6. \end{aligned} \tag{VIII.1.39}$$

The product $2\kappa_{11}^2 T_{M2}$ has units of length to the sixth power, matching L^6; the resulting flux count is dimensionless. For this purely electric solution $G_4 \wedge G_4 = 0$. With no additional internal C_3 holonomy, the classical Chern–Simons contribution to the Page integral also vanishes in the gauge used here. This does not turn (VIII.1.39) into an exact finite-N charge law.

The distinction between electric flux and Page charge is visible before any quantum correction is computed. In the stated bulk convention, away from an explicit source the four-form equation reads

$$d*G_4 + \frac{1}{2} G_4 \wedge G_4 = 0, \qquad d\left(*G_4 + \frac{1}{2} C_3 \wedge G_4 \right) = 0. \tag{VIII.1.40}$$

For the electric ansatz, G_4 contains all three worldvolume directions and one radial direction; wedging it with itself repeats those directions and gives zero. With the stated zero internal holonomy, the second term in the Page form also has no angular integral on Y_7. That is why the classical charge calculation above can use $*G_4$. The Page form has a gauge-dependent representative, and finite-charge curvature terms are outside this exterior calculation.

For a fixed local L the quotient has $1/k$ of the covering volume. Writing the two fluxes side by side gives

$$N_{\text{cover}} = \frac{6L^6\,\text{Vol}(S^7)}{(2\pi)^6\ell_p^6} = kN_{\text{quotient}}, \qquad \frac{N_{\text{quotient}}}{N_{\text{cover}}} = \frac{\text{Vol}(S^7/\mathbb{Z}_k)}{\text{Vol}(S^7)} = \frac{1}{k}. \quad \text{(VIII.1.41)}$$

At $k = 2$, a proposed radius with the covering coefficient but called "quotient charge N" would yield $N/2$ through the quotient surface. This is a physical normalization error, not a different name for the same integer. At $k = 1$ the ordinary unquotiented result returns. Identifying this leading N with equal-rank worldvolume data is useful later, but the flux integral alone establishes no finite-N rank identity. The next step uses L as the radius of the quotient sphere and asks how its Hopf circle appears in type IIA units.

VIII.1.6 The Hopf circle and type IIA units

The angular space is a circle bundle over $\mathbb{CP}^3$. The quotient shortens its fiber, so an observer who reduces along that circle sees a ten-dimensional string background. We must keep three lengths distinct: the sphere scale L, the proper fiber radius L/k, and the coefficient of the base metric measured in string units.

Start with a covering Hopf coordinate ψ of period 2π. The common-phase $\mathbb{Z}_k$ identification reduces its period to $2\pi/k$. Setting $\phi = k\psi$ restores a period-2π coordinate on the quotient, while preserving the local horizontal metric:

$$d\Omega_{7,k}^2 = ds_{\mathbb{CP}^3}^2 + (d\psi + \omega)^2 = ds_{\mathbb{CP}^3}^2 + \frac{1}{k^2}(d\phi + k\omega)^2, \qquad \phi \sim \phi + 2\pi. \quad \text{(VIII.1.42)}$$

At fixed base point the physical circle circumference is $2\pi L/k$. Thus its radius is $R_{11} = L/k$, whereas the base metric in the eleven-dimensional throat has coefficient L^2. These are distinct proper scales. Let g_s be the type IIA string coupling and ℓ_s its string length, with $\ell_s^2 = \alpha'$. The circle relations $R_{11} = g_s\ell_s$ and $\ell_p^3 = g_s\ell_s^3$ then give the coefficient L_{str}^2 of the $\mathbb{CP}^3$ unit metric in string frame, as well as the circle and coupling scales:

$$\begin{aligned} \frac{R_{11}}{\ell_p} &= (32\pi^2)^{1/6}\left(\frac{N}{k^5}\right)^{1/6}, \\ g_s &= \left(\frac{L}{k\ell_p}\right)^{3/2} = (32\pi^2)^{1/4}\left(\frac{N}{k^5}\right)^{1/4}, \\ \frac{L_{\text{str}}^2}{\ell_s^2} &= \frac{L^3}{k\ell_p^3} = \sqrt{32\pi^2\frac{N}{k}}. \end{aligned} \quad \text{(VIII.1.43)}$$

To see the frame conversion explicitly, use the constant-dilaton reduction in dimensionless metrics:

$$\frac{ds_{11}^2}{\ell_p^2} = g_s^{-2/3}\frac{ds_{10,\mathrm{str}}^2}{\ell_s^2} + g_s^{4/3}(d\phi + k\omega)^2, \qquad \frac{L_{\mathrm{str}}^2}{\ell_s^2} = g_s^{2/3}\frac{L^2}{\ell_p^2} = \frac{L^3}{k\ell_p^3}. \tag{VIII.1.44}$$

The fiber coefficient gives $g_s^{2/3} = L/(k\ell_p)$. The same horizontal conversion acts on the AdS metric, leaving its coefficient $L_{\mathrm{str}}^2/4$. This step uses the constant dilaton of this throat; it is not an equality between arbitrary warped coordinate radii. Written as a ten-dimensional metric, the result is

$$\frac{ds_{10,\mathrm{str}}^2}{\ell_s^2} = \frac{L^3}{k\ell_p^3}\left(\frac{1}{4}ds_{\mathrm{AdS}_4,\mathrm{unit}}^2 + ds_{\mathbb{CP}^3,\mathrm{unit}}^2\right). \tag{VIII.1.45}$$

The factor $1/4$ belongs to the AdS factor, while the coefficient of the $\mathbb{CP}^3$ metric is the string-frame radius squared. The circle has disappeared as a geometric coordinate of this metric; its size is encoded in g_s and in the Kaluza–Klein connection. The next section tests whether this ten-dimensional background has both weak coupling and weak curvature.

The algebra behind the string-frame expression can be done without guessing a radius. The circle relations imply

$$\ell_s = \left(\frac{\ell_p^3}{R_{11}}\right)^{1/2}, \qquad g_s = \frac{R_{11}}{\ell_s} = \left(\frac{R_{11}}{\ell_p}\right)^{3/2}, \qquad \frac{L^2}{\ell_s^2} = \frac{L^2 R_{11}}{\ell_p^3} = \frac{L^3}{k\ell_p^3}. \tag{VIII.1.46}$$

The metric conversion above identifies this horizontal coefficient with $L_{\mathrm{str}}^2/\ell_s^2$. In a warped reduction the local metric relation, rather than the circle length alone, determines the scale.

The fixed-N comparison is also instructive. Equation (VIII.1.39) gives $L(k = 2)/L(k = 1) = 2^{1/6}$, hence

$$\frac{R_{11}(k=2)}{R_{11}(k=1)} = 2^{-5/6}, \qquad \frac{(L_{\mathrm{str}}^2/\ell_s^2)_{k=2}}{(L_{\mathrm{str}}^2/\ell_s^2)_{k=1}} = 2^{-1/2}. \tag{VIII.1.47}$$

The fiber is not simply halved at fixed charge, because the sphere radius itself grows with k. At fixed L, by contrast, the geometric fiber radius is exactly divided by k.

VIII.1.7 Controlled regimes and physical comparisons

The throat is a classical solution, but a classical solution need not be a reliable approximation. We ask independently whether local curvature is small and whether the circle description is appropriate. Then we can state what a vacuum-space, protected-operator or gravity comparison actually tests.

A single exponent organizes the growing-N cases. Put $k = cN^a$ with fixed $c > 0$. Equations (VIII.1.39) and (VIII.1.43) give

$$\frac{L}{\ell_p} \propto N^{(1+a)/6}, \qquad \frac{R_{11}}{\ell_p} \propto N^{(1-5a)/6}, \qquad g_s \propto N^{(1-5a)/4}, \qquad \frac{L_{\rm str}^2}{\ell_s^2} \propto N^{(1-a)/2}. \tag{VIII.1.48}$$

Thus $a < 1/5$ enlarges the M-theory circle, whereas $1/5 < a < 1$ simultaneously weakens the IIA coupling and enlarges the string-frame curvature radius. The boundary exponents must still be read with their fixed numerical prefactors, as the worked cases below show. These are approximation windows, not phase transitions.

Gravity needs more than a throat. Eleven-dimensional supergravity needs both $L/\ell_p \gg 1$ for small local curvature and $R_{11}/\ell_p \gg 1$ for a large quotient circle. From (VIII.1.39) and (VIII.1.43), these are

$$\left(\frac{L}{\ell_p}\right)^6 = 32\pi^2 kN \gg 1, \qquad \left(\frac{R_{11}}{\ell_p}\right)^6 = 32\pi^2 \frac{N}{k^5} \gg 1. \tag{VIII.1.49}$$

Parametrically these are $Nk \gg 1$ and $N/k^5 \gg 1$. When the circle shrinks, type IIA supergravity is useful if its string coupling is small and the $\mathbb{CP}^3$ curvature radius is large in string units. Put $\lambda = N/k$ for the ratio that enters this comparison. Then

$$\frac{L_{\rm str}^2}{\ell_s^2} = \sqrt{32\pi^2\lambda} \gg 1, \qquad g_s^2 = \sqrt{32\pi^2}\,\frac{\lambda^{5/2}}{N^2} \ll 1. \tag{VIII.1.50}$$

At the level of scaling powers, the conditions are $\lambda \gg 1$ and $\lambda^{5/2}/N^2 \ll 1$. The displayed constants determine the chosen units; neither inequality defines a sharp phase boundary. For a growing window with both hierarchies improving as N increases, one can write $N^{1/5} \ll k \ll N$, with fixed numerical factors understood. The left inequality makes the circle small and the IIA coupling weak, while the right increases the string-frame radius. The exponents follow by substituting $k = cN^a$ into both IIA measures:

$$g_s^2 \propto N^{(1-5a)/2}, \qquad \frac{L_{\rm str}^2}{\ell_s^2} \propto N^{(1-a)/2}, \qquad \frac{1}{5} < a < 1. \tag{VIII.1.51}$$

Both required measures improve only in this open exponent interval.

It helps to separate an N-driven statement from validity at a large but fixed parameter. If k is fixed and N grows, both L/ℓ_p and R_{11}/ℓ_p grow. The eleven-dimensional description improves; its circle does not shrink. If $k = N^{1/2}$, then

$$\frac{R_{11}}{\ell_p} \propto N^{-1/4}, \qquad g_s \propto N^{-3/8}, \qquad \frac{L_{\rm str}^2}{\ell_s^2} \propto N^{1/4}, \tag{VIII.1.52}$$

with fixed factors suppressed. The type IIA approximation improves in both of its required measures.

At $k = cN$ with fixed $c > 0$, the ratio $\lambda = 1/c$ stays fixed. The coupling falls as N^{-1}, but the string curvature measure remains $\sqrt{32\pi^2/c}$: increasing N alone does not

improve it. A small fixed c can nevertheless give a large fixed radius. For instance $N = 10^{12}$, $k = 10^6$, and $c = 10^{-6}$ give $\lambda = 10^6$ and

$$\frac{L_{\rm str}^2}{\ell_s^2} = \sqrt{32\pi^2\, 10^6} \simeq 1.78 \times 10^4, \qquad g_s = (32\pi^2)^{1/4} 10^{-9/2} \simeq 1.33 \times 10^{-4}. \tag{VIII.1.53}$$

This is a useful IIA approximation according to the stated curvature and coupling tests, even though its curvature hierarchy does not improve with further N at fixed c. In contrast, $k = N$ keeps $\lambda = 1$, so the same large-N operation supplies no large curvature hierarchy.

The exponent boundary deserves the same care. For $k = cN^{1/5}$ with fixed positive c,

$$\frac{R_{11}}{\ell_p} = (32\pi^2)^{1/6} c^{-5/6}, \qquad g_s = (32\pi^2)^{1/4} c^{-5/4}, \tag{VIII.1.54}$$

while $L_{\rm str}^2/\ell_s^2$ grows as $N^{2/5}$. The powers of N leave the coupling and circle at fixed values. Their fixed prefactors decide whether either description has a numerical hierarchy; the exponent $1/5$ alone cannot decide it. The corresponding comparison is summarized in Figure VIII.1.4.

Scaling of the leading throat at fixed stated prefactors

k choice	circle and coupling	curvature test
fixed k	$R_{11}/\ell_p \to \infty$	11d curvature improves
$N^{1/2}$	$g_s \to 0$	$L_{\rm str}^2/\ell_s^2 \to \infty$
cN	$g_s \to 0$	$L_{\rm str}^2/\ell_s^2 = \sqrt{32\pi^2/c}$

$k = cN^{1/5}$ keeps g_s and R_{11}/ℓ_p fixed; their values depend on c.

Figure VIII.1.4: Controlled-regime comparison for the leading zero-torsion geometry as $N \to \infty$. In each row the displayed k prescription and its fixed prefactors are held fixed while N varies; L changes through $L^6 = 32\pi^2 kN\ell_p^6$. The cN row says only that curvature has no N-driven improvement. For sufficiently small fixed c, hence large fixed $\lambda = 1/c$, the IIA curvature and coupling tests can both hold. The $cN^{1/5}$ row marks an exponent boundary, not a sharp phase line.

We can now distinguish four comparisons that will appear later in the volume. A generic position branch compares vacuum coordinates with separated M2 locations. A protected operator comparison tests selected quantum numbers and may require magnetic dressing. A supergravity calculation estimates an observable only where the relevant curvature and coupling measures permit it. The near-horizon limit selects the background but does not itself establish any of those QFT statements. For instance, the same N, k can admit a quotient position branch while neither classical gravity description is controlled at small N.

A finite-charge correction illustrates the boundary. In the zero-torsion case, the sourced orbifold contribution to asymptotic M2 charge is

$$\Delta N_{\rm orb} = -\frac{1}{24}\left(k - \frac{1}{k}\right), \qquad \Delta N_{\rm orb}(k=1) = 0. \tag{VIII.1.55}$$

This is a higher-derivative sourced result, not a term produced by the classical flux integral here. Source, Page and Maxwell charges can differ; the leading N in our radius formula is the classical quotient charge. Unequal ranks and torsion are treated in Chapter 4, while Chapters 11 and 12 return to protected and large-N observables.

VIII.1.8 Exercises

These problems connect membrane fluctuations and candidate gauge theories to the charge-normalized geometry and its reduction. Use each question's stated domain and explain the physical meaning of your calculation.

1. **One-membrane displacement.** For one planar M2 in flat eleven-dimensional space, expand the induced area term to quadratic order. Give the coefficient in $S^{(2)} = qT_{M2}\int d^3x\,\partial_\mu X^I \partial^\mu X^I$, the power b in $\phi^I = T_{M2}^b X^I$, the engineering mass dimensions of T_{M2}, X^I, ϕ^I, and the connected Euclidean X^3 correlator around $X^3 = v$. Express the latter as $c\pi^p T_{M2}^t r^u + wv^2$. Use mostly-plus signature, static gauge, eight transverse coordinates, $T_{M2} > 0$, one membrane, a flat infinite worldvolume, the Gaussian approximation, $r > 0$ and vanishing background three-form pullback.

2. **Positions and operators.** Classify what a single-M2 position field, a generic stack eigenvalue and a chiral primary can measure or compare in their stated domains. Use one flat M2 at $k = 1$ and, separately, an $N > 1$ stack at a generic point. For each object, state its domain and distinguish local gauge invariance from a protected-sector match. Give a reasoned prose answer.

3. **Two ABJM routes.** Draw the two ABJM route chains and label the T_6, M-lift, moduli-comparison and protected-test arrows with their logical status. Assume $N, k > 0$; use source fivebrane charge order (NS5, D5) and book order (D5, NS5). Submit two labelled chains and a short explanation of what each arrow establishes.

4. **Three-dimensional gauge dimensions.** With $D_\mu = \partial_\mu + iA_\mu$ in three dimensions, give the mass dimensions of the measure, derivative, gauge field, field strength, Yang–Mills coupling squared and fundamental-trace Chern–Simons level. State only what dimension counting establishes about a CS-matter fixed-point candidate. Use natural units, $(2+1)$ dimensions, the fundamental trace and the terms in (VIII.1.17).

5. **Flux and the quotient throat.** For N coincident positive-charge M2 sources at the tip of $\mathbb{C}^4/\mathbb{Z}_k$ with common-phase action and zero discrete torsion, start from $H = 1 + L^6/r^6$ and $G_4 = \mathrm{vol}_{012} \wedge d(H^{-1})$. Derive the near-horizon AdS and

sphere radii and determine L^6 in terms of N, k and ℓ_p by an electric flux integral. Show the $k = 1$ limit.

Use positive integers N, k, the leading classical solution, $2\kappa_{11}^2 = (2\pi)^8 \ell_p^9$ and $T_{M2} = 1/((2\pi)^2 \ell_p^3)$. Take the mostly-plus orientation $\alpha = e^{012r}$, outward angular β, and $\mathrm{vol}_{11} = -\alpha \wedge \beta$, so $*\alpha = +\beta$. The surrounding unit S^7 quotient is free. In your derivation explain why the cover charge and quotient charge differ. The optional structured submission records the radial dimension and power, the two angular volumes, the Hodge coefficient and flux integral, the charge-radius result, both radii, and the $k = 1$ limit. Include units where applicable.

6. **Hopf reduction and controlled regimes.** Using $L^6 = 32\pi^2 k N \ell_p^6$ and the Hopf metric $ds_7^2 = ds_{\mathbb{CP}^3}^2 + k^{-2}(d\phi + k\omega)^2$ with ϕ of period 2π, derive R_{11}/ℓ_p, g_s and the $\mathbb{CP}^3$ curvature radius squared in string units. Classify fixed k with N large, $k = N^{1/2}$, and $k = cN$ with fixed $c > 0$ by N-driven control. Separately derive the type IIA validity inequalities in $\lambda = N/k$ and N, and analyze the $a = 1/5$ boundary for $k = N^a$.

   Use $R_{11} = g_s \ell_s$, $\ell_p^3 = g_s \ell_s^3$, and the sphere radius L with AdS radius $L/2$. Eleven-dimensional supergravity needs large curvature and circle scales in Planck units; type IIA needs weak coupling and small curvature in string units. Explain the inequalities and the fixed-prefactor boundary in words. These two explanations are written reasoning; the optional structured submission records the circle, coupling and curvature scales and the three N-driven classifications.

Status and sources

Sources by section. Source coordinates and scope qualifications follow.

§VIII.1.1. The sourced M2 area action is used only at the stated single-brane scope; its determinant expansion is [MATH] conditional on that action (Bergshoeff et al. 1987, §2).

§VIII.1.2. Gaussian propagator and radial Green function are [MATH] on the flat $r > 0$ domain, using the membrane normalization of Bergshoeff et al. 1987, §2.

§VIII.1.3. Dimensional counting is [MATH] in the fundamental-trace convention (Chern–Simons trace and levels; Aharony, Bergman, et al. 2008, §2). The IIB suspension-circle route is conditional [DUAL] (Aharony, Bergman, et al. 2008, §3). The position-sector comparison is [GEO-X], without quantum equivalence (Aharony, Bergman, et al. 2008, §2.3). The protected sector is a sourced premise with no specified BPS fraction (Aharony, Bergman, et al. 2008, §2.4). The leading gravity regime is [SUGRA] (Aharony, Bergman, et al. 2008, §4.1). Action and closure are [MATH] conditional on the BLG algebra and equations, not a general-N membrane identification (Bagger and Lambert 2008, §§3–4).

§VIII.1.4. Radial throat formulas are [MATH] conditional on the sourced classical M2 solution [SUGRA] of Maldacena 1998, §3.2.

§VIII.1.5. Leading flux and radius algebra is [MATH] under zero torsion and classical charge; the physical radius input is [SUGRA], Aharony, Bergman, et al. 2008, §4.1.

§VIII.1.6. Hopf-circle and type-IIA unit conversions are conditional [MATH] using the stated membrane and compact reduction conventions; the reduction dictionary is sourced, Aharony, Bergman, et al. 2008, §4.1.

§VIII.1.7. Scale inequalities are [MATH] under the leading solution; finite-charge corrections remain sourced [SUGRA] inputs, Bergman and Hirano 2009, §3.1.

§VIII.1.8. These exercises reuse the preceding conditional [MATH] calculations with brane-action units and Chern–Simons trace and levels using the stated membrane and compact reduction conventions (Bergshoeff et al. 1987, §2; Aharony, Bergman, et al. 2008, §4.1).

The single-brane area action and the classical M2 solution are sourced physical premises. The determinant, Green function, radial, flux and unit-conversion formulas are conditional algebra under those premises. The chapter uses metric signature, spinor conventions, brane-action units, Chern–Simons trace and levels, orbifold action, quiver gauge groups and Chern–Simons matter conventions, and the specified M2, compact gauge and geometric conventions. The gravity statements use leading equal-rank, zero-torsion classical charge. No finite-N charge equality or complete quantum duality follows.

Single membrane, §VIII.1.1 and §VIII.1.2. The induced-area premise is in Bergshoeff et al. (1987), §2, equations (3)–(5). The expansion, units, Gaussian propagator and unit-source flux follow from it. The sinusoidal-bend, complex-chart and doubled-distance displays are explanatory substitutions of the same formulas. The flat Gaussian, $r > 0$ domain is essential.

Several membranes, §VIII.1.3. The BLG candidate is sourced to Bagger and Lambert (2008), §§3–4. The CS/YM comparison and ABJM field-theory route use Aharony, Bergman, et al. (2008), §§2.1–2.4 and 3.1–3.3. The zero-axion compact construction uses the primitive flux, scalar and spin conventions stated above. The geometric comparison concerns the position sector.

Classical geometry, §VIII.1.4 and §VIII.1.5. The M2 solution and decoupling variable are in Maldacena (1998), §3.2, equation (3.3). The quotient and radius normalization are in Aharony, Bergman, et al. (2008), §4.1, equations (4.1)–(4.4). The membrane tension and gravitational coupling are in Giombi and Tseytlin (2023), §2, equation (2.7) and footnote 6. The electric orientation uses the M2 charge and flux orientation. The same classical solution determines the radial and flux algebra; the r^{-4} and cover/quotient examples illustrate those formulas.

Reduction and regimes, §VIII.1.6 and §VIII.1.7. The Hopf metric, string-frame bridge and regime scales use Aharony, Bergman, et al. (2008), §4.1, equations (4.3)–(4.7). The finite-charge orbifold correction is sourced to Bergman and Hirano (2009), §3.1, equation (3.8), and the distinct charge definitions to Aharony, Hashimoto, et al. (2010), introduction and Appendix A. These are source statements, not corrections inserted into the leading radius formula. The exercise companion tests the stated finite calculations; it does not assess the written physical explanations.

References

Aharony, O., O. Bergman, et al. (2008). "N=6 superconformal Chern-Simons-matter theories, M2-branes and their gravity duals". In: *JHEP* 10, p. 091. DOI: 10.1088/1126-6708/2008/10/091. arXiv: 0806.1218 [hep-th].

Aharony, O., A. Hashimoto, et al. (2010). "D-brane Charges in Gravitational Duals of 2+1 Dimensional Gauge Theories and Duality Cascades". In: *JHEP* 01, p. 072. DOI: 10.1007/JHEP01(2010)072. arXiv: 0906.2390 [hep-th].

Bagger, J. and N. Lambert (2008). "Gauge symmetry and supersymmetry of multiple M2-branes". In: *Phys. Rev. D* 77, p. 065008. DOI: 10.1103/PhysRevD.77.065008. arXiv: 0711.0955 [hep-th].

Bergman, O. and S. Hirano (2009). "Anomalous radius shift in AdS(4)/CFT(3)". In: *JHEP* 07, p. 016. DOI: 10.1088/1126-6708/2009/07/016. arXiv: 0902.1743 [hep-th].

Bergshoeff, E., E. Sezgin, and P. K. Townsend (1987). "Supermembranes and Eleven-Dimensional Supergravity". In: *Phys. Lett. B* 189, pp. 75–78. DOI: 10.1016/0370-2693(87)91272-X.

Giombi, S. and A. A. Tseytlin (2023). "Wilson Loops at Large N and the Quantum M2-Brane". In: *Phys. Rev. Lett.* 130.20, p. 201601. DOI: 10.1103/PhysRevLett.130.201601. arXiv: 2303.15207 [hep-th].

Maldacena, J. M. (1998). "The Large N limit of superconformal field theories and supergravity". In: *Adv. Theor. Math. Phys.* 2, pp. 231–252. DOI: 10.4310/ATMP.1998.v2.n2.a1. arXiv: hep-th/9711200.

Chapter VIII.2

From BLG to ABJM

A stack of M2-branes should have interacting fields for motion in eight transverse directions. The first explicit coupling with all sixteen classical supercharges used a metric three-bracket. Its four-generator example turns the bracket into an ordinary $\mathfrak{so}(4)$ gauge algebra and two opposite Chern–Simons factors. It teaches how a ternary matter interaction can coexist with gauge invariance, but its internal four-dimensional vector space is not an arbitrary number of membranes.

The arbitrary-rank candidate arises from a different construction. A circular IIB D3 suspension provides two rank-N intervals. After conditional T-duality and an M-theory lift, its transverse geometry has an extra torus period. A full compact $U(N)_k \times U(N)_{-k}$ Chern–Simons matter theory gives the same local one-brane position space. The two routes meet at a specified $\mathbb{C}^4/\mathbb{Z}_k$ action. This agreement concerns local vacuum coordinates; the proposed infrared dynamics, multi-brane branches and monopole operators need separate arguments.

We take positive integer k. On the brane route the IIB axion is zero and $0 < g_s^{\mathrm{B}} < \infty$. The compact groups, bare fundamental-trace levels and scalar charts will be declared at their first use.

VIII.2.1 The three-bracket and its gauge algebra

What algebraic operation can couple transverse scalar fields while generating ordinary local gauge transformations? The three-bracket answers this question only when its inner maps close and act as derivations.

Let $\mathcal{A}$ be a real vector space with a positive inner product $\langle\ ,\ \rangle$. A metric three-bracket is a trilinear, totally antisymmetric operation $[u, v, w] \in \mathcal{A}$ for which $\langle [u, v, w], z\rangle$ is antisymmetric in all four entries. Define the inner map $D_{u,v}w = [u, v, w]$. Metric invariance makes it skew-adjoint, since

$$\langle D_{u,v}w, z\rangle = -\langle w, D_{u,v}z\rangle. \tag{VIII.2.1}$$

This is the infinitesimal form of an orthogonal action on the matter space. It does not yet say that the maps $D_{u,v}$ close under commutators.

Closure comes from the *fundamental identity* (FI), required for every $u, v, x, y, z \in \mathcal{A}$:

$$[u, v, [x, y, z]] = [[u, v, x], y, z] + [x, [u, v, y], z] + [x, y, [u, v, z]]. \tag{VIII.2.2}$$

The left side is $D_{u,v}$ acting on a three-bracket; the right side says that it acts separately on the three inputs. Apply both sides to an arbitrary z and antisymmetrize the two successive actions. One obtains

$$[D_{u,v}, D_{x,y}] = D_{[u,v,x],y} + D_{x,[u,v,y]}. \tag{VIII.2.3}$$

Thus the inner maps span an ordinary Lie algebra, even though matter is coupled by a ternary product. A gauge connection can take values in this Lie algebra, and its covariant derivative can act on every bracket. Total antisymmetry by itself cannot do this job, as the counterexample below shows.

The worked example has an oriented orthonormal basis $e_1, \ldots, e_4$, $\epsilon_{1234} = +1$, and a nonzero real coefficient q:

$$\langle e_a, e_b \rangle = \delta_{ab}, \qquad [e_a, e_b, e_c] = q\epsilon_{abcd} e_d. \tag{VIII.2.4}$$

The invariant tensor of a metric bracket of this type is a four-form. It vanishes below dimension four, so this is the smallest positive-metric example with a nonzero bracket; smaller abelian examples exist. We take $q > 0$ when matching the positive first-node level below. Here $\langle [e_a, e_b, e_c], e_d \rangle = q\epsilon_{abcd}$, so the metric condition is immediate. To prove FI for *all* real arguments, rather than for a selection of basis tuples, observe that an orientation-preserving orthogonal map R preserves both the metric and the volume form. Hence $R[x, y, z] = [Rx, Ry, Rz]$. Differentiate this equation at the identity along any $T \in \mathfrak{so}(4)$:

$$T[x, y, z] = [Tx, y, z] + [x, Ty, z] + [x, y, Tz]. \tag{VIII.2.5}$$

Every $D_{u,v}$ is skew-adjoint by (VIII.2.1); putting $T = D_{u,v}$ in (VIII.2.5) proves (VIII.2.2). The orientation is essential: a reflection reverses the volume form and is not a symmetry of this fixed bracket.

The six D_{ab}, $a < b$, rotate the six coordinate planes. For example, $D_{12}e_3 = qe_4$ and $D_{12}e_4 = -qe_3$, while e_1, e_2 are fixed. Figure VIII.2.1 makes the sign and the unaffected directions explicit. In the column convention where column b is the image of e_b,

$$D_{12} = q \begin{pmatrix} 0 & 0 & 0 & 0 \\ 0 & 0 & 0 & 0 \\ 0 & 0 & 0 & -1 \\ 0 & 0 & 1 & 0 \end{pmatrix}, \qquad D_{13} = q \begin{pmatrix} 0 & 0 & 0 & 0 \\ 0 & 0 & 0 & 1 \\ 0 & 0 & 0 & 0 \\ 0 & -1 & 0 & 0 \end{pmatrix}. \tag{VIII.2.6}$$

Their commutator is

$$[D_{12}, D_{13}] = q^2 \begin{pmatrix} 0 & 0 & 0 & 0 \\ 0 & 0 & -1 & 0 \\ 0 & 1 & 0 & 0 \\ 0 & 0 & 0 & 0 \end{pmatrix} = qD_{14}. \tag{VIII.2.7}$$

Each pair rotates a different plane, so these six independent matrices span the six-dimensional $\mathfrak{so}(4) \simeq \mathfrak{su}(2)_+ \oplus \mathfrak{su}(2)_-$. Equation (VIII.2.7) is one concrete component

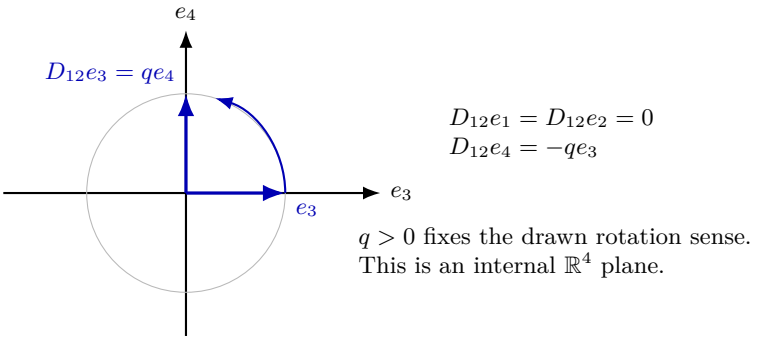


Figure VIII.2.1: Direction-only sketch of one inner derivation on the oriented orthonormal A_4 basis. The axes are internal basis directions, not membrane worldvolume coordinates. For fixed $q > 0$, D_{12} rotates the e_3, e_4 plane in the indicated infinitesimal sense and fixes e_1, e_2. Arrow lengths are schematic: $\|D_{12}e_3\|/\|e_3\| = q$. No membrane position or gauge group is inferred from this rotation.

of the general closure law (VIII.2.3). The four-dimensional matter space here is an algebraic representation; its dimension is not a count of membranes.

An explicit failed bracket shows why the FI is a separate condition. In an orthonormal real six-space, define the fully antisymmetric four-form

$$F_{abcd} = \epsilon^{1234}_{abcd} + t\epsilon^{1256}_{abcd}, \qquad [e_a, e_b, e_c] = \sum_d F_{abcd} e_d, \qquad t \neq 0, \tag{VIII.2.8}$$

where each four-plane symbol is $+1$ on its displayed ordered indices and vanishes outside that plane. The metric is still positive and invariant. Choose $(u, v, x, y, z) = (e_1, e_3, e_1, e_4, e_5)$. Since $[e_1, e_4, e_5] = 0$, the left side of FI is zero. Its first and third right-side terms vanish, whereas the middle term is

$$[e_1, e_3, e_4] = e_2, \qquad [e_1, [e_1, e_3, e_4], e_5] = [e_1, e_2, e_5] = te_6. \tag{VIII.2.9}$$

Consequently the FI residual, with left minus right as declared in (VIII.2.2), is $-te_6$. At $t = 0$ this bracket reduces to A_4 on $e_1, \ldots, e_4$ plus two central directions. The example establishes failure for this deformation; it is not a classification of positive-metric three-algebras. This gauge algebra is the input for the classical action in the next section.

VIII.2.2 The BLG action and the two SU(2) factors

What does the A_4 bracket produce as a field theory, and which part of the answer can be extended to arbitrary membrane number? The local action uses its inner derivations, while the compact group requires a separate choice.

The FI supplies the gauge algebra needed by an interacting action. Let $X^I = X^I_a e_a$ be eight real scalar fields, $I = 3, \ldots, 10$, and let $\Psi = \Psi_a e_a$ be their fermionic partners

on the $(2+1)$-dimensional worldvolume. The gauge connection acts through inner derivations, with $D_\mu X = \partial_\mu X - \widetilde{A}_\mu X$ in the real-vector chart. For mostly-plus worldvolume signature, the classical BLG matter and Chern–Simons terms can be written in a real-index chart as

$$\begin{aligned}\mathcal{L}_{\mathrm{BLG}} = & -\frac{1}{2}\langle D_\mu X^I, D^\mu X^I\rangle + \frac{i}{2}\langle\bar{\Psi}, \Gamma^\mu D_\mu \Psi\rangle + \frac{i}{4} f^{abcd}\bar{\Psi}_b \Gamma^{IJ} X^I_c X^J_d \Psi_a \\ & - V(X) + \mathcal{L}_{\mathrm{CS}}, \\ V(X) = & \frac{1}{12}\sum_{I,J,K} \left\| [X^I, X^J, X^K] \right\|^2 \geq 0,\end{aligned} \tag{VIII.2.10}$$

where $f^{abcd} = \langle [e_a, e_b, e_c], e_d\rangle$ and the repeated transverse indices are summed. The Yukawa contraction and gamma conventions follow the original classical action. The potential is sixth order in scalars and is nonnegative for the positive metric used here. It vanishes when every triple bracket of the scalar values vanishes. For A_4, this means those values span at most a two-plane in the internal $\mathbb{R}^4$; a vanishing potential alone is not a complete quantum moduli-space calculation.

The twisted $\mathcal{L}_{\mathrm{CS}}$ is a twisted Chern–Simons term built from f^{abcd} and the antisymmetric connection $A_{\mu ab}$. It contains one $A\partial A$ and one A^3 term, with no Yang–Mills kinetic term. After the A_4 split, it takes a particularly transparent form. Use Hermitian 2×2 connections $A, \widehat{A}$ and set

$$\mathrm{CS}_2(A) = \mathrm{tr}_{\mathbf{2}}\left(A\wedge dA + \frac{2i}{3}A\wedge A\wedge A\right), \qquad S_{\mathrm{CS}} = \frac{k}{4\pi}\int \big(\mathrm{CS}_2(A) - \mathrm{CS}_2(\widehat{A})\big). \tag{VIII.2.11}$$

Both bare levels refer to the fundamental trace and are $(+k, -k)$, with positive integer k. The connection is locally nonpropagating in this pure Chern–Simons action. Its field equation instead relates gauge curvature to the matter current. The classical construction has 16 supersymmetry transformations whose algebra closes on shell, after the fermion, scalar and gauge equations of motion are used. This is a statement about that classical action, not an off-shell transformation algebra or a quantum M2 identification.

The reason the FI is needed by this action can be seen before the supersymmetry transformations are considered. If the connection is a linear combination of inner derivations, its action on a bracket is the sum of its actions on the three inputs. Thus

$$D_\mu[X, Y, Z] = [D_\mu X, Y, Z] + [X, D_\mu Y, Z] + [X, Y, D_\mu Z]. \tag{VIII.2.12}$$

Consequently the squared bracket in the scalar potential transforms as an ordinary norm under the local inner-derivation algebra. Without the FI, a general antisymmetric tensor need not yield this covariance; the six-space example in the previous section supplies an explicit failure. This explains why the algebraic condition enters the Lagrangian rather than being an aesthetic restriction on a ternary product.

For a simple field configuration, let all eight scalar values lie in one fixed internal two-plane, $X^I = \alpha^I e_1 + \beta^I e_2$. Antisymmetry then makes every bracket in $V(X)$ vanish:

$$[X^I, X^J, X^K] = 0 \quad \text{for all } I, J, K, \qquad V(X) = 0. \tag{VIII.2.13}$$

This example exhibits a classical zero-potential locus. It does not determine which configurations remain after compact gauge identifications or quantum effects. That distinction will matter again when the ABJM abelian superpotential vanishes but its compact gauge fields still impose a quotient.

To see how the four real components enter the two-node description, let σ_j be Pauli matrices with $\mathrm{tr}_{\mathbf{2}}(\sigma_i\sigma_j) = 2\delta_{ij}$ and write

$$\mathsf{X}(x) = \frac{1}{2}\left(x_4\mathbf{1} + i\sum_{j=1}^{3} x_j\sigma_j\right), \qquad \sigma_2\mathsf{X}^*\sigma_2 = \mathsf{X}, \qquad \mathrm{tr}_{\mathbf{2}}(\mathsf{X}^\dagger\mathsf{X}) = \frac{1}{2}\sum_{a=1}^{4} x_a^2. \tag{VIII.2.14}$$

Indeed the mixed terms cancel under the trace, while $\mathrm{tr}_{\mathbf{2}}\,\mathbf{1} = 2$. This coefficient is just what converts $-\mathrm{tr}_{\mathbf{2}}(D_\mu\mathsf{X})^\dagger D^\mu\mathsf{X}$ to the $-\frac{1}{2}\sum_a (D_\mu x_a)^2$ kinetic term in (VIII.2.10). The matrix is constrained by the pseudoreality condition inherited from four real coordinates; it is not an unconstrained complex bifundamental. For Hermitian connections,

$$D_\mu\mathsf{X} = \partial_\mu\mathsf{X} + iA_\mu\mathsf{X} - i\mathsf{X}\widehat{A}_\mu, \qquad \mathsf{X} \longmapsto g_+\mathsf{X}g_-^{-1}. \tag{VIII.2.15}$$

The fermions obey the analogous real representation condition. Thus there are eight *real* scalar bifundamentals X^I, not eight independent complex chiral multiplets. Figure VIII.2.2 shows the representation and the fixed levels.

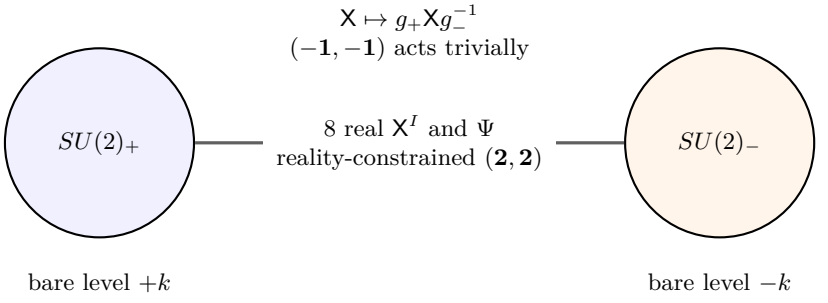


Figure VIII.2.2: The local A_4 BLG matter representation on the same (2+1)-dimensional worldvolume at both nodes. The nodes denote the declared simply connected $SU(2)_+ \times SU(2)_-$ group with unchanged rank two, positive k and bare fundamental-trace levels $(+k, -k)$. The unoriented link records the real bifundamental; it is not a directed chiral arrow. The diagonal central pair acts trivially on the displayed local fields, while the chosen compact group still controls global bundles and Wilson lines. There is no geometric displacement or axis.

The gauge split can be seen at quadratic order. Decompose the original antisymmetric connection into self-dual and anti-self-dual pieces in the fixed A_4 orientation:

$$A^{\mathrm{old}}_{\mu ab} = -\frac{A^+_{\mu ab} + A^-_{\mu ab}}{2q}, \qquad A^\pm_{\mu ab} = \pm\frac{1}{2}\epsilon_{abcd}A^\pm_{\mu cd}, \qquad A_\mu = A^+_{\mu 4i}\sigma_i, \quad \widehat{A}_\mu = A^-_{\mu 4i}\sigma_i. \tag{VIII.2.16}$$

Writing $a_i = A^+_{4i}$ and $b_i = A^-_{4i}$, the epsilon contraction in the twisted quadratic term gives

$$\frac{q}{2}\epsilon_{abcd}A^{\rm old}_{ab}\wedge dA^{\rm old}_{cd} = \frac{1}{q}\big(a_i\wedge da_i - b_i\wedge db_i\big) = \frac{1}{2q}\,\mathrm{tr}_{\mathbf{2}}(A\wedge dA - \widehat{A}\wedge d\widehat{A}). \quad \text{(VIII.2.17)}$$

The opposite signs follow from the two Hodge eigenvalues, while $\mathrm{tr}_{\mathbf{2}}(\sigma_i\sigma_j) = 2\delta_{ij}$ fixes the factor of two. The full bifundamental rewrite gives the corresponding cubic reduction and complete coefficient $[\mathrm{CS}_2(A) - \mathrm{CS}_2(\widehat{A})]/(2q)$. Equating it to $k/(4\pi)$ in (VIII.2.11) fixes

$$\frac{1}{2q} = \frac{k}{4\pi}, \qquad q = \frac{2\pi}{k}. \quad \text{(VIII.2.18)}$$

This relation uses the orientation of (VIII.2.4) and the first-node sign in (VIII.2.11). The seemingly different $\lambda = \pi/k_{\rm BL}$ in the original vector-trace presentation uses a vector trace $\mathrm{Tr}_{\mathbf{4}} = 2\,\mathrm{tr}_{\mathbf{2}}$ on each simple factor. In that presentation $k = 2k_{\rm BL}$ when k denotes the bare fundamental level here. The trace conversion does not ban odd fundamental levels or settle quantization for every quotient group. In particular, the two numerical coupling statements compare different normalizations of the same local factor:

$$\mathrm{Tr}_{\mathbf{4}}\big|_{\mathfrak{su}(2)_\pm} = 2\,\mathrm{tr}_{\mathbf{2}}, \qquad q = \frac{2\pi}{k}, \quad \lambda = \frac{\pi}{k_{\rm BL}}, \quad k = 2k_{\rm BL}. \quad \text{(VIII.2.19)}$$

Reading q and λ as directly comparable numbers without the two trace factors would create a false factor-of-two discrepancy. The self-dual split fixes local coefficients; it does not choose whether the compact group is a simply connected product or a quotient. Reflecting one worldvolume coordinate reverses each Chern–Simons term; exchanging the two nodes at the same time restores their sum. The matter transformation includes $\mathsf{X}\leftrightarrow\mathsf{X}^\dagger$.

The Lie algebra found above permits distinct compact groups. For the worked action we declare $G_{\rm sc} = SU(2)_+\times SU(2)_-$, with the bare levels in (VIII.2.11). Its diagonal central $\mathbb{Z}_2$ acts trivially on X and Ψ, so their *local* action factors through $G_{\rm diag} = (SU(2)_+\times SU(2)_-)/\mathbb{Z}_2^{\rm diag} \simeq SO(4)$. This fact alone does not identify the two quantum gauge theories. A choice of compact group also chooses which bundles and magnetic cocharacters may occur and which Wilson representations are genuine.

For a precise contrast, write a Cartan magnetic cocharacter in each factor as $H_\pm = \mathrm{diag}(h_\pm, -h_\pm)$. In the simply connected product, a loop closes only when

$$(h_+, h_-)\in\mathbb{Z}^2. \quad \text{(VIII.2.20)}$$

For the diagonal quotient it may close up to the common central pair, giving

$$(h_+, h_-)\in\mathbb{Z}^2 \;\cup\; \big(\mathbb{Z}+\tfrac{1}{2}\big)^2, \qquad h_+ - h_-\in\mathbb{Z}. \quad \text{(VIII.2.21)}$$

The flux $(\frac{1}{2},\frac{1}{2})$ is allowed only in the quotient, whereas a mixed half-integer/integer pair closes in neither group. Conversely a Wilson line in $(\mathbf{2},\mathbf{1})$ is a representation of the simply connected product but does not descend through the diagonal quotient. The real bifundamental is insensitive to precisely this difference in local transformations.

The construction below uses the full $U(N)_k \times U(N)_{-k}$ ABJM group. It has a different flux lattice again. A cocharacter of one full $U(N)$ factor has integer eigenvalues m_i, with trace flux $\sum_i m_i$ and central flux $(\sum_i m_i)/N$ for its charge-one central connection. At $N = 2$, the primitive $(1, 0)$ cocharacter has trace flux one and central flux one half, correlated with an $SU(2)$ center twist. Replacing it by a pure central cocharacter would erase this sector. These are global-group statements, not a new local interaction term.

The difference has a concrete consequence even before an operator spectrum is attempted. In one specified finite-gauge quotient route that compares a special-unitary description with the full product, a residual element $l \in \mathbb{Z}_k$ must come from a solution of

$$N l_B \equiv l \pmod{k}. \tag{VIII.2.22}$$

Multiplication by N reaches every class precisely when $\gcd(N, k) = 1$. For $N = k = 2$ its image contains only the zero class, so $l = 1$ has no preimage. This is an obstruction to that particular quotient route, not a theorem that every theory with these local Lie algebras is inequivalent. It also shows why one must specify the compact group before comparing two proposed descriptions at rank two.

The two proposed rank-two comparisons use distinct global inputs. The level-one proposal pairs full $U(2)_1 \times U(2)_{-1}$ ABJM with the diagonal-$\mathbb{Z}_2$ quotient of level-one BLG. The level-two proposal pairs full $U(2)_2 \times U(2)_{-2}$ ABJM with the simply connected $SU(2)_2 \times SU(2)_{-2}$ BLG group. These proposals are quantum identifications under study, not results of the local trace conversion above. The reported index and partition-function comparisons, together with their qualifications, are treated in Chapter 3. Here their role is to show that a common local $\mathfrak{su}(2) \oplus \mathfrak{su}(2)$ algebra cannot choose the bundle and line sectors of an arbitrary-rank theory.

The contrast with full $U(N)$ ABJM is the reason to seek an independent arbitrary-rank construction. The detailed rank-two comparison, its protected quantities and magnetic operators are left to Chapter 3.

VIII.2.3 A circular brane route to arbitrary rank

How can two gauge nodes of arbitrary common rank arise without enlarging the four-dimensional A_4 matter space? A circular Hanany–Witten suspension provides two intervals carrying the same N D3-branes and opposite level signs.

Let x^6 parametrize a circle of circumference $2\pi R_6$. Suspend N D3-branes along 0126 between an NS5-brane along 012345 and a second fivebrane carrying book-order $(D, NS) = (k, 1)$ charge. The two complementary arcs each carry the same rank N. In the source charge order (NS, D), the second brane is called $(1, k)$; changing the order of the two entries is a notation translation, not a duality operation. Figure VIII.2.3 shows the common starting objects and the orientations used below.

The suspension fixes the two node ranks before any low-energy field theory is proposed. The D3 worldvolume has the common directions 012, and each of the two arcs supplies one rank-N gauge sector. The fivebranes bound both arcs, so the interval count is two even though the x^6 direction is a single circle. In a compact notation the

starting configuration is

object	worldvolume or tangent directions	charge or rank
D3	0126	N on each arc
NS5	012345	$(D, NS) = (0, 1)$
rotated fivebrane	$012[3,7]_\theta[4,8]_\theta[5,9]_\theta$	$(D, NS) = (k, 1)$

(VIII.2.23)

The bracketed pairs mean equal rotations in the three indicated planes; they do not introduce six additional worldvolume directions. For the illustrated $N = 2$, $k = 3$ configuration, both arcs therefore carry rank two, while the second fivebrane has book charge $(3, 1)$ and source charge $(1, 3)$. The charge-entry swap preserves the same physical fivebrane.

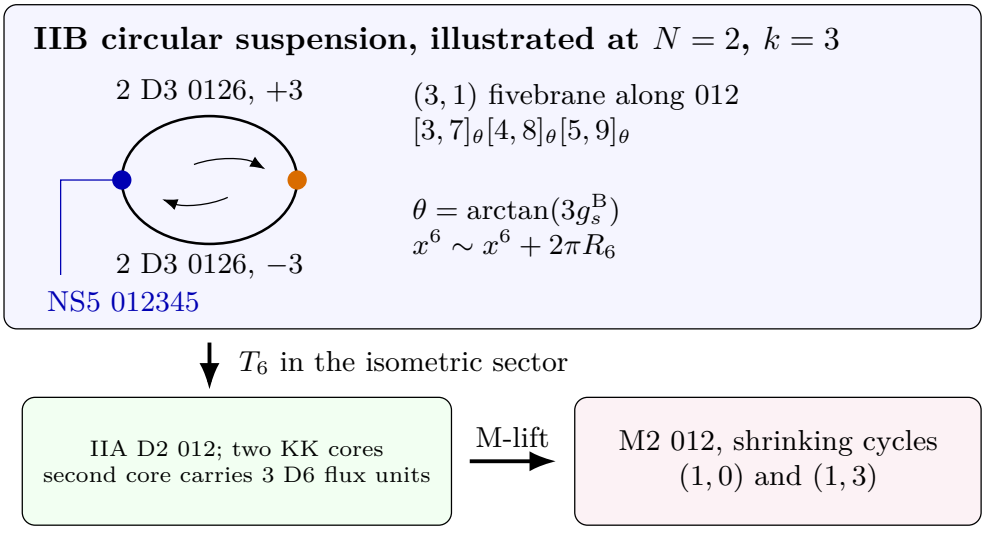


Figure VIII.2.3: At the illustrated $N = 2$, $k = 3$, the same D3-branes and fivebranes bound both oriented arcs of the compact x^6 circle. The second fivebrane makes equal angles in the 37, 48 and 59 planes. The displayed $+3, -3$ are bare interval levels. The arrows denote distinct conditional T_6 and M-lift steps, not an infrared proof. Equations in the text use general positive k.

The angle is a physical condition, not a convenient sketching choice. At $C_0 = 0$ and $0 < g_s^{\mathrm{B}} < \infty$, the equal rotation in the 37, 48 and 59 planes obeys

$$\tan\theta = k g_s^{\mathrm{B}}, \qquad 0 < \theta < \frac{\pi}{2}. \tag{VIII.2.24}$$

The suspended system then has six real supercharges in the ultraviolet. The charged fivebrane is obtained through a mass flow from a simpler web and assigns opposite bare levels to the two intervals. With the first arc oriented from NS5 to the rotated brane, the assignment is

$$(N_1, N_2) = (N, N), \qquad (k_1, k_2) = (+k, -k). \tag{VIII.2.25}$$

Reversing the arc orientation exchanges the entries. It does not make the two levels equal, and it does not change either rank. This sign data will reappear in the Chern–Simons action below. Neither the six-supercharge count nor that mass flow follows from a charge matrix. The count is specific to this zero-axion branch. For example, a special nonzero-axion locus at $k = 2$ has a different eight-supercharge asymptotic configuration, so the angle formula at arbitrary axion cannot be used to extend the present statement.

The angle is expressed using the complex IIB parameter $\tau_{\mathrm{B}} = C_0 + i/g_s^{\mathrm{B}}$. In the specified branch,

$$\theta = \arg \tau_{\mathrm{B}} - \arg(k + \tau_{\mathrm{B}}), \qquad C_0 = 0 \Longrightarrow \theta = \arctan(k g_s^{\mathrm{B}}). \tag{VIII.2.26}$$

For positive k and finite positive coupling this is strictly between zero and $\pi/2$, as drawn. The restriction on C_0 matters because changing the axion changes the asymptotic charge geometry and which supercharge statement applies. The special $k = 2$ case occurs at $\tau_{\mathrm{B}} = -1 + i$ and is not a limit of the generic zero-axion row. We keep the two cases separate.

The charged fivebrane is obtained through a mass deformation of a simpler web and then studies the equal-angle suspension. The preliminary web and the final circle setup are different configurations. The web argument supplies the proposed levels and flow, while the final orientation supplies the stated ultraviolet six-supercharge configuration. A drawing of final charges and tangents alone cannot reproduce the massive-mode integration or the worldvolume supersymmetry projectors.

Each interval has its own length L_i and coupling. In the conventions of this brane construction, $g_{3,i}^2 = 4\pi g_s^{\mathrm{B}}/L_i$. The proposed low-energy route requires energies below both interval Kaluza–Klein scales and the vector topological masses $|k| g_{3,i}^2/(4\pi)$. Its flow to the $\mathcal{N} = 6$ Chern–Simons matter theory is a dynamical premise. The six real ultraviolet charges and twelve real charges of that infrared candidate describe different regimes; we do not infer the latter from the brane orientations.

The two interval lengths need not be equal. Keeping them separate makes the condition on the proposed infrared description explicit:

$$g_{3,i}^2 = \frac{4\pi g_s^{\mathrm{B}}}{L_i}, \qquad m_{\mathrm{CS},i} = \frac{k g_{3,i}^2}{4\pi} = \frac{k g_s^{\mathrm{B}}}{L_i}, \qquad E \ll \min_{i=1,2}\{L_i^{-1}, m_{\mathrm{CS},i}\}. \tag{VIII.2.27}$$

The hierarchy says which interval modes are omitted in the candidate description. It does not derive the infrared supercharges from a mass formula. The ultraviolet six-charge statement is tied to the specified equal-angle branch; its proposed enhancement in the infrared is a separate property of the proposed field-theory flow.

Because the two arcs cover one circle, their lengths satisfy

$$L_1 + L_2 = 2\pi R_6, \qquad \frac{g_{3,1}^2}{g_{3,2}^2} = \frac{L_2}{L_1}, \qquad \frac{m_{\mathrm{CS},1}}{m_{\mathrm{CS},2}} = \frac{L_2}{L_1}. \tag{VIII.2.28}$$

This is a useful check on what the two-node description remembers. At equal arc lengths the couplings and topological masses coincide, while the two Chern–Simons levels remain opposite in sign. If one fivebrane is moved along x^6, the interval scales vary inversely with their lengths. The integers N and k do not vary with that motion.

A continuous change of interval lengths therefore cannot be used as a substitute for changing a compact charge or a bare level. The field theory is proposed in a regime below the smaller of the four thresholds L_i^{-1} and $m_{\mathrm{CS},i}$; a statement made at one choice of lengths need not describe energies above a threshold after the branes move.

The equal-angle condition and this energy condition have different logical roles. The angle specifies the ultraviolet fivebrane arrangement with the stated six supercharges. The energy inequality chooses a regime in which the interval vector multiplets and nonzero Kaluza–Klein modes are treated as massive. For the illustrated charge $k = 3$, the equal rotation is

$$\theta = \arctan(3g_s^{\mathrm{B}}), \qquad m_{\mathrm{CS},1} = \frac{3g_s^{\mathrm{B}}}{L_1}, \quad m_{\mathrm{CS},2} = \frac{3g_s^{\mathrm{B}}}{L_2}. \tag{VIII.2.29}$$

The example checks the dependence on the source charge k and the two separate interval lengths. The configuration drawing fixes orientations and integer data, while these scales enter the low-energy approximation. Neither input alone calculates the proposed infrared fixed point.

To compare the suspended D3 system with a transverse membrane geometry, T-dualize along the compact x^6 in an isometric, zero-mode description. The D3 becomes a D2 along 012, the NS5 becomes a KK degeneration of the dual circle, and the charged fivebrane becomes KK geometry with k D6 flux units. It is not a collection of k freely separated D6-branes. The directions and conserved data along the proposed route may be read as

frame	probe	fivebrane or core data
IIB on S^1_6	N D3 along 0126	$(0,1),(k,1)$ in book order
T_6 image	N D2 along 012	KK core, k D6 flux units
M lift	N M2 along 012	$(1,0),(1,k)$ shrinking torus cycles

(VIII.2.30)

The rank N belongs to the probe in each row. The integer k instead appears in the second core's flux and torus cycle. Treating k as a number of independently movable D6-branes would change the configuration. The dual radius and coupling are

$$\widetilde{R}_6 = \frac{\alpha'}{R_6}, \qquad g_s^{\mathrm{A}} = g_s^{\mathrm{B}}\frac{\sqrt{\alpha'}}{R_6}, \qquad R_{10} = g_s^{\mathrm{A}}\sqrt{\alpha'}. \tag{VIII.2.31}$$

Substituting the IIA coupling into the lift radius makes the common circle dependence visible:

$$R_{10} = \frac{g_s^{\mathrm{B}}\alpha'}{R_6}, \qquad \frac{R_{10}}{\widetilde{R}_6} = g_s^{\mathrm{B}}. \tag{VIII.2.32}$$

This ratio is a relation between the two circle radii in the stated duality regime. It does not say that their angles or shrinking cycles are interchangeable. In the next section both angular periods remain 2π, while the fivebrane charge chooses different primitive cycles. For example, decreasing the original radius at fixed α' raises both $\widetilde{R}_6$ and R_{10} by the same factor in these formulas; their ratio remains g_s^{B}. That simple consistency check helps separate a radius change from the finite identification caused by k. The latter comes from which cycles degenerate, not from simply dividing either circle radius

by k. Both shrinking cycles are primitive, since their integer components have greatest common divisor one:

$$v_{\mathrm{NS}} = (1,0), \qquad v_{(k,1)} = (1,k), \qquad \gcd(1,0) = \gcd(1,k) = 1. \tag{VIII.2.33}$$

Primitivity says each isolated core is locally a unit-cycle degeneration. Their joint period lattice can nevertheless have a nontrivial index, which we compute next. This is the precise sense in which the second core carries k units in the compact construction without splitting into k separate cores. Together these relations describe the IIA-to-M lift in which the D2 becomes an M2. The duality and lift links are physical inputs in this restricted regime. In particular, this chain alone does not prove an exact localized transverse T-duality or equality of full quantum theories.

VIII.2.4 The torus period becomes a complex quotient

Which representation of the finite torus-period group acts on the M2's transverse coordinates? The shrinking cycles determine its order, while the local metric determines the four complex phases.

The M-theory torus has angles $\phi = (\phi_1, \phi_2)^T = (\widetilde{x}^6/\widetilde{R}_6, x^{10}/R_{10})^T$, each with period 2π. In our book charge order, a (p_D, q_{NS}) fivebrane makes the cycle (q_{NS}, p_D) shrink. The two primitive cycles are therefore the columns of

$$v_1 = \begin{pmatrix} 1 \\ 0 \end{pmatrix}, \qquad v_2 = \begin{pmatrix} 1 \\ k \end{pmatrix}, \qquad L = (v_1\ v_2) = \begin{pmatrix} 1 & 1 \\ 0 & k \end{pmatrix}, \qquad \mathbb{Z}^2/L\mathbb{Z}^2 \simeq \mathbb{Z}_k. \tag{VIII.2.34}$$

Subtracting the first column from the second gives Smith diagonal $(1, k)$, and $|\det L| = k$. The quotient is trivial at $k = 1$. This integer calculation gives the order of an extra torus identification; it leaves open whether the generator rotates all four complex coordinates, only two, or some other combination. At $k = 0$ the matrix loses rank and there is no finite group of this form.

For the fixed $k = 3$ drawing, the second cycle winds once around the first angular direction and three times around the second. An integral column subtraction and a row ordering give

$$L_3 = \begin{pmatrix} 1 & 1 \\ 0 & 3 \end{pmatrix} \longrightarrow \begin{pmatrix} 1 & 0 \\ 0 & 3 \end{pmatrix}, \qquad \mathbb{Z}^2/L_3\mathbb{Z}^2 \simeq \mathbb{Z}_3. \tag{VIII.2.35}$$

The row and column operations are integral, so they preserve the period lattice. This step answers how many distinct identifications remain. It does not tell a scalar which phase to acquire. A determinant-three action that fixes two complex directions would have the same abstract group but a different fixed locus and a different transverse cone.

The cycle matrix describes degenerating torus fibers. The M2's transverse scalars instead use Cartesian coordinates on the local eight-real-dimensional space near the joint core. To compare the two, one must transport a primitive angular period through the local metric into those Cartesian coordinates. This requires the local two-core geometry and its period choice. The index alone leaves the representation of $\mathbb{Z}_k$ undetermined.

The local two-core Gibbons–Hawking metric supplies the missing action. Let $\vec{x}_1, \vec{x}_2$ be three-vector base coordinates and put $h_1 = 1/(2|\vec{x}_1|)$ and $h_2 = 1/(2|\vec{x}_1 + k\vec{x}_2|)$. At the common core we omit the asymptotic constant in the harmonic matrix. With $B = L^T$, the metric data diagonalize as

$$\begin{gathered} U = h_1 v_1 v_1^T + h_2 v_2 v_2^T, \qquad B = \begin{pmatrix} 1 & 0 \\ 1 & k \end{pmatrix}, \\ \vec{x}' = B\vec{x}, \qquad \phi' = B^{-T}\phi, \\ U' = B^{-T} U B^{-1} = \operatorname{diag}(h_1, h_2). \end{gathered} \tag{VIII.2.36}$$

Here $\vec{x}$ denotes the column of two three-vectors; the matrix acts only on the two-center label. The angle transformation is contragredient so that the base and fiber pairing is preserved. It is a local diagonalization, not an integral change of torus basis. In fact, the old second period becomes

$$\phi_1' = \phi_1 - \frac{\phi_2}{k}, \qquad \phi_2' = \frac{\phi_2}{k}, \qquad \vec{x}_1' = \vec{x}_1, \quad \vec{x}_2' = \vec{x}_1 + k\vec{x}_2. \tag{VIII.2.37}$$

This is why each h_a depends on only one primed base vector. The fractional coefficients in the angle map simultaneously show why the new angles cannot each be declared an independent period-2π circle. Doing that would erase the finite group found in the primitive lattice. The base-fiber pairing explains the contragredient transformation:

$$(\phi')^T d\vec{x}' = (B^{-T}\phi)^T B\, d\vec{x} = \phi^T d\vec{x}. \tag{VIII.2.38}$$

This is shorthand for the same two-label contraction in each of the three base-space components. It explains why B acts on the two base vectors while its inverse transpose acts on the angles. Applying B to both would lose the stated pairing and misread the periods. The actual image of the old second period is

$$(\phi_1, \phi_2) \longmapsto (\phi_1, \phi_2 + 2\pi) \quad \Longrightarrow \quad (\phi_1', \phi_2') \longmapsto (\phi_1' - 2\pi/k, \phi_2' + 2\pi/k). \tag{VIII.2.39}$$

The fractional shifts retain precisely the group found in (VIII.2.34). Their effect on Cartesian coordinates still requires one more step.

At $k = 3$, one turn of the original second circle shifts the primed angles by $(-2\pi/3, +2\pi/3)$. Three turns return both primed angles by integer 2π periods. The local order-three action is therefore represented by

$$(\Delta\phi_1', \Delta\phi_2') = \frac{2\pi}{3}(-1, +1), \qquad 3(\Delta\phi_1', \Delta\phi_2') = 2\pi(-1, +1). \tag{VIII.2.40}$$

The second equality checks the order without assuming a complex representation. To obtain that representation we need the unit-core metric, whose circle fiber is the primed angle itself.

The diagonal harmonic function of either factor is $h = 1/(2r)$, so the base radius r is not the flat radial distance. Setting $\rho = \sqrt{2r}$ gives the useful intermediate check

$$h\, dr^2 = \frac{dr^2}{2r} = d\rho^2, \qquad r = \frac{\rho^2}{2}. \tag{VIII.2.41}$$

The angular terms then carry the coefficient $\rho^2/4$ of the unit Hopf metric. This is why a period-2π shift of ϕ' is a full turn on the local complex pair. A different fiber period would change the local identification and the finite action.

For either diagonal unit-charge factor, write $r = |\vec{x}'|$, $\rho = \sqrt{2r}$, and use polar base angles (ϑ, ψ). With connection $\frac{1}{2}\cos\vartheta\, d\psi$, its near-core metric is

$$\begin{aligned} ds^2 &= d\rho^2 + \frac{\rho^2}{4}\left[d\vartheta^2 + \sin^2\vartheta\, d\psi^2 + (2d\phi' + \cos\vartheta\, d\psi)^2\right], \\ u &= \rho\cos\frac{\vartheta}{2}e^{i(\phi'+\psi/2)}, \qquad v = \rho\sin\frac{\vartheta}{2}e^{i(\phi'-\psi/2)}, \qquad ds^2 = |du|^2 + |dv|^2. \end{aligned} \tag{VIII.2.42}$$

Differentiating the two displayed complex coordinates gives the metric on the first line. In particular, a fiber shift $\phi' \mapsto \phi' + \delta$ multiplies both u and v by $e^{i\delta}$. Thus the geometric phase is fixed by the same coordinate that appears in the fiber one-form. One can verify the metric identity in an intermediate form before collecting the square:

$$|du|^2 + |dv|^2 = d\rho^2 + \frac{\rho^2}{4}d\vartheta^2 + \rho^2\left(d\phi'^2 + \cos\vartheta\, d\phi' d\psi + \frac{1}{4}d\psi^2\right). \tag{VIII.2.43}$$

The cross term follows from the opposite $\psi/2$ phases of u and v, weighted by $\cos^2(\vartheta/2)$ and $\sin^2(\vartheta/2)$. Their difference is $\cos\vartheta$. Collecting the last three terms reproduces the fiber square in (VIII.2.42). In this local chart both Cartesian coordinates carry exactly one unit of the ϕ' phase. The result comes from the metric, not from a choice of four phase weights made after computing $\det L$. Thus (VIII.2.39) acts on (u_1, v_1, u_2, v_2) with phase weights $(-1, -1, +1, +1)$ modulo k. Keeping the two doublets together displays the missing information from the lattice index:

$$(u_1, v_1, u_2, v_2) \longmapsto (\omega^{-1}u_1, \omega^{-1}v_1, \omega u_2, \omega v_2), \qquad \omega = e^{2\pi i/k}. \tag{VIII.2.44}$$

At $k = 3$ the first doublet rotates in the opposite complex sense from the second. This is one real eight-dimensional rotation, expressed in a particular complex chart. Its fixed set for nontrivial $k = 2$ inversion is only the origin, unlike an inversion of just two complex coordinates, which would fix a complex two-plane. The distinction is already visible at the level of local geometry. Choose the conjugated complex chart

$$z = (\bar{u}_1, \bar{v}_1, u_2, v_2), \qquad z^I \longmapsto \omega z^I \quad (I = 1, 2, 3, 4), \qquad \omega = e^{2\pi i/k}. \tag{VIII.2.45}$$

Conjugation changes the displayed complex structure of the first real four-plane but leaves its real metric and isometry intact. Equation (VIII.2.45), rather than the determinant of L, identifies the local $\mathbb{C}^4/\mathbb{Z}_k$ representation relevant to the membrane coordinates. The construction specifies a compatible local complex chart; it has not selected a worldvolume Lagrangian. The conjugation can be checked without an appeal to the name of the cone. The first doublet carries ω^{-1}, so its conjugate carries ω; the second doublet already carries ω:

$$(\bar{u}_1, \bar{v}_1, u_2, v_2) \longmapsto (\omega\bar{u}_1, \omega\bar{v}_1, \omega u_2, \omega v_2). \tag{VIII.2.46}$$

This is a change of complex description of the same real action. It adds no transverse directions and gives no supersymmetry proof. The scalar chart in the field theory below will have the same conjugated slots, allowing a comparison of the actual transformations.

The common phase can also be read directly as an eight-real-coordinate rotation. For each $z^I = x^I + iy^I$, with $\alpha = 2\pi/k$, the generator acts by

$$\begin{pmatrix} x^I \\ y^I \end{pmatrix} \longmapsto \begin{pmatrix} \cos\alpha & -\sin\alpha \\ \sin\alpha & \cos\alpha \end{pmatrix} \begin{pmatrix} x^I \\ y^I \end{pmatrix}, \qquad I = 1, 2, 3, 4. \tag{VIII.2.47}$$

At $k = 2$ each block is $-I_2$; at $k = 3$ each is a 120-degree rotation. Thus the four complex slots describe one simultaneous rotation on eight real displacements. This makes explicit why the conjugation of the first local doublet changes the complex weights but not the underlying real metric. It also supplies a direct comparison with the C scalar chart of the quiver, whose last two entries are conjugated in the same way. Figure VIII.2.4 records the lattice and the induced phase for the same $N = 2$, $k = 3$ example used in the brane and quiver figures.

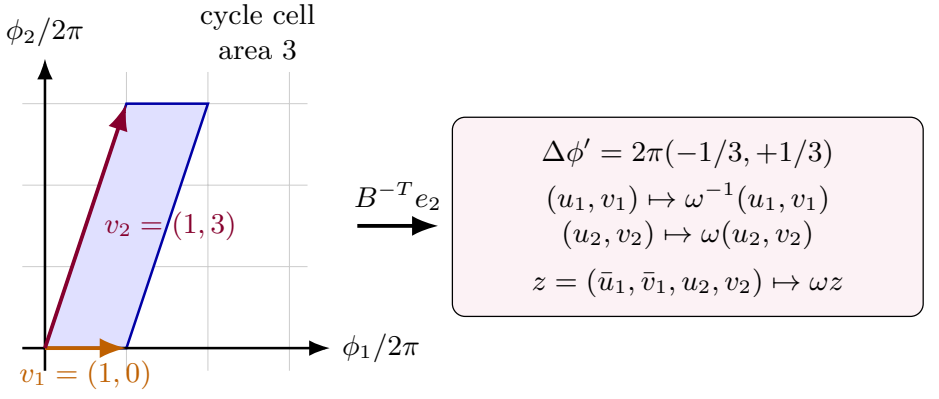


Figure VIII.2.4: For $k = 3$, the two primitive shrinking cycles span an index-three sublattice of the period lattice. The arrow acts on the old primitive second angle period $e_2 = (0, 1)$, not on the shrinking cycle $v_2 = (1, 3)$. The right panel uses its fractional transformed period and the Cartesian Hopf phases. Conjugating the first doublet produces the uniform generator. The lattice area alone does not determine that representation. The rank $N = 2$ labels the same illustrated brane and quiver configuration but does not enter this local transverse lattice calculation.

The first small orders make this distinction concrete. For $k = 1$ the period is ordinary and the local target is $\mathbb{C}^4$. At $k = 2$ the generator sends every z^I to $-z^I$, with only the origin fixed. A different order-two action, $(-z^1, -z^2, +z^3, +z^4)$, would instead have a two-complex-dimensional fixed locus. At $k = 3$ the old second angle period shifts the two local fibers by $(-2\pi/3, +2\pi/3)$, and conjugating the first doublet yields $z^I \mapsto e^{2\pi i/3} z^I$ for all I. The index three did not supply these phase assignments.

In equations, the fixed-point comparison at $k = 2$ is

$$\mathrm{Fix}(-1,-1,-1,-1) = \{0\}, \qquad \mathrm{Fix}(-1,-1,+1,+1) = \{z^1 = z^2 = 0\} \simeq \mathbb{C}^2. \tag{VIII.2.48}$$

Both transformations have abstract order two. Only the first is the action derived for the specified near-core metric and conjugated chart. The distinction matters because an M2 probe can move along the fixed two-plane in the second hypothetical geometry, whereas in the first only the tip is fixed. This example is a local geometric comparison; it says nothing by itself about the worldvolume interaction or protected operator spectrum.

VIII.2.5 The ABJM fields and quartic interaction

Now begin with a field theory rather than the cone. Take the full compact $U(N)_k \times U(N)_{-k}$ product. Two $\mathcal{N} = 2$ chiral multiplets A_a, $a = 1, 2$, transform as $(\mathbf{N}, \overline{\mathbf{N}})$; two B_a transform as $(\overline{\mathbf{N}}, \mathbf{N})$. The arrows and levels in Figure VIII.2.5 specify which ordered matrix products can be traced. By the book arrow rule, A_a points from node 1 to node 2 and is an $N_1 \times N_2$ matrix. As a linear map it is $A_a : V_2 \to V_1$; $B_a : V_1 \to V_2$ goes the other way. Thus the drawn arrows reverse the direction of maps in the mathematical quiver-representation convention. The chiral scalar list is $Z = (A_1, A_2, B_1, B_2)$. A different scalar chart, $C = (A_1, A_2, B_1^\dagger, B_2^\dagger)$, will display the geometric $SU(4)$ action. Its last two entries are conjugated scalar components, not extra chiral multiplets.

The field content can be read without guessing which matrix products exist. Node one acts on $V_1 \simeq \mathbb{C}^N$ and node two on $V_2 \simeq \mathbb{C}^N$. We use the following $\mathcal{N} = 2$ chart:

multiplet	$U(N)_1 \times U(N)_2$	matrix map	$U(1)_{\mathrm{rel}}$ charge
A_1, A_2	$(\mathbf{N}, \overline{\mathbf{N}})$	$V_2 \to V_1$	$+1$
B_1, B_2	$(\overline{\mathbf{N}}, \mathbf{N})$	$V_1 \to V_2$	-1
Φ_1	$(\mathrm{adj}, \mathbf{1})$	$V_1 \to V_1$	0
Φ_2	$(\mathbf{1}, \mathrm{adj})$	$V_2 \to V_2$	0

(VIII.2.49)

The Φ_i are auxiliary adjoint chirals in the auxiliary-field derivation of the quartic interaction. Eliminating them leaves the four displayed matter chirals. The charge column refers to the relative connection defined in the next section; it will make the abelian quotient immediate. Write $\mathrm{CS}_N(A) = \mathrm{Tr}_{\mathbf{N}}(A \wedge dA + \frac{2i}{3} A \wedge A \wedge A)$, the Hermitian form already used for $SU(2)$. The full compact product and its fundamental traces set the bare action

$$S_{\mathrm{CS}}^{\mathrm{ABJM}} = \frac{k}{4\pi} \int \big[\mathrm{CS}_N(A) - \mathrm{CS}_N(\widehat{A})\big], \qquad k \in \mathbb{Z}_{>0}. \tag{VIII.2.50}$$

Here the two $U(N)$ connections are independent compact fields. Writing only their common or relative Lie-algebra combinations at this point would hide the primitive flux lattice needed for the vacuum quotient.

The arrow convention and the matrix-map convention can be checked by applying a gauge transformation. For $g_i \in U(N)_i$,

$$A_a \longmapsto g_1 A_a g_2^{-1}, \qquad B_a \longmapsto g_2 B_a g_1^{-1}, \qquad M_1 \longmapsto g_1 M_1 g_1^{-1}, \quad M_2 \longmapsto g_2 M_2 g_2^{-1}. \tag{VIII.2.51}$$

This verifies that M_1 and M_2 are adjoints at their respective nodes and explains the placement of $\Phi_1 M_1$ and $\Phi_2 M_2$ in the superpotential. It also shows that a trace must follow a closed alternating word. The charge column in the field table is the abelian specialization of this transformation. Keeping both views matters because a word can have net zero abelian charge yet still fail as a well-typed nonabelian matrix product.

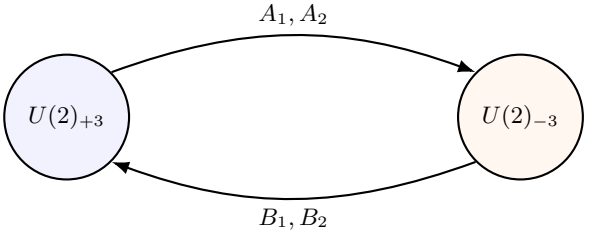
The matter kinetic terms make the same node assignment operational. With Hermitian connections and $D = d + iA$, the bifundamentals have

$$D_\mu A_a = \partial_\mu A_a + iA_\mu A_a - iA_a \widehat{A}_\mu, \qquad D_\mu B_a = \partial_\mu B_a + i\widehat{A}_\mu B_a - iB_a A_\mu. \quad \text{(VIII.2.52)}$$

In the first formula the last A_a is the chiral field, whereas A_μ is the node-one connection. The opposite ordering in the second formula records the reverse representation. Together with the opposite bare Chern–Simons factors, these terms fix the gauge and matter part of the $\mathcal{N} = 2$ action. Its scalar kinetic term is the sum of the corresponding positive Hermitian norms with the Lorentzian sign,

$$\mathcal{L}_{\text{scalar}} = -\sum_{a=1}^{2} \operatorname{Tr}\big[(D_\mu A_a)^\dagger D^\mu A_a + (D_\mu B_a)^\dagger D^\mu B_a\big] - V. \qquad \text{(VIII.2.53)}$$

The potential V is determined by the auxiliary-field elimination. We only need its abelian vacuum cancellation below; an explicit general matrix potential is not required for that quotient. The $\mathcal{N} = 2$ action includes the corresponding fermion terms, while the full infrared $\mathcal{N} = 6$ identification uses the proposed dynamical flow. The displayed bosonic terms by themselves are not a supersymmetry proof.



$$W = \frac{4\pi}{3} \operatorname{Tr}(A_1 B_1 A_2 B_2 - A_1 B_2 A_2 B_1)$$

Figure VIII.2.5: The same illustrated $N = 2$, $k = 3$ has two bifundamental chiral arrows in each direction and opposite bare levels. Every displayed quartic word follows a closed path from node one back to node one. The group is the full compact product; the equations in the text retain general N and positive k.

Why is the quartic interaction the one displayed? In the $\mathcal{N} = 2$ description, auxiliary adjoint chirals Φ_1, Φ_2 couple to the two moment-map words $M_1 = \sum_a A_a B_a$ and $M_2 = \sum_a B_a A_a$. Their superpotential is

$$W_{\text{aux}} = \frac{k}{8\pi} \operatorname{Tr}(\Phi_2^2 - \Phi_1^2) + \operatorname{Tr}(\Phi_1 M_1 + \Phi_2 M_2), \qquad \Phi_1 = \frac{4\pi}{k} M_1, \qquad \Phi_2 = -\frac{4\pi}{k} M_2. \qquad \text{(VIII.2.54)}$$

The stationary values follow by differentiating with respect to each adjoint. Substituting them back and using cyclicity of the trace yields

$$\frac{\partial W_{\rm aux}}{\partial \Phi_1} = -\frac{k}{4\pi}\Phi_1 + M_1 = 0, \qquad \frac{\partial W_{\rm aux}}{\partial \Phi_2} = \frac{k}{4\pi}\Phi_2 + M_2 = 0. \tag{VIII.2.55}$$

The opposite quadratic signs are essential. They make the stationary values opposite in sign and ultimately leave a difference of two cyclic matrix traces. Before rearranging any matrices, the substitution is

$$W_{\text{on shell}} = \frac{2\pi}{k}\left[\mathrm{Tr}_{V_1}(M_1^2) - \mathrm{Tr}_{V_2}(M_2^2)\right]. \tag{VIII.2.56}$$

Although the two traces act on different node spaces, a closed alternating product can be cyclically rotated between them. That is the allowed manipulation; swapping adjacent noncommuting fields is not.

$$\begin{aligned} W &= \frac{2\pi}{k}\,\mathrm{Tr}(M_1^2 - M_2^2) \\ &= \frac{4\pi}{k}\,\mathrm{Tr}(A_1B_1A_2B_2 - A_1B_2A_2B_1) \\ &= \frac{2\pi}{k}\epsilon^{ab}\epsilon^{cd}\,\mathrm{Tr}(A_aB_cA_bB_d). \end{aligned} \tag{VIII.2.57}$$

The equal-index terms in M_1^2 and M_2^2 cancel after a cyclic rotation. The two mixed orderings survive with opposite signs. This cyclic step is essential. Matrix multiplication itself cannot be commuted to make the surviving words disappear.

One can follow the cancellation term by term. At either node the words with both flavor indices equal have the same trace after a cyclic rotation. For the mixed terms, the node-two trace rotates into the opposite node-one ordering. Consequently

$$\begin{aligned} \mathrm{Tr}_{V_1}(M_1^2) - \mathrm{Tr}_{V_2}(M_2^2) = {}& 2\,\mathrm{Tr}_{V_1}(A_1B_1A_2B_2) \\ & - 2\,\mathrm{Tr}_{V_1}(A_1B_2A_2B_1). \end{aligned} \tag{VIII.2.58}$$

For example, $B_1A_2B_2A_1$ is a legitimate cycle traced at node two, and its cyclic rotation is $A_1B_1A_2B_2$ at node one. The alternating maps are what make both expressions well typed. An attempted word $A_1B_1A_2A_1$ fails the same typing test, before any F-term equation is considered.

The epsilon notation in (VIII.2.57) is compact, but its sign can be checked from the four flavor choices. With $\epsilon^{12} = +1$ there are two positive copies of the first trace cycle and two negative copies of the second. The two traces are independent for noncommuting matrices, as the matrix-unit example below demonstrates. For one-dimensional node spaces they collapse to the same number. This is the point where the interaction distinguishes the matrix theory from its abelian vacuum coordinates.

The invalid ordering supplies another diagnostic. Under the relative $U(1)$, it has charge

$$Q_{\rm rel}(A_1B_1A_2A_1) = 1 - 1 + 1 + 1 = 2, \qquad Q_{\rm rel}(A_1B_1A_2B_2) = 0. \tag{VIII.2.59}$$

The first word also ends with the wrong matrix map for a node-one trace. The second is a closed alternating path. Gauge invariance checks this distinction, while the relative minus sign in the actual superpotential comes from eliminating the adjoints.

For an explicit real 2×2 witness, let E_{ij} be matrix units and set

$$\begin{aligned} &A_1 = B_1 = E_{11}, \qquad A_2 = E_{12}, \qquad B_2 = E_{21}, \\ &\mathrm{Tr}(A_1 B_1 A_2 B_2) = 1, \qquad \mathrm{Tr}(A_1 B_2 A_2 B_1) = 0. \end{aligned} \tag{VIII.2.60}$$

The matrix-unit rule $E_{ij}E_{kl} = \delta_{jk}E_{il}$ lets the two answers be checked without a numerical matrix multiplication. The first closed word survives, while the second vanishes at its first two factors:

$$E_{11}E_{11}E_{12}E_{21} = E_{11}, \qquad E_{11}E_{21}E_{12}E_{11} = 0. \tag{VIII.2.61}$$

Their traces are therefore one and zero. The example is deliberately small but genuinely noncommutative. It proves that the two cyclic words cannot be identified by commuting fields inside the trace. At $N = 1$ the matrix-unit distinction disappears because every field is a complex number. That is why the same quartic expression becomes zero on the one-brane branch without making the nonabelian action trivial for $N > 1$. The two quartic words are gauge invariant because the arrows alternate and close. By comparison, $\mathrm{Tr}(A_1 B_1 A_2 A_1)$ does not form a closed node-one path and already has relative abelian charge $+2$. Gauge invariance alone would still allow a wrong plus sign between the two valid cycles; that mutation would remain nonzero for one brane and fail the vacuum comparison below.

At $N = 1$ all four scalar products commute, so

$$W_{N=1} = 0, \qquad \partial W_{N=1} = 0. \tag{VIII.2.62}$$

The abelian D-field and σ equations cancel the remaining scalar potential on the vacuum branch. Four complex scalar coordinates are therefore available before gauge identification. In this limit the same two traces in (VIII.2.56) become the same ordinary product, so their difference vanishes without imposing any relation among the four scalar values. This is a useful internal check on the relative sign. A gauge-invariant quartic with a plus sign between the two valid cycles would generally survive for one brane and could not reproduce this vacuum calculation. The vanishing of W is one step, however; the D- and σ-field cancellation and the compact gauge identification are still needed. Equation (VIII.2.62) alone would suggest an ordinary $\mathbb{C}^4$; the compact gauge fields make the answer different.

The comparison with BLG can now be made without conflating their matter spaces. BLG starts with eight real A_4-valued scalars and a reality-constrained matrix chart. The ABJM presentation starts with four independent $\mathcal{N} = 2$ complex chiral multiplets in two opposite bifundamental representations, for any declared positive integer N. Its C chart conjugates the last two scalar components only to display a common action on real transverse positions. It does not turn those components into new chiral multiplets. The local two-node Chern–Simons pattern is a useful bridge from BLG, while the full compact $U(N)$ groups, their flux sectors and the quartic interaction are fresh data in the arbitrary-rank construction.

This also explains the division of labor between the two routes. The brane and lift calculation fixes a candidate local cone and a physical path to M2 probes under stated duality conditions. The $\mathcal{N} = 2$ action fixes gauge transformations and interactions. They are compared first on a single abelian vacuum coordinate space, where the superpotential cancels. Higher-rank eigenvalues, singular configurations and monopole sectors require the later analysis of Chapter 3. Matching the number of scalar components at $N = 2$ would not replace a comparison of the compact groups or their allowed operators.

VIII.2.6 The compact abelian quotient and its scope

Why do four apparently free abelian scalars have a finite identification? The common compact gauge field retains a BF coupling that turns its integral flux sum into a periodic dual scalar.

Start at $N = 1$ with two independently compact connections a_1, a_2 and fluxes $(m_1, m_2) \in \mathbb{Z}^2$. The A scalars have relative charge $+1$ and the B scalars charge -1. A useful integral change of connection is

$$\begin{gathered} b = a_1 - a_2, \qquad c = a_2, \\ \begin{pmatrix} a_1 \\ a_2 \end{pmatrix} = \begin{pmatrix} 1 & 1 \\ 0 & 1 \end{pmatrix} \begin{pmatrix} b \\ c \end{pmatrix}, \qquad (m_b, m_c) = (m_1 - m_2, m_2) \in \mathbb{Z}^2. \end{gathered} \tag{VIII.2.63}$$

The matrix has determinant one, so this basis retains every compact bundle sector. Matter couples to b and is neutral under the common connection c. The latter remains in the action through the BF term. The determinant statement concerns the lattice, not merely linear algebra over $\mathbb{R}$. Its inverse map is integral:

$$\begin{pmatrix} m_1 \\ m_2 \end{pmatrix} = \begin{pmatrix} 1 & 1 \\ 0 & 1 \end{pmatrix} \begin{pmatrix} m_b \\ m_c \end{pmatrix}, \qquad \det \begin{pmatrix} 1 & 1 \\ 0 & 1 \end{pmatrix} = 1. \tag{VIII.2.64}$$

Every allowed integer flux pair in the new basis therefore comes from exactly one pair in the full compact product. This is the property needed when the dual scalar is introduced. A real change of variables with a different lattice index could reproduce the local differential form but change the flux sum and its residual finite group. To see its origin, retain the original two compact fields until after the change of basis. With one-form wedge products understood,

$$a_1 \wedge da_1 - a_2 \wedge da_2 = (b + c) \wedge d(b + c) - c \wedge dc \simeq b \wedge db + 2b \wedge dc. \tag{VIII.2.65}$$

The last equality is after integration by parts on a patch without a boundary contribution. The $c \wedge dc$ pieces cancel because the bare levels are opposite. This leaves c linearly coupled to the relative field, despite the absence of direct matter charge under c. Expanding the opposite levels, up to a boundary term, gives

$$S_{\mathrm{CS}} = \frac{k}{4\pi} \int (b \wedge db + 2b \wedge dc), \qquad K_{(b,c)} = \begin{pmatrix} k & k \\ k & 0 \end{pmatrix}. \tag{VIII.2.66}$$

Discarding c merely because no scalar carries its direct charge would discard the compact constraint that creates the finite quotient.

The widespread sum-and-difference pair is useful for local formulas but does not give two independent primitive fluxes. Indeed,

$$\begin{pmatrix} m_b \\ m_+ \end{pmatrix} = \begin{pmatrix} 1 & -1 \\ 1 & 1 \end{pmatrix} \begin{pmatrix} m_1 \\ m_2 \end{pmatrix}, \qquad m_+ = m_1 + m_2, \qquad m_b \equiv m_+ \pmod 2. \tag{VIII.2.67}$$

The determinant is two. A putative sum-and-difference flux $(1,0)$ would give $(m_1, m_2) = (1/2, -1/2)$ and is not in the original product theory. In the equal-flux sector $m_1 = m_2 = n$, the sum connection has flux $2n$ and its curvature periods are $4\pi\mathbb{Z}$. This is why its dual scalar normalization cannot be read as if it were a separate primitive $U(1)$.

The inverse flux map makes the parity restriction tangible:

$$m_1 = \frac{m_+ + m_b}{2}, \qquad m_2 = \frac{m_+ - m_b}{2}, \qquad (m_b, m_+) = (1,0) \Longrightarrow (m_1, m_2) = \left(\tfrac{1}{2}, -\tfrac{1}{2}\right). \tag{VIII.2.68}$$

It is therefore incorrect to integrate independently over every integer m_b and m_+. The primitive (b, c) basis avoids this mistake. For an equal-flux example $(m_1, m_2) = (n, n)$, one instead has $(m_b, m_+) = (0, 2n)$.

This doubled equal-flux period fixes the sum-connection multiplier if one chooses the nonprimitive sum-and-difference notation. On the equal-flux sector, the curvature $F_+ = d(a_1 + a_2)$ has periods in $4\pi\mathbb{Z}$. The primitive normalization used here translates to

$$S_{\tau,+} = \frac{1}{4\pi} \int \tau \, dF_+, \qquad S_{\tau,+} = \frac{1}{8\pi} \int d^3x \, \tau \epsilon^{\mu\nu\rho} \partial_\mu F_{+,\nu\rho} \quad \text{when } F_+ = \tfrac{1}{2} F_{+,\mu\nu} dx^\mu \wedge dx^\nu. \tag{VIII.2.69}$$

The factor of two between form and component coefficients follows from the displayed definition of F_+. It is easy to lose if the sum connection is treated as primitive. The form and component coefficients must be kept distinct under this fixed curvature convention. The primitive (b, c) derivation below avoids using the nonprimitive pair as two independent compact connections.

For the primitive pair, replace dc locally by an integral-period two-form f and impose its Bianchi identity with a scalar τ of period 2π. The terms needed to perform the dualization are

$$S_{\text{top}} = \frac{k}{4\pi} \int b \wedge db + \frac{k}{2\pi} \int b \wedge f + \frac{1}{2\pi} \int \tau \, df, \qquad kb = d\tau. \tag{VIII.2.70}$$

The final equation follows by integrating the multiplier term by parts and varying f. The period 2π is enforced by the sum over integral c-curvature sectors; it is not an optional local normalization. The variation can be displayed before gauge fixing:

$$S_f = \frac{1}{2\pi} \int (kb - d\tau) \wedge f, \qquad \frac{\delta S_f}{\delta f} = 0 \Longrightarrow kb = d\tau. \tag{VIII.2.71}$$

This local equation is compatible with a discrete leftover gauge transformation because τ is angular. It would be a different field-space problem if the multiplier took values on the real line without its compact period. The $b \wedge db$ term does not undo the period condition imposed by the integral c-flux sectors. For an arbitrary local value τ_0, a

relative gauge transformation with $\lambda_b = \tau_0/k$ sends it to zero. But the same angular value can be represented by $\tau_0 + 2\pi n$. These representatives give gauge-fixing parameters that differ by

$$\tau_0 \sim \tau_0 + 2\pi n \quad \Longrightarrow \quad \frac{\tau_0}{k} \sim \frac{\tau_0}{k} + \frac{2\pi n}{k}. \tag{VIII.2.72}$$

The ambiguity is a transformation of the charge-one matter field, not a new free scalar direction. It is precisely the finite phase that survives the gauge choice. For a noncompact multiplier there would be no identification $\tau_0 \sim \tau_0 + 2\pi n$, and hence no such residual transformation. This step is where the compact flux sum enters the vacuum geometry in an observable way. Under $b \mapsto b - d\lambda_b$, a charge-one C scalar transforms as $C \mapsto e^{i\lambda_b} C$, and the dual equation is preserved by $\tau \mapsto \tau - k\lambda_b$. Fix $\tau = 0$. Its residual transformations have $\lambda_b = 2\pi n/k$, so the local vacuum coordinates obey

$$b \longmapsto b - d\lambda_b, \qquad \tau \longmapsto \tau - k\lambda_b, \qquad C^I \longmapsto e^{i\lambda_b} C^I, \qquad \lambda_b\big|_{\tau=0} = \frac{2\pi n}{k}. \tag{VIII.2.73}$$

For generic nonzero C this is a finite orbit of order k. At the origin it collapses to a fixed point, producing the cone point for $k > 1$. The quotient therefore concerns a genuine compact-gauge identification, not an arbitrary notation for four free scalars. The first three values of k show the mechanism without a formal quotient symbol. At $k = 1$ the residual generator is the identity. At $k = 2$ it inverts all four complex coordinates. At $k = 3$ it is a simultaneous third-root rotation:

k	λ_b after $\tau = 0$	C^I orbit
1	$2\pi n$	C^I
2	πn	$\{C^I, -C^I\}$
3	$2\pi n/3$	$\{C^I, \omega C^I, \omega^2 C^I\}$

(VIII.2.74)

These are orbits of the full $U(1) \times U(1)$ action in the period-2π dual-scalar chart. If one instead takes $\tau \in \mathbb{R}$, fixing $\tau = 0$ leaves no nontrivial periodic shift and loses the second and third rows. This directly shows why the compact flux premise changes the vacuum answer.

$$C^I \sim \omega C^I, \qquad \mathcal{M}_{N=1}^{\text{local}} = \mathbb{C}^4/\mathbb{Z}_k. \tag{VIII.2.75}$$

Locally, $b = d\tau/k$ is exact after gauge fixing and the $b \wedge db$ term does not change this coordinate quotient. This reasoning neither identifies global flat sectors nor equates line operators and partition functions. If τ were treated as noncompact, gauge fixing it would leave no finite $\mathbb{Z}_k$ stabilizer and would incorrectly produce $\mathbb{C}^4$ at $k = 2$.

The two scalar charts make the same real action look different. Label the four ordered slots separately from the fields that occupy them. Under the residual generator,

slot	1	2	3	4
Z fields	A_1	A_2	B_1	B_2
Z phases	ω	ω	ω^{-1}	ω^{-1}
C fields	A_1	A_2	$B_1^\dagger$	$B_2^\dagger$
C phases	ω	ω	ω	ω

(VIII.2.76)

The last two C entries are $B_a^\dagger$. A neutral composite A_aB_b is invariant in the chiral chart. At $k=2$, inverse and direct phases coincide and all four coordinates invert. At $k=3$ they differ, so assigning a positive ω phase to the chiral B scalar would give the neutral composite a spurious phase ω^2. The uniform C action agrees with (VIII.2.45) after choosing the compatible geometric complex chart. A determinant-one test of the chiral weights does not replace this physical chart translation or a supersymmetry argument.

For $k=3$ the neutral product gives a short check of the opposite chiral weights:

$$A_aB_b \longmapsto (\omega A_a)(\omega^{-1}B_b) = A_aB_b, \qquad C^I \longmapsto \omega C^I. \tag{VIII.2.77}$$

At $k=2$ inverse and direct phases coincide, so that example alone would not detect an incorrect sign for the B charge. At $k=3$ it does. The real eight-dimensional rotation is the same in both charts; conjugating B changes the displayed complex weights.

For $N>1$, the group in the quiver remains the full compact $U(N)\times U(N)$, with $U(N)=[SU(N)\times U(1)]/\mathbb{Z}_N$ for each factor. Write a connection as $A=A_{\mathfrak{su}}+aI_N$. Since $\operatorname{Tr} I_N^2 = N$, the central quadratic term in a bare fundamental-trace level-k action has coefficient $Nk/(4\pi)$. This number must be read together with the cocharacter lattice. An integral diagonal magnetic cocharacter is $m=\operatorname{diag}(m_1,\dots,m_N)$ with all $m_i\in\mathbb{Z}$. Its trace flux is $\sum_i m_i$ while its central a-flux is $(\sum_i m_i)/N$. In particular,

$$m=\operatorname{diag}(1,0,\dots,0) \quad\Longrightarrow\quad \frac{1}{2\pi}\int \operatorname{Tr} F = 1, \qquad \frac{1}{2\pi}\int da = \frac{1}{N}. \tag{VIII.2.78}$$

For $N=2$, the primitive trace-one flux has central flux $1/2$. The pure central cocharacter $\operatorname{diag}(1,1)$ has central flux one and trace charge two. The cocharacter $\operatorname{diag}(2,0)=I_2+\operatorname{diag}(1,-1)$ also has central flux one and trace charge two, but carries an additional traceless magnetic component. Thus unit central flux alone does not determine the eigenvalue fluxes. The fractional central flux is correlated with an $SU(N)$ center twist; treating the two factors as independently quantized would change the theory.

The central coefficient and the primitive flux should be read together. In the fundamental trace normalization of the full group,

$$A=A_{\mathfrak{su}}+aI_N, \qquad \operatorname{Tr}(I_N^2)=N, \qquad \frac{k}{4\pi}\operatorname{Tr}(A\wedge dA) \supset \frac{Nk}{4\pi}a\wedge da. \tag{VIII.2.79}$$

For $N=2$, the flux $\operatorname{diag}(1,0)$ has central flux $1/2$, whereas $\operatorname{diag}(1,1)$ has central flux one. The coefficient $2k$ in the central term therefore cannot be read with an independently integer-quantized central flux. The full $U(2)$ cocharacter lattice correlates the fraction with the traceless part. The one-brane calculation above uses the declared full compact product; Chapter 3 must revisit global sectors at higher rank.

The geometric route gave an actual generator on four local complex coordinates in (VIII.2.45). The independent compact gauge calculation gave the same generator in (VIII.2.75). Their agreement is stronger than matching the abstract group $\mathbb{Z}_k$, because it also matches the action on all eight real transverse positions. It is narrower than an equality of quantum theories. The brane-flow argument that selects the infrared $\mathcal{N}=6$ action, the T-duality and lift, and the generic diagonal mass argument are physical

premises beyond the integer and matrix calculations. Local vacuum positions do not determine interactions, monopole spectra, currents or line sectors.

The computations can be placed side by side in compatible complex charts:

$$z = (\bar{u}_1, \bar{v}_1, u_2, v_2), \quad C = (A_1, A_2, B_1^\dagger, B_2^\dagger), \quad z^I \sim \omega z^I, \quad C^I \sim \omega C^I. \tag{VIII.2.80}$$

The first common-phase action is a local target-space result under the conditional geometric route. The second is a classical vacuum-coordinate result for the declared full compact product. The phase is the comparison; equality of positions alone neither derives the proposed infrared flow nor tests the operator algebra. The theory at arbitrary N is specified by the compact product and interaction above, not by extrapolating the one-brane quotient alone.

This distinction gives a practical reading rule for the following chapters. Chapter 1 supplies the leading M2 near-horizon geometry once a cone and charge are specified. Here we constructed that cone from the compact brane system and from one abelian vacuum branch of a proposed worldvolume theory. Chapter 3 will test the nonabelian and monopole physics, including low-rank comparisons with BLG. Chapter 11 will compare protected observables in regimes where they are defined. No geometric match in the present chapter substitutes for those tests.

VIII.2.7 Exercises

The first three problems study BLG; the following five develop the ABJM construction. Use the stated compact groups and orientations throughout.

BLG algebra and global form

E1. Build the A_4 inner-derivation algebra. For the oriented orthonormal real basis and nonzero symbolic q in (VIII.2.4), prove FI by differentiating volume-form invariance. Compute F_{1234} and F_{2134}, the full 4×4 column-image matrices D_{12} and D_{13}, their commutator $D_{12}D_{13} - D_{13}D_{12}$, and the rank of the span of all six D_{ab}. Explain in words why the result supplies a Lie algebra but does not choose a compact global group. The optional submitted part accepts exactly those two tensor components, three matrices and the rank; the general proof and global interpretation are reader work.

E2. Test a bracket that fails FI. In the positive-metric six-space of (VIII.2.8), take nonzero symbolic t and

$$(u, v, x, y, z) = (e_1, e_3, e_1, e_4, e_5).$$

Compute $F_{1234}, F_{1256}, F_{2156}$. Give the coordinate vectors of

$$[e_1, e_3, e_4], \qquad [e_1, e_2, e_5].$$

Then calculate the middle FI term $[e_1, [e_1, e_3, e_4], e_5]$, the FI left side and the left-minus-right residual. Explain which metric and antisymmetry properties survive the failure. The optional submitted part checks these three components and five six-vectors; the explanation remains reader work.

E3. Read the two-node dictionary. With positive integer k, fundamental $SU(2)$ traces and declared group $SU(2)_+ \times SU(2)_-$, derive the trace identity in (VIII.2.14) and the level relation in (VIII.2.18). Explain the reality condition on the eight scalar matrices and compare (VIII.2.20) with (VIII.2.21). State which extra global and operator information would be needed to compare this theory with full $U(2) \times U(2)$ ABJM. This is a written derivation with no submitted-answer route here.

For E1 and E2, provide both the named components and matrices and a written account of the general proof and its physical interpretation.

Compact construction and ABJM action

Each exercise uses the full compact product, $k > 0$, zero IIB axion and the declared charge order. Give the mathematical entries requested and explain the physical step in words. Include a written explanation alongside the mathematical entries.

E4. At $k = 3$, start with source-order (NS, D) fivebrane charges $(1, 0)$ and $(1, 3)$. Convert both to book order, find the ordered bare interval levels, and construct the primitive cycle matrix in the ordered torus-angle basis $(\phi_1, \phi_2) = (\widetilde{x}^6/\widetilde{R}_6, x^{10}/R_{10})$ defined at the opening of §VIII.2.4. Compute its Smith diagonal. Explain separately which physical assumptions enter T_6 and the M-lift, and why a lattice calculation does not give the ultraviolet supercharge count or the infrared flow.

E5. At $k = 3$, use the rows $(1, 0)$ and $(1, 3)$ for B. Find the shift of ϕ' caused by one old ϕ_2 period, the four phases on (u_1, v_1, u_2, v_2), and the four phases after the first doublet is conjugated. Derive the phase of u and v from (VIII.2.42). At $k = 2$, give the complex dimension of the fixed locus of the resulting action and compare it with a two-coordinate inversion.

E6. At $k = 3$, eliminate both adjoints from (VIII.2.54). Expand the two expressions in (VIII.2.57) into cyclic trace words and explain why cyclicity does not permit arbitrary reordering. Evaluate the two trace words for (VIII.2.60), then set $N = 1$. Finally decide whether $A_1B_1A_2A_1$ can be traced as a gauge-invariant node-one loop and compute its relative abelian charge.

E7. At $N = 1, k = 2$, compute the integer matrix taking (b, c) to (a_1, a_2), its determinant, and the resulting Chern–Simons matrix. Compute the determinant of the difference-and-sum flux map and invert its purported flux $(1, 0)$. Give the period and gauge shift of τ, then determine the residual matter action after $\tau = 0$. Explain what changes if τ is incorrectly made noncompact.

E8. At $N = 1, k = 3$, compare the residual weights in the geometric z chart, the scalar C chart, and the chiral Z chart. Check the charge of A_1B_1. At $N = 2$, use the cocharacter $\mathrm{diag}(1, 0)$ to compute trace flux, central flux and the central bare level divided by k. Explain why matching these local positions does not identify the full quantum theory.

Take-home message of this chapter

The fundamental identity makes the A_4 three-bracket a consistent source of local gauge transformations and two opposite $SU(2)$ Chern–Simons factors. The arbitrary-rank ABJM candidate has a separate compact brane and field-theory construction. Its one-brane compact quotient agrees with the local transverse $\mathbb{C}^4/\mathbb{Z}_k$ action after the scalar charts are matched. That position-space agreement is narrower than an identification of full quantum theories.

Status and sources

Sources by section. Source coordinates and scope qualifications follow.

§VIII.2.1. The bracket, fundamental identity and counterexample are conditional [MATH] for the stated metric algebras; the C04 classical action and supersymmetry are sourced to Bagger and Lambert 2008b, §§2–4.

§VIII.2.2. Old VIII3-C05 and The A_4 and two-factor coefficient rewrite is conditional [MATH] in the stated trace conventions; C06 fixes the global group, while on-shell closure remains a sourced physical premise, Van Raamsdonk 2008, §3.

§VIII.2.3. The IIB to M construction is conditional [DUAL] under the stated circle and lift hypotheses, with IR flow a sourced proposal; Aharony et al. 2008, §3.1.

§VIII.2.4. Torus-lattice and Cartesian phase algebra is conditional [MATH] under the sourced brane setup, Aharony et al. 2008, Appendix B.

§VIII.2.5. Auxiliary-adjoint elimination and the quartic action are conditional [MATH] under the sourced full-product action, Aharony et al. 2008, §2.2.

§VIII.2.6. The compact abelian quotient is conditional [MATH]; local vacuum-coordinate matching is [GEO-X] in the local position sector; generic separated-eigenvalue extension remains [CONJ+], Aharony et al. 2008, §§2.3–2.5.

§VIII.2.7. Exercises reuse the conditional [MATH] above. Inherited conventions: Chern–Simons trace and levels, the compact ABJM and membrane frame; Bagger and Lambert 2008b, §§2–4; Aharony et al. 2008, §§2.2–2.3, Appendix B. Explanations remain written work.

The BLG bracket, positive metric, fundamental identity and A_4 action use Bagger and Lambert 2008b, §§2–4 and Appendix A. The early ungauged three-product proposal is Bagger and Lambert 2007; on-shell closure of the classical action is source-supported, not a new gamma-matrix calculation. The real bifundamental and two-factor rewrite use Van Raamsdonk 2008, §3. Its fundamental-trace coefficient and the vector-trace convention in Bagger and Lambert 2008a, §3, are kept distinct. The global-form distinction uses Lambert and Papageorgakis 2010, §3. Its restricted rank-two comparisons, including the source-reported protected quantities in Bashkirov and Kapustin 2011 and Honda and Honma 2013, belong to Chapter 3. The BLG discussion uses the stated restricted trace and compact-group conventions. Local bracket and coefficient algebra

is [**MATH**]; the complete on-shell supercharge count is a sourced classical premise. No classification of all metric three-algebras or arbitrary-rank BLG construction is inferred.

The congruence in (VIII.2.22) is the restricted construction of Lambert and Papageorgakis 2010, §3 (59)–(65), not an obstruction to every possible rank-two identification. The same source's abstract and summary support the simply connected level-two proposal, while its printed p. 13 body and footnote 4 conflict on the named quotient; the conflict remains unresolved. The reported refined-index comparisons of Bashkirov and Kapustin 2011 extend through x^4, with a literal Table 7 fugacity inconsistency. Honda and Honma 2013, Appendix A, reports one undeformed level-two S^3 equality in its measure. These are [**CONJ+**] comparisons, not a full quantum equivalence or a check of all line operators and contact terms.

The IIB fivebrane orientation, interval levels, sourced six-supercharge ultraviolet statement and proposed infrared flow follow Aharony et al. 2008, §3.1 and Fig. 4, under $C_0 = 0$ and finite positive coupling. The isometric T_6 step and M lift are conditional steps in the IIB-to-M-theory construction [**DUAL**]. The torus lattice and near-core metric use the same paper's Appendix B, especially (B.7)–(B.12). The explicit Cartesian phase follows from the torus lattice [**MATH**]. The charge-order permutation is passive notation, not a duality link.

The full-product $\mathcal{N} = 2$ field action and auxiliary-adjoint elimination use Aharony et al. 2008, §2.2 (2.4)–(2.6). The compact vacuum quotient uses §2.3 (2.7)–(2.9) with the primitive compact flux convention [**MATH**]. The source's printed component multiplier in (2.9) is twice the coefficient compatible with a period-2π dual scalar and $kb = d\tau$ under $F = F_{\mu\nu} dx^\mu \wedge dx^\nu/2$. We use $(4\pi)^{-1} \int \tau \, dF_+$, or component coefficient $(8\pi)^{-1}$. The old source's printed monopole dressing sign also requires $\tau_{\mathrm{op}} = -\tau$ in this chart; no monopole formula is used here. The full $U(N)$ global form and primitive central flux follow §2.5 under the stated compact-group convention [**MATH**]. The local geometric and vacuum-coordinate agreement concerns the local position sector [**GEO-X**]. The sourced generic separated-eigenvalue claim is conjectural [**CONJ+**]; its detailed analysis is in Chapter 3. The exercises apply the finite algebraic calculations under these premises.

References

Aharony, O. et al. (2008). "N=6 superconformal Chern-Simons-matter theories, M2-branes and their gravity duals". In: *JHEP* 10, p. 091. DOI: 10.1088/1126-6708/2008/10/091. arXiv: 0806.1218 [hep-th].

Bagger, J. and N. Lambert (2007). "Modeling Multiple M2's". In: *Phys. Rev. D* 75, p. 045020. DOI: 10.1103/PhysRevD.75.045020. arXiv: hep-th/0611108.

Bagger, J. and N. Lambert (2008a). "Comments on multiple M2-branes". In: *JHEP* 02, p. 105. DOI: 10.1088/1126-6708/2008/02/105. arXiv: 0712.3738 [hep-th].

Bagger, J. and N. Lambert (2008b). "Gauge symmetry and supersymmetry of multiple M2-branes". In: *Phys. Rev. D* 77, p. 065008. DOI: 10.1103/PhysRevD.77.065008. arXiv: 0711.0955 [hep-th].

Bashkirov, D. and A. Kapustin (2011). "Dualities between N = 8 superconformal field theories in three dimensions". In: *JHEP* 05, p. 074. DOI: 10.1007/JHEP05(2011)074. arXiv: 1103.3548 [hep-th].

Honda, M. and Y. Honma (2013). "3d superconformal indices and isomorphisms of M2-brane theories". In: *JHEP* 01, p. 159. DOI: 10.1007/JHEP01(2013)159. arXiv: 1210.1371 [hep-th].

Lambert, N. and C. Papageorgakis (2010). "Relating U(N)xU(N) to SU(N)xSU(N) Chern-Simons Membrane theories". In: *JHEP* 04, p. 104. DOI: 10.1007/JHEP04(2010)104. arXiv: 1001.4779 [hep-th].

Van Raamsdonk, M. (2008). "Comments on the Bagger-Lambert theory and multiple M2-branes". In: *JHEP* 05, p. 105. DOI: 10.1088/1126-6708/2008/05/105. arXiv: 0803.3803 [hep-th].

Chapter VIII.3

ABJM moduli spaces and monopole operators

VIII.3.1 The separated positions and their finite identifications

Two membranes moving far apart have two transverse positions. The compact gauge theory of Chapter 2 explains why each position lies in $\mathbb{C}^4/\mathbb{Z}_k$. Yet a list of positions does not tell us which local operator creates magnetic flux, whether a charged scalar survives at the conformal point, or whether a second gauge theory has the same protected states. These questions become particularly sharp for two membranes at $k = 1, 2$. In those cases monopole operators supply the charged scalar multiplets needed for the proposed enhancement from $\mathcal{N} = 6$ to $\mathcal{N} = 8$.

We use the full compact $U(N)_k \times U(N)_{-k}$ product, with positive integer k, fundamental traces and $D = d + iA$. No common-center quotient is implicit. The four transverse complex coordinates are $C = (A_1, A_2, B_1^\dagger, B_2^\dagger)$, which all have positive weight under the relative phase. The holomorphic $\mathcal{N} = 2$ fields (A_1, A_2, B_1, B_2) instead have weights $(1, 1, -1, -1)$. This distinction will matter when we dress a monopole with B fields.

We first follow the gauge identifications on a separated diagonal branch. Magnetic insertions then expose information that positions cannot carry. At the end, two rank-two BLG comparisons test the role of compact global form and protected observables.

For one membrane the compact abelian calculation in Chapter 2 leaves the phase $C^I \mapsto \omega C^I$, where $\omega = e^{2\pi i/k}$. Its periodic dual scalar is essential. In the primitive integral gauge basis $b = A_1 - A_2$, $c = A_2$, the Chern–Simons matrix is $\left(\begin{smallmatrix} k & k \\ k & 0 \end{smallmatrix}\right)$; a 2π-period dual scalar obeys $kb = d\tau$. Fixing $\tau = 0$ leaves precisely $\lambda_b = 2\pi r/k$. Thus the local one-membrane vacuum coordinates are $\mathbb{C}^4/\mathbb{Z}_k$, with no residual continuous phase quotient.

It helps to keep the transformation, not just the name of the quotient. In the

conventions of Chapter 2, a relative transformation acts by

$$C^I \longmapsto e^{i\lambda_b} C^I, \qquad \tau \longmapsto \tau - k\lambda_b, \qquad \tau = 0 \implies \lambda_b = \frac{2\pi r}{k} \pmod{2\pi}. \quad \text{(VIII.3.1)}$$

The last implication uses the periodicity of τ and the compact, primitive gauge basis. At $k = 1$ it leaves no nontrivial phase; at $k = 2$ it identifies C with $-C$. In the holomorphic chiral chart $Z = (A_1, A_2, B_1, B_2)$, the same operation has weights $(1, 1, -1, -1)$, so conjugating the B coordinates is essential to the common-phase position chart.

At a generic point of the classical N-membrane vacuum locus, the four bifundamental matrices admit a common diagonal presentation $C^I = \mathrm{diag}(z_1^I, \ldots, z_N^I)$. Work on the generic locus with nonzero diagonal entries and massive off-diagonal fluctuations. Distinct $\mathbb{Z}_k$ orbits alone do not guarantee this mass condition. Each eigenline inherits the compact one-membrane phase, independently. A permutation of the first gauge-node basis must be accompanied by the same permutation at the second node to retain nonzero diagonal bifundamental entries. Hence the finite action is

$$C^I \longmapsto U C^I \widetilde{U}^{-1}, \qquad U = \mathrm{diag}(e^{i\alpha_a}), \quad \widetilde{U} = \mathrm{diag}(e^{i\widetilde{\alpha}_a}), \qquad z_a^I \longmapsto e^{i(\alpha_a - \widetilde{\alpha}_a)} z_a^I. \quad \text{(VIII.3.2)}$$

On this branch the Cartan Chern–Simons form is a sum of N copies of the one-eigenline form:

$$K_{\mathrm{Cartan}} = \bigoplus_{a=1}^{N} \begin{pmatrix} k & k \\ k & 0 \end{pmatrix}_{(b_a, c_a)}, \qquad k b_a = d\tau_a, \quad \tau_a \sim \tau_a + 2\pi. \quad \text{(VIII.3.3)}$$

The direct sum makes explicit why the residual phases are independent on this branch; it uses the same compact dualization as the one-membrane result. Fixing all $\tau_a = 0$ leaves $\alpha_a - \widetilde{\alpha}_a = 2\pi r_a / k$. The common phases $\alpha_a = \widetilde{\alpha}_a$ act trivially on these position coordinates. For the permutation part, $U = P_\pi$ and $\widetilde{U} = P_\pi$ preserve diagonal support, whereas a generic independent pair of permutations does not. These statements give the finite action

$$(r, \pi) \cdot z_a = \omega^{r_a} z_{\pi^{-1}(a)}, \qquad r \in (\mathbb{Z}_k)^N, \quad \pi \in S_N, \qquad G_{N,k} = (\mathbb{Z}_k)^N \rtimes S_N. \quad \text{(VIII.3.4)}$$

The permutation acts on phase labels by $\pi r \pi^{-1} = (r_{\pi^{-1}(1)}, \ldots, r_{\pi^{-1}(N)})$. This is the open separated part of $\mathrm{Sym}^N(\mathbb{C}^4/\mathbb{Z}_k)$; it has real dimension $8N$.

The semidirect product also fixes the order of operations. If (r, π) acts first and (s, σ) second, their combined phases obey

$$(s, \sigma)(r, \pi) = (s + \sigma r, \sigma\pi), \qquad (\sigma r)_a = r_{\sigma^{-1}(a)}. \quad \text{(VIII.3.5)}$$

Thus one may exchange eigenlines and then phase the newly assigned lines. The two phase factors are independent; replacing them by one diagonal $\mathbb{Z}_k$ changes the position quotient.

For an explicit orbit, take $N = 2$, $k = 3$, $z_1 = (1, 0, 0, 0)$ and $z_2 = (0, 2, 0, 0)$. With $\pi = (12)$ and $r = (1, 2)$, equation (VIII.3.4) sends (z_1, z_2) to $(\omega z_2, \omega^2 z_1)$. The group has $3^2 \cdot 2 = 18$ elements. A single common $\mathbb{Z}_3$ would miss $(\omega z_1, z_2)$; two unrelated

permutations would spoil the generic diagonal support. Figure VIII.3.1 displays these two independent phases and the exchange on a real slice of the position chart.

$$(z_1, z_2) \xrightarrow{((1,2),(12))} (\omega z_2, \omega^2 z_1), \qquad (z_1, z_2) \xrightarrow{((1,0),e)} (\omega z_1, z_2). \tag{VIII.3.6}$$

The second arrow gives a concrete identification absent from a common-phase quotient. One can also test the action on coordinate functions. For any selected complex direction I,

$$M^I{}_J = \sum_{a=1}^{N} z_a^I \bar{z}_a^J, \qquad H^I = \sum_{a=1}^{N} (z_a^I)^k \tag{VIII.3.7}$$

are unchanged by every independent phase and by every simultaneous permutation. By contrast, $\sum_a z_a^I$ fails the phase test when $k > 1$. The first invariant is a real-coordinate function and the second is holomorphic in this position chart. Their invariance checks the finite action; it does not identify an unrestricted set of local chiral operators in the interacting gauge theory. Figure VIII.3.1 depicts the operations schematically on selected complex-coordinate planes.

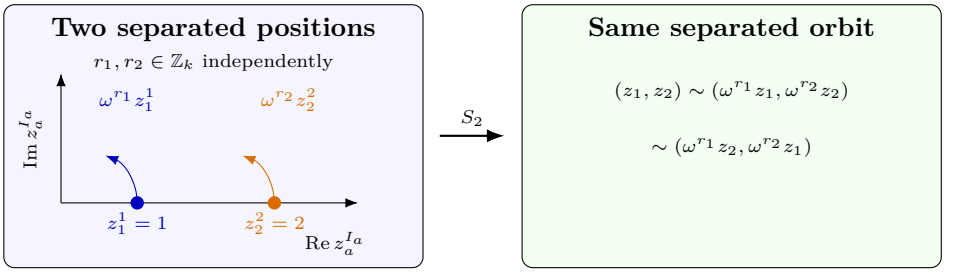


Figure VIII.3.1: The left panel overlays the two selected complex-coordinate planes z_1^1 and z_2^2 of the fixed example; horizontal separation is schematic, not a common spatial coordinate. The curved arrows indicate discrete phase operations schematically; their drawn angles and radii are not complex-plane trajectories. Each eigenline's other three complex components receive its own phase. The right panel applies those phases and a simultaneous exchange to the same two membranes. The diagonal derivation does not cover coincident positions.

The off-diagonal mass argument need not apply on nongeneric configurations, including coincidence and the origin. At $k = 3$, set $z_1 = v$, $z_2 = e^{i\pi/3} v$. These positions lie in different $\mathbb{Z}_3$ orbits, but every $C^I = v^I D$ shares one matrix $D = \mathrm{diag}(1, e^{i\pi/3})$. For any $U \in U(2)$,

$$(U, D^{-1}UD): \quad C^I \longmapsto U(v^I D)(D^{-1}UD)^{-1} = C^I. \tag{VIII.3.8}$$

The continuous off-diagonal stabilizer therefore survives orbit separation. The separate massive-fluctuation premise in the generic-branch argument cannot be deduced just from unequal discrete orbits. The diagonal description is a useful classical branch calculation, not a proof that all vacua are diagonal or that the quantum metric and

singular strata equal those of a symmetric product. Even a complete equality of position spaces would not fix sums over gauge bundles or line operators. Magnetic insertions offer more information.

VIII.3.2 A primitive flux and its electric charge

A local monopole insertion is specified by the magnetic flux through a small linking S^2. For each full $U(N)$ factor, choose integral eigenvalue cocharacters

$$\frac{1}{2\pi}\int_{S^2} F = \operatorname{diag}(m_1,\dots,m_N), \qquad \frac{1}{2\pi}\int_{S^2} \widetilde{F} = \operatorname{diag}(\widetilde{m}_1,\dots,\widetilde{m}_N), \qquad m_i,\widetilde{m}_j \in \mathbb{Z}. \tag{VIII.3.9}$$

Each Weyl group acts before a convenient pairing is chosen. The insertion creates a disorder boundary condition and is generally gauge charged. It is not an ordinary polynomial in the bifundamental fields.

The rank-two flux $(1,0)$ is primitive in $U(2)$. Write its Lie-algebra generator as

$$\operatorname{diag}(1,0) = \frac{1}{2}I_2 + \frac{1}{2}\operatorname{diag}(1,-1), \qquad \operatorname{diag}(1,1) = I_2. \tag{VIII.3.10}$$

The first has trace charge $t = 1$, central flux $1/2$, and a correlated traceless twist. The second is pure central flux one and has $t = 2$. The central connection has bare level $2k$, but multiplying that level by the primitive central flux $1/2$ gives k, not $2k$. Replacing the primitive insertion by the pure central one would change the operator. Figure VIII.3.2 fixes the relevant fluxes and Cartan weights.

Variation of the Cartan Chern–Simons terms gives the bare electric weights $(km_i; -k\widetilde{m}_j)$. Let a_{ij} count scalar $A^i{}_j$ occupations and b_{ji} count $B^j{}_i$ occupations, summed over the two flavors. Their gauge weights are respectively $(+e_i; -\widetilde{e}_j)$ and $(-e_i; +\widetilde{e}_j)$. A neutral scalar dressing must solve every component of

$$km_i + \sum_j (a_{ij} - b_{ji}) = 0, \qquad -k\widetilde{m}_j + \sum_i (b_{ji} - a_{ij}) = 0. \tag{VIII.3.11}$$

Summing gives the necessary equality

$$t := \sum_i m_i = \sum_j \widetilde{m}_j = \frac{\sum b - \sum a}{k} \in \mathbb{Z}. \tag{VIII.3.12}$$

Equal totals alone neither solve each Cartan equation nor establish a physical protected state. For example, with $m = \widetilde{m} = (1,0)$ and $k = 2$, setting every occupation to zero leaves residual weights $(2,0;-2,0)$. Inserting one $B^1{}_1$ changes them to $(1,0;-1,0)$, which still fails Gauss' law. A second insertion gives $(0,0;0,0)$. This component-by-component calculation explains why the trace equation alone is insufficient: it sees the required total number of B fields, but it does not say on which eigenline they must act. The same test at general k requires k copies on this line.

For $m = \widetilde{m} = (1,0)$ at $N = 2$, the bare weights are $(k, 0; -k, 0)$ and the matter magnetic-charge matrix is

$$(m_i - \widetilde{m}_j)_{ij} = \begin{pmatrix} 0 & 1 \\ -1 & 0 \end{pmatrix}. \tag{VIII.3.13}$$

The component ${B^1}_1$ sees zero magnetic flux and has weight $(-1, 0; +1, 0)$. Exactly k such components cancel all four Cartan charges. In the chosen flux gauge one may write $T_{(1,0),(1,0)}({B^1}_1)^k$; the physical local operator includes the appropriate nonabelian gauge contraction and Weyl completion. A bare ${B^1}_1$ polynomial has no such meaning. The resulting charge-neutral configuration is the input for the radial-energy calculation in the next section; neutralization itself says nothing about its conformal dimension. Reversing the paired flux gives a useful sign check. For $m = \widetilde{m} = (-1, 0)$, the bare weight is $(-k, 0; +k, 0)$, while ${A^1}_1$ has $(+1, 0; -1, 0)$. Thus k copies of this zero-flux component solve the opposite-charge Gauss equations. The two dressings are conjugate charge families, but neither can be obtained by erasing the monopole insertion. The calculation also makes clear why B is the correct holomorphic field for positive flux in our $D = d + iA$ convention, whereas a notation inherited from a differently signed Chern–Simons action may reverse that appearance.

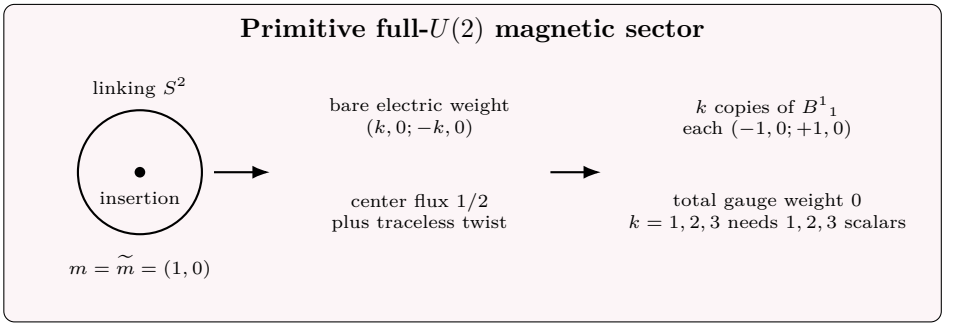


Figure VIII.3.2: A small sphere detects the primitive magnetic boundary condition in the full compact $U(2)_k \times U(2)_{-k}$ group. The displayed Cartan weights show how the B dressing cancels the Chern–Simons charge. The pure central flux $(1, 1)$ is a different sector. The diagram establishes no spectral protection by itself.

VIII.3.3 Bare energy, low dressings and the scalar families

Charge cancellation is only one requirement. In a supersymmetric radial calculation on a unit S^2, the sourced one-loop energy assigned to the bare magnetic vacuum is

$$E_0(m, \widetilde{m}) = \sum_{i,j} |m_i - \widetilde{m}_j| - \sum_{i<j} |m_i - m_j| - \sum_{i<j} |\widetilde{m}_i - \widetilde{m}_j|. \tag{VIII.3.14}$$

This formula uses a particular supersymmetric deformation, gauge fixing, monopole-harmonic spectrum and common regulator subtraction. We take that physical calculation as an input. The bare vacuum is usually gauge charged, so $E_0 = 0$ does not by itself exhibit a dimension-zero local primary.

There is an independent exact identity for the expression in (VIII.3.14). Let $A(x) = \#\{i : m_i > x\}$ and $B(x) = \#\{j : \widetilde{m}_j > x\}$. The identity $|u - v| = \int_{\mathbb{R}} |\mathbf{1}_{u>x} - \mathbf{1}_{v>x}|\, dx$ counts the interval between two flux values. At each x, its cross-node and two same-node contributions are

$$\begin{aligned} &\sum_{i,j} |m_i - \widetilde{m}_j| : \ A(N-B) + B(N-A), \\ &\sum_{i<j} |m_i - m_j| : \ A(N-A), \qquad \sum_{i<j} |\widetilde{m}_i - \widetilde{m}_j| : \ B(N-B). \end{aligned} \tag{VIII.3.15}$$

For instance, a flux value above x at the first node pairs with $N - B$ values below x at the second. Subtracting the two same-node counts cancels every term except the square:

$$E_0 = \int_{-\infty}^{\infty} [A(x) - B(x)]^2 \, dx \geq 0. \tag{VIII.3.16}$$

It vanishes exactly when the two flux multisets coincide, up to Weyl permutations. This is a proof of nonnegativity of the supplied finite expression, not a derivation of the radial regulator. Equal totals are weaker: $(m_1, m_2) = (1, -1)$ and $(\widetilde{m}_1, \widetilde{m}_2) = (0, 0)$ have equal $t = 0$, but $E_0 = 4 - 2 = 2$.

For $m = \widetilde{m} = (1, 0)$, equation (VIII.3.14) gives $E_0 = 2-1-1 = 0$. The zero-flux $B^1{}_1$ oscillator has spin $j = 0$ and energy $1/2$ in the radial calculation. Its k-fold symmetric dressing has regulator energy and R charge $k/2$, assuming the sourced scalar mode spectrum. The charge computation itself is exact for the stated cocharacter.

k	primitive dressing	$SU(2)_B$ representation	$E_{\text{radial}} = R$
1	B	**2**	$\frac{1}{2}$
2	$\mathrm{Sym}^2 B$	**3**	1
3	$\mathrm{Sym}^3 B$	**4**	$\frac{3}{2}$

(VIII.3.17)

Taking these energies to undeformed scaling dimensions uses the chiral protection and continuation argument below. At $k = 1$, the protected dimension-1/2 components, together with the unitary scalar bound, imply a free local scalar sector under that continuation. This conclusion concerns local operators, not every line or topological sector.

Enhancement asks specifically for charged dimension-one scalars. Restrict first to nonnegative, paired, zero-bare-energy flux and exactly two lowest scalar oscillators. Gauss' law requires $k \sum_i m_i = 2$. For $N = 2$ the allowed Weyl partitions are

k	$t = 2/k$	nonnegative paired flux
1	2	$(2, 0),\ (1, 1)$
2	1	$(1, 0)$
3	nonintegral	none

(VIII.3.18)

The $(1,1)$ family at $k=1$ is pure central and cannot be replaced by a Weyl copy of $(2,0)$. Both have total flux $t=2$, hence the same total induced electric charge, but their residual groups differ. The vector $(2,0)$ selects one eigenline, leaving a Cartan centralizer; $(1,1)$ is central and leaves the whole $U(2)$ factor unbroken. Two independent B matrices must therefore be contracted into a singlet of this residual nonabelian action. Its representative contracts both gauge index pairs,

$$T_{(1,1),(1,1)}\,\epsilon^{ij}\epsilon_{pq}B^{p}{}_{i,(a}B^{q}{}_{j,b)}. \tag{VIII.3.19}$$

Interchanging the two commuting scalars changes the sign of each epsilon tensor, so their flavor indices (a,b) are symmetric. They form the $SU(2)_B$ triplet. This manual residual-group and flavor argument is necessary; the finite charge and partition arithmetic alone does not assess it. The component Gauss equations also give a useful lower bound when some flux entries are negative. Apply the triangle inequality first within each row and then to all scalar occupations:

$$n_{\text{scalar}}=\sum_{i,j}(a_{ij}+b_{ji})\geq\sum_{i}\left|\sum_{j}(a_{ij}-b_{ji})\right|=k\sum_{i}|m_i|. \tag{VIII.3.20}$$

This bound uses the paired low-mode scalar dressing and the declared component Gauss laws. For nonzero integral flux and $k\geq 3$, two scalars cannot cancel the charge. It does not rule out all charged operators or the familiar neutral dimension-one moment maps.

VIII.3.4 When scalar states imply extra currents

The needed group-theory pattern can be derived without assuming that the charged operators exist. In a triality frame with transverse scalars in 8_v, assign a temporary phase weight $u(C)=1$. Then $8_v=4_{+1}\oplus\overline{4}_{-1}$. Since $\mathrm{Sym}^2 4=10$, $\Lambda^2 4=6$ and $4\otimes\overline{4}=15\oplus 1$, removing the single symmetric trace gives

$$\begin{aligned}\mathrm{Sym}^2(4_{+1}\oplus\overline{4}_{-1})&=10_{+2}\oplus(15\oplus 1)_0\oplus\overline{10}_{-2},\\ \Lambda^2(4_{+1}\oplus\overline{4}_{-1})&=6_{+2}\oplus(15\oplus 1)_0\oplus 6_{-2}.\end{aligned} \tag{VIII.3.21}$$

The trace is the neutral singlet in the first line. Removing it produces the scalar traceless-symmetric representation, while the second line already has the required antisymmetry:

$$\begin{aligned}35_v=\mathrm{Sym}^2_0(8_v)&\longrightarrow 10_{+2}\oplus 15_0\oplus\overline{10}_{-2},\\ 28=\Lambda^2(8_v)&\longrightarrow 6_{+2}\oplus(15\oplus 1)_0\oplus 6_{-2}.\end{aligned} \tag{VIII.3.22}$$

The dimensions add to 35 and 28. The source's triality name for its scalar 35 differs from this geometric 8_v chart; the displayed $SU(4)$ content is the invariant comparison. For the holomorphic dressed representatives above, $u=-kt$. The source's normalized topological label is $T_{\mathrm{BK}}=kt/2=-u/2$. Therefore the charged scalar $\overline{10}$ has positive $T_{\mathrm{BK}}=1$ at either $k=1$ with $t=2$ or $k=2$ with $t=1$. Its conjugate has negative

charge. Calling both primitive charge one would erase this distinction.

k	paired two-scalar flux $m = \widetilde{m}$	t	$T_{\rm BK} = -u/2$
1	$(2,0)$ or $(1,1)$	2	1
2	$(1,0)$	1	1
3	none in this construction	–	–

(VIII.3.23)

This table concerns charged two-scalar families. The primitive $k = 1$ dressing has one scalar, $t = 1$ and $T_{\rm BK} = 1/2$; it has a different role in the spectrum.

To see the flavor triplet inside the charged 10, choose the stated $\mathcal{N} = 2$ embedding

$$4 \longrightarrow (2,1)_{1/2} \oplus (1,2)_{-1/2}, \qquad 10 \longrightarrow (3,1)_1 \oplus (2,2)_0 \oplus (1,3)_{-1}, \tag{VIII.3.24}$$

with $\overline{10} \to (3,1)_{-1} \oplus (2,2)_0 \oplus (1,3)_1$. The two triplets follow from the symmetric squares of the two doublets, and the four middle states from their cross term. The charged highest components supplied by the dressed monopoles can occupy the appropriate triplets; the rest of each 10 is obtained after Spin(6) is restored at the undeformed conformal point. The complete 10 is not chiral under one fixed $\mathcal{N} = 2$ choice. For example, the two B flavor indices in (VIII.3.19) are symmetric, giving the $(1,3)_1$ piece of the $\overline{10}$ in this embedding. Its conjugate arises from the corresponding negative-flux A dressing. The four mixed states are part of the restored $SU(4)$ representation; the displayed B component alone does not construct them.

Here is the physical bridge, with its hypotheses in the order in which they matter. The sourced radial construction supplies gauge-invariant scalar states with $E = R = 1$ in the flux families of (VIII.3.18). Within a fixed four-real-Poincaré-supercharge $\mathcal{N} = 2$ subalgebra, the selected chiral components are annihilated by two of the four complexified Poincaré components. Their short label is therefore 2/4 for these components only. To transport them from the weakly coupled radial deformation to the undeformed conformal theory, one needs controlled continuation without escape into a continuum. The source excludes the relevant recombination partners in the radial Fock spectrum: the dangerous fermionic channels have $(E, R) = (1/2, 0)$ or $(3/2, 2)$ and the required Spin(4) and topological charges. The exclusion is more specific than a generic claim that all chiral states are protected: a recombining long multiplet would have to carry exactly the charges of a partner for these selected scalar components. The radial construction searches those channels and finds none in its spectrum. Carrying that conclusion to the interacting conformal point still needs the source's control of the deformation and no escape into a continuum. This is a physical spectral argument, not a consequence of (VIII.3.22).

At the conformal point, the source uses highest weights and restored Spin(6) to place the surviving scalars in $10_{-1} \oplus \overline{10}_{+1}$, now labelled by $T_{\rm BK}$. Its $\mathcal{N} = 6$ superconformal argument supplies the spin-one descendants and tests that their norms are nonzero; a free $\mathcal{N} = 8$ stress-tensor multiplet serves only as a representation witness for the norm. The conditional chain is

$$\begin{aligned} \left(10_{-1} \oplus \overline{10}_{+1}\right)_{\Delta=1} &\xrightarrow[\text{nonzero norm}]{\text{two supercharges}} (6_{-1} \oplus 6_{+1})_{\Delta=2,\, j=1}\,, \\ \|\partial\cdot J\|^2 &\propto (\Delta - 2)\|J\|^2 = 0. \end{aligned} \tag{VIII.3.25}$$

The arrow requires the source's continuation without recombination and the nonzero-norm step. For a nonzero spin-one primary in a unitary three-dimensional conformal theory, the $\Delta = 2$ bound makes the divergence descendant null and the current conserved. These charged currents join the neutral $15_0 \oplus 1_0$ to fill the 28 of (VIII.3.22). The representation count supplies none of the spectral premises.

The neutral 15 has familiar representatives $\mathrm{Tr}(C^I C_J^\dagger) - \delta^I_J \,\mathrm{Tr}(CC^\dagger)/4$. A direct search for vector states is less secure because possible fermionic partners can permit recombination. The scalar route explains why protection must be established before making a current claim. Geometric spinor counting in Chapter 2 is a separate input and does not construct these quantum currents.

VIII.3.5 Global form in the rank-two BLG comparison

The local A_4 three-algebra of Chapter 2 becomes a real bifundamental of two $SU(2)$ factors. Fix $\langle e_a, e_b\rangle = \delta_{ab}$, $[e_a, e_b, e_c] = q\epsilon_{abcd}e_d$ with $\epsilon_{1234} = +1$, and

$$X = \frac{x_4 I + i\sum_{j=1}^{3} x_j\sigma_j}{2}, \qquad \mathrm{tr}_2(X^\dagger X) = \frac{1}{2}\sum_{a=1}^{4} x_a^2, \qquad \mathrm{tr}_2(\sigma_i\sigma_j) = 2\delta_{ij}. \quad \text{(VIII.3.26)}$$

The Pauli identity has a short direct check. Multiplying $X^\dagger$ by X, the antisymmetric Pauli cross terms cancel because each $x_i x_j$ is symmetric. The remaining matrix is $\frac{1}{4}(x_4^2+\sum_j x_j^2)I_2$, whose fundamental trace gives (VIII.3.26). The mapped Chern–Simons coefficient $[CS_2(A) - CS_2(\widehat{A})]/(2q)$ equals the book's fundamental-trace $k[CS_2(A) - CS_2(\widehat{A})]/(4\pi)$ when $q = 2\pi/k$. This step ties a real four-vector kinetic normalization to the two complex-matrix gauge factors; forgetting the factor of two would assign the wrong compact level before any flux comparison. A vector-trace formula in the original A_4 presentation uses $\mathrm{Tr}_4\,/(4\lambda)$. Restriction of the real four-vector to one factor contains two doublets, so

$$\mathrm{Tr}_4((t\otimes I)(s\otimes I)) = 2\,\mathrm{tr}_2(ts), \qquad \frac{\mathrm{Tr}_4}{4\lambda} = \frac{\mathrm{tr}_2}{2\lambda}, \qquad k_{\mathrm{fund}} = 2k_{\mathrm{BL}} \qquad \text{(VIII.3.27)}$$

for that source's $\lambda = \pi/k_{\mathrm{BL}}$. The displayed trace conversion does not impose an odd-fundamental-level ban on the simply connected theory. Orientation reversal exchanges the node signs.

Local bifundamental matter does not specify the global group. Write the two Cartan fluxes as $H_\pm = \mathrm{diag}(h_\pm, -h_\pm)$. For the candidate integer and half-integer cocharacters, the endpoint of a Cartan loop in one factor is computed without invoking the local action:

$$e^{2\pi i H_\pm} = \mathrm{diag}(e^{2\pi i h_\pm}, e^{-2\pi i h_\pm}) = \begin{cases} I, & h_\pm \in \mathbb{Z}, \\ -I, & h_\pm \in \mathbb{Z} + \frac{1}{2}. \end{cases} \qquad \text{(VIII.3.28)}$$

A lift closes in $SU(2)\times SU(2)$ only when both endpoints are I. In the diagonal quotient, it may instead end at $(-I, -I)$; a mixed endpoint does not lie in the quotient kernel.

Thus both $h_\pm$ are integers or both are half-integers:

BLG global group	allowed (h_+, h_-)
$SU(2) \times SU(2)$	$\mathbb{Z} \times \mathbb{Z}$
$(SU(2) \times SU(2))/\mathbb{Z}_2^{\text{diag}}$	$\{(h_+, h_-) : h_\pm \in \frac{1}{2}\mathbb{Z},\ h_+ - h_- \in \mathbb{Z}\}$

(VIII.3.29)

The endpoint test can be performed before naming a monopole operator. In the order $(h_+, h_-) = (0,0), (1/2,1/2), (1/2,0), (1,-1)$, the lifted loops end at

(h_+, h_-)	endpoint in $SU(2)^2$	$SU(2)^2$	$(SU(2)^2)/\mathbb{Z}_2^{\text{diag}}$
$(0,0)$	(I, I)	✓	✓
$(1/2,1/2)$	$(-I, -I)$	×	✓
$(1/2,0)$	$(-I, I)$	×	×
$(1,-1)$	(I, I)	✓	✓

(VIII.3.30)

Thus $(1/2,1/2)$ belongs only to the quotient lattice and $(1/2,0)$ belongs to neither. Conversely a Wilson representation $(2,1)$ descends only to the simply connected product: the diagonal central element acts as -1 on that line. Neither group has a hidden $U(2)$ trace connection. The level, line spectrum and bundle sum must accompany any proposed comparison.

One proposed route reduces the full $U(N)$ product to a $\mathbb{Z}_k$ identification of $(SU(N) \times SU(N))/\mathbb{Z}_N$. An eigenline phase assignment with exponent sum ℓ has determinant ω^ℓ. A common phase with exponent ℓ_B has determinant $\omega^{N\ell_B}$, so this route requires

$$N\ell_B = \ell \pmod{k} \quad \text{for every } \ell \in \mathbb{Z}_k \quad \Longleftrightarrow \quad \gcd(N,k) = 1. \tag{VIII.3.31}$$

Bezout supplies the inverse when the gcd is one. At $(N,k) = (2,3)$, $\ell_B = 2\ell$ works; at $(2,2)$, $\ell = 1$ has no solution. This obstructs that reduction only. It is not a theorem excluding every other low-rank duality.

Indeed, at $k = 2$ a distinct simply connected BLG comparison has the same classical signed-permutation position action. On the ordered pair of real eight-vectors, choose

$$s = \begin{pmatrix} 1 & 0 \\ 0 & -1 \end{pmatrix}, \qquad a = \begin{pmatrix} 0 & 1 \\ -1 & 0 \end{pmatrix}, \qquad a^2 = -I, \quad s^2 = I, \quad sas = a^{-1}. \tag{VIII.3.32}$$

Then s flips the second vector, $sa^2 = \text{diag}(-1,1)$ flips the first, and $sa = \left(\begin{smallmatrix} 0 & 1 \\ 1 & 0 \end{smallmatrix}\right)$ exchanges them. The eight matrices are $\{\pm I, \pm s, \pm a, \pm sa\}$, so the generated action is $(\mathbb{Z}_2)^2 \rtimes S_2$. This establishes the classical quotient $\text{Sym}^2(\mathbb{R}^8/\mathbb{Z}_2)$, not equality of quantum theories. The explicit generators distinguish this $k = 2$ route from the failed common-phase congruence in (VIII.3.31).

The two precise candidates should therefore stay distinct. At $k = 1$ compare full $U(2)_1 \times U(2)_{-1}$ ABJM with $(SU(2)_1 \times SU(2)_{-1})/\mathbb{Z}_2^{\text{diag}}$ BLG. At $k = 2$ compare full $U(2)_2 \times U(2)_{-2}$ ABJM with simply connected $SU(2)_2 \times SU(2)_{-2}$ BLG. Their proposed full equivalences have finite supporting evidence and remain conjectural.

VIII.3.6 Protected comparisons beyond the quotient

For the $k = 1$ pair there are two directions of comparison: the classical global/moduli reduction and a source-reported charge-refined index through finite order, including

half-integral powers of x. Here the BLG $U(1)_t$ charge equals the ABJM trace charge T, and the half-integral BLG flux sector probes the quotient global form. The printed $k = 1$ Table 7 zero-flux row literally pairs $15z^4x^4$ with $15z^{-8}x^4$, an asymmetric exponent compared with the corresponding Table 8 entry. We retain the printed row and do not infer an all-row equality from a silent correction. For the $k = 2$ pair there are three directions: the signed-permutation moduli action, a flux-resolved index through x^4, and one undeformed S^3 partition function. The two protected observables both rely on localization; they are correlated evidence, not two independent first-principles derivations of the full QFT.

The physical index is defined on the radial Hilbert space $\mathcal{H}_{S^2}$, equivalently by the $S^2 \times S^1$ path integral. Choose the source's $Q = Q_{12-}$ and radial adjoint $S = Q^\dagger$, with

$$\delta = \{Q, S\} = E - R - j_3, \qquad \mathcal{I}(x, z) = \mathrm{Tr}_{\mathcal{H}_{S^2}}(-1)^F e^{-\beta\delta} x^{E+j_3} z^{F_t}. \tag{VIII.3.33}$$

States with positive δ pair in the supertrace; the surviving quantity is protected under the source's spectral and localization assumptions. Use the undeformed conformal vacuum at zero masses and FI, $|x| < 1$, and generic unit-modulus z. This choice of one complex Q and its conformal adjoint does not determine a fraction of preserved real Poincaré supercharges for all index states. We assign no such fraction. This $S^2 \times S^1$ observable is distinct from the S^3 matrix integral below.

The charge fugacity must compare the same integer label on both sides. For the $k = 1$ quotient-group candidate the source identifies $F_t = T$, whereas the $k = 2$ simply connected candidate uses $F_t = 2T$, with $T = \sum_i m_i$ in ABJM. These are pair-specific translations, not a universal redefinition of the primitive magnetic cocharacter. In particular, a coefficient at z^{2j} in the $k = 2$ series belongs to ABJM trace charge $T = j$. With P_j denoting the printed charge-sector coefficient polynomials, the finite $k = 2$ comparison reads

$$\begin{aligned} P_0 &= 1 + 4x + 21x^2 + 32x^3 + 53x^4, \\ P_1 &= 3x + 16x^2 + 36x^3 + 48x^4, \\ P_2 &= 11x^2 + 36x^3 + 54x^4, \\ P_3 &= 22x^3 + 64x^4, \qquad P_4 = 45x^4, \\ \mathcal{I}(x, z) &= P_0 + \sum_{j=1}^{4} (z^{2j} + z^{-2j}) P_j + O(x^5). \end{aligned} \tag{VIII.3.34}$$

At $z = 1$, every positive-charge sector has a matching negative-charge coefficient. The contributions at successive powers of x are

x^n	x^0	x^1	x^2	x^3	x^4
P_0	1	4	21	32	53
$2\sum_{j=1}^{4} P_j$	0	6	54	188	422
sum	1	10	75	220	475

(VIII.3.35)

For example, the x^3 charged contribution is $2(36 + 36 + 22) = 188$. This is literal finite-series addition, with no evaluation of the path integral. It gives

$$\mathcal{I}(x, 1) = 1 + 10x + 75x^2 + 220x^3 + 475x^4 + O(x^5). \tag{VIII.3.36}$$

The other printed decomposition gives the same finite coefficients by adding $(1+10x+40x^2+76x^3+114x^4)+(35x^2+144x^3+196x^4)+165x^4$. These are arithmetic identities among published coefficients. They do not independently evaluate the physical trace. A source comparison with unequal rank has $230x^3$, rather than $220x^3$, showing that the displayed agreement is sensitive to the named theory.

For an additional $k=2$ number, take the source's explicit normalization of its convergent real integral

$$J(k)=\int_{\mathbb{R}} d\lambda\,\frac{\lambda}{\sinh(\pi k\lambda)}\tanh^2(\pi\lambda),\qquad Z_{SU}=\frac{k}{32}J(k),\qquad Z_U=\frac{1}{16}J(k). \tag{VIII.3.37}$$

The apparent point $\lambda=0$ is regular. The integrand has the limiting and large-argument behavior

$$\frac{\lambda\tanh^2(\pi\lambda)}{\sinh(\pi k\lambda)}=\frac{\pi}{k}\lambda^2+O(\lambda^4)\quad(\lambda\to 0),\qquad O\big(|\lambda|e^{-\pi k|\lambda|}\big)\quad(|\lambda|\to\infty). \tag{VIII.3.38}$$

The integral therefore converges for positive k. Dividing the two written prefactors gives $Z_{SU}/Z_U=k/2$, hence equality at $k=2$ for the specified simply connected and full-product global forms. The common-integral reduction imports the source's contour, trace-constraint measure and localization prescription; this chapter has not recomputed the original multidimensional matrix integrals. Physical equality is stated in that measure and background-contact convention. Neither the finite index nor this sphere number tests all line operators, discrete contact terms, arbitrary manifolds or OPE coefficients. The proposed full identifications remain conjectural comparisons and do not upgrade the geometric dictionary of Chapter 2.

VIII.3.7 Exercises

1. **VIII.3.E1: Separated orbit.** For the full $U(2)_3\times U(2)_{-3}$ product and $z_1=(1,0,0,0)$, $z_2=(0,2,0,0)$, give generators and a composition law for $(\mathbb{Z}_3)^2\rtimes S_2$. Exhibit a transformation sending (z_1,z_2) to $(\omega z_2,\omega^2 z_1)$ and one that phases only the first position. Explain why the answer requires the compact dual-scalar premise and why it does not cover coincident vacua. Equivalent generating sets and exponents modulo three are acceptable.

2. **VIII.3.E2: Primitive magnetic sector.** At $N=2$, compute the trace, center and traceless parts of $(1,0)$ and $(1,1)$. For $m=\widetilde{m}=(1,0)$ at $k=2$, compute all four bare CS electric weights, the 2×2 effective matter-flux matrix $(m_i-\widetilde{m}_j)$, and E_0; then compute the four Gauss residuals after two ${B^1}_1$ insertions. For each $k=1,2,3$, give the number of ${B^1}_1$ insertions needed to dress the same primitive paired flux and all four postdressing Gauss residuals, ordered by increasing k. Compute E_0 for the equal-total counterexample $m=(1,-1)$, $\widetilde{m}=(0,0)$. List the nonnegative paired two-scalar flux partitions at $k=1,2,3$. Explain why the $k=1$ $(1,1)$ operator requires both epsilon contractions and yields a flavor triplet; charge and energy arithmetic alone does not establish this last point. In a written

solution, a simultaneous Weyl move with its dressing moved to the corresponding eigenline is physically equivalent. Optional structured submissions use the stated first-eigenline flux and dressing.

3. **VIII.3.E3: Branching and charge.** Starting from $8_v = 4_{+1} \oplus \overline{4}_{-1}$ and $4 \to (2,1)_{1/2} \oplus (1,2)_{-1/2}$, derive both branchings in (VIII.3.22), their dimensions, and the 10 and $\overline{10}$ decompositions. Determine t and T_{BK} for each charged two-scalar family at $k = 1, 2$ and explain the $k = 3$ charge obstruction. Separately, for the primitive paired flux $(1, 0)$ at $k = 1$, compute u and T_{BK}; this is a one-scalar dressing, not a two-scalar current family. In a written solution, simultaneous reversal of u and conjugation of every representation is an equivalent convention if stated consistently. Optional structured submissions use the displayed u convention. Explain separately which physical conditions are needed to obtain nonzero conserved currents.

4. **VIII.3.E4: The same local action, two magnetic lattices.** From $X = (x_4 I + i x_i \sigma_i)/2$ derive $\mathrm{tr}_2(X^\dagger X)$ and the trace restriction in (VIII.3.27). Translate the source vector-trace level into the fundamental-trace level. For $(h_+, h_-) = (0,0), (1/2,1/2), (1/2,0), (1,-1)$, decide membership in both named BLG groups and give the endpoints of their lifted loops. Explain which global information is invisible to the local bifundamental action. Equivalent exact rational notation is acceptable.

5. **VIII.3.E5: Two routes at $k = 2$.** For $N = 2$ and $k = 1, 2, 3$, find the image of multiplication by two on $\mathbb{Z}_k$ and give a preimage or an obstruction for every residue. At $k = 2$, enumerate the matrices generated by $s = \mathrm{diag}(1, -1)$ and $a = \left(\begin{smallmatrix} 0 & 1 \\ -1 & 0 \end{smallmatrix}\right)$, taking the rightmost matrix to act first. Identify both sign flips and exchange. Add the five polynomials in (VIII.3.34) at $z = 1$ and also add the independent three printed contributions following (VIII.3.36). Explain why neither the order-eight matrix action nor these additions establish full quantum equivalence. Generator words related by the group relations are acceptable.

Take-home message of this chapter

The full compact ABJM group gives independent $\mathbb{Z}_k$ phases for separated membranes and integral primitive magnetic fluxes. The $(1, 0)$ monopole has central flux $1/2$ and needs k scalar B insertions to cancel its Chern–Simons charge. At $k = 1, 2$, two-scalar charged families can supply the protected $10 \oplus \overline{10}$ components used in the sourced current-enhancement argument. Their existence and survival are physical inputs beyond charge algebra. Low-rank BLG comparisons gain force from a named global form, flux-resolved index terms and a sphere number, while remaining finite tests of conjectured quantum identifications.

Status and sources

Sources by section. Source coordinates and scope qualifications follow.

§VIII.3.1. The finite orbit is conditional [MATH] on the full compact product and sourced diagonal-vacuum premise [GEO-X] in the local position sector; Aharony et al. 2008, §2.3. Quantum completeness is [FOLK].

§VIII.3.2. Primitive flux and Gauss-law arithmetic are conditional [MATH] under the restricted BLG trace and compact-group frame; radial-state inputs remain source premises, Bashkirov and Kapustin 2011b, §§2.2–2.7.

§VIII.3.3. Scalar partitions are conditional [MATH] on the sourced bare energy and mode spectrum; selected shortening is [BPS:1/2|short] only in the stated four-real-supercharge subalgebra, Bashkirov and Kapustin 2011b, Tables 2–3.

§VIII.3.4. Representation arithmetic is conditional [MATH]; extra physical currents require source-supported survival and nonzero descendants, Bashkirov and Kapustin 2011b, §§2.8–2.11 and Appendix B.

§VIII.3.5. Finite-group and trace conversions are conditional [MATH] under the restricted BLG trace and compact-group frame; the restricted rank-two pairings remain [CONJ+], Lambert and Papageorgakis 2010, equations (59)–(65).

§VIII.3.6. Index-coefficient additions and the common-integral ratio are conditional [MATH]; physical protected comparisons remain [CONJ+] with the stated source and contact limitations, Bashkirov and Kapustin 2011a, Tables 4–8 and Honda and Honma 2013, Appendix A.

§VIII.3.7. Five bounded exercises reuse the preceding conditional [MATH] calculations under the restricted BLG trace and compact-group frame and Chern–Simons trace and levels (Aharony et al. 2008, §2.3; Bashkirov and Kapustin 2011b, §§2.2–2.11; Lambert and Papageorgakis 2010, equations (59)–(65)).

The compact one-brane quotient in §VIII.3.1 reuses Chapter VIII.2 and the primitive compact flux and dual-scalar convention. The generic diagonal vacuum and massive off-diagonal premise are in Aharony et al. 2008, arXiv:0806.1218v4, §2.3, equations (2.7)–(2.9), printed pp. 7–9, physical PDF pp. 8–10. Equation (VIII.3.4) is conditional **[MATH]** on that premise and on the full compact product. Completeness of the quantum symmetric-product moduli is a non-load-bearing **[FOLK]** expectation, not a result at coincidence. The same source's §2.4, printed pp. 9–12, footnotes 6 and 8, retracts the earlier general Wilson-endpoint picture and cautions that its moduli-based large-rank chiral-spectrum argument is not an independent duality test. The distinction between compact global forms is in §§2.5–2.6, printed pp. 13–15.

The primitive flux and component Gauss laws (VIII.3.9)–(VIII.3.13) use spinor conventions, arrow orientation, Chern–Simons trace and levels, quiver gauge groups and Chern–Simons matter conventions and the restricted restricted BLG trace and compact-group frame normalization and charge translation. Their exact arithmetic, the center decomposition, (VIII.3.16), partitions, branchings and finite group action are conditional **[MATH]**. The bare energy (VIII.3.14), zero-flux scalar mode and $E = R$ radial assignments are sourced physical inputs from Bashkirov and Kapustin 2011b, arXiv:1007.4861v1, §§2.2–2.7, equations (9)–(13), printed pp. 4–10, Table 2 printed p. 8, and Appendix A equations (36)–(53), printed pp. 23–27. The common regulator, gauge fixing and mode spectrum are not consequences of the integral-square identity.

Equation (VIII.3.19) uses §§2.8–2.9, equations (17)–(20), printed pp. 10–12; its residual singlet and flavor symmetry are a manual argument outside the finite exercise checker.

The selected scalar-shortening statement uses the fixed four-real-supercharge $\mathcal{N} = 2$ subalgebra only and is **[BPS:1/2|short]** with denominator 2/4, conditional on the undeformed unitary conformal vacuum and the source continuation. The dimension-1/2 free-field inference is conditional on that survival and scalar unitarity. The physical current bridge in §VIII.3.4 follows Bashkirov and Kapustin 2011b, §§2.8–2.11, Table 3, equations (13)–(22), printed pp. 10–14, with the recombination exclusions in Appendix B printed p. 28, physical PDF p. 29. It requires survival under the radial deformation, restored Spin(6), absent partners and nonzero vector-descendant norms. The bare radial energy and current bridge come from the cited spectrum; the conditional spin-one current-bound lemma gives conservation only after a nonzero primary exists. The arithmetic branchings do not certify these spectral premises. Chapter VIII.2's geometric spinor result under the specified geometric quotient and spin lift is separate.

The A_4 map and fundamental coefficient are in Van Raamsdonk 2008, arXiv:0803.3803v3, §3, printed p. 4. The original vector trace is in Bagger and Lambert 2008, arXiv:0712.3738v2, §3, equations (10), (15)–(16), printed pp. 5–6. the restricted BLG trace and compact-group frame admits only the restricted trace, global-form and $T_{\mathrm{BK}} = kt/2$ conventions, not protection or quantum equivalence. The gcd route and signed-permutation $k = 2$ action are in Lambert and Papageorgakis 2010, arXiv:1001.4779v3, equations (59)–(65), printed pp. 11–14. Its printed p. 13 body and footnote 4 conflict about the $k = 2$ group; the comparison used here is the simply connected one stated in its abstract, introduction and summary and tested by the later primary sources. The two precise $k = 1, 2$ pairings are **[CONJ+]** comparisons of the stated observables. The $k = 1$ comparison has moduli and source-reported finite-index directions; the $k = 2$ comparison additionally has the sphere number. Line sectors, discrete contacts, arbitrary manifolds and full OPEs remain untested.

The concrete choice Q_{12-} comes from Bashkirov and Kapustin 2011b, §2.2, printed p. 4 and Table 1 p. 5. The physical index trace definition is from Bashkirov and Kapustin 2011a, arXiv:1103.3548v1, §§4.1–4.2, equations (1)–(3), printed pp. 7–8, physical PDF pp. 8–9. The charge-resolved $k = 2$ coefficients in (VIII.3.34) are Tables 4–5, printed pp. 12–13; their additions are **[MATH]** only. The source-computed index comparison has no established preserved-real-supercharge fraction. Its $k = 1$ Tables 7–8, printed pp. 13–15, include the literal Table 7 exponent asymmetry $15z^4x^4$ and $15z^{-8}x^4$ in the zero-flux row; no silent correction is used. The Table 7 continuation on printed p. 14 also ends the $|3\rangle|3\rangle$ row with $16z^8x^4 + 16z^{-4}x^4$; Table 8 has $16x^4$ in the $T = 8$, $|7, -1\rangle|7, -1\rangle$ sector. Both literal discrepancies remain source caveats. The unequal-rank x^3 counterexample is in §4.1, printed p. 7 and Table 3 p. 12. Equation (VIII.3.37) follows Honda and Honma 2013, arXiv:1210.1371v3, Appendix A equations (A.1)–(A.6), printed pp. 17–18, physical PDF pp. 18–19. Its $Z_{SU}/Z_U = k/2$ is a conditional identity of the written common integral and stated measure; the physical S^3 interpretation imports localization, contour and contact choices. Five bounded exercises test submitted finite objects; their manual physical explanations and the source-only spectral premises are outside that grading. S-035 records the localization machinery and S-036 the radial monopole spectrum and operator ring beyond this chapter's calculations.

References

Aharony, O. et al. (2008). "N=6 superconformal Chern-Simons-matter theories, M2-branes and their gravity duals". In: *JHEP* 10, p. 091. DOI: 10.1088/1126-6708/2008/10/091. arXiv: 0806.1218 [hep-th].

Bagger, J. and N. Lambert (2008). "Comments on multiple M2-branes". In: *JHEP* 02, p. 105. DOI: 10.1088/1126-6708/2008/02/105. arXiv: 0712.3738 [hep-th].

Bashkirov, D. and A. Kapustin (2011a). "Dualities between N = 8 superconformal field theories in three dimensions". In: *JHEP* 05, p. 074. DOI: 10.1007/JHEP05(2011)074. arXiv: 1103.3548 [hep-th].

Bashkirov, D. and A. Kapustin (2011b). "Supersymmetry enhancement by monopole operators". In: *JHEP* 05, p. 015. DOI: 10.1007/JHEP05(2011)015. arXiv: 1007.4861 [hep-th].

Honda, M. and Y. Honma (2013). "3d superconformal indices and isomorphisms of M2-brane theories". In: *JHEP* 01, p. 159. DOI: 10.1007/JHEP01(2013)159. arXiv: 1210.1371 [hep-th].

Lambert, N. and C. Papageorgakis (2010). "Relating U(N)xU(N) to SU(N)xSU(N) Chern-Simons Membrane theories". In: *JHEP* 04, p. 104. DOI: 10.1007/JHEP04(2010)104. arXiv: 1001.4779 [hep-th].

Van Raamsdonk, M. (2008). "Comments on the Bagger-Lambert theory and multiple M2-branes". In: *JHEP* 05, p. 105. DOI: 10.1088/1126-6708/2008/05/105. arXiv: 0803.3803 [hep-th].

Chapter VIII.4

ABJ theory and fractional M2-branes

VIII.4.1 One circle, two ranks

An M2-brane can move on $\mathbb{C}^4/\mathbb{Z}_k$ without carrying the discrete charge of a fractional brane. In the type-IIB circle construction this distinction is visible before any flux calculation. Put N D3-branes around the circle and suspend L additional D3 segments directly between an NS5 and a $(1,k)_5$, where the charge order is (NS,D). The winding branes pass through both intervals. We choose the first interval to have bare level $+k$ and the second $-k$, and put the extra segments in the second interval. The complete compact gauge theory in this chapter is

$$\mathcal{T}_{N,L,k} = U(N)_{+k} \times U(N+L)_{-k}, \qquad k \in \mathbb{Z}_{>0}, \quad N, L \in \mathbb{Z}_{\geq 0}. \tag{VIII.4.1}$$

The orientations are those of Section 2.3: D3 along 0126, NS5 along 012345, and the other fivebrane along $012[3,7]_\theta[4,8]_\theta[5,9]_\theta$, on the same equal-angle, zero-axion branch. Both factors are full unitary groups and the levels are bare fundamental-trace levels. Calling the second factor simply $U(L)$ would erase the N mobile pairs.

The ordered ranks can be read one interval at a time. If n_+ and n_- count D3 segments in the intervals with bare levels $+k$ and $-k$, the winding stack contributes equally and the direct stack contributes only to the latter:

$$n_+ = N, \qquad n_- = N + L, \qquad n_- - n_+ = L. \tag{VIII.4.2}$$

This subtraction identifies a candidate fractional sector. It does not establish that a suspended stack preserves supersymmetry or that crossing-related theories share an infrared fixed point. The circle is the x^6 direction: a winding D3 passes through both intervals, while a direct segment ends on the fivebranes.

At a generic point where the N pairs separate, the unmatched colors leave a pure $\mathcal{N} = 3$ $U(L)_{-k}$ Yang–Mills–Chern–Simons sector. The sourced bosonic shift of its nonabelian level is $K \mapsto K - L \operatorname{sign} K$. For $K = -k$ it gives

$$K_{SU(L),\mathrm{bos}} = -k + L = -(k - L). \tag{VIII.4.3}$$

This is the $SU(L)$ level. The central $U(1)$ level has no corresponding shift. For example, at $k = 5, L = 2$ the bare second-node level -5 becomes the nonabelian bosonic level -3. At $L = k$ this nonabelian level reaches zero, while the central abelian level is not shifted by this calculation:

$$(K, L) = (-5, 2) \Rightarrow K_{SU(2),\mathrm{bos}} = -3, \qquad L = k \Rightarrow K_{SU(k),\mathrm{bos}} = 0. \tag{VIII.4.4}$$

The generic-separation argument probes a particular pure sector; it does not classify the strongly coupled theory at the origin of the mobile branch. The source vacuum and index argument for the separated pure sector requires $L \leq k$. Independently, the generalized s-rule permits at most k supersymmetric direct D3 segments between these particular fivebranes. Crossing them creates k segments. Together these physical inputs give the direct-segment regulator window $0 \leq L \leq k$. Rank arithmetic alone gives neither the s-rule nor a quantum vacuum theorem. Other D3 configurations can wind around the circle; the direct-segment bound does not classify them. Extrapolating to the absence of every $L > k$ unitary superconformal fixed point is a conjecture in the source construction.

The original ABJ paper prints its rank difference l_A on the *larger positive-level* node. Its proposed crossing relation is

$$U(N + l_A)_{+k} \times U(N)_{-k} \;\simeq\; U(N)_{+k} \times U(N + k - l_A)_{-k}, \qquad L = k - l_A. \tag{VIII.4.5}$$

The equality sign denotes a proposed infrared relation, not equality of the displayed ultraviolet Lagrangians. The crossing preserves the winding stack and replaces l_A direct segments in one interval by $k - l_A$ in the other:

$$(n_+, n_-)_{\mathrm{before}} = (N + l_A, N), \qquad (n_+, n_-)_{\mathrm{after}} = (N, N + k - l_A). \tag{VIII.4.6}$$

For $N = 4$, $k = 5$, $l_A = 2$, its two ordered rank pairs are $(6, 4)$ at levels $(+5, -5)$ and $(4, 7)$ at those same ordered levels; the chapter's L is 3. Relabeling l_A as L without the crossing would give a different ordered theory. Parity also reverses the orientation and is a separate operation.

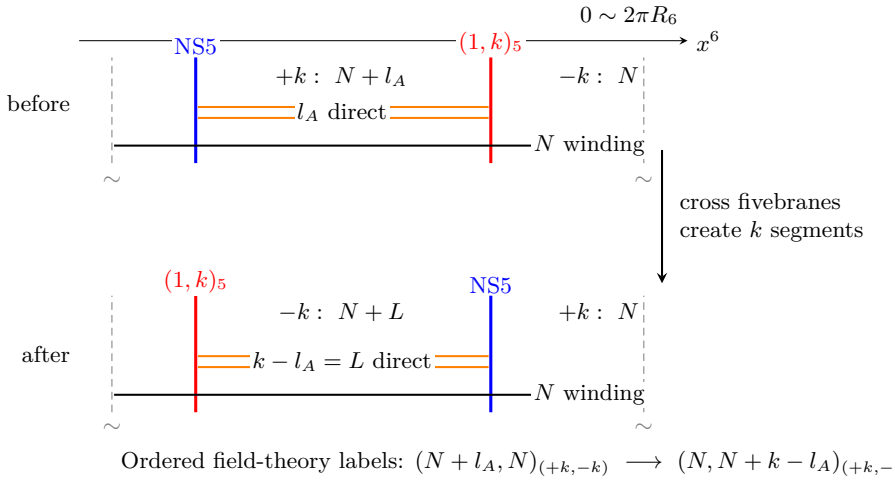


Figure VIII.4.1: The source crossing in the direct-segment regulator. Both panels contain the same two fivebranes and the same N winding D3-branes. In the upper panel l_A direct segments occupy the positive-level interval. Move the $(1,k)_5$ toward the NS5 in decreasing x^6, initially shortening the direct interval. Crossing creates k direct segments and leaves $k - l_A = L$ in the negative-level interval of the lower panel. The vertical D3 separation only distinguishes stacks; it is not a transverse-position modulus, and the vertical fivebrane strokes suppress their worldvolume orientations. The ordered node levels remain $(+k, -k)$ when their intervals are renamed as shown; the ordered ranks are $(N + l_A, N)$ and $(N, N + k - l_A)$, respectively. The creation and supersymmetry bound are brane inputs, while identification of the infrared field theories is proposed.

The fractional sector also has a discrete bulk label. The seven-dimensional lens space $S^7/\mathbb{Z}_k$ has one cell in each dimension from zero to seven, with its integral cellular boundary maps alternating between zero and multiplication by k. The relevant part of the cellular chain complex is

$$C_4 \xrightarrow{\partial_4 = k} C_3 \xrightarrow{\partial_3 = 0} C_2, \qquad C_j \simeq \mathbb{Z}. \tag{VIII.4.7}$$

A three-cycle can close while k copies bound a four-chain. Thus $H_3(S^7/\mathbb{Z}_k, \mathbb{Z}) = \mathbb{Z}_k$, and the universal coefficient sequence gives $H^4(S^7/\mathbb{Z}_k, \mathbb{Z}) = \mathrm{Ext}(H_3, \mathbb{Z}) = \mathbb{Z}_k$. In the selected brane dictionary we assign $t = [L]$. This group has k classes, and the proposed endpoint identification relates $L = k$ to $L = 0$, possibly with a topological sector. Therefore $L = 0, \ldots, k-1$ gives k candidate rank labels in this branch. Counting cohomology classes alone does not prove their rank assignment or the endpoint field-theory equivalence. The counts differ before the endpoint proposal:

$$\#H^4(S^7/\mathbb{Z}_k, \mathbb{Z}) = k, \qquad \#\{L : 0 \le L \le k\} = k + 1. \tag{VIII.4.8}$$

For $k = 3$ there are three classes $[0], [1], [2]$ but four direct counts $0, 1, 2, 3$. At $k = 1$ the

torsion group is trivial, and at $k = 2$ it has two classes. The larger-rank endpoint still needs the proposed identification even in these small cases.

VIII.4.2 Which charge does a rank measure?

A rank labels a brane construction, whereas fluxes depend on both the field strength and a choice of B-field representative. We use one fixed type-IIA orientation throughout. Let J be normalized by $\int_{\mathbb{CP}^j} J^j = 1$ for $j = 1, 2, 3$, let $\ell_s^2 = \alpha'$ and $R_{11} = g_s \ell_s$, and set

$$F_2 = 2\pi k R_{11} J, \qquad B_2 = (2\pi\ell_s)^2 b J, \qquad b \sim b + 1. \tag{VIII.4.9}$$

The b period is dimensionless in this normalization. D4 and D2 flux integrals below have been divided by $(2\pi\ell_s)^3 g_s$ and $(2\pi\ell_s)^5 g_s$, respectively. In the chosen D4 orientation $P_4 = \mu_4 \int_{\mathbb{CP}^2} (-\widehat{F}_4)$ with $\mu_4 = [(2\pi\ell_s)^3 g_s]^{-1}$. These units give $\mu_4 \int B_2 \wedge F_2 = kb$ and the analogous D2 quadratic term $kb^2/2$. They matter when comparing papers with different rank order or a string-unit convention.

The distinction between the two flux definitions can be seen before imposing the infrared condition. Schematically the Page forms absorb explicit B_2 terms from the gauge-invariant RR strengths; in the fixed source convention relevant here,

$$\widehat{F}_4 = \widetilde{F}_4 + B_2 \wedge F_2, \qquad \widehat{F}_6 = *\widetilde{F}_4 - B_2 \wedge (-\widehat{F}_4) - \frac{1}{2} B_2^2 \wedge F_2. \tag{VIII.4.10}$$

The wedge terms explain why a change of B representative shifts Page integrals while leaving Maxwell fields unchanged. They also fix the relative linear and quadratic powers of b that appear below. Neither a rank count nor torsion cohomology supplies the curvature contribution to the D2 charge.

The half-unit in the D4 charge has a physical origin. A D4 wrapped on $\mathbb{CP}^2$ is the di-baryon particle and encounters $w_2(\mathbb{CP}^2) = H \bmod 2 \neq 0$. The Freed–Witten condition requires a half-integral worldvolume flux. In the source's signed representative write $F = (2\pi\ell_s)^2 f J$ with $f = -1/2$. Its di-baryon endpoint equation is $L = P_4 - kf = P_4 + k/2$, and hence

$$P_4 = L - \frac{k}{2}. \tag{VIII.4.11}$$

This is an affine Page charge. For odd k it is half-integral in this representative. It is useful to leave the signed half-flux in the endpoint equation for one step:

$$L = P_4 - kf, \qquad f = -\frac{1}{2} \quad \Longrightarrow \quad L = P_4 + \frac{k}{2}. \tag{VIII.4.12}$$

The nonspin cycle supplies the half-integral class; the sign of its selected representative also uses the orientation and the source brane construction. A different signed representative must be accompanied by the corresponding Page-frame change. The choice $f = -1/2$ is not obtained merely by renaming the torsion class.

We distinguish the integer rank label $P_2^{\mathrm{rank}} = N$ from the inferred D2 Page flux in the corrected source prescription. The latter includes a D6 induced term $k/8$ and an orbifold curvature contribution

$$C_k = -\frac{k - k^{-1}}{24}, \qquad P_2^{\mathrm{flux}} = N + \frac{k}{8} + C_k = N + \frac{k}{12} + \frac{1}{24k}. \tag{VIII.4.13}$$

The coefficient C_k comes from the specified curvature inflow calculation. Neither it nor the FW shift follows from classical rank counting. The corrected Page expression is a source prescription; we do not infer a complete quantum Page lattice from it.

The two corrections entering the D2 Page-flux prescription should remain visible separately:

$$\frac{k}{8} + C_k = \frac{k}{8} - \frac{k - k^{-1}}{24} = \frac{k}{12} + \frac{1}{24k}. \tag{VIII.4.14}$$

The first term is induced by the source's D6/Freed–Witten bookkeeping and the second is the orbifold curvature inflow. Their sum is algebraic, but the two physical inputs are independent. This distinction will matter in the baryon-vertex check, which retains only the leading $k/12$ part.

The gauge-invariant Maxwell charges combine these Page values with b.

$$Q_4^M = P_4 + kb, \qquad Q_2^M = P_2^{\text{flux}} + bP_4 + \frac{k}{2}b^2. \tag{VIII.4.15}$$

The Maxwell flux can be fractional and spread through the bulk. The Page charge instead changes under a large B gauge transformation. A wrapped probe's induced source charge is a local wall quantity and has a third definition. Figure VIII.4.2 keeps these uses of the word charge apart.

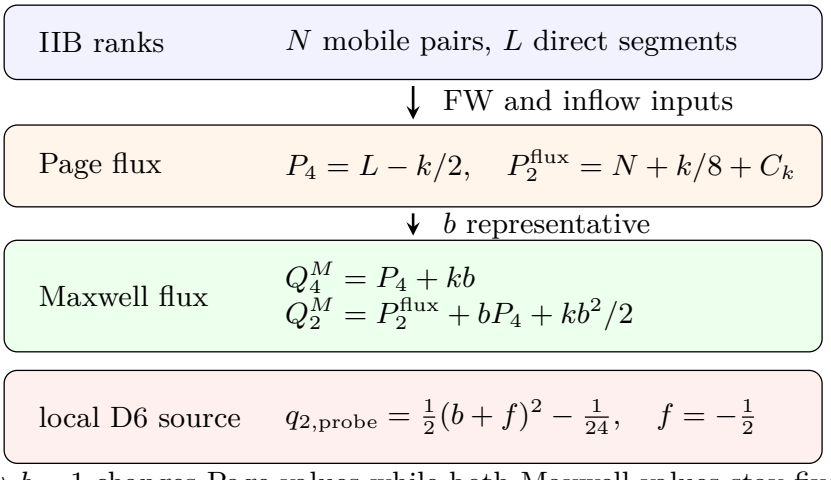


Figure VIII.4.2: The selected type-IIA charge relations with $\int_{\mathbb{CP}^j} J^j = 1$. Rank labels (N, L) specify the IIB diagram; the FW-shifted Page values depend on a B representative; Maxwell fluxes remain fixed when that representative changes. A wrapped D6 has a local Wess–Zumino and curvature source charge $q_{2,\text{probe}}$, shown separately from the background D2 Maxwell flux. Arrows encode the displayed definitions and physical inputs, not an exact wall-jump equation.

A quick algebraic test shows why Page and Maxwell values cannot be interchanged. At arbitrary b the derivative of the displayed Maxwell polynomial with respect to the representative is

$$\frac{\partial Q_2^M}{\partial b} = P_4 + kb = Q_4^M. \tag{VIII.4.16}$$

This is a derivative of a chosen polynomial at fixed Page data, not a physical variation at fixed Maxwell background. It makes the special role of vanishing internal four-form transparent: the selected value of b is a stationary point of that polynomial in this fixed Page frame.

The selected infrared $AdS_4 \times \mathbb{CP}^3$ background imposes the additional physical condition of vanishing internal Maxwell four-form, $Q_4^M = 0$. Equations (VIII.4.11) and (VIII.4.15) then fix a representative

$$b_0 = \frac{1}{2} - \frac{L}{k}, \qquad Q_4^M(b_0) = 0. \tag{VIII.4.17}$$

This condition is an IR ansatz, not an algebraic identity for arbitrary backgrounds. In this frame the proposed torsion label is $[L]$ and the holonomy is b_0 mod 1; the holonomy alone does not choose a Page representative. The older unshifted ABJ assignment $b_A = l_A/k$ becomes $1 - L/k$ after (VIII.4.5); it differs by a half-unit from (VIII.4.17).

Completing the square in the same prescription is a useful intermediate calculation:

$$Q_2^M = P_2^{\text{flux}} - \frac{P_4^2}{2k} + \frac{(P_4 + kb)^2}{2k}. \tag{VIII.4.18}$$

At the selected infrared point $Q_4^M = 0$, only the first two terms survive. This exposes which input actually makes the final expression symmetric under $L \leftrightarrow k - L$: the square of $P_4 = L - k/2$. It does not derive parity or an infrared duality.

Now insert (VIII.4.17) into the D2 relation. Keeping the source's curvature term visible, we find

$$\begin{aligned} Q_2^M &= N + \frac{k}{8} + C_k + \left(\frac{1}{2} - \frac{L}{k}\right)\left(L - \frac{k}{2}\right) + \frac{k}{2}\left(\frac{1}{2} - \frac{L}{k}\right)^2 \\ &= N + \frac{L(k-L)}{2k} + C_k. \end{aligned} \tag{VIII.4.19}$$

This is exact algebra within the retained corrected prescription. It is a leading-geometry charge parameter, not an all-order quantum theorem for a finite-N radius. In eleven-dimensional units, the electric Maxwell flux is measured in $(2\pi)^6 \ell_p^6 = 2\kappa_{11}^2 T_{\text{M2}}$ units. The magnetic form $F_4/(2\pi\ell_p)^3$ has a shifted lattice on a suitable smooth spin filling.

In particular, for the two direct-segment endpoints the completed square gives

$$Q_2^M(N,0,k) = Q_2^M(N,k,k) = N + C_k, \qquad P_4(N,k,k) - P_4(N,0,k) = k. \tag{VIII.4.20}$$

The equal Maxwell value is an algebraic consequence of the corrected prescription. The two Page representatives and the corresponding field-theory descriptions still require the separately proposed endpoint relation.

A torsion C_3 holonomy on $S^7/\mathbb{Z}_k$ is invisible to local de Rham F_4, so it cannot be read from that form integral alone.

VIII.4.3 A rational example and a change of representative

The formulas become less abstract at $(N, L, k) = (10, 1, 3)$. Equation (VIII.4.17) gives $b_0 = 1/6$; the FW and curvature terms give $P_4 = -1/2$ and $C_3 = -1/9$. Thus

$$P_2^{\text{rank}} = 10, \quad P_2^{\text{flux}} = 10 + \frac{3}{8} - \frac{1}{9} = 10 + \frac{19}{72}, \quad Q_4^M = -\frac{1}{2} + 3\left(\frac{1}{6}\right) = 0, \tag{VIII.4.21}$$

and direct substitution into the second Maxwell relation gives

$$Q_2^M = 10 + \frac{19}{72} - \frac{1}{12} + \frac{1}{24} = \frac{92}{9}. \tag{VIII.4.22}$$

The rank 10, Page flux $10 + 19/72$ and Maxwell flux $92/9$ answer different questions. Their disagreement is the point of the calculation.

The numbers in this example are intentionally awkward: they prevent the rank label from hiding inside an integer flux. The torsion contribution to the final Maxwell expression is $L(k - L)/(2k) = 1/3$, and the curvature term is $-1/9$. These combine to a net shift $2/9$ above N:

$$\frac{L(k-L)}{2k} = \frac{1}{3}, \qquad C_3 = -\frac{1}{9}, \qquad Q_2^M - N = \frac{2}{9}. \tag{VIII.4.23}$$

The local wall source charge computed in the next section will be $1/72$, smaller and of a different type. Thus none of N, P_2^{flux}, Q_2^M, and $q_{2,\text{probe}}$ should be substituted for another just because all carry a D2 label.

For a large gauge change $b' = b - 1$ at fixed physical Maxwell flux, (VIII.4.15) requires

$$P_4' = P_4 + k, \qquad (P_2^{\text{flux}})' = P_2^{\text{flux}} + P_4 + \frac{k}{2}. \tag{VIII.4.24}$$

The D4 transformation follows first from $Q_4^{M\prime} = Q_4^M$:

$$P_4' + k(b-1) = P_4 + kb \quad \Longrightarrow \quad P_4' - P_4 = k. \tag{VIII.4.25}$$

For the D2 charge, insert this result and expand every term rather than assuming an analogous shift:

$$\begin{aligned} 0 = Q_2^{M\prime} - Q_2^M = P_2^{\text{flux}\prime} - P_2^{\text{flux}} + (b-1)(P_4 + k) - bP_4 \\ + \frac{k}{2}\big[(b-1)^2 - b^2\big] = P_2^{\text{flux}\prime} - P_2^{\text{flux}} - P_4 - \frac{k}{2}. \end{aligned} \tag{VIII.4.26}$$

The cancellation of the b terms is the useful check. It shows that the Page shift is a bookkeeping change compatible with one physical Maxwell background.

There is a second way to check the transformation that avoids expanding the b polynomial twice. The completed-square form (VIII.4.18) has two pieces: one depends on the Page representative and the other on the Maxwell four-charge. Under the derived Page shift, the representative-dependent combination is actually invariant:

$$P_2^{\text{flux}\prime} - \frac{(P_4')^2}{2k} = P_2^{\text{flux}} + P_4 + \frac{k}{2} - \frac{(P_4 + k)^2}{2k} = P_2^{\text{flux}} - \frac{P_4^2}{2k}. \tag{VIII.4.27}$$

Since Q_4^M is also invariant, the completed-square equation immediately implies invariance of Q_2^M. This argument explains the cancellation structurally: the large gauge change moves explicit B dependence between the Page entries without changing the bulk Maxwell charge. It is still a statement about charge representatives. The operation neither creates a new dynamical vacuum nor decides whether a circular IIB configuration with additional winding segments exists. In particular, the change $L \mapsto L + k$ leaves the torsion residue fixed because it moves within one class of $\mathbb{Z}_k$; that fact is weaker than the proposed endpoint relation between quantum theories.

At fixed k the rank form of this transformation is

$$(N, L, b) \longmapsto (N + L, L + k, b - 1). \tag{VIII.4.28}$$

Indeed $P_4' = L + k - k/2 = P_4 + k$ and $(P_2^{\text{flux}})' = N + L + k/8 + C_k$. Substituting them into (VIII.4.15) gives $Q_4^{M\prime} = Q_4^M$ and $Q_2^{M\prime} = Q_2^M$. For the numerical background, the transformed Page values are

$$P_4' = -\frac{1}{2} + 3 = \frac{5}{2}, \qquad P_2^{\text{flux}\prime} = 10 + \frac{19}{72} - \frac{1}{2} + \frac{3}{2} = 11 + \frac{19}{72}. \tag{VIII.4.29}$$

Inserting $b' = -5/6$ gives an independent numerical check:

$$Q_4^{M\prime} = \frac{5}{2} + 3\left(-\frac{5}{6}\right) = 0, \qquad Q_2^{M\prime} = 11 + \frac{19}{72} - \frac{25}{12} + \frac{25}{24} = \frac{92}{9}. \tag{VIII.4.30}$$

The transformed pair is outside the chosen direct-segment regulator, yet the flux calculation remains well defined. This separation between the domain of an algebraic representative change and the domain of a brane vacuum is essential.

The torsion residue $[L]$ also stays fixed. In the worked example the new labels are $(N', L', k, b') = (11, 4, 3, -5/6)$, with the same Maxwell charges. This is a representative identity. Since $L' = 4 > 3$, it does not create an additional direct-segment SCFT. The related IIB fivebrane slide has its own geometric direction; the sign of b' here is fixed by the Maxwell equations.

One can also test the proposed rank-frame exchange against the charge polynomial without treating the test as a proof of duality. At fixed N, k, its torsion part obeys

$$\frac{L(k - L)}{2k} = \frac{(k - L)L}{2k}. \tag{VIII.4.31}$$

The symmetry is a property of this quadratic expression in the selected infrared frame. The crossing relation acts on ordered ranks and involves a physical fivebrane move; it cannot be reconstructed merely by observing this equality. For instance, both $L = 1$ and $L = 2$ at $k = 3$ give $1/3$, but the corresponding ordered ultraviolet rank pairs differ.

At $L = 0$, the selected IR representative has $b_0 = 1/2$, $P_4 = -k/2$, and $Q_2^M = N + C_k$. At $L = k$, (VIII.4.19) returns the same Maxwell value, while the direct-segment endpoint remains a distinct rank description before the proposed field-theory identification. The $k = 1$ curvature term vanishes. These limits check the algebra, but the endpoint equivalence and torsion-to-rank assignment still use the brane proposal.

The limits of the charge formula are particularly instructive when one varies the rank difference without changing the level. In the selected IR frame the quadratic part is nonnegative throughout the direct-segment window:

$$0 \le \frac{L(k-L)}{2k} \le \frac{k}{8} \qquad (0 \le L \le k), \tag{VIII.4.32}$$

where the maximum occurs at the midpoint when that midpoint is an allowed integer. This is a statement about the polynomial, not about stability of every point. At $k = 2$, for instance, the candidates $L = 0, 1, 2$ have quadratic contributions $0, 1/4, 0$; the endpoints are proposed to represent the same torsion class, while $L = 1$ represents the nonzero class. At $k = 1$, $C_1 = 0$ and the two direct counts $0, 1$ are proposed endpoint descriptions of the sole torsion class:

$$(k, L) = (2, 0), (2, 1), (2, 2): \quad \frac{L(k-L)}{2k} = 0, \frac{1}{4}, 0; \qquad C_1 = 0. \tag{VIII.4.33}$$

The computation makes the endpoint proposal legible but cannot prove it. The distinction is sharper outside the regulator. Continuing the same formula to $k = 3, L = 4$ gives

$$b_0 = -\frac{5}{6}, \qquad P_4 = \frac{5}{2}, \qquad Q_2^M = N - \frac{2}{3} - \frac{1}{9} = N - \frac{7}{9}. \tag{VIII.4.34}$$

These are consistent substitutions into the charge prescription. They do not demonstrate a supersymmetric direct-segment vacuum for four suspended D3-branes between the specified fivebranes. The earlier large-gauge representative with $(N', L') = (11, 4)$ makes this point especially concrete: its Maxwell flux equals the original $(10, 1)$ background even though its formal L' is outside the canonical window. A representative identity, a brane existence statement and a field-theory duality have different hypotheses.

VIII.4.4 A wrapped wall and the accuracy of the comparison

One wrapped D6 on the nonspin $\mathbb{CP}^2$ supplies a local check of the flux dictionary. Its Wess–Zumino coupling uses $B_2 + F$, while its curvature coupling contributes $-1/24$ to the D2 source charge in the chosen orientation. At $f = -1/2$ and $b = b_0$, $b_0 + f = -L/k$, so the local result is

$$q_{2,\mathrm{probe}} = \frac{1}{2}(b_0 + f)^2 - \frac{1}{24} = \frac{L^2}{2k^2} - \frac{1}{24}. \tag{VIII.4.35}$$

This is a source charge on the probe, not a Maxwell flux measured at infinity. Reversing the wall orientation reverses its induced D4 Page sign; in the displayed orientation the signed half-flux induces $-1/2$ D4 Page unit.

The square in the Wess–Zumino term is a local worldvolume operation. At the chosen infrared representative it becomes

$$b_0 + f = \left(\frac{1}{2} - \frac{L}{k}\right) - \frac{1}{2} = -\frac{L}{k}, \qquad \frac{1}{2}(b_0 + f)^2 = \frac{L^2}{2k^2}. \tag{VIII.4.36}$$

Its curvature contribution remains $-1/24$, independent of the rank polynomial's orbifold term. The D4 sign follows the orientation of the wall, so reversing the wall reverses that signed source charge; simply changing k in a background formula does not perform this orientation reversal.

We can independently take a finite difference of the retained background polynomial at fixed N, L, for $k > 1$ and $L \le k-1$ so both direct-segment configurations lie in their respective windows. The result is

$$\begin{aligned} Q_2^M(N,L,k) - Q_2^M(N,L,k-1) &= \frac{L^2}{2k(k-1)} - \frac{1}{24} - \frac{1}{24k(k-1)}, \\ \left[Q_2^M(k) - Q_2^M(k-1)\right] - q_{2,\mathrm{probe}} &= \frac{12L^2 - k}{24k^2(k-1)}. \end{aligned} \tag{VIII.4.37}$$

The finite-difference calculation can be followed term by term. Writing the selected background polynomial as

$$Q_2^M(N,L,k) = N + \frac{L}{2} - \frac{L^2}{2k} - \frac{k}{24} + \frac{1}{24k}, \tag{VIII.4.38}$$

the constant $N + L/2$ cancels when k changes by one. The remaining three contributions are

$$\begin{aligned} -\frac{L^2}{2}\left(\frac{1}{k} - \frac{1}{k-1}\right) &= \frac{L^2}{2k(k-1)}, \\ -\frac{k-(k-1)}{24} &= -\frac{1}{24}, \\ \frac{1}{24}\left(\frac{1}{k} - \frac{1}{k-1}\right) &= -\frac{1}{24k(k-1)}. \end{aligned} \tag{VIII.4.39}$$

This transparent subtraction prevents an apparently plausible but false replacement of the denominator $k(k-1)$ by k^2. That replacement is only a large-k approximation.

For $k = 3, L = 1$, the probe gives $1/72$ and the finite background difference gives $5/144$, leaving $1/48$. The source wall argument compares the leading large-k pieces, which agree. Equation (VIII.4.37) is an exact finite difference *of the displayed background polynomial*; it does not establish an exact finite-k physical wall-jump law. In particular, the nonzero remainder cannot be erased by calling both expressions a D2 charge.

The order of the comparison can be read from the exact remainder in (VIII.4.37). If L stays fixed as k grows, the terms scale differently from a sequence with L/k fixed:

$$\Delta Q_2^M - q_{2,\mathrm{probe}} = O(k^{-2}) \quad (L \text{ fixed}), \qquad = O(k^{-1}) \quad (L/k \text{ fixed}). \tag{VIII.4.40}$$

The leading probe comparison must state which regime it uses. For example $L = 1$ at $k = 3$ is far from an asymptotic test, so its $1/48$ remainder is a diagnostic of the distinction, not a failure of an exact wall law that was never asserted. The calculation also requires $L \le k-1$ so that the two compared direct-segment configurations lie in their respective windows.

The numerical wall comparison can be made without subtracting the closed formula. Keeping $N = 10, L = 1$, the adjacent background has $k = 2$ and remains inside the

direct-segment window:

$$Q_2^M(10,1,2) = 10 + \frac{1}{4} - \frac{1}{16} = \frac{163}{16}, \qquad Q_2^M(10,1,3) = \frac{92}{9}. \tag{VIII.4.41}$$

Their difference is $92/9 - 163/16 = 5/144$, while the wrapped D6 source is $1/72 = 2/144$. The remaining $3/144 = 1/48$ is exactly the finite-polynomial remainder. One must keep the same N, L during the subtraction: changing the rank labels at the same time would compare a different path through the family of backgrounds.

The two wrapped D6 computations also have different geometrical jobs. The wall D6 wraps the nonspin $\mathbb{CP}^2$ and spans a codimension-one object in the noncompact theory, so the induced D2 charge in (VIII.4.35) is localized on that probe. The baryon vertex wraps $\mathbb{CP}^3$ and is a particle-like object to which fundamental strings may attach. Its endpoint count depends on the integrated Page bookkeeping and the curvature term on this different worldvolume. The shared D6 label therefore does not make their curvature terms interchangeable. One may use the wall computation as a leading consistency check of how the background charge changes when the flux level changes, and the baryon computation as a leading consistency check of an integer endpoint count. Neither computes a complete finite-k quantum observable by itself.

A second wrapped-brane check uses a D6 baryon vertex on $\mathbb{CP}^3$. Its source curvature term is $-k/12$. Applied to the leading Page expression $N + k/12$, it leaves N string endpoints. If we instead retain the full polynomial (VIII.4.13), the same displayed subtraction leaves

$$\left(N + \frac{k}{12} + \frac{1}{24k}\right) - \frac{k}{12} = N + \frac{1}{24k}. \tag{VIII.4.42}$$

The truncation can be displayed without conflating it with the wall result:

$$P_{2,\mathrm{lead}}^{\mathrm{flux}} - \frac{k}{12} = N, \qquad P_2^{\mathrm{flux}} - P_{2,\mathrm{lead}}^{\mathrm{flux}} = \frac{1}{24k}, \quad P_{2,\mathrm{lead}}^{\mathrm{flux}} = N + \frac{k}{12}. \tag{VIII.4.43}$$

The first relation is the source's leading string-endpoint cancellation. The second records the term kept in the corrected flux polynomial but not evaluated by that leading baryon analysis. A physical number of string endpoints would require the complete worldvolume and bulk treatment at the same order.

No finite-k completion of that baryon calculation has been established here. The remainder is a comparison of truncated and retained expressions, not a prediction of a fractional number of physical strings.

VIII.4.5 Historical variables and the remaining QFT question

The historical eleven-dimensional expression of Bergman and Hirano uses a torsion label l_B and contains $l_B^2/(2k) + C_k$. For a nonendpoint comparison through the proposed ABJ map, $l_B = k - L \pmod k$. Keeping the same N, k and no unprovided rank offset, its difference from the selected AHHO/DMP charge is

$$\left[N + \frac{(k-L)^2}{2k} + C_k\right] - \left[N + \frac{L(k-L)}{2k} + C_k\right] = \frac{(k-L)(k-2L)}{2k}. \tag{VIII.4.44}$$

For $k = 3, L = 1$, $l_B = 2$, the historical expression gives $95/9$, versus $92/9$ in (VIII.4.22); the difference is $1/3$. This is a located disagreement between finite expressions after the stated conditional map. The FW-supported AHHO prescription, subsequently used by Drukker, Mariño and Putrov, is the selected physical rank-to-flux dictionary here. The historical M-theory calculation has not been fully reconciled at fixed shifted quantum charge conventions. Its note on a possible parity-anomaly half-shift does not by itself turn the positive square into the AHHO quadratic term. In particular, the auxiliary disk-bundle filling used in the historical calculation has a spin subtlety at odd k, so a smooth-spin flux rule cannot simply be applied to it without further work.

The historical comparison also has a simple falsification test. Merely replacing l_B by L would give

$$\left[N + \frac{L^2}{2k} + C_k\right] - Q_2^M = \frac{L(2L-k)}{2k}, \tag{VIII.4.45}$$

which is a different expression from (VIII.4.44). For $k = 3, L = 1$ it yields $-1/6$ rather than $1/3$. This difference is a quick way to detect a silent frame swap. The source-level map $l_B = k - L$ follows a proposed crossing; it is neither a renaming nor a proof that the two historical charge conventions coincide.

The discrepancy formula also has zeros, and these zeros are useful controls rather than a reconciliation. At the midpoint of an even-level window, $L = k/2$, the two displayed torsion polynomials agree under the conditional historical map:

$$\left.\frac{(k-L)(k-2L)}{2k}\right|_{L=k/2} = 0. \tag{VIII.4.46}$$

For $k = 2, L = 1$, both finite expressions evaluate to $N + 3/16$ because $C_2 = -1/16$ and the quadratic contribution is $1/4$. Their agreement at that one class does not identify the full charge lattices or resolve the odd-k filling issue. Conversely, $k = 3, L = 1$ produces a nonzero difference. A good source comparison needs both kinds of test: a coincidence can reveal a symmetry of the algebra, while a counterexample shows why that symmetry is insufficient as a general physical dictionary.

The chapter's evidence therefore has a definite hierarchy. The ordered UV Lagrangian specifies a theory; the generic separated pure sector and s-rule constrain one brane regulator; the FW-corrected flux equations calculate a conditional background parameter; and the crossing suggests an infrared relation. A direct test of the last step would have to match observables sensitive to global data, such as line-operator sectors or contact terms, in a common convention. The Maxwell polynomial alone is too coarse for that task, even when it agrees at the endpoints or midpoint. Likewise, a leading supergravity radius comparison cannot settle a finite-rank partition function. These are distinct questions for the later protected-observable and large-N chapters.

The full infrared field-theory relation in (VIII.4.5) remains a **conjectural** global statement. The fivebrane crossing tests ordered ranks, the torsion and Maxwell calculations test the selected charge assignment, and parity provides another limited consistency check. They do not establish equivalence of all line operators, contact terms, partition functions or possible decoupled topological sectors. The proposed absence of an out-of-window unitary fixed point also needs dynamics beyond the direct-segment s-rule. Chapter 2 constructed the equal-rank orbifold theory and Chapter 3 followed its mobile

branch; the extra suspended segments here supply the new discrete sector. Chapter 9 treats relevant mass deformations, while Chapters 11 and 12 provide protected and large-N observables. Those later comparisons must keep the brane picture, a protected observable, and a quantum endpoint distinct.

VIII.4.6 Exercises

The four submitted calculations use the fixed full-unitary AHHO frame, exact rational numbers and the declared source premises. Give the requested exact values and explain their physical meaning in a written argument.

1. **Crossing and rank order.** Start from the printed ABJ theory $U(N + l_A)_{+k} \times U(N)_{-k}$ at $N = 4$, $k = 5$, $l_A = 2$. Give the ordered ranks and levels of the proposed partner, its chapter variable L and its torsion residue. Identify the generalized s-rule and proposed endpoint relation as physical premises. Explain why the rank equation alone does not prove an infrared equivalence. In the companion form for this problem, the input field L denotes l_A, while the answer field L denotes $k - l_A$.

2. **Four kinds of charge.** For $(N, L, k) = (10, 1, 3)$ calculate b_0, P_4, P_2^{rank}, P_2^{flux}, Q_4^M, Q_2^M, C_k and the local wrapped-D6 D2 source charge. State separately that the FW half-flux comes from nonspin $\mathbb{CP}^2$ and that the curvature terms use orbifold inflow and the D6 worldvolume coupling. Compare the D6 value with the finite background difference by hand and identify the approximation under which the wall argument is used.

3. **One background, two Page representatives.** With symbolic $k > 0, N, L, b$, impose $b' = b-1$ and fixed Q_4^M, Q_2^M. Derive ΔP_4, ΔP_2^{flux}, ΔN and ΔL, then verify both Maxwell residuals vanish. Express the changes in the basis $(N, L, k, b, 1)$. Explain why the formal transformed pair need not be a direct-segment SCFT.

4. **A source comparison with a domain test.** At $k = 3, L = 1, N = 10$, use the proposed ABJ map to determine l_B, evaluate the BH and AHHO expressions and their difference, and evaluate the AHHO polynomial formally at $L = 4$. State why the BH comparison remains unresolved at the full M-theory level while the FW-corrected AHHO/DMP frame is the one used here. Explain why evaluating a polynomial outside the direct-segment window is not a fixed-point argument.

Take-home message of this chapter

For the declared unequal-rank theory, N counts mobile pairs and $[L] \in \mathbb{Z}_k$ is the proposed fractional sector. In the selected FW-corrected IIA frame the IR charge is $Q_2^M = N + L(k - L)/(2k) - (k - k^{-1})/24$, conditional on the wrapped-brane and vanishing internal four-form inputs. Page flux, Maxwell flux and a local wrapped-wall charge have different definitions. The direct-segment window and the proposed infrared rank relation require physical brane and quantum premises beyond the charge algebra.

Status and sources

§VIII.4.1. [**MATH**] is the ordered-rank and nonabelian-level arithmetic conditional on the full compact group and source shift. The direct-segment s-rule and proposed infrared relation are [**CONJ+**]; [**MATH**] counts torsion classes, while [**CONJ+**] assigns $[L]$ to a physical sector. Aharony, Bergman, et al. 2008, arXiv:0807.4924v3, §§2.1–2.2, Figures 1–2 and (2.1), printed pp. 3–8 / PDF pp. 4–9; Chern–Simons trace and levels, the compact ABJM and membrane frame and the ordered ABJ charge frame.

§VIII.4.2. The signed Freed–Witten half-flux and orbifold inflow use [**ANOM**] evidence. The selected Page, Maxwell and infrared inputs use [**SUGRA**] evidence. [**MATH**] is the completed square conditional on those premises, not an all-order charge law. Aharony, Hashimoto, et al. 2010, arXiv v2, §2.5 (2.64)–(2.67) and §§3.3–3.4 (3.23)–(3.28), printed pp. 17, 30–32 / PDF pp. 18, 31–33; Bergman and Hirano 2009, arXiv:0902.1743v2 (3.8), p. 6; Chern–Simons trace and levels and the ordered ABJ charge frame.

§VIII.4.3. The rational example, large-gauge identity and formal out-of-window substitution are [**MATH**] under the stated charge normalizations and background premises. They establish no vacuum outside the direct-segment window. Aharony, Hashimoto, et al. 2010, arXiv v2, §§3.1–3.4, especially (3.21)–(3.28), printed pp. 25–32 / PDF pp. 26–33; Chern–Simons trace and levels and the ordered ABJ charge frame.

§VIII.4.4. The local D6 value and truncated baryon coupling are sourced [**SUGRA**] inputs. The comparison of the retained background polynomial is conditional [**MATH**]; the probe value is not an exact finite-background jump. Aharony, Hashimoto, et al. 2010, arXiv v2 (3.29), (3.35)–(3.37), (3.43)–(3.49), printed pp. 32–35 / PDF pp. 33–36; Chern–Simons trace and levels and the ordered ABJ charge frame.

§VIII.4.5. [**MATH**] is the conditional historical-polynomial difference, not a reconciliation. The infrared endpoints and beyond-window fixed points are source proposals [**CONJ+**]. Bergman and Hirano 2009, v2 (3.24), printed/PDF p. 8; Aharony, Bergman, et al. 2008, v3, §2.1 (2.1), printed pp. 4–6 / PDF pp. 5–7; Chern–Simons trace and levels, the ordered ABJ charge frame. The shifted M-theory reconciliation remains open.

§VIII.4.6. The exercises use the same level, charge and physical premises as the calculations above.

The ranks, s-rule, crossing and torsion proposal follow Aharony, Bergman, et al. 2008, arXiv:0807.4924v3, §2.1, Figures 1–2 and (2.1), printed pp. 3–7 / PDF pp. 4–8. The direct-segment window and endpoint relation are source-supported [**CONJ+**]; universal out-of-window SCFT absence, global lines and contact terms are untested. The H^4 count is [**MATH**], while $t = [L]$ is proposed. Chern–Simons trace and levels and the compact ABJM and membrane frame fix the full compact product and bare levels; The charge comparison uses the stated ordered fivebrane frame. Source fivebrane order $(\mathrm{NS}, \mathrm{D}) = (1, k)$ becomes book order $(\mathrm{D}, \mathrm{NS}) = (k, 1)$.

Page/Maxwell forms and units use Aharony, Hashimoto, et al. 2010, arXiv v2, §2.5 (2.64)–(2.67), printed p. 17 / PDF p. 18. Its §3.1–3.4, printed pp. 25–35 / PDF

pp. 26–36, supply the signed FW half-flux [**ANOM**], IR four-form and endpoint inputs [**SUGRA**], D6 local value (3.35)–(3.37), leading wall comparison (3.29), and truncated baryon cancellation (3.43)–(3.49). Orbifold inflow C_k is [**ANOM**] from Bergman and Hirano 2009, arXiv:0902.1743v2 (3.8), printed/PDF p. 6, and Aharony, Hashimoto, et al. 2010 (3.24)–(3.26), printed pp. 31–32 / PDF pp. 32–33. Equations (VIII.4.19), (VIII.4.24), (VIII.4.37) and (VIII.4.44) are conditional [**MATH**], not all-order charge laws.

The AHHO-citing corrected expression appears in Drukker et al. 2011, arXiv v4 (5.7)–(5.10), printed p. 20 / PDF p. 21. The historical positive-square term and note are Bergman and Hirano 2009 (3.24), printed/PDF pp. 8 and 3. Their full shifted M-theory reconciliation remains open. The result distinguishes a local probe from a finite background. Four bounded exercises check arithmetic and controlled origin/scope fields, not the physical premises or exact duality.

References

Aharony, O., O. Bergman, and D. L. Jafferis (2008). "Fractional M2-branes". In: *JHEP* 11, p. 043. DOI: 10.1088/1126-6708/2008/11/043. arXiv: 0807.4924 [hep-th].

Aharony, O., A. Hashimoto, et al. (2010). "D-brane Charges in Gravitational Duals of 2+1 Dimensional Gauge Theories and Duality Cascades". In: *JHEP* 01, p. 072. DOI: 10.1007/JHEP01(2010)072. arXiv: 0906.2390 [hep-th].

Bergman, O. and S. Hirano (2009). "Anomalous radius shift in AdS(4)/CFT(3)". In: *JHEP* 07, p. 016. DOI: 10.1088/1126-6708/2009/07/016. arXiv: 0902.1743 [hep-th].

Drukker, N., M. Marino, and P. Putrov (2011). "From weak to strong coupling in ABJM theory". In: *Commun. Math. Phys.* 306, pp. 511–563. DOI: 10.1007/s00220-011-1253-6. arXiv: 1007.3837 [hep-th].

Chapter VIII.5

From Calabi–Yau fourfolds to Chern–Simons theories

An M2-brane sees an eight-real-dimensional transverse space. Reducing its M-theory circle leaves a D2-brane moving through a seven-real-dimensional space, and the lost angular coordinate reappears as a compact degree of freedom in the three-dimensional gauge theory. For a toric Calabi–Yau fourfold, this observation is more useful than a dimension count. A chosen circle produces a family of Calabi–Yau threefolds, its curvature supplies Ramond–Ramond (RR) two-form flux, and that flux fixes the Chern–Simons (CS) levels carried by wrapped fractional branes.

The choice of circle and of fractional-brane classes is part of the construction. We will calculate its consequences, rather than try to recover a unique quantum theory from an arbitrary fourfold. The conifold gives a complete local example: its exceptional curve has flux period $-k$, while the two ordered brane classes yield levels $(k, -k)$. We then use a three-node suspended pinch point (SPP) to test two independent curve periods. The distinction between a circle that twists and one that actually collapses will identify where D6-branes may enter.

VIII.5.1 What does a membrane circle leave behind?

The reduction has to retain both the position along the base and the circle angle. Start with $m + 4$ complex GLSM coordinates z_i and an integral rank-m charge matrix Q_i^a. In a chamber with regular quotient, the fourfold is

$$X_4 = \big\{ z : \mu_a(z) = r_a \big\}/U(1)^m, \qquad \mu_a(z) = \sum_{i=1}^{m+4} Q_i^a |z_i|^2, \quad \sum_i Q_i^a = 0. \tag{VIII.5.1}$$

The row-sum condition preserves the holomorphic volume form on the regular Calabi–Yau quotient. It does not, by itself, choose a reduction circle. The GLSM variables are homogeneous coordinates. The moment equations and the m gauge phases remove m

complex directions, so in this regular chamber

$$\dim_{\mathbb{C}} X_4 = (m+4) - m = 4. \tag{VIII.5.2}$$

This count assumes an effective action on a populated stable locus. The charge matrix alone does not identify the circle that should be reduced or the chamber explored by a D2-brane. The row-sum condition has a direct holomorphic interpretation. The coordinate top form $dz_1 \wedge \cdots \wedge dz_{m+4}$ has weight $\sum_i Q_i^a$ under the ath complexified gauge action. Contracting it with the m gauge vector fields gives a candidate holomorphic four-form of the quotient. If every row sum vanishes, that form has no residual gauge weight on the smooth locus. Requiring $\sum_i q_i = 0$ makes the corresponding fixed-s threefold Calabi–Yau on its regular locus:

$$\mathrm{wt}_{Q^a}(dz_1 \wedge \cdots \wedge dz_{m+4}) = \sum_i Q_i^a = 0, \qquad \mathrm{wt}_q = \sum_i q_i = 0. \tag{VIII.5.3}$$

This canonical-bundle test does not guarantee smoothness in every chamber or settle the global circle stabilizers. There is a useful redundancy in the choice of the extra charge row. If t_a are integers and $q_i' = q_i + \sum_a t_a Q_i^a$, then on the original moment shell

$$\mu_{q'} = \mu_q + \sum_a t_a \mu_a = s + \sum_a t_a r_a. \tag{VIII.5.4}$$

The corresponding phase rotations differ by an action already gauged in X_4. They describe the same circle on the quotient, with a shifted origin for its moment coordinate. A genuinely different primitive row modulo the old charge lattice can instead select a different circle. This calculation shows why specifying only the fourfold variety does not supply a unique reduction dictionary: one must also specify the circle in the quotient lattice and its chamber. Choose an additional primitive integral row q_i, independent of the Q^a rows, with $\sum_i q_i = 0$. Write its moment value as the real variable

$$s = \mu_q(z) = \sum_i q_i |z_i|^2, \qquad z_i \longmapsto e^{iq_i\lambda} z_i, \qquad \lambda \sim \lambda + 2\pi. \tag{VIII.5.5}$$

The square on $|z_i|$ matters: this is the Hamiltonian moment map for phase rotation with the ordinary flat Kähler form. Replacing it by $|z_i|$ changes the geometry, even if the two expressions have the same zeros on a coordinate axis. For $z = x + iy$, rotation by $v = -y\partial_x + x\partial_y$ contracts the flat symplectic form as

$$\iota_v(dx \wedge dy) = -x\,dx - y\,dy = -d\left(\frac{|z|^2}{2}\right). \tag{VIII.5.6}$$

The overall sign depends on the generator convention; the quadratic dependence does not. This check fixes the moment equation used below.

To display the circle explicitly, add an angle $\theta \sim \theta + 2\pi$ and identify

$$(z_i, \theta) \sim (e^{iq_i\lambda} z_i, \theta + \lambda). \tag{VIII.5.7}$$

Gauge fixing θ on a free orbit recovers the original z-space. No fifth complex coordinate has been created. At fixed s, however, we quotient the z_i by one more $U(1)$ and obtain

$$X_3(s) = \{\mu_a = r_a,\ \mu_q = s\}/U(1)^{m+1}, \qquad \dim_{\mathbb{R}} X_3(s) = 2(m+4) - 2(m+1) = 6. \tag{VIII.5.8}$$

The order of these operations matters conceptually. If we first fix s and discard θ, we obtain only one member of the threefold family. If we keep θ but forget the extra phase identification, we incorrectly enlarge the dimension. The augmented space has one new real coordinate and one periodic coordinate, but the additional $U(1)$ removes precisely the added angle on each free orbit. The surviving circle of the original fourfold is a relative angular coordinate whose local representative depends on the chosen gauge chart. This is why a global angle need not exist when the resulting bundle has nonzero Chern class. On the free locus, s and the residual angle add two real directions to this six-dimensional fiber. The result has the expected eight real dimensions. At special s the quotient can change chamber or acquire a singular fiber; the dimension count is local to a regular stratum. At fixed s the quotient has a definite Kähler class. Across different s, its complex affine cone can remain the same even as an exceptional cycle grows, contracts, or flops. The circle above the family retains information that one fixed-s quotient discards.

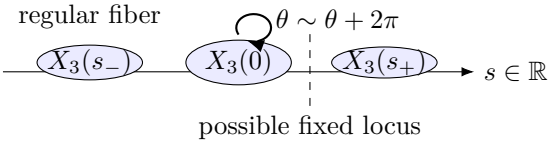


Figure VIII.5.1: A chosen circle presents the fourfold over the real moment value s. A regular $X_3(s)$ has a circle above each base point. The dashed position marks a possible degeneration, not a claim that every fiber is smooth or that the circle always collapses.

The simplest moving threefold is the conifold quotient. Take four coordinates A_1, A_2, B_1, B_2 and the extra row

$$q = (1, 1, -1, -1), \qquad s = |A_1|^2 + |A_2|^2 - |B_1|^2 - |B_2|^2. \tag{VIII.5.9}$$

At fixed positive s the A doublet cannot vanish, so its projective ratio describes an exceptional $\mathbb{P}^1$. At negative s, the B doublet instead gives the other small resolution. At $s = 0$ the affine quotient contracts the curve. A D2-brane can move through these chambers because s is its transverse scalar, rather than a fixed coupling of a single four-dimensional theory. At $s > 0$, setting $B_1 = B_2 = 0$ leaves $|A_1|^2 + |A_2|^2 = s$. Its three-sphere divided by the relative $U(1)$ is precisely the exceptional $\mathbb{P}^1$, with area proportional to s. For $s < 0$ the same test with $A_1 = A_2 = 0$ produces the flopped curve from the B doublet:

$$s > 0 :\ B = 0,\ [A_1 : A_2] \in \mathbb{P}^1; \qquad s < 0 :\ A = 0,\ [B_1 : B_2] \in \mathbb{P}^1. \tag{VIII.5.10}$$

The singular value $s = 0$ is not a third smooth resolution.

The augmented presentation depends on a genuinely integral circle. If θ shifted by $p\lambda$ instead of λ, gauge fixing it would leave a $\mathbb{Z}_{|p|}$ identification. Likewise, a nonprimitive charge row can hide a finite stabilizer. We therefore keep the primitive action explicit before interpreting the threefold family or its RR flux. The quiver vacuum calculation in Chapter 6 will meet the same integer lattice from the worldvolume side. For $p = 3$, setting $\theta = 0$ still permits $\lambda = 0, 2\pi/3, 4\pi/3$. If a coordinate has unit q charge, the last two transformations rotate it nontrivially, so the quotient is genuinely divided by $\mathbb{Z}_3$. If all q_i shared a factor three, the action would not be effective and the residual group would need to be recomputed from the faithful lattice. This finite identification is invisible in the real moment equations. It will become the $\mathbb{Z}_k$ position quotient in the conifold example once the CS level fixes the angle shift. The real moment coordinate and the integral circle generator play different roles. A positive real rescaling of s can amount to a change of symplectic units. Multiplying the circle generator by an integer changes the compact lattice and may change the finite quotient. One can rescale the horizontal axis in Figure VIII.5.1; one cannot replace a primitive circle by an ineffective multiple and keep the same bundle.

VIII.5.2 The circle remembers a two-form

A varying family of threefolds does not yet determine CS levels. Those levels need the curvature of the circle over the threefold. On a patch where a charged coordinate w is nonzero, put $\beta = \arg w$. For the local transformation $w \mapsto e^{-i\lambda}w$ and $\theta \mapsto \theta + p\lambda$, the real one-form

$$\eta = d\theta + p\, d\beta, \qquad \delta_\lambda \eta = p\, d\lambda - p\, d\lambda = 0 \tag{VIII.5.11}$$

is invariant. Different nonzero coordinates give different local angle charts. Their transition functions, rather than an everywhere-defined angle, describe the circle bundle.

We use charge-normalized RR fields from the outset. If C_1 is the dimensionful IIA potential and μ_0 is the D0 RR charge, set

$$\mathcal{C}_1 = \mu_0 C_1, \qquad \mathcal{F}_2 = d\mathcal{C}_1, \qquad c_1(S^1) = \left[\frac{\mathcal{F}_2}{2\pi}\right] \tag{VIII.5.12}$$

on the free circle locus. A unit D0 couples to $\int \mathcal{C}_1$; consequently $\mathcal{F}_2/(2\pi)$ has integer periods on closed two-cycles there. The local IIA/M reduction identifies this Chern class with RR two-form flux. The reduction is a physical duality input; the integral pairing that follows is an ordinary bundle calculation.

For a toric divisor $D_i = \{z_i = 0\}$ and an oriented compact curve $C \subset X_3(s)$, a connection assembled from coordinate phases with integer coefficients n_i has period

$$\left[\frac{\mathcal{F}_2}{2\pi}\right] = \sum_i n_i [D_i], \qquad f_C := \int_C \frac{\mathcal{F}_2}{2\pi} = \sum_i n_i (D_i \cdot C). \tag{VIII.5.13}$$

The intersection is signed. It must be evaluated in the chosen chamber and curve orientation. In a patch description, $d(d\arg w)$ has a 2π distributional contribution at $w = 0$; globally the transition functions make that contribution a divisor class. A local

exact form does not make the class globally exact. For example, cover $C \simeq \mathbb{P}^1$ by north and south patches whose circle angles differ on the equator by winding $n\varphi$. Integrating the local curvatures and keeping the opposite boundary orientations gives

$$\frac{1}{2\pi}\int_C \mathcal{F}_2 = \frac{1}{2\pi}\int_{\text{equator}} (\mathcal{C}_{1,N} - \mathcal{C}_{1,S}) = n. \tag{VIII.5.14}$$

The construction has no global $\mathcal{C}_1$ when $n \neq 0$. Applying Stokes' theorem once to the entire closed C with such a fictitious potential would incorrectly set the period to zero. Locally, $d\arg w$ has zero ordinary exterior derivative wherever $w \neq 0$. On overlapping patches, however, the two angles can differ by a winding function. The transition $e^{in\varphi}$ cannot be removed by one continuous gauge choice on the sphere when $n \neq 0$. The period measures this global obstruction, which the toric description records as a divisor intersection in (VIII.5.13). An explicit free bundle makes the point concrete. Use polar angles (ϑ, φ) on a positively oriented S^2, and choose local normalized connections

$$\mathcal{C}_{1,N} = \frac{n}{2}(1 - \cos\vartheta)d\varphi, \qquad \mathcal{C}_{1,S} = -\frac{n}{2}(1 + \cos\vartheta)d\varphi. \tag{VIII.5.15}$$

The north form is regular near $\vartheta = 0$, the south form near $\vartheta = \pi$, and on the overlap they differ by $n\,d\varphi$. Their common curvature is

$$\mathcal{F}_2 = \frac{n}{2}\sin\vartheta\, d\vartheta \wedge d\varphi, \qquad \int_{S^2} \frac{\mathcal{F}_2}{2\pi} = n. \tag{VIII.5.16}$$

For every point of the base sphere the fiber is an honest circle; there is no D6 locus on this sphere. The same unit bundle can occur as the boundary of a region containing the fixed orbit in (VIII.5.17). The distinction is whether the circle action extends freely through the interior, not whether its boundary Chern number happens to vanish.

There are two geometrically different reasons for a nonzero flux integral. First, a free circle bundle may twist over a compact curve; its first Chern class is nonzero although no orbit collapses. Second, the circle may actually have a fixed locus. Only the latter has the local Kaluza–Klein monopole behavior that reduces to a D6 source. One can see this distinction without invoking a full brane construction. Consider

$$(u, v) \mapsto (e^{i\lambda}u, e^{-i\lambda}v), \qquad z = uv, \quad s = |u|^2 - |v|^2. \tag{VIII.5.17}$$

The orbit-space coordinates $(\Re z, \Im z, s)$ range over $\mathbb{R}^3$. For $(z, s) \neq (0, 0)$ at least one of u, v is nonzero, and the orbit is free. At $u = v = 0$, the whole circle fixes the point. Over a small sphere linking the origin in the orbit space, the circle is the Hopf bundle, with one unit of first Chern number after choosing its orientation. The preimage of that linking sphere is a three-sphere, rather than $S^2 \times S^1$. Moving the sphere without crossing the origin leaves its period unchanged; shrinking it through the origin meets the degeneration. A compact curve in a region where the circle is everywhere free can carry a nonzero period without this local magnetic source. One can verify the orbit-space claim directly. With $a = |u|^2$ and $b = |v|^2$, the invariants obey $ab = |z|^2$ and $a - b = s$. Thus

$$a = \frac{s + \sqrt{s^2 + 4|z|^2}}{2}, \qquad b = \frac{-s + \sqrt{s^2 + 4|z|^2}}{2}. \tag{VIII.5.18}$$

Both are nonnegative for every (z, s), and their phases are unique up to the circle action away from the origin. At $(z, s) = (0, 0)$, $a = b = 0$, so the stabilizer jumps from trivial to the whole circle. On a small sphere $|u|^2 + |v|^2 = \varepsilon^2$ in $\mathbb{C}^2$, the same circle action has no fixed point. Its orbit space is a two-sphere. The north chart may use the phase of u to fix the circle, while the south chart uses the phase of v; on their overlap the two gauge choices differ by one full winding. This is the elementary clutching construction of the Hopf bundle. It calculates the unit period in (VIII.5.19) without assuming it from a D6-brane label. The D6 interpretation then uses the IIA reduction of precisely this local fixed-circle geometry.

$$\int_{S^2_{\mathrm{link}}} \frac{\mathcal{F}_2}{2\pi} = +1, \qquad d\mathcal{F}_2 = 2\pi\,\delta_{\mathrm{fixed}} \quad \text{in the local transverse model.} \tag{VIII.5.19}$$

Here the delta form indicates the magnetic source after extending across the fixed locus. Reversing the circle orientation changes both signs.

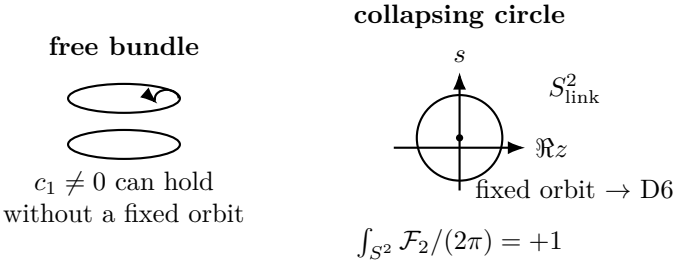


Figure VIII.5.2: A twisted free circle and a collapsing circle are different situations. The right panel is the local (z, s) orbit space of (VIII.5.17); its linking sphere detects a D6 magnetic source. Both panels use the same positive circle orientation.

The D6 interpretation requires the stated local smooth reduction near the primitive fixed orbit. A nonzero divisor pairing elsewhere does not diagnose a D6-brane. Chapter 8 will use actual D6 loci to introduce flavors and their quantum monopole relations. Here the immediate job of f_C is to determine the CS term of a brane wrapped on C.

VIII.5.3 Why RR flux writes a Chern–Simons level

A fractional D2-brane can carry D4 charge on a compact curve in the threefold. Put a positively oriented D4 on $M_3 \times C$ with $M_3 = \mathbb{R}^{2,1}$ locally. In the book convention $D = d + iA$ and the Hermitian fundamental-trace CS form is

$$\omega_3(A) = \mathrm{Tr_f}\left(A\,dA + \frac{2i}{3}A^3\right), \qquad d\omega_3(A) = \mathrm{Tr_f}(F \wedge F). \tag{VIII.5.20}$$

This equation fixes the cubic sign. A change to anti-Hermitian gauge fields requires a correlated change of convention; changing the cubic term alone would spoil the transgression identity. For a single $U(1)$ factor the cubic term vanishes and $\omega_3 = A \wedge dA$.

The full expression is needed for a stack of fractional branes, where the worldvolume connection is matrix valued. The fundamental trace is the same trace used to state the book's integer bare level. A different trace normalization would rescale the numerical coefficient that one reads from the WZ term. The sign of a level also depends on the orientation of M_3; throughout the calculation that orientation is held fixed while wrapped-brane charge or curve flux is varied.

The relevant D4 Wess–Zumino term is second order in its gauge field. With $B = 0$ and the RR charge convention $\mu_p = (2\pi)^{-p}\alpha'^{-(p+1)/2}$, its coefficient is

$$S_{\mathrm{WZ}} \supset \frac{\mu_4(2\pi\alpha')^2}{2}\int_{M_3\times C} C_1 \wedge \mathrm{Tr_f}(F\wedge F), \qquad \frac{\mu_4(2\pi\alpha')^2}{2\mu_0} = \frac{1}{8\pi^2}. \tag{VIII.5.21}$$

The factor $1/2$ from the exponential and the 2π normalization are both needed. Omitting the former would double the level. The brane tension is μ_4/g_s, but the RR WZ charge in this expression is μ_4. Substitution shows every factor explicitly:

$$\mu_4 = \frac{1}{(2\pi)^4\alpha'^{5/2}}, \qquad \mu_0 = \alpha'^{-1/2}, \qquad \frac{\mu_4(2\pi\alpha')^2}{2\mu_0} = \frac{1}{2(2\pi)^2}. \tag{VIII.5.22}$$

The last expression is $1/(8\pi^2)$. A bare integer period for the dimensionful dC_1 would conceal the D0 normalization and obscure this result. The book quotes the bare ultraviolet level in the action $K\omega_3/(4\pi)$. A quantum effective level can change when massive fermions are integrated out. Such a shift depends on a specified spectrum and regulator; it does not change the classical RR period in (VIII.5.12). This distinction becomes useful when D6 fixed loci add charged flavors. We calculate the WZ-induced bare term here and leave the flavored effective theory to Chapter 8.

One must interpret the five-dimensional term globally. On a nontrivial RR bundle, $\mathcal{C}_1$ cannot be chosen everywhere on C; also a purely external $F\wedge F$ vanishes pointwise on a three-manifold. The level arises from WZ descent on overlapping patches, or from a four-dimensional extension of the external gauge field. In that extension the transgression is

$$S_{\mathrm{WZ}} \rightsquigarrow \frac{1}{8\pi^2}\int_{M_3\times C}\mathcal{F}_2\wedge\omega_3(A) = \frac{1}{4\pi}\left(\int_C \frac{\mathcal{F}_2}{2\pi}\right)\int_{M_3}\omega_3(A). \tag{VIII.5.23}$$

The arrow denotes the globally defined descended coupling, with the extension ambiguity fixed modulo the quantized CS action. It is not a global integration by parts using an everywhere-defined RR potential. Equivalently, choose a spin-compatible four-dimensional filling W_4 of the external M_3 and extend the gauge connection. This uses the spin Chern–Simons prescription appropriate to the fermionic brane theory. The integral of $\mathrm{Tr}\,F^2$ over W_4 records the difference of boundary CS forms. Changing the spin-compatible extension changes the phase by an integer multiple of 2π under the stated flux and gauge quantization. Arbitrary oriented fillings are insufficient: at odd abelian level an odd self-intersection of an integral first Chern class would instead produce a π ambiguity. This is why the coefficient is an integer level instead of a freely chosen real coupling. In this language the descended topological expression is

$$\frac{1}{8\pi^2}\int_{C\times W_4}\mathcal{F}_2\wedge\mathrm{Tr_f}(F\wedge F) = \frac{f_C}{4\pi}\int_{W_4}\mathrm{Tr_f}(F\wedge F). \tag{VIII.5.24}$$

Its boundary variation is $f_C\omega_3/(4\pi)$. This expression does not require a globally defined $\mathcal{C}_1$ on C, and the four-dimensional field strength is allowed to have a nonzero square. It makes explicit which two separate dimensional operations were compressed into the three-dimensional CS term: first integrate RR flux over the internal curve, then take the boundary transgression of the gauge characteristic form. The two-dimensional flux and three-dimensional CS form also carry independent orientations. Reversing C flips f_C with its class held fixed; reversing M_3 flips $\int\omega_3$. We fix M_3 once and use the complex orientation of each curve. A source formula with suppressed orientations cannot then decide by itself which ordered node has $+k$. For positive wrapped D4 orientation we therefore read the integer bare level

$$K_C = \int_C \frac{\mathcal{F}_2}{2\pi}. \tag{VIII.5.25}$$

An anti-D4 on the same oriented C has level $-K_C$. A pure D2 charge does not contribute to this $\mathcal{F}_2$ pairing. Thus a D4 and anti-D4 with $f_C = n$ have ordered levels $(n, -n)$, even when one of the two constituents also carries a pointlike D2 charge. For a curve of period -4, the positive D4 receives -4 and the anti-D4 receives $+4$. Placing the anti-D4 at the first node gives $(+4, -4)$. Reversing the curve orientation together with the wrapping charge preserves the physical pairing; reversing only one changes its sign. This distinction is useful in quiver examples because node labels are ordered by the actual constituents. A relabeling of nodes exchanges the ordered pair, while a reversal of the RR class changes both levels without relabeling. The operations may produce similar-looking vectors, but they act differently on the geometric dictionary.

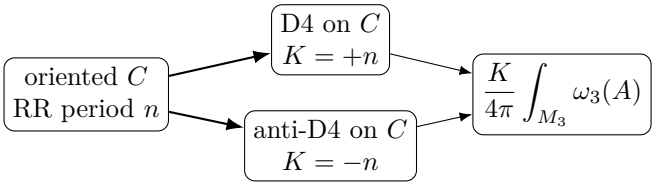


Figure VIII.5.3: The same oriented two-form period pairs with opposite wrapped D4 charges. The WZ descent fixes each CS coefficient; the drawing does not determine infrared dynamics.

More generally write the charges of a chosen fractional basis as

$$\Delta_\alpha = c_\alpha[\mathrm{pt}] + \sum_C m_{\alpha C}[C] + \sum_D h_{\alpha D}[D]. \tag{VIII.5.26}$$

For the D4 component under the present hypotheses the pairing is

$$K^{(2)}_\alpha = \sum_C m_{\alpha C} f_C, \qquad f_C = \int_C \frac{\mathcal{F}_2}{2\pi}. \tag{VIII.5.27}$$

Wrapped D6 charge may contribute through independently normalized four-form flux. Nonzero B, curvature and Freed–Witten shifts, and Romans mass also require their own

treatment. Equation (VIII.5.27) is the exact two-form contribution under the declared local assumptions; it is not a general all-flux formula. The superscript (2) names the two-form contribution. If a constituent has D6 charge $h_{\alpha D}[D]$, its higher-form pairing must be normalized and included before the full K_α is quoted. A background B field can also shift induced lower-dimensional charges. These effects are not hidden inside c_α: pointlike D2 charge does not enter the $\mathcal{F}_2$ term in (VIII.5.27).

If a regular D2 is a combination $[\mathrm{pt}] = \sum_\alpha n_\alpha \Delta_\alpha$, cancellation of its wrapped charges gives

$$\sum_\alpha n_\alpha m_{\alpha C} = 0, \qquad \sum_\alpha n_\alpha K_\alpha^{(2)} = 0. \tag{VIII.5.28}$$

The multiplicities n_α and the individual D2 charges c_α are different numbers. In examples with all $n_\alpha = 1$, the second relation becomes an ordinary sum of levels. It does not justify an unweighted sum in an arbitrary fractional basis. We use the no-F_0 regular-brane pairing in the two examples below. The distinction can be tested with a hypothetical two-constituent charge basis. Suppose one regular D2 contains two copies of Δ_1 and one copy of Δ_2, and their D4 charges on a single oriented curve are $m_1 = 1$, $m_2 = -2$. Then

$$2m_1 + m_2 = 0, \qquad (K_1^{(2)}, K_2^{(2)}) = (f_C, -2f_C), \qquad 2K_1^{(2)} + K_2^{(2)} = 0. \tag{VIII.5.29}$$

The unweighted sum is $-f_C$ and need not vanish. This elementary example prevents a statement valid for unit-multiplicity regular branes from being promoted to an arbitrary fractional basis. It also shows why $n_1 = 2$ is not a claim that Δ_1 itself has twice the pointlike D2 charge: multiplicity in the regular-brane combination and the coefficient c_1 in an individual charge class answer different questions.

VIII.5.4 From FI slope to the missing circle coordinate

The WZ calculation supplies integers, but the D2 still has to move through the family $X_3(s)$. On a connected geometric branch of a three-dimensional $\mathcal{N} = 2$ quiver, an occupied bifundamental joining nodes α and β contributes a nonnegative term

$$V_{\alpha\beta} \supset |\phi_{\alpha\beta}|^2(\sigma_\alpha - \sigma_\beta)^2, \qquad \phi_{\alpha\beta} \neq 0 \implies \sigma_\alpha = \sigma_\beta = s. \tag{VIII.5.30}$$

Connectivity propagates this equality across the populated support. It is a branch statement, not an identity on every component of the vacuum space. For three nodes with nonzero arrows $1 \to 2$ and $2 \to 3$, the two positive terms separately force $\sigma_1 = \sigma_2$ and $\sigma_2 = \sigma_3$. If the second arrow vanishes on another component, this conclusion need not hold there. The common scalar belongs to the connected brane-position component.

The supersymmetric completion of each bare CS term includes a $K_\alpha D_\alpha \sigma_\alpha$ coupling. In the source FI normalization, eliminating the auxiliary fields on this branch yields

$$r_\alpha = K_\alpha s + r_\alpha^{(0)}, \qquad \sum_\alpha n_\alpha K_\alpha = 0 \quad \text{for the specified regular D2.} \tag{VIII.5.31}$$

The constants $r_\alpha^{(0)}$ select a reference chamber. With them set to zero, moving the common scalar s moves the D-term levels along the ray selected by the RR periods. The slope is therefore the worldvolume expression of the circle-family geometry. Multiplying the node equations by regular-brane multiplicities and summing eliminates the s-dependent part by (VIII.5.28). Thus the center-of-mass regular D2 does not acquire a spurious FI force. For two unit-multiplicity nodes, the levels $(k, -k)$ give

$$(r_1, r_2) = (ks, -ks), \qquad r_1 + r_2 = 0, \qquad r_1 - r_2 = 2ks. \tag{VIII.5.32}$$

The last factor of two belongs to this particular relative variable; the conifold equation below uses its directly normalized moment level.

The angular coordinate is more delicate because the compact gauge group remembers finite quotients. In the two-node case retain the full $U(1)_1 \times U(1)_2$ and choose the unimodular basis

$$b = A_1 - A_2, \qquad c = A_2, \qquad \begin{pmatrix} A_1 \\ A_2 \end{pmatrix} = \begin{pmatrix} 1 & 1 \\ 0 & 1 \end{pmatrix} \begin{pmatrix} b \\ c \end{pmatrix}. \tag{VIII.5.33}$$

Its determinant is one, so integral flux sectors are preserved. For ordered levels $(k, -k)$ the symmetric CS matrix becomes

$$\begin{pmatrix} 1 & 0 \\ 1 & 1 \end{pmatrix} \begin{pmatrix} k & 0 \\ 0 & -k \end{pmatrix} \begin{pmatrix} 1 & 1 \\ 0 & 1 \end{pmatrix} = \begin{pmatrix} k & k \\ k & 0 \end{pmatrix}, \qquad S_{\mathrm{CS}} = \frac{k}{4\pi} \int b\, db + \frac{k}{2\pi} \int b\, dc. \tag{VIII.5.34}$$

The c field is the primitive common connection. A half-sum or a nonprimitive diagonal shortcut would change the integral lattice and could lose the finite $\mathbb{Z}_k$ action. For example, the symmetric variables $b' = A_1 - A_2$ and $c' = A_1 + A_2$ have determinant two relative to the original connections. They cover only a sublattice unless an additional parity condition is imposed on flux sectors. A Lie-algebra calculation can miss this while still reproducing a local BF term. The unimodular choice in (VIII.5.33) avoids that loss.

Dualize c by replacing dc with an independent integral-period two-form f and imposing its Bianchi identity with a scalar $\tau \sim \tau + 2\pi$. Locally the first-order terms and their equation are

$$S_{\mathrm{first}} = \frac{k}{2\pi} \int b \wedge f + \frac{1}{2\pi} \int \tau\, df, \qquad kb = d\tau. \tag{VIII.5.35}$$

The local equation follows by integrating the τdf term once on a patch and varying f. Its global use requires the compact period of τ and the integral flux lattice of c. A real, noncompact Lagrange multiplier would impose the same differential equation but would fail to identify the discrete gauge transformations that survive after τ is fixed. Conversely, retaining only a discrete quotient without the equation $kb = d\tau$ would lose the continuous angular coordinate paired with s. The relation has a simple test on a closed loop γ in a local region with no insertion. If the compact scalar winds m times, then

$$\oint_\gamma d\tau = 2\pi m, \qquad \oint_\gamma b = \frac{2\pi m}{k}. \tag{VIII.5.36}$$

Thus a full turn of the scalar corresponds locally to a fraction of the relative gauge holonomy when $k > 1$. The statement is local because nontrivial bundles, monopole insertions and global flux sectors require the complete compact treatment of the theory. For the present one-brane geometric branch, it already reveals why the angle cannot simply be discarded after imposing the D-term equation. It carries precisely the periodic information needed to restore the fourth complex direction. With $b \mapsto b - d\lambda$, the constraint is invariant when

$$\tau \mapsto \tau - k\lambda, \qquad \tau = 0 \implies \lambda = \frac{2\pi j}{k} \pmod{2\pi}. \tag{VIII.5.37}$$

For $k = 1$ no finite group remains. For $k = 3$, the three values $j = 0, 1, 2$ produce a $\mathbb{Z}_3$ action on the chiral coordinates. If a matter field has relative charge one, the jth transformation multiplies it by $e^{2\pi i j/k}$; a charge-minus-one field gets the inverse phase. For a faithful matter representation these are k distinct identifications. At $k = 3$ they act as

$$(A, B) \mapsto (\zeta^j A, \zeta^{-j} B), \qquad \zeta = e^{2\pi i/3}, \quad j = 0, 1, 2. \tag{VIII.5.38}$$

The source angle used for the conifold circle below transforms with the opposite sign: $\theta_{\mathrm{AG}} = -\tau$ after matching matter gauge conventions. The two descriptions therefore recover one compact angular direction, while s supplies its real partner. At $k = 1$, the residual transformation in (VIII.5.37) is the identity, so the four complex position coordinates are unrestricted by a finite group. At $k = 3$, the generator rotates each A by $e^{2\pi i/3}$ and each B by its inverse. These two calculations use the same primitive gauge basis; the difference is entirely in the integer BF coefficient. If one kept only the local equation for s, both cases would look like a four-complex-dimensional family. Their coordinate rings differ because the compact scalar is identified differently. The sign map is a coordinate statement, not a claim that the two formulas for a local connection have the same literal appearance. In the book gauge convention the relative field transforms as $b \mapsto b - d\lambda$, and τ transforms by $-k\lambda$. In the source's conifold phase convention B_1 has charge minus one and its angle transforms by $-\lambda$; the corresponding source angle transforms by $+k\lambda$. Thus $\theta_{\mathrm{AG}} = -\tau$ is forced by the paired transformations. The next section checks the actual invariant real one-form, including its sign.

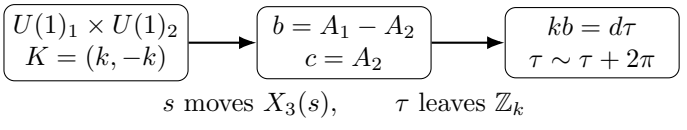


Figure VIII.5.4: The FI motion and the dual circle use the same ordered level pair. The original two compact gauge factors remain explicit until the integer basis is fixed.

These steps are the local classical mechanism. They do not, on their own, establish an infrared fixed point or identify the metric of the full M2 moduli space. Chapter 6 proves the corresponding compact quotient in a broader class of quivers, including conditions on the F-term component and the populated vacuum branch.

VIII.5.5 The conifold calculation returns ABJM

We can now run the entire chain for one compact curve. The conifold threefold has relative charges $q = (1, 1, -1, -1)$ on (A_1, A_2, B_1, B_2). Its four basic invariant monomials are

$$x = A_1B_1, \qquad y = A_2B_2, \qquad u = A_1B_2, \qquad v = A_2B_1, \qquad xy = uv. \tag{VIII.5.39}$$

At $s = 0$, the coordinate ring is $\mathbb{C}[x, y, u, v]/(xy - uv)$, a complex threefold singularity. For $s > 0$ the two A coordinates cannot vanish together and define $[A_1 : A_2] \in \mathbb{P}^1$. The B coordinates have charge -1, so each is a fiber coordinate of $\mathcal{O}(-1)$ over this curve:

$$X_3(s > 0) = \mathrm{Tot}\big(\mathcal{O}(-1) \oplus \mathcal{O}(-1) \longrightarrow \mathbb{P}^1\big). \tag{VIII.5.40}$$

The two small resolutions exchange the roles of A and B across $s = 0$. Their complex affine cone is the same, while their Kähler chambers differ. The invariant relation follows from the rank-one matrix

$$M = \begin{pmatrix} A_1B_1 & A_1B_2 \\ A_2B_1 & A_2B_2 \end{pmatrix}, \qquad \det M = xy - uv = 0. \tag{VIII.5.41}$$

Conversely, a nonzero rank-one matrix factors as an A column times a B row, uniquely up to their relative $\mathbb{C}^*$ scaling. The affine relation captures the generic complex quotient, while the real moment value chooses the Kähler resolution. This is why the exceptional curve used in the flux calculation belongs to the chosen positive chamber.

Let $C = \mathbb{P}^1$ in the positive chamber, oriented by its complex structure. The divisor $D_{B_1} = \{B_1 = 0\}$ restricts to a section of $\mathcal{O}(-1)$ on C. Hence

$$D_{B_1} \cdot C = \deg \mathcal{O}(-1) = -1, \qquad \left[\frac{\mathcal{F}_2}{2\pi}\right] = k[D_{B_1}], \quad k > 0. \tag{VIII.5.42}$$

The circle orientation and this divisor choice are physical input to the local reduction. Their signed period is not $+k$:

$$f_C = \int_C \frac{\mathcal{F}_2}{2\pi} = k(D_{B_1} \cdot C) = -k. \tag{VIII.5.43}$$

This minus sign is the point of carrying the curve orientation through the derivation. If the RR flux were chosen with the opposite class while the fractional basis stayed fixed, the ordered levels would reverse. The line-bundle degree can be checked in two patches. On $A_1 \neq 0$ use $t = A_2/A_1$, while on $A_2 \neq 0$ use $t' = 1/t$. The B_1 fiber coordinate transforms with one inverse power of the base transition, the defining transition of $\mathcal{O}(-1)$. Thus its restriction to C has degree -1. The intersection was computed from the resolution, not chosen to obtain a desired CS sign. More explicitly, choose gauge-invariant fiber coordinates $p = A_1B_1$, $q = A_1B_2$ on the first chart. On the second chart use $p' = A_2B_1$, $q' = A_2B_2$. Over their overlap,

$$t' = t^{-1}, \qquad p' = tp, \qquad q' = tq. \tag{VIII.5.44}$$

The zero section is $p = q = 0$ in the first chart and $p' = q' = 0$ in the second. The locus $B_1 = 0$ is $p = 0$ or $p' = 0$; restricting its associated line bundle to that zero section gives the degree in (VIII.5.42). The coordinate relation also shows why the fiber divisor is a legitimate geometric object even though the homogeneous field B_1 itself is not a gauge-invariant function on the quotient.

The specified fractional classes are

$$\Delta_1 = [\mathrm{pt}] - [C], \qquad \Delta_2 = [C], \qquad \Delta_1 + \Delta_2 = [\mathrm{pt}]. \tag{VIII.5.45}$$

The first constituent contains an anti-D4 on C and one unit of D2 charge; the second contains a D4. Their $\mathcal{F}_2$ pairings are therefore

$$(K_1, K_2) = (-f_C, +f_C) = (k, -k). \tag{VIII.5.46}$$

This is an ordered statement: node 1 has bare level $+k$. The D2 charge in Δ_1 makes the sum a regular brane but does not change either level in the present two-form WZ calculation. The charge computation can be displayed as a one-row matrix multiplication. In the ordered basis (Δ_1, Δ_2), the D4 charge vector on C is $(-1, +1)$, so

$$\begin{pmatrix} K_1 \\ K_2 \end{pmatrix} = \begin{pmatrix} -1 \\ +1 \end{pmatrix} f_C = \begin{pmatrix} -1 \\ +1 \end{pmatrix} (-k). \tag{VIII.5.47}$$

The regular-brane multiplicities are $(1, 1)$, and their sum annihilates the D4 vector. This explains the zero-sum levels from brane charge cancellation rather than imposing them as a separate quiver rule.

For clarity, we can see the same sign in an angular patch. Put $\beta = \arg B_1$ where $B_1 \neq 0$. The source's local circle action may be written

$$B_1 \mapsto e^{-i\lambda} B_1, \qquad \theta_{\mathrm{AG}} \mapsto \theta_{\mathrm{AG}} + k\lambda, \qquad \eta = d\theta_{\mathrm{AG}} + k\, d\arg B_1. \tag{VIII.5.48}$$

Both shifts cancel in η. Its transition at $B_1 = 0$ gives $k[D_{B_1}]$, whose curve period is $-k$. With the book's dual scalar in (VIII.5.35), the angle dictionary is

$$\theta_{\mathrm{AG}} = -\tau, \qquad \tau \mapsto \tau - k\lambda. \tag{VIII.5.49}$$

The real connection in (VIII.5.48) is the quantity used here. A complex logarithmic expression with a different sign cannot be substituted for it without checking its gauge transformation and its real part. Indeed $\delta\beta = -\lambda$, so the two terms in η change by $+k\, d\lambda$ and $-k\, d\lambda$. Their cancellation forces the plus sign in the real form. The divisor class is then fixed by the positively oriented angle around $B_1 = 0$ and the negative degree of the B_1 fiber on C.

The D-term level now moves with the same k. In a convention where s is the relative moment level, the one-brane branch obeys

$$|A_1|^2 + |A_2|^2 - |B_1|^2 - |B_2|^2 = ks. \tag{VIII.5.50}$$

For each set of four chiral coordinates, this equation determines s. The connected relative gauge action can be absorbed by the periodic angle, leaving only its finite stabilizer. After fixing $\tau = 0$ the remaining action is

$$(A_1, A_2, B_1, B_2) \sim (\zeta A_1, \zeta A_2, \zeta^{-1} B_1, \zeta^{-1} B_2), \qquad \zeta^k = 1. \tag{VIII.5.51}$$

At $k = 1$ the quotient is $\mathbb{C}^4$. At $k = 2$, $\zeta = -1$ reverses the sign of all four coordinates. At $k = 3$, the chiral chart has weights $(1, 1, -1, -1)$, so its last two coordinates transform by ζ^{-1}. These weights should not be called uniform in this complex chart. At $k = 3$, the product A_1B_1 is invariant, whereas A_1^2 and B_1^2 are not. For $k = 2$, every quadratic monomial is invariant because the generator flips all four signs. These low-degree tests expose the finite quotient that a dimension count would miss. They also explain why the shorthand $\mathbb{C}^4/\mathbb{Z}_k$ needs a declared complex coordinate chart when $k > 2$. At $k = 3$, the chiral invariant ring admits both mixed bilinears A_iB_j and pure cubic monomials in either the A or B variables. The bilinears alone reproduce the conifold coordinate ring (VIII.5.39); the cubic invariants record the additional angular direction of the fourfold quotient. For instance,

$$A_1^3, \quad B_1^3, \quad A_1B_1 \quad \text{are } \mathbb{Z}_3\text{-invariant}, \qquad (A_1^3)(B_1^3) = (A_1B_1)^3. \tag{VIII.5.52}$$

This relation is a small visible part of the fourfold coordinate ring. It illustrates why the quotient contains more information than the conifold base at one fixed s. It is not a substitute for an all-generator presentation of $\mathbb{C}^4/\mathbb{Z}_3$.

The standard membrane position coordinates use the conjugate B variables. Define the real-scalar chart

$$C = (A_1, A_2, B_1^\dagger, B_2^\dagger). \tag{VIII.5.53}$$

Complex conjugation turns the last two factors of (VIII.5.51) into ζ, so in this distinct complex-structure chart

$$C^I \sim \zeta C^I, \qquad \mathcal{M}_{N=1}^{\text{position}} = \mathbb{C}^4/\mathbb{Z}_k. \tag{VIII.5.54}$$

The ordered levels and the one-brane position quotient agree with the ABJM construction of Chapters 2 and 3. Matching these quantities is a consistent local IIA/M picture. It is not, by itself, a proof of quantum equivalence or of supersymmetry enhancement. The change from B_i to $B_i^\dagger$ is not a holomorphic change of the chiral coordinates. In the chiral chart the finite action preserves the evident $\mathcal{N} = 2$ complex structure and has two positive and two negative weights. In the real scalar position chart the same group acts uniformly on four complex coordinates. Both descriptions concern one real eight-dimensional position space, but they organize its complex coordinates differently. In particular, calling the chiral action uniform would erase the very sign that the conifold divisor calculation supplied.

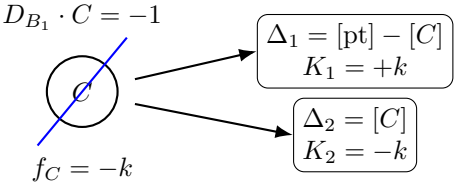


Figure VIII.5.5: Conifold divisor and brane pairing. The positive exceptional curve has negative intersection with the B_1 fiber divisor. The same oriented period $-k$ pairs with an anti-D4 and a D4 to give the ordered ABJM levels. The diagram records charges; the IR identification uses additional physical input.

VIII.5.6 Two curve periods test the construction

Figure VIII.5.5 summarizes the preceding one-curve calculation. The conifold has only one compact curve, so it cannot test whether the brane pairing keeps track of several independent periods. The suspended pinch point supplies two compact curve classes C_1, C_2 and three fractional constituents. This example has a narrower premise: we specify the oriented RR periods and derive their level pairing, but do not identify the supplied flux with the source's printed circle angle.

Choose the fractional classes

$$\Delta_1 = [C_1], \qquad \Delta_2 = [C_2], \qquad \Delta_3 = [\mathrm{pt}] - [C_1] - [C_2], \qquad \sum_{\alpha=1}^{3} \Delta_\alpha = [\mathrm{pt}]. \tag{VIII.5.55}$$

For any supplied oriented period vector $f = (f_1, f_2)$, the two-form pairing has the integer matrix form

$$\begin{pmatrix} K_1 \\ K_2 \\ K_3 \end{pmatrix} = \begin{pmatrix} 1 & 0 \\ 0 & 1 \\ -1 & -1 \end{pmatrix} \begin{pmatrix} f_1 \\ f_2 \end{pmatrix}, \qquad f_i = \int_{C_i} \frac{\mathcal{F}_2}{2\pi}. \tag{VIII.5.56}$$

The first two rows ask separately for each curve period; the third uses the negative of both because Δ_3 contains both anti-D4 charges. For $f = (k, -k)$ the result is

$$(K_1, K_2, K_3) = (k, -k, 0), \qquad K_1 + K_2 + K_3 = 0. \tag{VIII.5.57}$$

The vanishing unweighted sum holds because all three regular-brane multiplicities in (VIII.5.55) are one. It is a special case of (VIII.5.28). The full two-parameter form is instructive. If one changes only f_1 by one unit, the levels change by $(1, 0, -1)$; if one changes only f_2, they change by $(0, 1, -1)$. These are linearly independent deformations of the ordered level vector within the two-form pairing. At $f = (k, -k)$ they cancel in the third node, but the zero there does not mean that the third constituent carries no wrapped D4 charge. It carries minus one unit on each of the two curves, and its two induced contributions happen to cancel:

$$K_3 = -f_1 - f_2 = -k - (-k) = 0. \tag{VIII.5.58}$$

This is a useful physical reason to keep the full charge vector instead of remembering only the numerical level zero.

The abelian geometric component can be described by six homogeneous coordinates in the order $p = (a_1, a_2, b_1, b_2, B_1, B_2)$. They factor the quiver fields as

$$A_1 = a_1 b_1, \quad A_2 = a_2 b_2, \quad C_1^{\mathrm{field}} = a_1 b_2, \quad C_2^{\mathrm{field}} = a_2 b_1, \quad \Phi = B_1 B_2. \tag{VIII.5.59}$$

We distinguish the fields C_i^{field} from the curve classes C_i. On this component the homogeneous charge rows are

	a_1	a_2	b_1	b_2	B_1	B_2
Q_1	1	−1	0	0	0	0
Q_2	0	1	−1	0	−1	1
Q_3	0	1	0	−1	1	−1
Q_{aux}	−1	−1	1	1	0	0

(VIII.5.60)

Their sum is zero and their rank is three. At fixed chamber they therefore describe a threefold quotient of $\mathbb{C}^6$. The Q_1 row moves along the FI line while the remaining zero-level continuous rows can be taken as

$$H_1 = Q_1 + Q_2 = (1,0,-1,0,-1,1), \qquad H_2 = Q_{\text{aux}} = (-1,-1,1,1,0,0). \quad \text{(VIII.5.61)}$$

At $k=1$ their quotient has complex dimension $6-2=4$. For $k>1$ the stated source gauge leaves a $\mathbb{Z}_k$ action on (a_1,a_2) with weights $(1,-1)$. The dimension count and finite action describe this specified geometric component; they do not classify every F-flat branch. It is useful to see how the row relation works before eliminating any variable. If $\rho_j = |p_j|^2$ in the displayed coordinate order, the four moment functions are

$$\begin{aligned} \mu_1 &= \rho_{a_1} - \rho_{a_2}, \\ \mu_2 &= \rho_{a_2} - \rho_{b_1} - \rho_{B_1} + \rho_{B_2}, \\ \mu_3 &= \rho_{a_2} - \rho_{b_2} + \rho_{B_1} - \rho_{B_2}, \\ \mu_{\text{aux}} &= -\rho_{a_1} - \rho_{a_2} + \rho_{b_1} + \rho_{b_2}. \end{aligned} \quad \text{(VIII.5.62)}$$

Adding the four lines gives zero for every point, not only on a solution. The independent moment levels must satisfy the same linear relation. This is why eliminating the auxiliary row without tracking its integer coefficients can change a divisor class.

To verify the divisor periods, take the positive r_1 chamber where a_1 is nowhere zero. The integral reduced rows are

$$R_1 = Q_1 + Q_{\text{aux}} = (0,-2,1,1,0,0), \qquad R_2 = Q_2 = (0,1,-1,0,-1,1). \quad \text{(VIII.5.63)}$$

The first row gives the corrected reduced moment equation

$$|b_1|^2 + |b_2|^2 - 2|a_2|^2 = r_1 \quad \text{(VIII.5.64)}$$

after fixing a_1 in the chosen chamber. The factor two follows directly from the integral row and is needed for the correct divisor basis. In this reduced basis the divisor columns and curve pairings are

$$\mu_1 = r_1 > 0 \quad \Longrightarrow \quad |a_1|^2 = r_1 + |a_2|^2 > 0, \qquad \mu_1 + \mu_{\text{aux}} = -2|a_2|^2 + |b_1|^2 + |b_2|^2. \quad \text{(VIII.5.65)}$$

The calculation uses the actual nonvanishing of a_1, rather than declaring a coordinate to be one on a chamber where it could vanish. As a numerical check, take the six squared radii $(2,1,1,2,0,1)$. The four original moments are $(1,1,-2,0)$, and the reduced first moment is 1. Replacing $-2|a_2|^2$ by $-|a_2|^2$ would give 2 at the same point, so it is not an equivalent reduced row.

$$\begin{array}{c|cc} & C_1 & C_2 \\ \hline D_{a_1} & 0 & 0 \\ D_{b_1} & 1 & -1 \end{array}, \qquad \left[\frac{\mathcal{F}_2}{2\pi}\right] = k([D_{a_1}] + [D_{b_1}]). \quad \text{(VIII.5.66)}$$

Here the flux class is supplied independently with its orientation. It yields

$$\begin{pmatrix} f_1 \\ f_2 \end{pmatrix} = \begin{pmatrix} 0 & 1 \\ 0 & -1 \end{pmatrix} \begin{pmatrix} k \\ k \end{pmatrix} = \begin{pmatrix} k \\ -k \end{pmatrix}. \quad \text{(VIII.5.67)}$$

This matrix makes two wrong alternatives visible. kD_{a_1} alone has periods $(0,0)$ and cannot give $(k,-k,0)$. With the supplied $(k,-k)$ periods, the level vector $(k,k,-2k)$ fails (VIII.5.56) even though its entries sum to zero. An arbitrary zero-sum assignment is therefore weaker than a fractional-brane charge calculation. For $k=2$, for example, the period vector is $(2,-2)$. The proposed levels $(2,2,-4)$ would require periods $(2,2)$ for the first two constituents, contrary to the oriented divisor matrix. The sum of those proposed levels is still zero, so the regular-brane sum alone cannot detect the mistake. Likewise the isolated divisor $2D_{a_1}$ is cohomologically invisible to these two curves even though it has a nonzero coefficient in the chosen divisor presentation. These checks separate a basis-dependent divisor expression from the curve periods that the D4 constituents actually measure.

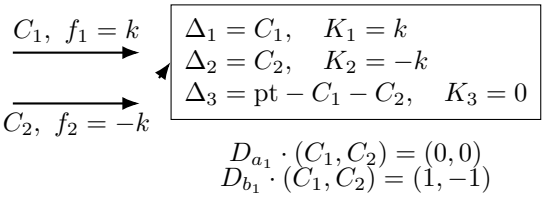


Figure VIII.5.6: Two oriented SPP curves give three ordered levels after pairing with the stated fractional classes. The displayed divisor pairings act on the supplied flux coefficients (k,k); the source's printed circle angle is not used to establish that class.

There is a useful algebraic check on the fixed-s threefold in the $a_1 \neq 0$ chamber. After setting $a_1 = 1$, the two residual rows are (VIII.5.63). The four monomials

$$U = a_2 b_1^2 B_2, \qquad V = a_2 b_2^2 B_1, \qquad Z = a_2 b_1 b_2, \qquad T = B_1 B_2 \tag{VIII.5.68}$$

are neutral under those reduced rows. Their exponents immediately give

$$UV = Z^2 T, \qquad \mathbb{C}[U,V,Z,T]/(UV - Z^2 T). \tag{VIII.5.69}$$

This relation is not just an identity among four examples. The homogeneous variables in (VIII.5.68) give a presentation of the neutral semigroup. Under the reduced rows R_1, R_2, a monomial $a_2^a b_1^b b_2^c B_1^d B_2^e$ is neutral precisely when

$$-2a + b + c = 0, \qquad a - b - d + e = 0, \quad \text{or} \quad b + c = 2a,\ e = b + d - a. \tag{VIII.5.70}$$

If $b \geq a$, the equations give $c = 2a - b$ and $e = b + d - a$. The monomial is then exactly

$$U^{b-a} Z^{2a-b} T^d, \qquad b \geq a. \tag{VIII.5.71}$$

If $b \leq a$, nonnegativity of e gives $d \geq a - b$, and the same monomial is

$$V^{a-b} Z^b T^e, \qquad b \leq a. \tag{VIII.5.72}$$

Thus every neutral monomial is generated by U, V, Z, T, and their primitive relation is $UV = Z^2 T$. The precise geometric component is the one selected by the factorization

(VIII.5.59); other F-flat components are not removed by the ring calculation. For a concrete $b \geq a$ instance, take $(a, b, c, d, e) = (2, 3, 1, 1, 2)$. The two neutrality equations hold, and the monomial is UZT. In the opposite case take $(a, b, c, d, e) = (2, 1, 3, 2, 1)$; it is VZT.

$$\begin{aligned} a_2^2 b_1^3 b_2 B_1 B_2^2 &= UZT, \\ a_2^2 b_1 b_2^3 B_1^2 B_2 &= VZT. \end{aligned} \tag{VIII.5.73}$$

The two formulas are not separate generators for two disconnected parts. They meet at $b = a$, where both descriptions reduce to $Z^a T^d$ with $e = d$. Multiplying the primitive relation lets one move between different factorizations of the same neutral monomial. This is the semigroup reason the single equation in (VIII.5.69) is sufficient on this component. For example, the field configuration in which all A_i, C_i, B_i vanish but $\Phi = 1$ can satisfy the abelian F equations of the source quiver. It is absent from the factorization $\Phi = B_1 B_2$ when both B_i vanish. The displayed ring therefore describes the selected geometric component in its stated chamber, not a claim that the full F-flat scheme has only this component.

The SPP example also marks an orientation limit. In the source's printed angular variables, $\arg a_1 + \arg b_1$ and its θ shift produce an invariant real connection whose class is $-k(D_{a_1} + D_{b_1})$, opposite to the class supplied in (VIII.5.66). We have therefore used the latter only as a specified flux for the WZ pairing. An oriented translation of the entire SPP circle, base, and FI convention would be required before claiming the same full circle-to-position derivation as for the conifold.

The construction leaves a clear boundary for subsequent chapters. Chapter 6 analyzes which F-term components and compact quotients actually produce fourfold vacua. Chapter 7 develops toric methods beyond these two charge tables. Circle fixed loci can add D6-branes and flavors, treated in Chapter 8; D6-wrapped fractional constituents may also receive four-form contributions. Neither a fourfold coordinate ring nor a successful position match selects a unique full quantum Chern–Simons quiver.

The two worked examples test different parts of the dictionary. It is helpful to keep their input and output types side by side.

	Conifold	SPP preview
Compact curve basis	C	(C_1, C_2)
Oriented RR periods	$-k$ from the stated circle divisor	$(k, -k)$ supplied as a flux class
Wrapped charge rows	$(-1, +1)$	$(1, 0), (0, 1), (-1, -1)$
Ordered bare levels	$(k, -k)$	$(k, -k, 0)$
Geometric conclusion	$\mathbb{C}^4/\mathbb{Z}_k$ in the one-brane position chart	$UV = Z^2 T$ for the fixed-s geometric component

The last row does not assert the same kind of completed construction in both columns. The conifold computation follows one circle through its divisor curvature, wrapped

charges, FI line and finite position quotient. The SPP preview begins with an independently supplied oriented flux and tests two curve periods against three fractional charges; its displayed ring verifies the chosen threefold component. Its printed source angle would reverse the chosen flux class under the convention used here. Keeping these inputs distinct prevents a correct numerical level vector from being mistaken for a complete M-theory circle lift. There is one final algebraic reason not to guess levels from a threefold alone. The flux periods form a covector on compact curve charge. The ordered levels are obtained only after a basis of fractional-brane charges has been specified. If an integral change of charge basis is written $\Delta' = M\Delta$, its level vector changes by the same matrix, while the regular-brane multiplicities change contragrediently:

$$K' = MK, \qquad n' = (M^{\mathsf{T}})^{-1}n, \qquad (n')^{\mathsf{T}}K' = n^{\mathsf{T}}K. \tag{VIII.5.74}$$

This is a statement about the charge pairing, not a declaration that every integral change of basis produces a physical quiver duality. It identifies the invariant content of the regular-D2 zero-sum rule and the basis dependence of an individual node level. For the chosen conifold and SPP bases, the physical node order is fixed by the supplied fractional constituents. A different basis would require its own brane and quiver interpretation before its entries could be read as a new theory.

The take-home result is a chain of signed pairings. A chosen M-theory circle makes $X_3(s)$, its Chern class fixes f_C, and the wrapped charges of chosen fractional D2 constituents turn those periods into ordered bare CS levels. For the conifold the chain gives the ABJM pair $(k, -k)$ and its one-brane position quotient. For SPP, a supplied two-period vector gives $(k, -k, 0)$ and the geometric ring $UV = Z^2T$ on the specified component.

Exercises

1. **Conifold orientation.** With $D_{B_1} \cdot C = -1$, $[\mathcal{F}_2/2\pi] = 3[D_{B_1}]$, and ordered fractional classes $([\mathrm{pt}] - [C], [C])$, submit the signed period, the two bare levels, and the finite chiral action weights modulo three. Repeat the levels after reversing only the flux class.

2. **A wrapped-brane coefficient.** Using the stated μ_p, compute $8\pi^2\mu_4(2\pi\alpha')^2/(2\mu_0)$ and the ordered levels for a D4 and anti-D4 on a positive curve of period -4. State which missing factor would double both levels.

3. **SPP divisor and brane pairing.** For the divisor matrix in Figure VIII.5.6 and supplied coefficients $(2, 2)$, submit the two periods and three ordered levels. Compute the periods for coefficients $(2, 0)$. Also submit the third level in the proposed vector $(2, 2, -4)$ and explain why that vector does not describe the original supplied class.

4. **The geometric component.** Verify that U, V, Z, T in (VIII.5.68) are neutral under both reduced rows. Submit their exponent vectors and the primitive integer relation among them. Use the two equations in (VIII.5.70) to explain the two cases in the all-degree generator argument.

Status and sources

Sources by section. Source coordinates and scope qualifications follow.

§VIII.5.1. The toric quotient [MATH] is conditional on a primitive independent GLSM row and a regular free chamber (Aganagic 2010, §2.1); The inverse field-theory interpretation is a source-supported premise.

§VIII.5.2. [MATH] gives integral curvature and periods on the free circle locus; [DUAL] is the restricted IIA/M interpretation using the local M-theory circle (Aganagic 2010, §2.1).

§VIII.5.3. The WZ coupling is a sourced premise; The level pairing [MATH] is the conditional level sum for actual fractional classes and $F_0 = 0$ (Aganagic 2010, §3.1–3.3; Witten 2003, §2.1).

§VIII.5.4. The branch interpretation is a sourced premise; The dual-scalar argument [MATH] is the compact dual-circle calculation with primitive compact flux (Aganagic 2010, §3.1–3.3).

§VIII.5.5. The oriented periods are source inputs; The geometric calculation [MATH] is the local $\mathbb{C}^4/\mathbb{Z}_k$ quotient conditional on it (Aganagic 2010, §4).

§VIII.5.6. The flux is a supplied premise; The resulting quotient [MATH] is only the corrected conditional GLSM and level pairing (Aganagic 2010, §6–6.1).

The spin-compatible extension used in the CS descent follows Witten (2003), Section 2.1: the book's level-one abelian functional is one half of that source's $I(A)$. The even intersection form on a spin filling removes the odd-level extension ambiguity.

This chapter establishes a specified local circle, chamber, flux and fractional-brane construction. The IIA/M identification and the D2 quiver are sourced physical premises. The integral GLSM dimensions, divisor periods, WZ coefficient, conifold ordered levels and SPP supplied-flux pairings are conditional calculations. They do not establish a unique inverse theory for every Calabi–Yau fourfold, full quantum equivalence, or the SPP source-angle translation. The construction uses the stated brane-action units, Chern–Simons trace and level conventions, and local IIA circle and flux-to-level map. The general inverse interpretation remains a geometric proposal [GEO-E]. The local IIA/M-circle construction and the IIB suspension-circle construction use separate hypotheses. The ABJM comparison concerns its local positions.

Circle family and curvature, §VIII.5.1 and §VIII.5.2. Aganagic (2010), §2.1, printed pages 6–9, equations (2.1)–(2.8), supplies the chosen GLSM circle, divisor curvature and fixed-locus discussion. Its added charge row in (2.4) and (2.6) is printed with an unsquared modulus; the Hamiltonian moment equation here uses $|z_i|^2$, as its ordinary GLSM equation (2.2) requires. A nonzero free-bundle class is distinct from a D6 fixed locus.

WZ descent and FI slope, §VIII.5.3 and §VIII.5.4. Aganagic (2010), §3.1–3.3, printed pages 11–17, equations (3.1)–(3.9), supplies the fractional-brane and FI/dual circle route, with 2π factors suppressed in its WZ display. Equations (VIII.5.21)–(VIII.5.25) restore the book normalization. Their descent is global or patchwise; an

everywhere-defined potential and a direct three-dimensional $F \wedge F$ argument would be invalid. Four-form flux, B shifts, Freed–Witten effects and F_0 are outside the two-form coefficient derived here.

Conifold and SPP, §VIII.5.5 and §VIII.5.6. Aganagic (2010), §4, printed pages 18–20, equations (4.1)–(4.6), supplies the conifold classes and divisor period. Its θ in (4.5) is $-\tau$ in the book compact quotient. The printed complex-log connection is not used as the invariant real form; equation (VIII.5.48) states that form explicitly. The SPP charge rows and classes are in §6–6.1, printed pages 23–25, equations (6.1)–(6.3). The reduced row in (6.3) needs the factor $-2|a_2|^2$. The supplied SPP flux has the opposite class from the source's printed angle under the conifold orientation convention, so only the conditional period-to-level pairing is used. The SPP ring is the stated geometric component, not the entire F-flat variety.

References

Aganagic, M. (2010). "A Stringy Origin of M2 Brane Chern-Simons Theories". In: *Nucl. Phys. B* 835, pp. 1–28. DOI: 10.1016/j.nuclphysb.2010.01.007. arXiv: 0905.3415 [hep-th].

Witten, E. (2003). *SL(2,Z) action on three-dimensional conformal field theories with Abelian symmetry*. arXiv: hep-th/0307041 [hep-th].

Chapter VIII.6

Vacuum geometry of Chern–Simons quivers

An M2-brane moving on a Calabi–Yau fourfold needs four complex position coordinates. A four-dimensional quiver built from a Calabi–Yau threefold seems to supply only three. The missing pair has a simple physical origin in three dimensions. The vector-multiplet scalar can move the D-term level along one real direction, while a compact scalar dual to a diagonal photon supplies its angular partner. Neither scalar can be counted without first asking which vacua exist and how the full compact gauge group identifies them.

We study classical vacua of a specified abelian quiver. Its gauge group is the full product $U(1)^G$, $G \geq 2$, with integer bare Chern–Simons levels $k = (k_1, \ldots, k_G)$ satisfying $\sum_i k_i = 0$ and $k \neq 0$. Matter consists only of bifundamental chiral fields, with no additional common-center quotient. This setting gives a precise construction of a geometric branch. The resulting affine quotient is a fourfold only when the F-term component and its populated stable orbits obey further conditions, which we will test in two contrasting examples.

VIII.6.1 Which vacuum remembers a membrane?

In the two-node ABJM example of Chapter 3, one membrane has four complex transverse coordinates with a finite $\mathbb{Z}_k$ identification. That calculation already shows the role of a compact gauge variable. A general quiver has more nodes and a superpotential, so the same answer cannot be inferred from the number of arrows or from a formal quotient by all node phases. We must find the actual vacuum equations, retain the gauge torus's integer lattice, and inspect whether the quotient has a populated generic part.

The worldvolume question is local and classical. A point of an F-term variety, together with real scalar expectation values, should represent a vacuum only if every positive term in the potential vanishes. Gauge-equivalent solutions then represent the same position. A finite quotient can change that position space even when it leaves the complex dimension unchanged. This chapter calculates that quotient and the conditions

under which its complex dimension is four. Equality of a classical position space does not by itself establish an infrared fixed point, a metric, or an M2 duality.

The familiar ABJM branch supplies a useful standard of precision. The level is an integer because the gauge fields are compact; a finite phase survives even though the local Lie algebra calculation sees no continuous residual gauge direction. Once more nodes are present, that finite phase can act differently on different arrows. Meanwhile a superpotential can impose enough F equations to lower the dimension or leave components with distinct support. For this reason, the argument has three stages. We first solve the auxiliary vacuum equations on a connected populated support. We then dualize the compact diagonal connection in an integral basis and compute the residual action on fields. Finally, we inspect an actual F-term component and its closed orbits. Each stage has an example in which omitting it would change the conclusion.

VIII.6.2 Auxiliary fields select the geometric branch

Let an arrow $e : a \to b$ carry a complex scalar ϕ_e of charge $+1$ at its tail a and -1 at its head b. We use $D = d + iA$. If W is the holomorphic superpotential, the ordinary abelian F-term equations define the affine variety

$$\mathcal{F} = \{\phi \in \mathbb{C}^{|E|} : \partial_{\phi_e} W = 0 \text{ for every } e\}. \tag{VIII.6.1}$$

The subset relevant to a chosen branch may be one irreducible component of $\mathcal{F}$. This choice must be made before counting its dimension.

The signed incidence matrix Q has $Q_{ie} = +1$ at the tail, -1 at the head, and zero otherwise. Its moment maps therefore satisfy

$$\mu_i = \sum_{e:\, t(e)=i} |\phi_e|^2 - \sum_{e:\, h(e)=i} |\phi_e|^2 = \sum_e Q_{ie} |\phi_e|^2, \qquad \sum_i \mu_i = 0. \tag{VIII.6.2}$$

Every arrow contributes once with each sign. The last equality expresses the fact that the common diagonal $U(1)$ is uncharged by bifundamentals.

For a single arrow, the sign convention can be checked without any superpotential. If $e : 1 \to 2$ and $\rho = |\phi_e|^2$, its contribution is $(\mu_1, \mu_2) = (\rho, -\rho)$. Reversing the arrow while retaining the same charge assignment would describe the conjugate representation. This observation matters in a many-node calculation because a reversed sign in one incidence column changes the D equations at both endpoints. The incidence matrix also makes $\mathbf{1}^T Q = 0$ manifest.

Write σ_i for the real scalar and D_i for the auxiliary field at node i. In the convention just declared, the bosonic auxiliary potential needed for this calculation is

$$V_{\mathrm{aux}} = -\sum_i \frac{k_i}{2\pi} D_i \sigma_i + \sum_i D_i \mu_i + \sum_{e:a\to b} |\phi_e|^2 (\sigma_a - \sigma_b)^2. \tag{VIII.6.3}$$

Here D_i is linear and imposes a constraint. It should not be confused with the positive final potential obtained after eliminating auxiliary fields. Varying it gives

$$\frac{\partial V_{\mathrm{aux}}}{\partial D_i} = 0 \quad \Longrightarrow \quad \mu_i = \frac{k_i \sigma_i}{2\pi}. \tag{VIII.6.4}$$

The residual nonnegative scalar term makes every populated edge equate the two scalars at its ends,

$$|\phi_e|^2(\sigma_{t(e)} - \sigma_{h(e)})^2 = 0, \qquad \phi_e \neq 0 \implies \sigma_{t(e)} = \sigma_{h(e)}. \tag{VIII.6.5}$$

Thus the support graph, retaining only arrows with nonzero vacuum values, controls the kernel of this quadratic form. It is the support of the solution, not merely the drawn quiver, that must be connected.

There is a useful linear-algebra form of this statement. Let $R_e = |\phi_e|^2$ and let B be the oriented incidence matrix of the populated edges. The edge potential is $\sigma^T B \,\mathrm{diag}(R_e) B^T \sigma$. Its vanishing follows from positivity,

$$\sigma^T B \,\mathrm{diag}(R_e) B^T \sigma = \sum_{e \in E_{\mathrm{pop}}} R_e (B^T\sigma)_e^2 = 0 \quad \Longleftrightarrow \quad B^T\sigma = 0. \tag{VIII.6.6}$$

The kernel consists of vectors constant on each connected component of the populated graph. If that graph has r components, the edge term alone leaves r constants. The D equations may remove some or all of them. This is why graph connectivity is a condition on a vacuum.

For clarity, compare the source convention in one edge. Its arrow $1 \to 2$ has $\mathcal{D}_{\mathrm{MS}} = (\rho, -\rho)$ for $\rho = |\phi|^2$. The same representation is the book arrow $2 \to 1$, for which $\mu_{\mathrm{book}} = (-\rho, \rho)$. Keeping A and k fixed while setting $\sigma_{\mathrm{book}} = -\sigma_{\mathrm{MS}}$ and $D_{\mathrm{book}} = -D_{\mathrm{MS}}$ maps the entire bosonic auxiliary expression to (VIII.6.3). In particular,

$$\mu_{\mathrm{book}} = -\mathcal{D}_{\mathrm{MS}}, \qquad -\frac{kD_{\mathrm{MS}}\sigma_{\mathrm{MS}}}{2\pi} = -\frac{kD_{\mathrm{book}}\sigma_{\mathrm{book}}}{2\pi}, \qquad D_{\mathrm{MS}}\mathcal{D}_{\mathrm{MS}} = D_{\mathrm{book}}\mu_{\mathrm{book}}. \tag{VIII.6.7}$$

This is a translation between two descriptions of the same bosonic calculation. It changes no scalar coordinate established in preceding chapters. It also explains why copying a source moment-map sign without reversing the arrow would give the wrong FI direction.

On a connected populated support, equation (VIII.6.5) propagates along paths and gives $\sigma_i = s$ for every node. Summing (VIII.6.4) now yields

$$\sigma_1 = \cdots = \sigma_G = s, \qquad 0 = \sum_i \mu_i = \frac{s}{2\pi}\sum_i k_i. \tag{VIII.6.8}$$

For levels of zero total sum, the remaining equations resemble a family of four-dimensional D-terms with one real FI direction,

$$\mu_i = \zeta_i(s), \qquad \zeta_i(s) = \frac{k_i s}{2\pi}, \qquad \sum_i \zeta_i(s) = 0. \tag{VIII.6.9}$$

This is a possible direction in level space. It is populated only at those s for which (VIII.6.1) and (VIII.6.9) have a common solution. A zero entry k_i simply fixes $\mu_i = 0$; it does not invalidate the construction.

We can derive the reduced moment equations directly, rather than guessing them from the number of nodes. Let $\mathfrak{h}_{\mathbb{R}} = \{v \in \mathbb{R}^G : k \cdot v = 0\}/\mathbb{R}\mathbf{1}$, where $\mathbf{1} = (1, \ldots, 1)$.

Because both $k \cdot \mathbf{1}$ and $\mathbf{1} \cdot \mu$ vanish, the pairing $v \cdot \mu$ is well-defined on this quotient. The zero moment equation for the residual connected torus is

$$v \cdot \mu = 0 \quad \text{for all } v \in \mathbb{R}^G \text{ with } k \cdot v = 0. \tag{VIII.6.10}$$

The annihilator of $\ker k$ is the line spanned by k. Thus (VIII.6.10) implies $\mu = \lambda k$ for a real λ, and conversely every such vector obeys it. Comparing with (VIII.6.4) gives $\lambda = s/(2\pi)$ on connected support. The reduced moment equation has $G-2$ independent real components: one of the $G-1$ directions in $\ker k$ is the ineffective diagonal. This calculation explains the quotient rank without silently dividing by every relative phase.

The distinction between a moment-map equation and a solution is visible even in elementary arithmetic. The vector λk always satisfies the linear constraints, but each μ_i is a signed sum of nonnegative $|\phi_e|^2$ subject to the F equations. Positivity, the incidence pattern and the superpotential can obstruct a chosen λ. We will use the all-positive-weight example later to exhibit an obstruction that survives even though the complexified group acts effectively on generic fields.

Figure VIII.6.1 fixes the same three-node cycle, $W = 0$, and levels $(1, -1, 0)$ in both panels. Setting two of its three edge values to zero changes the support and frees one relative value of σ. Both panels admit actual D-flat vacua. Thus the picture compares solutions of one theory, not merely two graphs that look different.

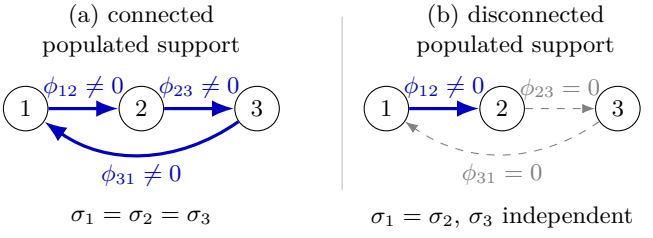


Figure VIII.6.1: The same $U(1)^3$ quiver, cycle arrows, $W = 0$ and bare levels $(1, -1, 0)$ in both panels. Solid arrows carry nonzero vacuum values; dashed arrows remain in the theory but have zero value. At $s = 2\pi$, panel (a) permits squared magnitudes $(x, y, z) = (2, 1, 1)$ and panel (b) permits $(1, 0, 0)$. The third scalar can differ in panel (b) because its level and moment map both vanish.

The caption's values can be checked directly. For the cycle $1 \to 2 \to 3 \to 1$, put $(x, y, z) = (|\phi_{12}|^2, |\phi_{23}|^2, |\phi_{31}|^2)$. With $k = (1, -1, 0)$, the connected choice $(2, 1, 1)$ gives $(\mu_1, \mu_2, \mu_3) = (1, -1, 0) = k\, s/(2\pi)$ at $s = 2\pi$. The disconnected choice $(1, 0, 0)$ gives the same moment vector. Since $k_3 = 0$ and $\mu_3 = 0$, its D equation leaves σ_3 independent, while the populated $1 \to 2$ edge fixes $\sigma_1 = \sigma_2 = 2\pi$. An isolated node of nonzero level would instead obey $k_3\sigma_3 = 0$. This comparison separates the edge-potential kernel from the full vacuum equations.

One can solve the real equations explicitly before turning to more general geometry. Temporarily take a three-edge cycle with $W = 0$, one arrow on each edge, and levels $(1, 1, -2)$. Write their squared magnitudes as x, y, z in cyclic order. Equation (VIII.6.4)

becomes

$$x - z = \frac{s}{2\pi}, \qquad y - x = \frac{s}{2\pi}, \qquad z - y = -\frac{2s}{2\pi}. \tag{VIII.6.11}$$

The third equation follows from the first two, as it must from the uncharged diagonal. At $s = 2\pi$ the choice $(x, y, z) = (2, 3, 1)$ is positive and gives populated connected support. More generally, set $z = r > 0$, $x = r + s/(2\pi)$ and $y = r + 2s/(2\pi)$ whenever all three are positive. This example shows how an FI direction becomes a family of actual vacua for this particular W. A different superpotential can remove the example through its F equations.

An individual zero level behaves differently from an identically zero level vector. Take a four-node directed cycle with one field on each edge, $W = 0$, and $k = (1, 0, -1, 0)$. Denote squared edge magnitudes in cyclic order by x_1, x_2, x_3, x_4. Connected support requires all four to be positive. The D equations at a common scalar value are

$$x_1 - x_4 = t, \qquad x_2 - x_1 = 0, \qquad x_3 - x_2 = -t, \qquad x_4 - x_3 = 0, \qquad t = \frac{s}{2\pi}. \tag{VIII.6.12}$$

For every finite t, choose $r > \max(0, -t)$ and set $(x_1, x_2, x_3, x_4) = (r + t, r + t, r, r)$. This is an F- and D-flat populated solution. The two zero-level nodes impose genuine equalities of adjacent magnitudes; they do not remove the scalar direction. The corresponding compact character is nontrivial and primitive, as the next section's construction will show.

VIII.6.3 A circle survives the gauge quotient

The common diagonal gauge field does not act on bifundamental matter. Yet its Chern–Simons cross term supplies a constraint that changes the quotient. To keep global identifications honest, we first choose an integral basis of the original gauge torus. Choose node G as reference and write

$$b_i = A_i - A_G \quad (i < G), \qquad c = A_G, \qquad A_i = b_i + c \quad (i < G), \quad A_G = c. \tag{VIII.6.13}$$

The same formulas hold for the integral flux lattice. Their inverse uses only integer coefficients, so this basis is unimodular. In particular c is a compact primitive connection. Replacing it by the sum of all A_i would multiply one lattice direction by G.

This integer claim can be checked on fluxes. If $n_i = (2\pi)^{-1} \int_\Sigma dA_i \in \mathbb{Z}$ on a closed two-cycle, then $n_{b_i} = n_i - n_G$ and $n_c = n_G$. Conversely $n_i = n_{b_i} + n_c$ for $i < G$. Both directions send integral vectors to integral vectors:

$$(n_{b_1}, \ldots, n_{b_{G-1}}, n_c) = (n_1 - n_G, \ldots, n_{G-1} - n_G, n_G) \in \mathbb{Z}^G. \tag{VIII.6.14}$$

The continuous classical action alone would allow a real change of basis. The compact theory admits only integral unimodular changes when we wish to preserve this flux lattice exactly.

Let $\kappa = (k_1, \dots, k_{G-1})^T$ and let M send (b, c) to the original vector A. The transformation of the diagonal level matrix is

$$M = \begin{pmatrix} I_{G-1} & \mathbf{1} \\ 0 & 1 \end{pmatrix}, \qquad K' = M^T \operatorname{diag}(k_1, \dots, k_G) M = \begin{pmatrix} \operatorname{diag}(\kappa) & \kappa \\ \kappa^T & \sum_i k_i \end{pmatrix}. \tag{VIII.6.15}$$

Thus the diagonal $c\,dc$ entry vanishes when $\sum_i k_i = 0$, while the cross term survives. Up to a boundary term the abelian action reads

$$S_{\mathrm{CS}} = \frac{1}{4\pi} \int \sum_{i<G} k_i b_i \wedge db_i + \frac{1}{2\pi} \int c \wedge \sum_{i<G} k_i db_i. \tag{VIII.6.16}$$

The apparently inactive diagonal connection is therefore paired with a specific integral combination of relative connections. Treating it as an ordinary redundant phase would erase this pairing.

For the three-node choice $k = (1, 1, -2)$, one can calculate without general matrix notation. Substitute $(A_1, A_2, A_3) = (b_1 + c, b_2 + c, c)$ into $A_1 dA_1 + A_2 dA_2 - 2A_3 dA_3$:

$$K' = \begin{pmatrix} 1 & 0 & 1 \\ 0 & 1 & 1 \\ 1 & 1 & 0 \end{pmatrix}, \qquad S_{\mathrm{CS}} \simeq \frac{1}{4\pi} \int (b_1 db_1 + b_2 db_2 + 2c\, d(b_1 + b_2)). \tag{VIII.6.17}$$

Here $\simeq$ means equality modulo a boundary term. One sees in the same line why c has no self-level and why setting it to zero before dualization would discard an equation.

We can dualize the compact diagonal connection locally. Introduce its field strength $f = dc$ as an independent two-form and a scalar τ with period 2π. In the first-order action the relevant terms are

$$S_{\mathrm{first}} = \frac{1}{2\pi} \int f \wedge \left(\sum_{i<G} k_i b_i - d\tau \right), \qquad \tau \sim \tau + 2\pi. \tag{VIII.6.18}$$

Integration by parts relates the first term to (VIII.6.16). The periodicity of τ follows from the integral flux of primitive c. Varying f produces the local relation

$$\sum_{i<G} k_i b_i = d\tau. \tag{VIII.6.19}$$

This equation shows explicitly how the compact angular coordinate couples to the matter gauge quotient. It is a local description of the relevant branch, not a statement equating all possible flat or torsion sectors.

The 2π period has a direct first-order meaning. Changing τ by 2π changes its coupling to f by an integer multiple of 2π when $(2\pi)^{-1} \int f$ is integral. Thus the exponentiated action is unchanged. A smaller period would require a correspondingly restricted flux lattice; no such restriction was made for primitive $c = A_G$. This converts the local differential equation into a global residual character, rather than merely its tangent-space kernel.

Let β_i be relative gauge parameters. With $D = d + iA$, a field of relative charge q_e transforms by $e^{iq_e\cdot\beta}$. Covariance of (VIII.6.19) requires

$$b_i \longmapsto b_i - d\beta_i, \qquad \phi_e \longmapsto e^{iq_e\cdot\beta}\phi_e, \qquad \tau \longmapsto \tau - \sum_{i<G} k_i\beta_i. \tag{VIII.6.20}$$

Fixing $\tau = 0$ leaves the gauge transformations for which the last shift is a multiple of 2π. This residual group includes continuous and possibly disconnected parts.

This formulation also locates the difference from the ordinary four-dimensional parent quiver. After its ineffective diagonal is removed, that parent divides F-flat matter configurations by $L = U(1)^G/U(1)_{\text{diag}}$, a torus of dimension $G-1$. The level character descends to a surjective map from L to $U(1)$, because a nonzero integer row has image the whole circle. Its kernel is precisely H:

$$1 \longrightarrow H \longrightarrow L \xrightarrow{\chi_k} U(1) \longrightarrow 1. \tag{VIII.6.21}$$

The kernel can be disconnected when the character is nonprimitive; surjectivity does not force a connected kernel. At a stable generic point the three-dimensional construction divides by one fewer continuous phase than the parent. The dual scalar and variable real moment level are the physical partners of that retained complex direction. The exact sequence specifies the phase identification; the F and D equations decide whether the corresponding positions exist.

Figure VIII.6.2 pictures the real and angular directions on a selected populated regular patch. The finite group is still applied to the matter coordinates. A circle drawn above an s value does not prove a globally trivial bundle. The example in (VIII.6.11) supplies populated points for every finite s after choosing r sufficiently large.

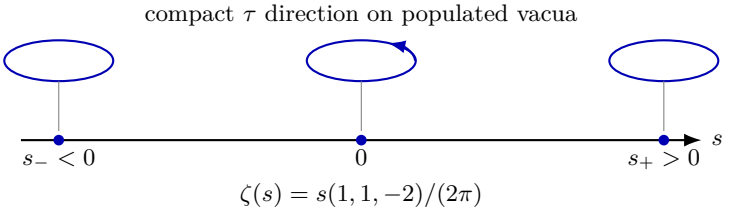


Figure VIII.6.2: A local physical picture for the three-edge $W = 0$ cycle with levels $(1, 1, -2)$. At each marked s, positive edge magnitudes can be chosen as in (VIII.6.11). The circles indicate the periodic dual coordinate over selected regular solutions. They are distinct from the residual gauge circle H^0 that is divided out. The schematic does not specify a global fibration or metric.

For $G = 2$ and $k = (m, -m)$, the transformed matrix and first-order relation are particularly transparent,

$$K' = \begin{pmatrix} m & m \\ m & 0 \end{pmatrix}, \qquad b = A_1 - A_2, \quad c = A_2, \quad mb = d\tau. \tag{VIII.6.22}$$

After fixing τ, the relative phase is $\beta = 2\pi r/m$. On the transverse holomorphic coordinates of ABJM this produces the familiar finite $\mathbb{Z}_{|m|}$ orbit. No continuous relative gauge quotient remains, so the four complex position coordinates keep their dimension.

For example, $m = 2$ leaves $\beta = 0, \pi$. In $\mathcal{N} = 2$ holomorphic notation the two A fields carry relative charge $+1$ and the two B fields charge -1, so the nontrivial element acts as -1 on all four at this particular level:

$$(A_1, A_2, B_1, B_2) \longmapsto (-A_1, -A_2, -B_1, -B_2) \quad (m = 2). \tag{VIII.6.23}$$

At general m, the B phases are inverse to the A phases in these holomorphic variables. When the transverse coordinates are written as $(A_1, A_2, B_1^\dagger, B_2^\dagger)$, all four instead carry the same relative phase. The conjugation must be kept in view when comparing a holomorphic superpotential quotient with physical transverse positions.

For three nodes with $k = (1, 1, -2)$, take $c = A_3$. The dual relation is

$$(b_1, b_2) = (A_1 - A_3, A_2 - A_3), \qquad b_1 + b_2 = d\tau. \tag{VIII.6.24}$$

The remaining continuous transformations have $\beta_1 + \beta_2 = 0$. They remove one complex direction from a suitable F-term component, while the real scalar s and the dual angle give the corresponding physical picture of the surviving circle over its allowed real levels.

At a fixed nonzero value of s for which F- and D-flat solutions exist, the real equations select a slice of the complexified $(G-2)$-torus orbits. As s varies, the slice moves along the FI line. The dual scalar supplies a periodic coordinate along this family. That physical picture does not replace the affine quotient at $s = 0$. The circle can degenerate or the set of populated solutions can change at special levels. The fourfold statement below is therefore phrased with an explicit dense stratum, not an unexamined product of a threefold and a cylinder.

There is a useful comparison with the nonprimitive source variables. Writing $a_{\mathrm{MS}} = \sum_i A_i = \sum_{i<G} b_i + Gc$ and $b_{\mathrm{MS}} = \sum_i k_i b_i / h$, where $h = \gcd(k_i)$, gives locally

$$h b_{\mathrm{MS}} = \sum_{i<G} k_i b_i = d\tau = G\, d\tau_{\mathrm{MS}}. \tag{VIII.6.25}$$

On the connected diagonal-flux branch used for that source coordinate, τ_{MS} has period $2\pi/G$. The primitive τ here has period 2π. The local relation is $\tau = G\tau_{\mathrm{MS}}$ up to a constant on that branch. Transferring a period between these bases without their flux lattices would change the finite quotient.

VIII.6.4 The integer lattice fixes the finite quotient

The last gauge transformation in (VIII.6.20) is a compact character, not a linear equation over real numbers. On the original product torus it is

$$\chi_k(e^{i\theta_1}, \ldots, e^{i\theta_G}) = \exp\left(i \sum_{j=1}^{G} k_j \theta_j \right), \qquad H = \ker \chi_k / U(1)_{\mathrm{diag}}. \tag{VIII.6.26}$$

The diagonal group lies in the kernel because $\sum k_i = 0$. Since it is connected, dividing by it does not remove disconnected components of the character kernel.

In the primitive relative basis the character has integer row $(k_1, \dots, k_{G-1})$. Elementary integer row and column operations reduce a nonzero row to its gcd $h = \gcd(k_1, \dots, k_G)$; the last level is minus the sum of the others. The exact compact result is

$$H^0 \simeq U(1)^{G-2}, \qquad \pi_0(H) \simeq \mathbb{Z}_h, \qquad H \simeq U(1)^{G-2} \times \mathbb{Z}_h \quad \text{noncanonically.} \tag{VIII.6.27}$$

Its Lie algebra remembers only $G-2$. Its component group remembers the integer normalization of the levels. To know the geometry, we must also compute how the components act on the fields.

The integer reduction can be seen without invoking an abstract classification theorem. Since the row $(k_1, \dots, k_{G-1})$ has gcd h, the Euclidean algorithm produces an integral unimodular matrix U that takes it to $(h, 0, \dots, 0)$. In the transformed compact angles γ, the kernel condition is

$$h\gamma_1 = 0 \pmod{2\pi}, \qquad \gamma_1 = \frac{2\pi r}{h}, \quad r = 0, \dots, h-1, \qquad \gamma_2, \dots, \gamma_{G-1} \in S^1. \tag{VIII.6.28}$$

This displays the h connected components and the $G-2$ unconstrained circles. The matrix U is not canonical, so the description of an individual finite generator depends on the chosen basis. Its action on a specified field is basis-independent once all charges are transformed with it.

The four-node example from (VIII.6.12) tests this group formula when some, but not all, levels vanish. With node four as reference, $k = (1, 0, -1, 0)$ gives $\chi_k = e^{i(\beta_1 - \beta_3)}$. Its compact kernel has $\beta_1 = \beta_3 = u$, while $\beta_2 = v$ is free; there is no disconnected component since the gcd is one. The four cycle fields therefore transform by

$$(\phi_{12}, \phi_{23}, \phi_{34}, \phi_{41}) \longmapsto (e^{i(u-v)}\phi_{12}, e^{i(v-u)}\phi_{23}, e^{iu}\phi_{34}, e^{-iu}\phi_{41}). \tag{VIII.6.29}$$

The two parameters act independently on generic populated fields, as expected from $G-2 = 2$. The product of the four edge fields is invariant because its four charges sum to zero. This direct field action verifies both the continuous rank and the absence of a finite factor for an example with individual zero levels.

Consider a directed cycle $1 \to 2 \to 3 \to 1$ with three families X_i, Y_i, Z_i, $i = 1, 2, 3$, on the respective edges. This is a classical branch calculation: diagonal bare levels have a mixed gauge parity anomaly on the full compact lattice. Chapter 7 selects a mixed trace-product correction with zero row sums, preserving this common-σ branch and primitive BF character. This calculation alone does not define a complete quantum theory. Relative to $c = A_3$ the charge vectors are

$$q(X_i) = (1, -1), \qquad q(Y_i) = (0, 1), \qquad q(Z_i) = (-1, 0). \tag{VIII.6.30}$$

At levels $(1, 1, -2)$, the connected kernel has $(\beta_1, \beta_2) = (t, -t)$ modulo 2π. It acts by

$$(X_i, Y_i, Z_i) \longmapsto (e^{2it}X_i, e^{-it}Y_i, e^{-it}Z_i). \tag{VIII.6.31}$$

The cubic superpotential is compatible with both this circle and the finite component introduced below. Every term $X_iY_jZ_k$ follows the closed cycle and has total relative charge

$$q(X_i) + q(Y_j) + q(Z_k) = (1,-1) + (0,1) + (-1,0) = (0,0). \tag{VIII.6.32}$$

Thus a gauge transformation of any component preserves W and maps its F locus to itself. This check is logically prior to computing invariant functions on that locus. In the doubled-level case the representative changes two of the three field families' signs, so each cubic term remains unchanged. Its action on $X_1Y_1^2$ can nevertheless be odd, since this polynomial is an observable on the F locus rather than a term required in W. Thus the indexed polynomial $X_1Y_1^2$ has continuous weight $2-1-1=0$. Its index matters, since it is an actual function of the fields, not merely an abstract charge vector.

One can classify monomials in a local polynomial chart by their weights. For $P = \prod_i X_i^{a_i} Y_i^{b_i} Z_i^{c_i}$, with nonnegative integer exponents, invariance under the connected circle means

$$2\sum_i a_i - \sum_i b_i - \sum_i c_i = 0. \tag{VIII.6.33}$$

For the doubled levels, this is only the first condition. The representative $(\pi, 0)$ multiplies the same monomial by $(-1)^{\sum_i (a_i+c_i)}$. The full invariant ring keeps exactly the connected-invariant combinations with even $\sum_i (a_i + c_i)$. The indexed monomial $X_1Y_1^2$ has $(a_1, b_1, c_1) = (1, 2, 0)$, so it meets the first condition and fails the second.

Three low-degree indexed invariants show more of the ring than one sign test. On the rank-one component introduced below, set

$$A = X_1Y_1^2, \qquad B = X_1Y_1Z_1, \qquad C = X_1Z_1^2, \qquad B^2 = AC. \tag{VIII.6.34}$$

All three have continuous weight zero. The displayed relation is an ordinary polynomial identity, so their values are not independent. Under the extra finite representative, $(A, B, C) \mapsto (-A, B, -C)$. The point with all matrix entries one has $A = B = C = 1$, while its finite partner has $A = C = -1$ and $B = 1$. The two are different points before the finite identification. This makes the effect on functions and on points agree.

The level multiplication has a general compact formulation. Start with a primitive level vector k and replace it by mk for a positive integer m. The new character is $\chi_{mk} = (\chi_k)^m$. Its differential has the same kernel as that of χ_k, while its compact kernel has m connected components. If the original gcd is h, the component order changes from h to mh. On a specified F component, the quotient map is induced by inclusion of invariant rings,

$$\mathbb{C}[F]^{H_{mk,\mathbb{C}}} \subseteq \mathbb{C}[F]^{H_{k,\mathbb{C}}}, \qquad F//H_{k,\mathbb{C}} \longrightarrow F//H_{mk,\mathbb{C}}. \tag{VIII.6.35}$$

The map can identify points even though both sides have the same complex dimension. Its degree on a given branch depends on the actual finite action, not solely on m. In our rank-one example the odd nonzero function $A = X_1Y_1^2$ proves that the extra $\mathbb{Z}_2$ action is effective on a dense locus.

Multiplying all levels by two changes the character while preserving its real nullspace. At levels $(2, 2, -4)$, the element $(\beta_1, \beta_2) = (\pi, 0)$ lies in the second component and acts

by

$$(X_i, Y_i, Z_i) \longmapsto (-X_i, Y_i, -Z_i), \qquad X_1 Y_1^2 \longmapsto -X_1 Y_1^2. \tag{VIII.6.36}$$

Hence the polynomial survives the connected quotient but is removed from the full invariant ring in the doubled-level theory. By contrast, $X_1^2 Y_1^4$ is even under this representative. This is a concrete geometric difference between the two compact theories despite identical Lie algebra quotients.

This distinction persists after imposing the cubic F equations used below. At the all-ones rank-one matrix, $X_1 Y_1^2 = 1$, so this polynomial does not vanish identically on the F locus. Its square also does not vanish there. The finite quotient therefore genuinely changes which functions separate points on that component. A gcd alone would say how many components the residual group has, but not whether its action on a particular branch is trivial. The field action supplies that missing information.

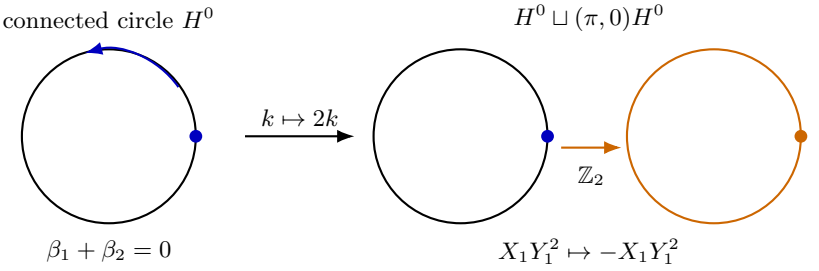


Figure VIII.6.3: The circles depict connected parameter components of the residual compact gauge group, rather than circles in the vacuum target. The arrow between the two right-hand circles is the representative $(\pi, 0)$ for the same fields and ranks on the three-node cycle. The levels change from $(1, 1, -2)$ to $(2, 2, -4)$. The displayed polynomial distinguishes the finite orbit, while the continuous orbit dimension remains one.

The figure separates two roles often compressed into the word "circle." The dual scalar τ is compact and makes the residual character condition possible. The circle H^0 is the continuous group by which solutions are divided. Their relation is fixed by the BF coupling and the integer lattice, and the resulting finite action depends on the matter charges.

VIII.6.5 When does the quotient have complex dimension four?

The tempting count starts with an F-flat space of complex dimension $G+2$ and subtracts $G-2$ continuous gauge dimensions. That count is correct only if the affine quotient actually sees a dense set of orbits of that dimension. At zero moment level, a nonclosed complex orbit can run toward the origin; polynomial invariants then identify it with the closed orbit in its closure. An effective action by itself does not prevent every nonconstant invariant from disappearing.

Let F be an irreducible affine F-term component. We require a dense stratum of closed complexified H^0 orbits of dimension $G-2$, each represented by a populated solution of the zero-H moment equations. If $\dim_{\mathbb{C}} F = G+2$, the generic fibers of the quotient on that stratum have dimension $G-2$, and therefore

$$\dim_{\mathbb{C}}(F/\!/H^0_{\mathbb{C}}) = (G+2)-(G-2) = 4. \tag{VIII.6.37}$$

The finite component group changes the invariant ring but not its Krull dimension. The closed-orbit and population conditions are what make the subtraction a statement about the affine vacuum geometry.

Why does the zero-H moment condition enter an algebraic quotient? For a compact torus acting linearly on an affine variety, a complex orbit has a representative at zero moment level when it is closed in the relevant zero-level setting. The quotient records the closed orbit in each orbit closure. The dimension of a generic orbit in the ambient F locus need not equal the dimension of a generic closed orbit represented in the zero-moment set. In the first example below, both dimensions agree on a dense populated patch. The counterexample has a dense set of one-dimensional orbits but only one closed orbit at zero moment level.

A three-node example realizes the conditions in detail. Use the cycle fields X_i, Y_i, Z_i above and the cubic superpotential

$$W = \epsilon_{ijk} X_i Y_j Z_k. \tag{VIII.6.38}$$

Its nine F equations say that the three row vectors are pairwise parallel. Equivalently, all 2×2 minors vanish in the matrix

$$\mathcal{M} = \begin{pmatrix} X_1 & X_2 & X_3 \\ Y_1 & Y_2 & Y_3 \\ Z_1 & Z_2 & Z_3 \end{pmatrix}, \qquad F = \{\mathcal{M} : \operatorname{rank}\mathcal{M} \le 1\}. \tag{VIII.6.39}$$

For instance, $\partial W/\partial Z_3 = X_1Y_2 - X_2Y_1$. This explicit derivative gives the reader a sign and index check before we use the entire determinantal ideal.

The other derivative families have the same concrete meaning:

$$\frac{\partial W}{\partial X_i} = \epsilon_{ijk} Y_j Z_k, \qquad \frac{\partial W}{\partial Y_j} = \epsilon_{ijk} X_i Z_k, \qquad \frac{\partial W}{\partial Z_k} = \epsilon_{ijk} X_i Y_j. \tag{VIII.6.40}$$

Each set is a cross product of two rows. If all derivatives vanish, every pair of rows is dependent. Conversely, rank at most one makes every cross product zero. This is an equivalence of the full F equations' zero locus with the determinantal locus.

On the chart $X_1 \neq 0$, four minors solve for four entries,

$$\begin{aligned} Y_2 &= Y_1X_2/X_1, \quad Y_3 = Y_1X_3/X_1, \\ Z_2 &= Z_1X_2/X_1, \quad Z_3 = Z_1X_3/X_1. \end{aligned} \tag{VIII.6.41}$$

Conversely, these relations make the Y and Z rows multiples of the X row, so every other minor vanishes. The five free coordinates are X_1, X_2, X_3, Y_1, Z_1 with X_1 invertible. This is a chart on the actual F locus, not just a tangent-space count.

The chart extends to the full determinantal component because every rank-one matrix factors as $\mathcal{M} = uv^T$. For nonzero matrices (u, v) and $(\lambda u, \lambda^{-1} v)$ give the same matrix, and the zero matrix lies in the closure. Hence

$$\dim_{\mathbb{C}} F = 3 + 3 - 1 = 5 = G + 2, \qquad F = \overline{\{uv^T : u, v \neq 0\}}. \tag{VIII.6.42}$$

The factorization also proves irreducibility. It prevents an unnoticed extra component at rank zero from spoiling the dimension statement.

It is helpful to see the quotient's four local coordinates rather than only its dimension. On the patch $X_1 Y_1 \neq 0$, the rank-one relations give $X_i = X_1 v_i$, $Y_i = Y_1 v_i$, $Z_i = Z_1 v_i$ with $v_1 = 1$. The connected complex gauge transformation sends $(X_1, Y_1, Z_1) \mapsto (t^2 X_1, t^{-1} Y_1, t^{-1} Z_1)$. A set of invariant rational chart coordinates is

$$R = X_1 Y_1^2, \qquad S = Z_1 / Y_1, \qquad P = X_2 / X_1, \qquad Q = X_3 / X_1. \tag{VIII.6.43}$$

They are algebraically independent on this open patch. For example, fixing the orbit parameter by $Y_1 = 1$ reconstructs $X_1 = R$, $Z_1 = S$, $X_2 = RP$, $X_3 = RQ$ and the remaining entries from (VIII.6.41). This chart argument does not claim that the entire affine quotient is $\mathbb{C}^4$ or that all four rational coordinates are globally regular.

The same patch illustrates what the fourth coordinate adds to the four-dimensional parent quiver. That parent divides by all relative node phases. Its gauge-invariant cubic monomials include $X_i Y_j Z_k$, since their three charge vectors sum to zero. On $X_1 Y_1 Z_1 \neq 0$ the invariant $T = X_1 Y_1 Z_1$ and the ratios P, Q give three local coordinates. In terms of the Chern–Simons quotient chart,

$$T = X_1 Y_1 Z_1 = RS, \qquad (R, S, P, Q) \longmapsto (T, P, Q) = (RS, P, Q). \tag{VIII.6.44}$$

The map forgets one complex direction. At fixed nonzero T, changing R and S inversely leaves every parent invariant of this local type unchanged, while the three-dimensional quotient still distinguishes the two configurations. This is the algebraic counterpart of the extra real FI parameter and compact dual scalar. It uses a stable open patch; it does not assert a globally trivial circle fibration over the parent threefold.

The same chart makes the finite quotient visible in coordinates a student can manipulate. For doubled levels $(2, 2, -4)$, the representative $(\pi, 0)$ acts on the four quantities in (VIII.6.43) as

$$(R, S, P, Q) \longmapsto (-R, -S, P, Q). \tag{VIII.6.45}$$

Since R is invertible on this chart, its finite-invariant functions may instead use

$$U = R^2, \qquad V = S/R, \qquad P, \qquad Q. \tag{VIII.6.46}$$

Here U is invertible. The continuous quotient has local coordinate R, while the doubled-level quotient remembers only R^2 together with a correspondingly adjusted S coordinate. Both charts have complex dimension four, yet the map between them is two-to-one on generic points. This exhibits exactly what the finite character does in the stable example.

For $k = (1, 1, -2)$, the connected residual action has row weights $(2, -1, -1)$ by (VIII.6.31). At a matrix with all three rows nonzero, both positive and negative weights occur. The orbit under $t \in \mathbb{C}^*$ cannot approach a finite point of F as $t \to 0$ or $t \to \infty$, and is closed. Its stabilizer is trivial because the row weights have gcd one. The moment equation for this circle is

$$\mu_H = 2\|X\|^2 - \|Y\|^2 - \|Z\|^2 = 0. \tag{VIII.6.47}$$

The matrix with all nine entries equal to one lies in F, has connected populated support, satisfies this equation, and has $X_1 Y_1^2 = 1$. Small variations within the nonzero-row locus give the required populated dense stratum of closed one-dimensional orbits. It follows that the affine connected quotient has complex dimension $5 - 1 = 4$. The finite action of the doubled-level version is nontrivial on an actual point of this locus, not only on a formal polynomial.

In fact this F component permits a populated solution at every real value of the candidate s for these levels. Put $t = s/(2\pi)$ and choose $r > \max(0, -t, -2t)$. Take a unit vector $v \in \mathbb{C}^3$ with every entry nonzero and choose the three rows proportional to it, with norms

$$\|X\|^2 = r + t, \qquad \|Y\|^2 = r + 2t, \qquad \|Z\|^2 = r. \tag{VIII.6.48}$$

All rows are nonzero and the matrix has rank one, so the F equations hold. The node moments are $(\|X\|^2 - \|Z\|^2, \|Y\|^2 - \|X\|^2, \|Z\|^2 - \|Y\|^2) = (t, t, -2t)$. This is precisely $k\, s/(2\pi)$. The free choice of sufficiently large r explains why no sign of s is excluded in this example. It also demonstrates how to check population rather than infer it from the formal FI line.

The moment-map representative can also be found along any generic complex orbit on this patch. Let the absolute value of its orbit parameter be $r > 0$. Then the three row norms become $r^4\|X\|^2$, $r^{-2}\|Y\|^2$, and $r^{-2}\|Z\|^2$. Setting the moment map to zero gives

$$r^6 = \frac{\|Y\|^2 + \|Z\|^2}{2\|X\|^2} > 0. \tag{VIII.6.49}$$

There is one positive solution. The remaining phase is the compact part of the orbit divided by H^0. This exhibits a zero-moment representative and explains why the mixed signs make the quotient stable on the nonzero-row locus.

The same dimension arithmetic fails in a simple effective action. Choose $G = 3$, $k = (1, -2, 1)$, $W = 0$, two arrows $1 \to 2$, two arrows $2 \to 3$, and one arrow $1 \to 3$. There are five free fields, so $F = \mathbb{C}^5$ has dimension $G + 2$. A generator of the residual connected group can be represented by node phases $(2, 1, 0)$. The five arrow weights are

$$(q_1, q_2, q_3, q_4, q_5) = (1, 1, 1, 1, 2). \tag{VIII.6.50}$$

They have gcd one and the generic orbit has dimension one. Still, every nonconstant monomial has positive weight, so

$$\mathbb{C}[x_1, \ldots, x_5]^{\mathbb{C}^*} = \mathbb{C}, \qquad \operatorname{Spec} \mathbb{C}[x_1, \ldots, x_5]^{\mathbb{C}^*} = \{\text{point}\}. \tag{VIII.6.51}$$

The zero moment equation supplies the same conclusion in real terms,

$$\mu_H = \sum_{a=1}^{4} |x_a|^2 + 2|x_5|^2 = 0 \quad \Longrightarrow \quad x_1 = \cdots = x_5 = 0. \tag{VIII.6.52}$$

The origin has no populated support. The generic complex orbit is effective but is not a closed zero-moment orbit. Its closure meets the origin, and the affine quotient collapses it. Thus a quiver with the right F dimension and the right Lie algebra count need not describe a fourfold. This intentionally elementary counterexample is not asserted to be a complete quantum membrane model.

The node D equations show how strongly population fails here. If $a = |x_1|^2 + |x_2|^2$, $b = |x_3|^2 + |x_4|^2$ and $c = |x_5|^2$, then the three moments and their proposed FI values are

$$(\mu_1, \mu_2, \mu_3) = (a + c, b - a, -b - c) = \frac{s}{2\pi}(1, -2, 1). \tag{VIII.6.53}$$

The first component requires $s \geq 0$ and the third requires $s \leq 0$. Hence $s = 0$, then $a = b = c = 0$. No value of the formal FI line has a populated connected solution. The algebraic result (VIII.6.51) and the real D equations therefore give the same answer for different reasons: invariant polynomials collapse all complex orbit closures, while positivity rules out a nonzero zero-moment representative.

One can see the collapse without invariant theory terminology. Under $t \in \mathbb{C}^*$, the five fields scale as $(tx_1, tx_2, tx_3, tx_4, t^2x_5)$. For any fixed point, the limit $t \to 0$ is the origin. Every polynomial constant on these orbits therefore has the same value at the given point as at the origin. The limit is a closure operation, not a gauge transformation by an element of $\mathbb{C}^*$. Confusing those two operations is what makes a generic orbit count look like a fourfold even though the affine quotient has one point.

VIII.6.6 Fields, monopoles and several branes

At higher ranks, the abelian result can be carried to a particular separated branch. Give every node equal rank N and take bifundamental matrices diagonal in matched eigenlines. Suppose their real scalar eigenvalues s_α, $\alpha = 1, \ldots, N$, are pairwise distinct, and the configurations on the chosen generic locus satisfy the required off-diagonal mass conditions. The edge term generalizes schematically to

$$\sum_{e:a\to b} \sum_{\alpha,\beta} |(\phi_e)_{\alpha\beta}|^2 (\sigma_{a,\alpha} - \sigma_{b,\beta})^2. \tag{VIII.6.54}$$

For unmatched distinct eigenvalues, vanishing of this term sets the corresponding off-diagonal bifundamental entries to zero. Matched diagonal entries obey the abelian F and D equations independently on the separated locus.

The matrix equation also explains why equal node ranks are assumed. An eigenline at one node must be matched to an eigenline at every node that carries nonzero bifundamental support. With ranks N_i that differ, such a complete matching need not cover all basis vectors. Extra unpaired directions can support different vacua or

unbroken gauge factors. The simple N-copy argument then has no reason to describe the entire moduli space.

For a superpotential built from traces of closed quiver paths, the diagonal ansatz splits the expression before taking derivatives. If the αth eigenline carries the abelian fields $\phi_e^{(\alpha)}$, then on this ansatz

$$W_{\text{matrix}}\big|_{\text{diag}} = \sum_{\alpha=1}^{N} W_{\text{abelian}}\big(\phi^{(\alpha)}\big), \qquad \left.\frac{\partial W_{\text{matrix}}}{\partial \phi_e^{(\alpha)}}\right|_{\text{diag}} = \frac{\partial W_{\text{abelian}}}{\partial \phi_e}\big(\phi^{(\alpha)}\big). \quad \text{(VIII.6.55)}$$

For the cubic cycle, this is just the sum of $\epsilon_{ijk} X_i^{(\alpha)} Y_j^{(\alpha)} Z_k^{(\alpha)}$ over eigenlines. It explains why the abelian F equations reappear on the separated branch. It does not establish that every matrix solution is simultaneously diagonalizable.

The Chern–Simons term splits just as explicitly when restricted to diagonal connections. Write $A_i = \operatorname{diag}(A_i^{(1)}, \dots, A_i^{(N)})$ on the separated patch. The fundamental trace contains no cross term between distinct eigenlines:

$$S_{\text{CS}}\big|_{\text{diag}} = \frac{1}{4\pi} \sum_{\alpha=1}^{N} \sum_{i=1}^{G} k_i \int A_i^{(\alpha)} \wedge dA_i^{(\alpha)}. \quad \text{(VIII.6.56)}$$

For each fixed α we may therefore choose $b_i^{(\alpha)} = A_i^{(\alpha)} - A_G^{(\alpha)}$ and $c^{(\alpha)} = A_G^{(\alpha)}$, exactly as in (VIII.6.13). On this diagonal patch the same matrix K' and first-order equation appear separately on every eigenline:

$$K'_\alpha = \begin{pmatrix} \operatorname{diag}(\kappa) & \kappa \\ \kappa^T & 0 \end{pmatrix}, \qquad \sum_{i<G} k_i b_i^{(\alpha)} = d\tau_\alpha, \quad \tau_\alpha \sim \tau_\alpha + 2\pi. \quad \text{(VIII.6.57)}$$

This derivation explains the separate abelian character conditions appearing in the scalar position calculation. A common Weyl permutation exchanges the full tuples $(\phi^{(\alpha)}, b^{(\alpha)}, c^{(\alpha)}, \tau_\alpha)$, not the matter fields alone. The derivation is restricted to the diagonal patch; the full compact $U(N)^G$ cocharacter lattice and non-diagonal vacua still require their own treatment.

For two eigenlines this means

$$\phi_e = \operatorname{diag}(\phi_e^{(1)}, \phi_e^{(2)}), \qquad \sigma_i = \operatorname{diag}(s_1, s_2), \qquad s_1 \neq s_2. \quad \text{(VIII.6.58)}$$

Each line carries its own instance of the abelian character quotient. The common Weyl transformation at all nodes exchanges the two lines, since an independent permutation at one node would make the generic diagonal arrows off-diagonal. Thus the separated configuration space has the local symmetric-product form

$$\big(\mathcal{M}_{1,\text{geom}}^{\text{sep}} \times \mathcal{M}_{1,\text{geom}}^{\text{sep}}\big)/S_2, \quad \text{(VIII.6.59)}$$

with the same conditions on each factor. For general N, replace S_2 by the common S_N. This describes a branch on the generic separated locus, not every nonabelian or coincident solution.

The two-line example makes the action concrete. If the abelian coordinates on the selected fourfold patch are p_1, p_2, a simultaneous Weyl exchange acts as

$$(\phi_e^{(1)}, \phi_e^{(2)}; s_1, s_2) \longmapsto (\phi_e^{(2)}, \phi_e^{(1)}; s_2, s_1), \qquad (p_1, p_2) \longmapsto (p_2, p_1). \tag{VIII.6.60}$$

Each p_α has already been identified by its own compact character kernel before this exchange. At a fixed point of the permutation, the off-diagonal fluctuations may become light and this coordinate patch ceases to prove a complete local description. In particular, pairwise distinct points in the quotient are not by themselves a substitute for the stated mass condition.

Magnetic operators remind us why the compact lattice matters beyond ordinary scalar coordinates. A magnetic insertion is specified by an integral cocharacter of the full gauge group. In $U(2)$, the diagonal matrix of fluxes $(1, 0)$ is primitive, whereas a flux assigned only to the central connection would have to respect the quotient linking central and special-unitary factors. The abelian basis (VIII.6.13) should therefore not be applied independently to each nonabelian center without checking that full $U(N)$ lattice.

For example, the loop $\mathrm{diag}(e^{i\varphi}, 1)$ for $0 \le \varphi \le 2\pi$ closes in $U(2)$ and has flux vector $(1, 0)$. The central loop $e^{i\varphi} I_2$ instead carries $(1, 1)$. Their determinant windings are one and two, respectively:

$$\frac{1}{2\pi i} \oint d \log \det \mathrm{diag}(e^{i\varphi}, 1) = 1, \qquad \frac{1}{2\pi i} \oint d \log \det(e^{i\varphi} I_2) = 2. \tag{VIII.6.61}$$

Treating the central phase as the only primitive magnetic variable would omit the first allowed insertion. This small example is enough to show why the global group has to remain in the statement of a multi-brane claim.

In the separated branch, diagonal magnetic data can be associated with each eigenline, and the Weyl group permutes those assignments with the scalar entries. This compatibility is useful when comparing geometric positions with monopole-dressed operators from Chapter 3. It does not calculate monopole operator products, quantum corrections, or the global structure of the coincident branch. Those require new input, especially when flavors are added in Chapter 8.

The two-line version of the three-node example gives a concrete position calculation. On the patch where each line has $X_1^{(\alpha)} Y_1^{(\alpha)} \neq 0$, write its abelian coordinates as $(R_\alpha, S_\alpha, P_\alpha, Q_\alpha)$ from (VIII.6.43). Before the common Weyl exchange, the two lines have eight independent complex chart coordinates. The exchange acts simultaneously on all four coordinates:

$$(R_1, S_1, P_1, Q_1;\, R_2, S_2, P_2, Q_2) \longmapsto (R_2, S_2, P_2, Q_2;\, R_1, S_1, P_1, Q_1). \tag{VIII.6.62}$$

For instance, $R_1 + R_2$ and $R_1 R_2$ do not label which eigenline carried which value, as required for indistinguishable separated branes. For doubled levels the finite representative acts independently on each local eigenline as $(R_\alpha, S_\alpha) \mapsto (-R_\alpha, -S_\alpha)$. The common permutation then exchanges the two finite orbits. This is a local description of scalar positions on the diagonal branch. It does not assert that independent central $U(1)$ fluxes exhaust the full $U(2)^G$ magnetic sectors.

An explicit two-line vacuum shows that the product in (VIII.6.59) contains actual solutions rather than just formal copies of an F component. Use the three-node cubic cycle at levels $(1, 1, -2)$ and let each eigenline's rows form a rank-one matrix. Choose

$$\mathcal{M}^{(1)} = \begin{pmatrix} 1 & 1 & 1 \\ 1 & 1 & 1 \\ 1 & 1 & 1 \end{pmatrix}, \qquad \mathcal{M}^{(2)} = \begin{pmatrix} 2/\sqrt{3} & 2/\sqrt{3} & 2/\sqrt{3} \\ \sqrt{5/3} & \sqrt{5/3} & \sqrt{5/3} \\ 1 & 1 & 1 \end{pmatrix}, \qquad (s_1, s_2) = (0, 2\pi). \tag{VIII.6.63}$$

All three rows of each matrix are proportional, so the F terms vanish. Their squared row norms are respectively $(3, 3, 3)$ and $(4, 5, 3)$. The corresponding node moments are

$$\mu^{(1)} = (0, 0, 0) = k\, s_1/(2\pi), \qquad \mu^{(2)} = (1, 1, -2) = k\, s_2/(2\pi). \tag{VIII.6.64}$$

Both supports are populated. The distinct values s_1, s_2 make the off-diagonal entries in (VIII.6.54) costly on this ansatz. Exchanging the two matrices and their scalar values is a common Weyl transformation, not a third membrane position. This check ties the symmetric-product notation to the actual classical vacuum equations.

There is also a useful diagnostic for leaving this patch. The quadratic term (VIII.6.54) vanishes for an off-diagonal entry whenever a matched pair of scalar eigenvalues becomes equal. Such an entry is then not removed by that mass term, and a diagonal solution may meet a noncommuting or singular stratum. The symmetric-product expression remains a correct description of the specified separated branch; extending it through this locus requires solving the full matrix F and D equations. This is the physical reason to keep the separated condition next to the multi-brane result.

VIII.6.7 Where the construction changes

The derivation has three separate hinges. Connected populated support gave a common s. A nonzero level vector of zero total sum gave a nontrivial BF character with an unrestricted *possible* FI direction. A populated dense closed-orbit stratum made the complex dimension count an affine-geometric statement. Dropping any one of these assumptions changes the result.

If $\sum_i k_i \neq 0$, the common-σ equation (VIII.6.8) forces $s = 0$. If the support graph splits into components C, the edge potential permits a separate s_C on each component; for a component with no matter leaving it, summing its D equations gives

$$s_C \sum_{i \in C} k_i = 0. \tag{VIII.6.65}$$

This is only a necessary equation on a disconnected candidate branch. Its F equations and remaining D equations still decide existence.

If every $k_i = 0$, the character is trivial and the BF mechanism used here disappears. That case cannot be recovered by assigning a gcd to the zero vector. By contrast, one vanishing level among nonzero levels is already covered. Fundamental flavors change the action of the overall diagonal group and the moment-map sum; quantum monopoles can change the coordinate ring. These are real changes of the physical problem, not alternative notation for the same quotient.

The zero-vector case can be compared on the stable rank-one F locus without making a new general claim. If its three levels were all zero, the usual bifundamental quotient would use the full relative torus L of dimension two. The same open rank-one chart has five complex coordinates and closed generic $L_{\mathbb{C}}$ orbits. Locally its invariants can be represented by (T, P, Q) from (VIII.6.44), so its quotient has complex dimension three on that patch. The nonzero level vector instead selects the one-dimensional H^0 quotient and leaves the four coordinates (R, S, P, Q). This comparison identifies the mechanism that changes the dimension. It is not an assertion about the full quantum theory at zero levels.

Likewise, add hypothetically a field q of charge $+1$ at node one. The common diagonal now acts on q, and the sum of node moments contains $|q|^2$:

$$\mu_i^{\mathrm{new}} = \mu_i + \delta_{i1}|q|^2, \qquad \sum_i \mu_i^{\mathrm{new}} = |q|^2. \tag{VIII.6.66}$$

The step $\sum_i \mu_i = 0$ in (VIII.6.8) no longer follows for a vacuum with $q \neq 0$. Nor is the common diagonal automatically an ineffective matter gauge group. The flavor problem needs its own quotient and monopole analysis, which is why it belongs to the next construction rather than to an unqualified extension of this chapter's formula.

The three principal examples can now be compared without suppressing the condition that made each result true.

Classical example	$\dim F$	$\dim H^0$	Populated closed stratum	Quotient dim.
Two-node ABJM position branch	4	0	present on the generic branch	4
Three-node rank-one matrix	5	1	mixed row weights, present	4
Five-arrow positive-weight model	5	1	absent at zero moment level	0

The first two rows have the same quotient dimension for different numbers of gauge nodes. The third has the same input dimensions as the second and a different answer. The finite group does not appear in the dimension column, yet it distinguishes functions in the doubled-level version of the second row. A calculation reporting only a quotient dimension therefore misses both the population question and the compact identification.

The construction combines vacuum equations with the integral compact quotient. Auxiliary fields expose a candidate FI line; primitive BF dualization gives a character kernel and finite field action. A populated closed complex orbit then determines whether the affine quotient is a fourfold. Chapter 7 builds toric examples; Chapter 8 adds flavor and monopole ingredients.

Exercises

1. **Primitive BF basis.** For compact $U(1)^3$ with $k = (2, -1, -1)$ and bifundamental matter, set $b_1 = A_1 - A_3$, $b_2 = A_2 - A_3$, $c = A_3$. Submit integer M in $A =$

$M(b_1, b_2, c)^T$, $\det M$, transformed K', its BF row to c, and the primitive dual-scalar period as a multiple of π. Explain why treating $A_1 + A_2 + A_3$ as primitive changes the flux lattice.

2. **A finite field action.** For the three-family cycle with $W = \epsilon_{ijk} X_i Y_j Z_k$, compare levels $(1, 1, -2)$ and $(2, 2, -4)$. Submit connected weights on (X_i, Y_i, Z_i), component groups, the second theory's action of $(\beta_1, \beta_2) = (\pi, 0)$, and the two signs on $X_1 Y_1^2$. Exhibit any nonzero F-flat, zero-H-moment point where this polynomial is nonzero, and give its value. For a structured submission, choose real rational coordinates with reduced numerator magnitude and positive denominator at most 1000; written solutions may use any valid complex point.

3. **A stable fourfold calculation.** On the rank-one matrix F locus at $X_1 \neq 0$, submit five free coordinates, four dependent formulas, the connected moment map and the affine connected quotient dimension, together with the F-locus and orbit dimensions. State the closed-orbit condition used. For a structured submission, order the free coordinates as X_1, X_2, X_3, Y_1, Z_1 and the dependent formulas as Y_2, Y_3, Z_2, Z_3; list each numerator as its row coordinate followed by its X coordinate, with common denominator X_1.

4. **A failed dimension subtraction.** For the five-arrow $W = 0$ model with $k = (1, -2, 1)$ above, submit the five integer weights, the invariant ring, the zero-H-moment solution set and its affine quotient dimension. State whether a populated closed orbit exists. Identify which hypothesis of (VIII.6.37) fails, despite generic effectiveness.

Status and sources

Sources by section. Source coordinates and scope qualifications follow.

§VIII.6.1. The geometric-branch question fixes the connected populated classical scope. The M2 interpretation is a source-supported premise, not a full IR identification (Martelli and Sparks 2008, §3; the connected abelian classical branch).

§VIII.6.2. Auxiliary-field equations and the common-σ consequence are conditional [MATH] under the sourced potential and mapped arrow signs (Martelli and Sparks 2008, §3).

§VIII.6.3. The primitive compact circle and BF reduction are conditional [MATH] under the full $U(1)^G$ lattice, the connected abelian classical branch (Martelli and Sparks 2008, §3).

§VIII.6.4. The component group and finite field action are conditional [MATH] under the stated character-kernel hypotheses (Martelli and Sparks 2008, §3).

§VIII.6.5. The fourfold dimension is conditional [MATH] on a populated dense closed-orbit stratum; generic effectiveness alone is insufficient (Martelli and Sparks 2008, §3).

§VIII.6.6. The separated higher-rank diagonal branch is a sourced classical ansatz; it yields no complete quantum moduli claim (Martelli and Sparks 2008, §4; the connected abelian classical branch and Chern–Simons trace and levels).

§VIII.6.7. The nine-chiral parity completion is an allowed [ANOM] choice under the classical tiling and gauge-parity frame, not a selected string completion (Benini et al. 2011, §6).

This chapter establishes a scoped classical geometric-branch quotient, not a complete moduli-space classification or an infrared duality. The bosonic potential, compact Chern–Simons premises and separated-branch ansatz are sourced physical inputs. The matrix transformation, graph constraint, finite field action, determinantal chart and contrasting invariant rings are conditional algebra. The connected abelian classical branch uses the stated arrow orientation, superpotential normalization, Chern–Simons trace and compact gauge group. The ABJM comparison uses the full compact product, and the nine-chiral example uses the specified gauge-parity completion.

Vacuum equations and signs, §VIII.6.2. The source potential and vacuum equations are in Martelli and Sparks (2008), §3, equations (3.3)–(3.17), physical PDF pages 6–8. Its arrow direction and $\mathcal{D}$ sign differ from the book convention; the correlated arrow, D and σ map in (VIII.6.7) is required. The source's FI-line discussion does not prove that every value is populated for an arbitrary quiver.

Primitive circle and finite quotient, §VIII.6.3 and §VIII.6.4. The compact gauge discussion and quotient are in Martelli and Sparks (2008), §3, equations (3.18)–(3.42), physical PDF pages 8–11. The source uses $a = \sum A_i$ and its branch-dependent dual period; the primitive $c = A_G$ construction here preserves the original integral torus. The local scalar relation does not identify all flux or flat sectors. The indexed polynomial and its finite action are explicit applications of the admitted character kernel.

For the nine-chiral example, Benini et al. (2011), §6, equations (6.1) and (6.3)–(6.6), printed pages 46–47, supplies the fermion-regulated spin Chern–Simons framework for trace-product terms. The zero-row-sum parity correction preserves the displayed branch and BF row; this framework does not select a string-theoretic completion.

Fourfold condition and branch scope, §VIII.6.5 and §VIII.6.6. The affine quotient viewpoint occurs in Martelli and Sparks (2008), §3, equations (3.39)–(3.42). The populated dense closed-orbit hypothesis, rank-one local chart and all-positive-weight counterexample state the extra conditions needed for the four-dimensional conclusion. The higher-rank diagonal ansatz is in Martelli and Sparks (2008), §4, equations (4.23)–(4.28), PDF pages 16–17. Only equal ranks and separated matched eigenvalues are used here. The source premises do not establish arbitrary-quiver quantum consistency, a complete nonabelian vacuum space, a metric, or an M2 duality.

References

Benini, F., C. Closset, and S. Cremonesi (2011). "Quantum moduli space of Chern-Simons quivers, wrapped D6-branes and AdS4/CFT3". In: *JHEP* 09, p. 005. DOI: 10.1007/JHEP09(2011)005. arXiv: 1105.2299 [hep-th].

Martelli, D. and J. Sparks (2008). "Moduli spaces of Chern-Simons quiver gauge theories and AdS(4)/CFT(3)". In: *Phys. Rev. D* 78, p. 126005. DOI: 10.1103/PhysRevD.78.126005. arXiv: 0808.0912 [hep-th].

Chapter VIII.7

Toric fourfolds from Chern–Simons tilings

A brane tiling on a two-torus ordinarily organizes a quiver whose regular-brane mesonic moduli space is a Calabi–Yau threefold. An M2-brane instead moves in a four-complex-dimensional transverse cone. In three dimensions a Chern–Simons (CS) level supplies an extra integral direction, but drawing an extra axis next to a tiling does not determine its lattice. The axis must come from actual edge weights and from the compact gauge quotient of the membrane theory.

We develop that dictionary on the connected, populated, single-brane geometric branch. The main example is the three-node cyclic quiver with nine fields and levels $(1, 1, -2)$. Its six perfect matchings yield the five external vertices of the toric diagram of the cone over $M^{1,1,1}$, together with one nonexternal matching. The same quotient gives a Hilbert series whose first nonconstant coefficient is 30. Doubling all levels preserves the connected charge matrix but changes that coefficient to 10. This comparison shows why a toric picture must retain the compact lattice, not only the real polytope.

The construction uses a specified classical coherent F-term component with a dense stratum of populated closed orbits represented by zero-moment vacua. The scalar expectation values have common σ on that stratum, as in Chapter 6. A toric diagram here describes its affine quotient. The stronger identification with a full quantum branch or an infrared SCFT requires additional input. This boundary will also help distinguish a CS-weighted two-torus tiling from an M-theory crystal or a D1 brane brick.

VIII.7.1 From a threefold tiling to a fourfold question

The familiar square tiling of the one-brane ABJM quiver is a compact warmup. Take $U(1)_k \times U(1)_{-k}$, two arrows $A_1, A_2 : 1 \to 2$, two arrows $B_1, B_2 : 2 \to 1$, and the quartic superpotential. For commuting fields its two terms cancel, so every F derivative vanishes. Each of the four tiling edges is a perfect matching. The connected residual quotient has rank zero, while the compact CS action retains a finite group. With the book's

physical tail-positive arrow charges its action is

$$(A_1, A_2, B_1, B_2) \longmapsto (\omega A_1, \omega A_2, \omega^{-1} B_1, \omega^{-1} B_2), \qquad \omega^k = 1. \tag{VIII.7.1}$$

Thus the specified single-brane branch is $\mathbb{C}^4/\mathbb{Z}_{|k|}$. At $|k| = 1$ the four matching rays form a primitive tetrahedron. At larger $|k|$, renormalizing every height difference to one would erase the orbifold action in (VIII.7.1). We need a route from the tiling to the *integral* ray lattice.

There is already an elementary flow check in this smallest model. With the head-positive convention that we define below, an A arrow contributes $(-1, 1)$ to the incidence and a B arrow contributes $(1, -1)$. For levels $(k, -k)$, assigning $n_{A_1} = -k$ and the other three edge weights zero gives

$$d_{\mathrm{ABJM}} n = (-k)(-1, 1) = (k, -k). \tag{VIII.7.2}$$

The four square-tiling matchings acquire four heights, one displaced by k relative to the others in this choice of cell. An integral change of the torus cycles moves which vertex appears displaced; the lattice height separation, together with the finite action, does not disappear. This warmup tells us what the third exponent of a weighted matching polynomial is supposed to measure.

Let a connected consistent bipartite tiling on an oriented T^2 have E edges and G quiver nodes. A perfect matching contains precisely one edge incident on each black and each white tiling vertex. If the matchings are p_α, define their edge-incidence matrix and monomial map by

$$P_{I\alpha} = \begin{cases} 1 & I \in p_\alpha, \\ 0 & I \notin p_\alpha, \end{cases} \qquad X_I = \prod_{\alpha=1}^{c} p_\alpha^{P_{I\alpha}}. \tag{VIII.7.3}$$

The p_α are homogeneous coordinates for the coherent F-term component; they need not represent different lattice points after quotient. The integer relations among these coordinates form

$$Q_F \text{ a primitive row basis of } \ker_{\mathbb{Z}} P, \qquad \mathcal{F}_{\mathrm{coh}} = \mathbb{C}^c /\!/ (\mathbb{C}^*)^{\mathrm{rk}\, Q_F}. \tag{VIII.7.4}$$

Only when the monomial chart and component in question have the expected properties does this quotient describe the relevant F-flat variety. We will verify them directly in the nine-field example.

The matching map is useful because it first solves the superpotential relations and only then performs gauge identifications. In a threefold tiling one often presents the resulting mesonic toric diagram after all four-dimensional D terms. A three-dimensional CS theory changes this last step. Its vector multiplet scalar and diagonal compact photon rearrange the quotient so that only $G - 2$ continuous matter directions are removed on the common-σ branch. That one-direction difference is where the extra complex dimension becomes possible. It is a dimension count to be checked on stable orbits, not a rule that every CS quiver has a fourfold component.

The extra toric coordinate is supplied by integer CS levels $k \in \mathbb{Z}^G$ with $\sum_a k_a = 0$ and $k \neq 0$. Denote the physical tail-positive charge of edge $I : a \to b$ by q_{aI}^{phys}, equal to

$+1$ at a and -1 at b. For the tiling calculation alone, use the head-positive incidence

$$d_{aI} = \delta_{a,h(I)} - \delta_{a,t(I)} = -q_{aI}^{\mathrm{phys}}. \tag{VIII.7.5}$$

This sign distinction is essential. The edge flow n below solves $dn = k$; in physical tail-positive variables its negative is the corresponding flow. Neither choice changes the physical arrows or levels.

VIII.7.2 Perfect matchings solve the F equations

Which F-flat component does the matching construction see? Consider $U_i : 1 \to 2$, $V_i : 2 \to 3$, and $W_i : 3 \to 1$ for $i = 1, 2, 3$, with

$$W = \epsilon_{ijk} U_i V_j W_k, \qquad k = (1, 1, -2). \tag{VIII.7.6}$$

The three triples are vectors in $\mathbb{C}^3$. Differentiation gives all nine equations, not merely a representative subset,

$$\frac{\partial W}{\partial U_i} = \epsilon_{ijk} V_j W_k, \quad \frac{\partial W}{\partial V_j} = \epsilon_{ijk} U_i W_k, \quad \frac{\partial W}{\partial W_k} = \epsilon_{ijk} U_i V_j. \tag{VIII.7.7}$$

They are the three components of each pairwise cross product. Consequently every 2×2 minor of the 3×3 matrix with rows U, V, W vanishes. For example, the W_3 equation is $U_1 V_2 - U_2 V_1 = 0$, while the U_1 equation is $V_2 W_3 - V_3 W_2 = 0$. Conversely, the vanishing minors give every derivative in (VIII.7.7). The coherent locus is the rank-at-most-one determinantal variety,

$$\mathcal{F}_{\mathrm{coh}} = \{(U, V, W) : \operatorname{rank} \begin{pmatrix} U_1 & U_2 & U_3 \\ V_1 & V_2 & V_3 \\ W_1 & W_2 & W_3 \end{pmatrix} \leq 1\}. \tag{VIII.7.8}$$

For completeness the three triples of minors can be displayed as

$$\begin{array}{lll} U_2 V_3 - U_3 V_2, & U_3 V_1 - U_1 V_3, & U_1 V_2 - U_2 V_1, \\ V_2 W_3 - V_3 W_2, & V_3 W_1 - V_1 W_3, & V_1 W_2 - V_2 W_1, \\ W_2 U_3 - W_3 U_2, & W_3 U_1 - W_1 U_3, & W_1 U_2 - W_2 U_1. \end{array} \tag{VIII.7.9}$$

The rows of (VIII.7.9) arise by differentiating with respect to W, U, and V, respectively, up to the cyclic order of the indices. A missing family would leave a larger reducible locus. Their joint vanishing says that any two nonzero rows are proportional; if only one row is nonzero the matrix still has rank one. Thus the rank condition captures the boundary points of this determinantal component as well as its open chart. On $U_1 \neq 0$, five coordinates U_1, U_2, U_3, V_1, W_1 are free and the other four satisfy $V_i = V_1 U_i / U_1$ and $W_i = W_1 U_i / U_1$ for $i = 2, 3$. This gives complex dimension five. It also shows explicitly why the coherent component contains populated points rather than only a formal monomial image.

A concrete populated point is $U = V = W = (1, 1, 1)$. It makes every minor zero. Its three row norms coincide, so the connected moment condition with weights $(2, -1, -1)$

is also zero. All arrows are nonzero and connect the three nodes. This point is therefore a transparent representative of the geometric branch used in the dimension count. It is not meant to parametrize every boundary stratum.

The six matchings have a simple description. For $i = 1, 2, 3$, p_i consists of the same-index triple $\{U_i, V_i, W_i\}$; q_1, q_2, q_3 consist of all three U, all three V, and all three W edges respectively. Their map is

$$U_i = p_i q_1, \qquad V_i = p_i q_2, \qquad W_i = p_i q_3. \tag{VIII.7.10}$$

The 9×6 matching matrix in the row order $(U_1, U_2, U_3, V_1, V_2, V_3, W_1, W_2, W_3)$ and column order $(p_1, p_2, p_3, q_1, q_2, q_3)$ is

$$P = \begin{pmatrix} 1 & 0 & 0 & 1 & 0 & 0 \\ 0 & 1 & 0 & 1 & 0 & 0 \\ 0 & 0 & 1 & 1 & 0 & 0 \\ 1 & 0 & 0 & 0 & 1 & 0 \\ 0 & 1 & 0 & 0 & 1 & 0 \\ 0 & 0 & 1 & 0 & 1 & 0 \\ 1 & 0 & 0 & 0 & 0 & 1 \\ 0 & 1 & 0 & 0 & 0 & 1 \\ 0 & 0 & 1 & 0 & 0 & 1 \end{pmatrix}. \tag{VIII.7.11}$$

The U_i, V_i, W_i equations (VIII.7.10) are therefore the direct incidence reading of the six matchings. A vector $(a_1, a_2, a_3, b_1, b_2, b_3)$ is in $\ker P$ precisely when $a_i + b_A = 0$ for every i, A. Hence all a_i coincide, all b_A are their negatives, and the primitive F charge is

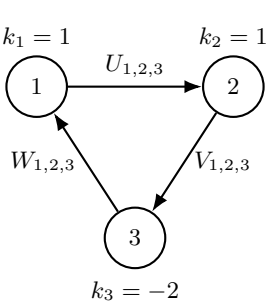
$$\operatorname{rank} P = 5, \qquad Q_F = (-1, -1, -1, 1, 1, 1). \tag{VIII.7.12}$$

This first quotient has dimension $6 - 1 = 5$; the CS gauge quotient is still to come. It is useful to keep this sequence distinct from directly counting mesonic operators. The latter already includes the second quotient.

The matching sets can be checked directly from the three-by-three bipartite matrix that appears later. Each of its six permanent terms chooses one entry in each row and column. The choices that take three fields of one species give q_1, q_2, q_3; the choices that take one field of each species with the same index give p_1, p_2, p_3. No seventh permutation remains. This explains the exact number six without reading it off from a picture. It also makes the duplicated planar position of the three q matchings less mysterious: they are distinct monomials even when the projection to the parent threefold draws them at the same point.

VIII.7.3 The compact gauge lattice determines the quotient

The three physical $U(1)$ phases do not all act as independent quotient directions on the common-σ branch. The uncharged diagonal phase is removed after its compact dual



$p_i = \{U_i, V_i, W_i\},\ i = 1, 2, 3$
$q_1 = \{U_1, U_2, U_3\}$
$q_2 = \{V_1, V_2, V_3\}$
$q_3 = \{W_1, W_2, W_3\}$

Schematic projection of the primitive height-one slice

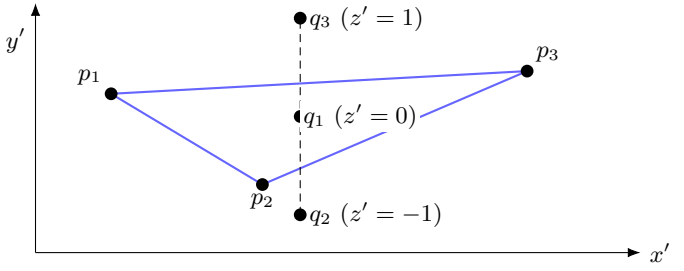


Figure VIII.7.1: The same nine-field model in three views. The physical arrows are tail-positive and carry levels $(1, 1, -2)$. Each listed matching contains three actual edges. The lower schematic projection retains the fixed labels $(p_1, p_2, p_3, q_1, q_2, q_3)$ and the vertical ordering, with q_1 between the tips. Exact reflected coordinates are in (VIII.7.30).

scalar is treated, leaving the character kernel of the CS level. Its full group is

$$H = \ker\Big[\chi_k : U(1)^G \to U(1), \quad (e^{i\theta_a}) \mapsto e^{i\sum_a k_a\theta_a}\Big] / U(1)_{\mathrm{diag}}. \tag{VIII.7.13}$$

On the branch just specified, the continuous part has dimension $G - 2$; the component group is $\mathbb{Z}_{\gcd(k_a)}$. Equation (VIII.7.13) is an assertion about the compact group, so the integer cocharacter lattice must be taken before a rational nullspace. With $\theta_G = 0$ as a primitive relative basis, its connected lattice is

$$L_H = \ker_{\mathbb{Z}}(k_1, \ldots, k_{G-1}) \quad \text{in } \mathbb{Z}^{G-1}. \tag{VIII.7.14}$$

For the present $k = (1, 1, -2)$, this gives the generator $\ell = (1, -1, 0)$. Merely solving the two orthogonality equations $\sum_a \ell_a = 0$ and $k \cdot \ell = 0$ is unsafe in another level vector. At $k = (1, 0, -1)$, it yields $(1, -2, 1)$, while the primitive relative generator is $(0, 1, 0)$; the former produces weights divisible by three. The issue can be seen directly from the phase coordinates. Write $(\theta_1, \theta_2, \theta_3) = (\beta_1, \beta_2, 0) + \theta_3(1, 1, 1)$. For $k = (1, 1, -2)$, the connected condition becomes

$$\beta_1 + \beta_2 = 0 \pmod{2\pi}, \qquad (\beta_1, \beta_2) = (\alpha, -\alpha) \quad \text{on the identity component.} \tag{VIII.7.15}$$

The period of α is 2π, and the vector $(1,-1)$ is primitive in the relative cocharacter lattice. With levels $(1,0,-1)$ instead, the condition is $\beta_1 = 0$ and β_2 is the primitive circle. The orthogonal vector $(1,-2,1)$ maps to three times its matter action after the diagonal quotient. This is why an integer kernel taken before specifying the quotient basis can be nonprimitive even though every entry of that vector has gcd one.

For our cyclic arrows, $\ell^T q^{\mathrm{phys}}$ assigns $(2,-1,-1)$ to each (U_i, V_i, W_i). The matching charge lifting this action satisfies $Q_D P^T = \ell^T q^{\mathrm{phys}}$. One convenient row is

$$Q_D = (0,0,0,2,-1,-1), \qquad Q_D P^T = (2,2,2,-1,-1,-1,-1,-1,-1). \quad \text{(VIII.7.16)}$$

Adding a multiple of Q_F changes this lift without changing field charges. Combining the F and connected gauge quotients gives

$$Q_t = \begin{pmatrix} -1 & -1 & -1 & 1 & 1 & 1 \\ 0 & 0 & 0 & 2 & -1 & -1 \end{pmatrix}, \qquad \mathcal{M}_{\mathrm{conn}} = \mathbb{C}^6 /\!/ (\mathbb{C}^*)^2_{Q_t}. \quad \text{(VIII.7.17)}$$

The mixed signs in the D row matter for existence. A generic rank-one matrix has three nonzero rows, its gauge orbit has dimension one and a closed representative on the zero-H-moment locus. Thus the affine quotient has dimension $5 - 1 = 4$. A formal subtraction without such a populated closed-orbit stratum would not establish a fourfold, as the all-positive-weight counterexample in Chapter 6 shows. For example, at the all-ones matrix, $|U|^2 = |V|^2 = |W|^2 = 3$ and the connected real moment map is

$$\mu_H = 2|U|^2 - |V|^2 - |W|^2 = 6 - 3 - 3 = 0. \quad \text{(VIII.7.18)}$$

A generic complexified orbit can be rescaled until this mixed-sign moment vanishes, and its stabilizer is trivial because all three rows remain nonzero. This explicit solution is what permits the dimension subtraction here. At a point with only the U row populated, the same moment has one sign and the origin may be the only closed orbit in its closure. The latter point cannot by itself justify the fourfold count.

The matching lift also has a useful ambiguity. For any integer m, $Q_D + mQ_F$ produces the same nine physical field weights, since $Q_F P^T = 0$. It acts differently on the auxiliary matching coordinates but yields an equivalent presentation of the affine quotient. It does not change the compact finite component, which must still be computed from k and its primitive field action. For the displayed rows, a 2×2 minor using a p column and q_2 column has absolute value one. This is a quick certificate that the row lattice of Q_t is primitive here; it cannot replace the separate finite-group test after doubling the levels.

There is also a quantum consistency condition before calling the diagonal-only nine-field action a complete theory. Let Q be the full tail-positive 3×9 charge matrix. In a fixed fermion-regulator spin prescription, the parity contact matrix from the chiral fermions is

$$\Pi = \frac{1}{2} Q Q^T = \begin{pmatrix} 3 & -\frac{3}{2} & -\frac{3}{2} \\ -\frac{3}{2} & 3 & -\frac{3}{2} \\ -\frac{3}{2} & -\frac{3}{2} & 3 \end{pmatrix}. \quad \text{(VIII.7.19)}$$

The diagonal bare matrix $\mathrm{diag}(1,1,-2)$ has half-integral mixed entries in $K + \Pi$ and fails the mixed gauge parity condition on the full primitive flux lattice. One allowed

completion within that spin prescription is

$$K = \mathrm{diag}(k) + \Lambda, \qquad \Lambda = \Pi, \qquad K + \Pi = \mathrm{diag}(k) + 2\Pi \in M_3(\mathbb{Z}), \qquad \Lambda\mathbf{1} = 0. \tag{VIII.7.20}$$

The row sums of Π vanish because each bifundamental has zero charge under the common diagonal $U(1)$. In the primitive gauge basis $b_1 = A_1 - A_3$, $b_2 = A_2 - A_3$, $c = A_3$, the completed matrix for $k = (1, 1, -2)$ becomes

$$K' = \begin{pmatrix} 4 & -\frac{3}{2} & 1 \\ -\frac{3}{2} & 4 & 1 \\ 1 & 1 & 0 \end{pmatrix}. \tag{VIII.7.21}$$

In particular, the c cross row is still $(1, 1)$, which is the primitive BF character whose kernel appears in (VIII.7.13). The parity repair can therefore be stated adjacent to this classical calculation without changing its toric answer. The mixed half-integers in K' are meaningful only together with the declared fermion regulator, and there is no inference here about a bare bosonic theory with that matrix alone. Here K is symmetric in $S_{\mathrm{CS}} = \sum_{a,b} K_{ab} A_a \, dA_b/(4\pi)$; off-diagonal entries already represent both ordered terms. The half-integral bare matrix is part of the combined regulated fermion/CS system, not an independent bosonic CS theory. Since $\Lambda\mathbf{1} = 0$, the common-σ moment line and primitive diagonal BF row remain those of (VIII.7.13). This choice preserves the classical branch calculated here. It is one allowed completion of the parity obstruction, not a string-theoretic selection of a unique quantum model. Other flux sectors, line operators and dynamics need separate analysis. At equal rank N the analogous correction couples $\mathrm{Tr}\, A_a$ to $d\,\mathrm{Tr}\, A_b$ and is not a shift of the nonabelian single-trace CS levels.

VIII.7.4 Edge flows lift the Kasteleyn polynomial

How can the integer level vector become the vertical coordinate of each matching? Use the head-positive d of (VIII.7.5) and solve $dn = k$ with one integer n_I for each of the nine edges. For a connected quiver, the integer incidence image is the sum-zero lattice, so the solution exists when $\sum k_a = 0$. Here the three distinct incidence columns, one per arrow family, are

$$d_U = (-1, 1, 0)^T, \quad d_V = (0, -1, 1)^T, \quad d_W = (1, 0, -1)^T. \tag{VIII.7.22}$$

Choose $n_{U_1} = -1$, $n_{V_1} = -2$, and all seven other edge weights zero. The full nine-edge incidence calculation is then

$$d_{\mathrm{full}} n = (-1) d_U + (-2) d_V = (1, 1, -2)^T = k. \tag{VIII.7.23}$$

The vector $(-1, -2, 0)$ records the *total* flow in the U, V, W families. Assigning these numbers to every edge of a family would give $3k$, an actual change of the level vector. There are many solutions of $dn = k$. A change of edge flow by an integer circulation m with $dm = 0$ modifies matching heights. To compare two pictures as the same integral toric presentation one must show the induced change is an integral affine transformation

of the declared character lattice. The equality $d(n+m)=k$ alone does not prove that every coordinate renormalization is allowed. In particular, division by a common visual height spacing can remove torsion. The fixed nine-edge choice makes the test concrete.

Let (u_I, v_I) be the oriented crossings of edge I with the chosen fundamental cycles of T^2. In a bipartite matrix, weight that edge by $X_I x^{u_I} y^{v_I} z^{n_I}$. Expanding the permanent enumerates the matchings and assigns

$$h(p_\alpha) = \left(\sum_{I \in p_\alpha} u_I, \sum_{I \in p_\alpha} v_I, \sum_{I \in p_\alpha} n_I \right). \tag{VIII.7.24}$$

The permanent is appropriate because it does not cancel matching terms. A signed determinant would need a separately verified Kasteleyn sign system. The z coordinate is an integer sum over *actual edges*, and its allowed affine changes are integral in the compact quotient lattice. The six terms can be enumerated directly from the matrix below. Number its rows and columns from one to three. Each permutation selects one edge from each row and column,

columns selected	edge product	matching
$(1,2,3)$	$U_1W_1V_1$	p_1
$(1,3,2)$	$U_1U_2U_3$	q_1
$(2,1,3)$	$V_2V_3V_1$	q_2
$(2,3,1)$	$V_2U_2W_2$	p_2
$(3,1,2)$	$W_3V_3U_3$	p_3
$(3,2,1)$	$W_3W_1W_2$	q_3

. (VIII.7.25)

This is a direct matching count rather than an inference from the shape of the toric diagram. The x, y factors of the six products come from torus crossings; the z factor is the sum of edge flows.

The source's three-by-three weighted matrix uses a different raw height prescription. With $a=-k_1+k_2$, $b=-k_1-2k_2$ and $c=2k_1+k_2$, it is

$$K_{\mathrm{src}} = \begin{pmatrix} U_1 z^a & V_2 x z^b & W_3 y^{-1} z^c \\ V_3 z^b & W_1 z^c & U_2 z^a \\ W_2 y z^c & U_3 z^a & V_1 x^{-1} z^b \end{pmatrix}. \tag{VIII.7.26}$$

At $(k_1,k_2)=(1,1)$, its permanent has exactly six terms,

$$\begin{aligned} \operatorname{perm} K_{\mathrm{src}} = {} & z^{-9} V_1V_2V_3 + U_1U_2U_3 + z^9 W_1W_2W_3 \\ & + x^{-1} U_1V_1W_1 + xy U_2V_2W_2 + y^{-1} U_3V_3W_3. \end{aligned} \tag{VIII.7.27}$$

The V, U, W cubic terms are q_2, q_1, q_3. The other three are p_1, p_2, p_3 in that order. The source exponents are useful for finding support, but their raw difference-of-level weights do not themselves solve (VIII.7.23). We use the physical compact lattice to fix the primitive scale. At $(1,1,-2)$ the source shorthand is $(a,b,c)=(0,-3,3)$, so the three pure-species products have raw heights $(0,-9,9)$. A plot that simply divides by nine happens to draw the desired shape for this example, but gives no reason that the

division is legal in the compact character lattice. The next integral shear supplies the normalization, and the quotient matrix independently checks it.

Retain the same (x, y) crossings as (VIII.7.26), but use the nine-edge flow of (VIII.7.23). The six matching coordinates, still in the fixed $(p_1, p_2, p_3, q_1, q_2, q_3)$ order, are

$$\begin{array}{c|cccccc} & p_1 & p_2 & p_3 & q_1 & q_2 & q_3 \\ \hline x & -1 & 1 & 0 & 0 & 0 & 0 \\ y & 0 & 1 & -1 & 0 & 0 & 0 \\ z & -3 & 0 & 0 & -1 & -2 & 0 \end{array} . \tag{VIII.7.28}$$

The affine shear $z_s = z - 2x + y + 1$ sets all three p heights to zero and sends (q_1, q_2, q_3) to $(0, -1, 1)$. Its linear part has determinant one. Finally apply the fixed-label planar reflection

$$(x', y', z') = (x - y, -y, z_s), \qquad \det \frac{\partial(x', y', z')}{\partial(x, y, z)} = -1. \tag{VIII.7.29}$$

This gives the integral ray matrix

$$G_t = \begin{pmatrix} 1 & 1 & 1 & 1 & 1 & 1 \\ -1 & 0 & 1 & 0 & 0 & 0 \\ 0 & -1 & 1 & 0 & 0 & 0 \\ 0 & 0 & 0 & 0 & -1 & 1 \end{pmatrix}, \qquad G_t Q_t^T = 0. \tag{VIII.7.30}$$

No p_2/p_3 exchange has occurred. The source's sheared raw heights are nine times the primitive q heights for this example; multiplication by nine is a comparison between prescriptions, not a permitted unimodular rescaling. The gcd of the two-by-two minors of Q_t is one, and the gcd of the maximal minors of G_t is one. These integral checks fix both the quotient row lattice and the ray-span lattice. For a general tiling, compatibility of heights with the charge equations alone does not prove saturation; it must be checked for the example at hand. As a diagnostic, changing just n_{V_1} from -2 to -1 changes the incidence to

$$(-1)d_U + (-1)d_V = (1, 0, -1)^T. \tag{VIII.7.31}$$

This is another level vector, not a harmless height gauge choice. The flow equation and the primitive quotient test are separate checks; both are visible in (VIII.7.23) and (VIII.7.30).

VIII.7.5 Reading and counting the toric fourfold

The height-one slice of (VIII.7.30) has a base triangle formed by p_1, p_2, p_3. The two vertical tips are q_2 and q_3; q_1 is their midpoint. Thus there are five external vertices and six homogeneous matchings. Projection to the $z' = 0$ plane recovers the parent $\mathbb{C}^3/\mathbb{Z}_3$ triangle, including a point whose multiplicity came from three different q matchings before the lift. The fourfold cone is the one conventionally associated with $M^{1,1,1}$. The geometrical reading uses the full lattice in (VIII.7.30), not a sketch of its convex hull alone.

An explicit inverse makes this statement stronger than a rational kernel calculation. A connected invariant character has exponent vector

$$v(j,a,b,c) = (j-a, j-b, j+a+b, j, j-c, j+c) \in \mathbb{Z}^6, \tag{VIII.7.32}$$

where (j,a,b,c) are integers and all six entries are nonnegative. Indeed the two Q_t charges of this vector vanish. Conversely an integer nonnegative vector $v = (p_1,p_2,p_3,q_1,q_2,q_3)$ with $Q_t v = 0$ has the integral inverse

$$j = q_1, \qquad a = j - p_1, \qquad b = j - p_2, \qquad c = q_3 - j. \tag{VIII.7.33}$$

The third p and the remaining q coordinates then follow from the charge equations. This proves integral saturation of the invariant character lattice for this model, and nonnegative exponents select its semigroup. It also explains why a matching coordinate by itself need not be a generator of the gauge-invariant ring. The inverse can be tested on the two monomials that distinguish the finite projection. The product $U_1 V_1^2$ has matching exponents $(3,0,0,1,2,0)$, so $(j,a,b,c) = (1,-2,1,-1)$. The product $U_1 V_1 W_1$ has exponents $(3,0,0,1,1,1)$ and gives $(j,a,b,c) = (1,-2,1,0)$. Both lie in the connected invariant semigroup. Their distinct c values are precisely what the finite component detects; a convex polytope without its ambient lattice cannot distinguish them.

To count that ring, assign degree one to each p_i and zero to each q_A. This is a formal fugacity convention. It does not assert that an elementary chiral field has scaling dimension one. A two-variable Molien projection of the charges in (VIII.7.17) is

$$H(t) = \oint \frac{dz}{2\pi i z} \oint \frac{dw}{2\pi i w} \frac{1}{(1-t/z)^3 (1-zw^2)(1-z/w)^2}. \tag{VIII.7.34}$$

One can evaluate it without contour technology. A nonnegative invariant has q_1 exponent j. The D charge forces the total q_2, q_3 exponent to be $2j$, and the F charge forces total p exponent $3j$,

$$|p| = 3j, \qquad |q_2, q_3| = 2j, \qquad q_1 = j, \qquad j \in \mathbb{Z}_{\geq 0}. \tag{VIII.7.35}$$

There are $\binom{3j+2}{2}$ degree-$3j$ monomials in three p's and $2j+1$ degree-$2j$ monomials in (q_2,q_3). Thus

$$H(t) = \sum_{j\geq 0} \binom{3j+2}{2} (2j+1) t^{3j} = \frac{1 + 26t^3 + 26t^6 + t^9}{(1-t^3)^4} = 1 + 30t^3 + 140t^6 + 385t^9 + \cdots . \tag{VIII.7.36}$$

Keeping $SU(3)$ and $SU(2)$ fugacities refines the same count to

$$H(t; x, y, \xi) = \sum_{j\geq 0} \chi^{SU(3)}_{[3j,0]}(x,y) \chi^{SU(2)}_{[2j]}(\xi) t^{3j}. \tag{VIII.7.37}$$

The first nonconstant sector is $\mathrm{Sym}^3 \mathbf{3} \otimes \mathrm{Sym}^2 \mathbf{2}$, with $10 \cdot 3 = 30$ components. Its monomials have the form $p_i p_j p_k q_1 q_A q_B$ for $A, B \in \{2,3\}$. In elementary fields, one example is $U_1 V_1 W_1$, while $U_1 V_1^2$ is another connected invariant. The pole order four

checks the complex dimension. A Reeb or superconformal dimension assignment requires further physical input; the formal exponent $3j$ alone does not provide it. For $j=2$, there are $\binom{8}{2}=28$ degree-six monomials in the three p variables and five monomials of degree four in the two tip variables. The first sectors can be displayed as

j	$\lvert p\rvert$	$\lvert q_2,q_3\rvert$	# invariants
0	0	0	1
1	3	2	$10\cdot 3=30$
2	6	4	$28\cdot 5=140$

. (VIII.7.38)

This count explains the first coefficients independently of a contour choice. It also clarifies the word *generator*: the thirty degree-three invariants span the first nonconstant graded piece, whereas a printed finite cyclic representative need not generate the component group of the compact quotient.

Now double the levels to $2(1,1,-2)$. The connected row Q_D remains the same, but the full group (VIII.7.13) has two components. Choose $\theta_3=0$. The identity component is $(\theta_1,\theta_2)=(\alpha,-\alpha)$, whereas $\beta=(\pi,0,0)$ represents its nontrivial component. In general, for levels $r(1,1,-2)$ the primitive representative acts by

$$(U,V,W)\mapsto(\omega U,V,\omega^{-1}W),\qquad (q_1,q_2,q_3)\mapsto(\omega q_1,q_2,\omega^{-1}q_3),\qquad \omega=e^{2\pi i/r}. \tag{VIII.7.39}$$

For the character (VIII.7.32), this phase is ω^{-c}. The full invariant sublattice therefore requires

$$c\in r\mathbb{Z}. \tag{VIII.7.40}$$

At $r=2$, $c=-1,0,1$ for $j=1$, and only $c=0$ survives. Each allowed q sector has ten p monomials, so the degree-three coefficient becomes 10 rather than 30. Concretely, $U_1V_1^2$ is odd under (VIII.7.39), whereas $U_1V_1W_1$ is even. Counting allowed c at every degree gives

$$H_r(t)=\sum_{j\geq 0}\binom{3j+2}{2}\left(\sum_{c=-j}^{j}\frac{1}{r}\sum_{s=0}^{r-1}e^{-2\pi isc/r}\right)t^{3j}. \tag{VIII.7.41}$$

The inner root-of-unity average is one exactly when r divides c and zero otherwise. This finite Molien projector is derived from the actual field action. For $r=2$ it yields

$$H_{r=2}(t)=\sum_{j\geq 0}\binom{3j+2}{2}\begin{cases}j+1, & j \text{ even},\\ j, & j \text{ odd}\end{cases}t^{3j}=1+10t^3+84t^6+165t^9+455t^{12}+\cdots. \tag{VIII.7.42}$$

Writing $s=t^3$, the same exact series is

$$H_{r=2}(s)=\frac{1+9s+71s^2+54s^3+71s^4+9s^5+s^6}{(1-s)^4(1+s)^3}. \tag{VIII.7.43}$$

Its leading pole has half the primitive leading coefficient, as a degree-two quotient requires. At $j=2$, the allowed values $c=-2,0,2$ leave three q monomials and therefore

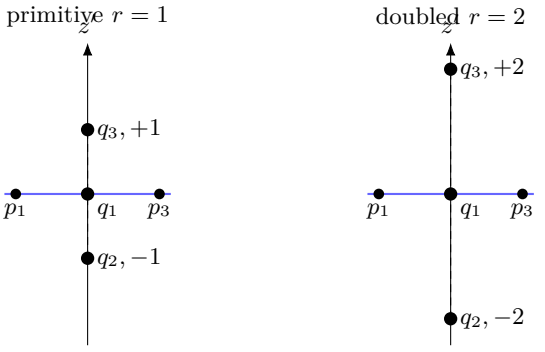


Figure VIII.7.2: The two vertical matching tips in one fixed compact ambient lattice. Their primitive heights ± 1 become ± 2 when the levels double, while the planar triangle and the connected charge row stay the same. The doubled ray span has index two, corresponding to the finite $\mathbb{Z}_2$ projection that removes twenty of the thirty degree-three connected invariants. This side view projects the planar base triangle onto a line; p_2 is not separately displayed. Horizontal positions are schematic; the vertical lattice spacing is the content of the comparison.

$28 \cdot 3 = 84$ states. This second sector checks the phase rule separately from the degree-three calculation. In the fixed ambient ray lattice the final row of (VIII.7.30) becomes $(0, 0, 0, 0, -r, r)$. The index-r ray span encodes precisely the finite invariant sublattice (VIII.7.40); dividing this height by r would lose the finite action.

The printed finite-action representative in the source's equation (6.11) does not always generate this component group. At these doubled levels it acts with phase ω^{2c} on a connected invariant, which is trivial at $r = 2$, and would incorrectly leave the coefficient at 30. The primitive representative in (VIII.7.39) is the one obtained from the compact relative basis. This is a specific source-formula limitation, not a change of the source's superpotential or its connected quotient.

VIII.7.6 Crystals and the boundary of the dictionary

The preceding extra coordinate arose from a level-weighted edge flow on T^2. A three-torus crystal builds a fourfold by a different geometric route. In the M-theory crystal proposal, a T-dual M5 configuration yields a periodic graph of atoms and bonds on T^3. A perfect matching chooses bonds in that graph. For two matchings, their oriented difference is a collection of closed cycles, hence a class in $H_1(T^3, \mathbb{Z})$,

$$\partial(m_\alpha - m_0) = 0. \tag{VIII.7.44}$$

At each atom a matching uses one incident bond. Subtracting two matchings therefore leaves balanced incoming and outgoing contributions there. The cancellation of this

boundary is the local reason the difference carries a homology class,

$$[m_\alpha - m_0] \in H_1(T^3, \mathbb{Z}) \simeq \mathbb{Z}^3. \tag{VIII.7.45}$$

The three integers are intrinsic winding numbers on the crystal's physical three-torus. In the CS tiling, by contrast, only the first two come from torus crossings; the third was an edge flow constrained by $dn = k$. Sharing a toric diagram does not identify these local constructions.

The $\mathbb{C}^4$ crystal provides a substantive test of (VIII.7.45). Choose one matching m_0 as origin. The four perfect matchings of the elementary crystal can be placed, after an integral basis choice, at

$$m_0 \mapsto (0,0,0), \quad m_1 \mapsto (1,0,0), \quad m_2 \mapsto (0,1,0), \quad m_3 \mapsto (0,0,1). \tag{VIII.7.46}$$

Their differences generate $H_1(T^3, \mathbb{Z})$, and the convex hull is a unit tetrahedron. Its cone is the toric $\mathbb{C}^4$ example. The integral test is the determinant of the three difference vectors from m_0,

$$\det \begin{pmatrix} 1 & 0 & 0 \\ 0 & 1 & 0 \\ 0 & 0 & 1 \end{pmatrix} = 1. \tag{VIII.7.47}$$

Using m_1 as reference instead gives the ordered differences to m_0, m_2, m_3,

$$((-1,0,0),(-1,1,0),(-1,0,1)), \qquad \det = -1. \tag{VIII.7.48}$$

The sign records the order and orientation; the absolute determinant still equals one. A sketch of a tetrahedron without this integral test would not distinguish $\mathbb{C}^4$ from a finite quotient. Adjoining the height-one row gives the four ray columns

$$G_{\mathbb{C}^4} = \begin{pmatrix} 1 & 1 & 1 & 1 \\ 0 & 1 & 0 & 0 \\ 0 & 0 & 1 & 0 \\ 0 & 0 & 0 & 1 \end{pmatrix}, \qquad |\det G_{\mathbb{C}^4}| = 1. \tag{VIII.7.49}$$

There is no nontrivial integral relation among these four rays. In the elementary affine coordinate ring, degree one for each of the four coordinates gives the standard count

$$H_{\mathbb{C}^4}(t) = \frac{1}{(1-t)^4} = \sum_{n \geq 0} \binom{n+3}{3} t^n. \tag{VIII.7.50}$$

The calculation relates the crystal tetrahedron to the familiar four-coordinate cone, while the matching-difference cycles explain where its three planar lattice coordinates came from. It does not give an inverse map from an arbitrary toric diagram to an M5 graph. Changing the reference matching translates all positions and does not change the simplex. The physical picture of intersecting M5 cycles motivates this construction; the matching-difference calculation is the precise toric statement used here. It does not derive the three-node CS quiver from that crystal.

There is a third three-torus object in this book. A D1 probe of a Calabi–Yau fourfold can lead to a two-dimensional $(0,2)$ brane-brick model. Its T^3 tessellation has chiral

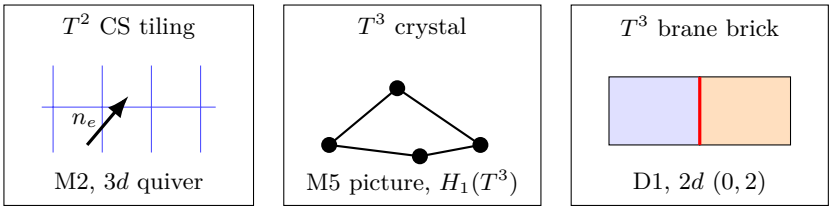


Figure VIII.7.3: Three constructions that can produce toric CY_4 information. Left, a CS-weighted T^2 dimer uses an assigned integer weight on each edge. Middle, an M-theory crystal on a physical T^3 has atoms and bonds; the difference between matchings winds around three cycles. Right, a D1 brane brick is a T^3 tessellation with distinct chiral and Fermi faces (schematically blue and orange). The panels encode different probes and worldvolume dimensions, even when their toric outputs agree.

and Fermi faces and encodes the corresponding interaction data. The following table and Figure VIII.7.3 compare the physical input rather than only the common toric output. The two three-tori in this comparison have different jobs. The crystal's cycles measure matching-difference homology, while the brick's periodic directions organize two-dimensional chiral and Fermi interactions. For the CS dimer the input remains T^2 even though its output rays live in $\mathbb{Z}^3$. A third output coordinate should not be mistaken for a third cycle of the input graph. The D1 brane-brick construction is developed in Volume VII, Chapter 10, where its Fermi interactions have their own geometric dictionary.

construction	probe/worldvolume	third toric coordinate
CS-weighted dimer on T^2	M2, $3d$ $\mathcal{N}=2$ candidate	integer edge flow $dn=k$
M-theory crystal on T^3	M5 geometric picture	matching difference in $H_1(T^3)$
brane brick on T^3	D1, $2d$ $(0,2)$	periodic brick geometry

The chapter's take-home message is that the CS level lifts perfect matchings only after an integer edge flow and a compact gauge lattice are fixed. In the nine-field example this produces a primitive $M^{1,1,1}$ diagram, an explicit invariant semigroup and a finite quotient whose first coefficient changes from 30 to 10 when the levels double. The crystal comparison shows an alternative route to fourfold toric geometry with different local data. There is no universal inverse algorithm here from a fourfold diagram to a unique tiling, crystal or infrared theory.

Exercises

1. **Nine-edge flow.** For the cyclic arrows and levels in (VIII.7.6), set $n_{U_1}=-1$ and $n_{V_1}=-2$, with every other edge flow zero. Compute the three components of $d_{\mathrm{full}}n$ and the six matching heights in the fixed $(p_1,p_2,p_3,q_1,q_2,q_3)$ order. Then assign the same two numbers to all three U and all three V edges and state the resulting level vector.

2. **Charges and rays.** Starting with (VIII.7.11), compute a primitive F charge, the displayed D charge and the 4×6 ray matrix. Submit the two integer matrix

products $Q_F P^T$ and $G_t Q_t^T$, and the determinant of the planar reflection. Explain why an unrecorded exchange of p_2 and p_3 would spoil the fixed-label comparison.

3. **The first two invariant sectors.** With the formal degree in (VIII.7.35), compute the coefficients of t^3 and t^6 for the primitive levels and for doubled levels. Submit the allowed values of c at $j = 1, 2$ in the doubled theory and the finite phases of $U_1 V_1^2$ and $U_1 V_1 W_1$.

4. **Crystal differences.** Take the four $\mathbb{C}^4$ crystal matching positions in (VIII.7.46). Compute the determinant of the three difference vectors from m_0, and repeat with m_1 as reference. Explain why the two descriptions give the same integral tetrahedron and why this does not fix a CS edge flow on T^2.

Status and sources

Sources by section. Source coordinates and scope qualifications follow.

§VIII.7.1. A connected populated one-brane coherent branch is the source-supported starting point. No full quantum identification follows (Hanany, Vegh, et al. 2009, §§2–3).

§VIII.7.2. C1 and The matching matrix and coherent F-term component are conditional [MATH] under the sourced tiling (Hanany, Vegh, et al. 2009, §§2–3 and 5.5).

§VIII.7.3. C1 and The saturated compact lattice and finite action are conditional [MATH] under the stated full gauge group; parity completion is only an allowed [ANOM] choice (Hanany and Zaffaroni 2008, §2 and §6; Benini et al. 2011, §6).

§VIII.7.4. The primitive edge-flow heights are conditional [MATH] for the given nine-edge incidence matrix (Hanany, Vegh, et al. 2009, equation (5.48)).

§VIII.7.5. Rays, Hilbert counts and the changed finite quotient are conditional [MATH] for the stated grading and levels (Hanany, Vegh, et al. 2009, equations (5.48)–(5.53)).

§VIII.7.6. The distinct crystal and brick dictionaries are sourced comparisons at their separate scopes. (Lee et al. 2007, §§2.2, 3.3, 4.1; Volume VII, Chapter 10).

The fourfold and series concern a connected, populated classical one-brane coherent branch and its compact quotient. The tiling and vacuum premises are sourced; the edge flow, matrices, finite action and counts are calculations under those premises. The spin parity completion is one allowed choice, with no string selection. This result does not establish a full quantum branch or exact IR duality.

Tilings, matchings and heights. Hanany, Vegh, et al. (2009), §§2–3 and 5.5, equations (5.45)–(5.53), PDF pages 5–10 and 30–32, supplies the nine-field quiver and weighted matching matrix. Its raw edge-level-difference exponent differs from the primitive flow (VIII.7.23). General M2 duality is proposed there. The inconsistent individual-field R-charge sentence after (5.56) is not used in the formal series.

Compact quotient and finite action. Hanany and Zaffaroni (2008), §2 and §6, PDF pages 4–6 and 14–15, supports the quotient and cyclic master space. Equation (6.11) fails to generate the $r = 2$ finite component. Chapter VIII.6 supplies the populated-orbit

condition. The mixed parity contact-term framework is in Benini et al. (2011), §6, equations (6.1), (6.3)–(6.6), PDF pages 47–48; it does not select (VIII.7.20) from M2 physics.

Crystal and brick comparison. Lee et al. (2007), §§2.2, 3.3 and 4.1 and Fig. 16, gives the M-theory crystal, matching-difference homology and the $\mathbb{C}^4$ tetrahedron. Volume VII, Chapter 10 develops the D1 $(0, 2)$ brick dictionary. The constructions do not identify the probe theories.

References

Benini, F., C. Closset, and S. Cremonesi (2011). "Quantum moduli space of Chern-Simons quivers, wrapped D6-branes and AdS4/CFT3". In: *JHEP* 09, p. 005. DOI: 10.1007/JHEP09(2011)005. arXiv: 1105.2299 [hep-th].

Hanany, A., D. Vegh, and A. Zaffaroni (2009). "Brane Tilings and M2 Branes". In: *JHEP* 03, p. 012. DOI: 10.1088/1126-6708/2009/03/012. arXiv: 0809.1440 [hep-th].

Hanany, A. and A. Zaffaroni (2008). "Tilings, Chern-Simons Theories and M2 Branes". In: *JHEP* 10, p. 111. DOI: 10.1088/1126-6708/2008/10/111. arXiv: 0808.1244 [hep-th].

Lee, S., S. Lee, and J. Park (2007). "Toric AdS4/CFT3 duals and M-theory Crystals". In: *JHEP* 05, p. 004. DOI: 10.1088/1126-6708/2007/05/004. arXiv: hep-th/0702120.

Chapter VIII.8

Flavors, monopoles, and quantum geometry

A conifold quiver remembers the four corners of a planar toric diagram. It does not remember how many lattice points lie above either corner. That lost height has a physical meaning. When the M-theory circle used to reduce a toric Calabi–Yau fourfold shrinks, its fixed locus becomes a D6 divisor in type IIA, and strings between that D6 and a D2 probe add chiral matter. A monopole operator on the D2 then carries information about the circle that the classical bifundamental quotient cannot see.

We follow one such lift all the way from geometry to an operator ring. The worked model has one flavor pair on each of two conifold arrows, a full $U(1)_1 \times U(1)_2$ gauge group, and zero displayed Chern–Simons levels. Its proposed geometric branch is the cone over the Segre embedding of $(\mathbb{P}^1)^3$. We will derive its eight invariant coordinates, nine quadratic equations, and Hilbert series. The link of this fourfold is $Q^{1,1,1}$, a seven-dimensional circle bundle over $(\mathbb{P}^1)^3$. The physical input that permits this algebraic answer is the proposed complete monopole presentation of the single-probe geometric branch. We state that input precisely where it enters.

VIII.8.1 Where the reduction circle ends

In Chapter 5 the M-theory circle was smooth. Reducing along it gave a Calabi–Yau threefold varying over a real line, with circle curvature providing Ramond–Ramond flux. A fixed circle changes the reduction. Its Kaluza–Klein monopole locus becomes a D6-brane, so the D2 probe sees new open-string states. We need both the planar toric projection and the vertical lattice coordinate to locate those states.

Choose the primitive circle $U(1)_M$ and let r_0 be its real moment-map coordinate. At a regular value, the reduction has the schematic form

$$Y_4/U(1)_M \longrightarrow \mathbb{R}_{r_0}, \qquad (Y_4/U(1)_M)_{r_0} \simeq X_3(r_0), \tag{VIII.8.1}$$

where $X_3(r_0)$ is a Calabi–Yau threefold in the toric construction. To see the extra operation explicitly, write ϕ_s for homogeneous coordinates and Q_s^0 for the chosen circle

charges. Introduce an angular variable θ_0 with period 2π and impose

$$\mu_0(\phi) = \sum_s Q_s^0 |\phi_s|^2 = r_0, \qquad (\phi_s, \theta_0) \sim (e^{i\lambda Q_s^0}\phi_s, \theta_0 + \lambda). \tag{VIII.8.2}$$

When r_0 is allowed to vary, this adds a redundant description of the original fourfold: the moment equation eliminates r_0 and the new gauge transformation eliminates θ_0. When r_0 is held fixed, quotienting the additional $U(1)$ instead constructs the threefold fiber. If Q_B denotes the charge rows defining the fourfold, the two operations can be summarized as

$$Y_4 = \{\mu_B = 0\}/U(1)^2, \qquad X_3(r_0) = \{\mu_B = 0,\ \mu_0 = r_0\}/U(1)^3 \tag{VIII.8.3}$$

for the six-coordinate example after its rows are given below. The extra $U(1)$ is a quotient used to examine a fiber, not a third gauge row in the fourfold coordinate ring. The source toric dictionary identifies the circle direction from the same charge vector. If $v_s = (1, x_s, y_s, z_s)$ is the ray of ϕ_s, then

$$v_M = \text{primitive}\left(\sum_s Q_s^0 v_s\right). \tag{VIII.8.4}$$

The Calabi–Yau charge condition $\sum_s Q_s^0 = 0$ makes its first coordinate vanish. In a lattice frame where v_M is vertical, the threefold diagram is the projection forgetting the last coordinate. The vector is oriented: replacing Q^0 by its negative reverses the circle and changes the sign of every M weight, even though it leaves the unoriented projection unchanged.

The circle radius vanishes at a codimension-two fixed locus. Under the regularity and external-edge assumptions of the source construction, a unit vertical interval between adjacent external toric points represents one D6 on the projected toric divisor at $r_0 = 0$. If a column contains $h+1$ consecutive external lattice points, its h unit intervals describe h coincident D6s. The source distinguishes these codimension-two fixed loci from several other possible degenerations. A circle can shrink on a divisor or a larger toric stratum, and nonprimitive local weights can leave a finite stabilizer. Those alternatives need not produce the single D6 flavor pair used here. The unit external edge and the regular quotient away from the chosen fixed divisor are therefore truth-changing conditions. A projected overlap alone is insufficient: the interval must belong to the specified primitive-circle fixed-locus construction.

The real line and the planar diagram play different roles. At fixed r_0, the reduction gives a threefold slice. Moving along r_0 changes the circle bundle; across a D6, its first Chern class jumps. The planar diagram describes the toric threefold fibers, whereas the vertical lattice coordinate records fixed-point data of the chosen circle. Collapsing a unit interval to one planar point loses one integral unit of that data. This explains why the number of D6s cannot be recovered by simply counting projected vertices.

For the example, order the six homogeneous coordinates as $(a_0, b_0, c_0, d_0, a_{-1}, c_1)$. Their source lattice positions are

	a_0	b_0	c_0	d_0	a_{-1}	c_1
(x, y, z)	$(0,0,0)$	$(0,1,0)$	$(1,1,0)$	$(1,0,0)$	$(0,0,-1)$	$(1,1,1)$.

(VIII.8.5)

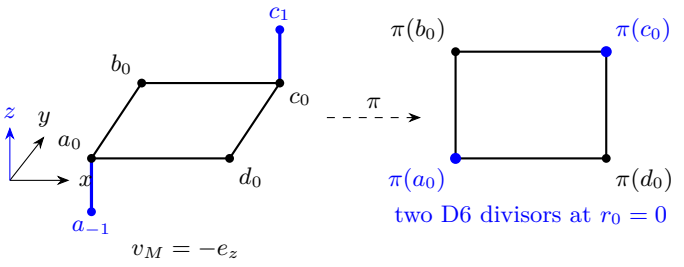


Figure VIII.8.1: The six source lattice points project to the conifold square. The blue unit intervals above two different corners retain the circle information erased by the planar projection. For the specified primitive circle and a regular codimension-two fixed locus, each interval gives one D6 divisor at $r_0 = 0$. The source circle orientation is $v_M = -e_z$.

Forgetting z leaves the conifold square. Yet the ordered differences are

$$v_{a_0} - v_{a_{-1}} = e_z, \qquad v_{c_1} - v_{c_0} = e_z. \tag{VIII.8.6}$$

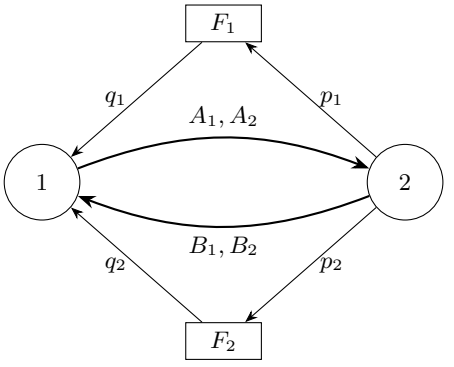
Under the projection $\pi(x, y, z) = (x, y)$ this statement is the two-line calculation

$$\pi(v_{a_{-1}}) = \pi(v_{a_0}) = (0, 0), \qquad \pi(v_{c_0}) = \pi(v_{c_1}) = (1, 1). \tag{VIII.8.7}$$

Both edges have lattice length one and project to distinct external corners. They therefore supply one D6 divisor each in the chosen reduction. The orientation of the source's global circle generator will turn out to be $v_M = -e_z$; the sign is fixed by its action on the homogeneous variables below, rather than guessed from this drawing. The other two projected corners, b_0 and d_0, have one point apiece in the listed configuration. They do not yield another unit vertical interval. Four planar corners therefore do not mean four D6 divisors.

The D6 divisor is the vanishing locus of an arrow X in the D2 quiver. Open D2–D6 strings provide two chiral fields whose cubic coupling is pXq in the rank-one theory. For our two vertical intervals, $X = A_1$ and $X = A_2$. This geometric assignment selects the two flavor pairs; it does not yet determine their quantum operator relations. The flavor group at the near-core point can also differ from a naive independent square-node symmetry, because a diagonal D6 flavor $U(1)$ can be gauged. We therefore use the squares to identify matter content, not to assert the full infrared global symmetry.

At the divisor where $X = 0$, a D2–D6 string can become light. The two open-string orientations give fields in conjugate endpoint representations; their product can couple to the D2 field whose vanishing defines the divisor. This argument identifies a cubic superpotential monomial after its representations are fixed. It cannot set the normalization of a product of disorder operators. That distinction becomes decisive when the monopole OPE enters.



$$k_1 = k_2 = 0, \quad m_{\text{diag}} = (1, 1)$$

Figure VIII.8.2: The two-node Abelian source model. Circles are the two compact gauge factors and squares identify D6 flavor pairs. Labels on flavor arrows follow the source's commuting rank-one fields; the indexed nonabelian product exchanges their p/q names. The zero bare levels are a specified parity-compatible choice, not a consequence of the diagram alone.

VIII.8.2 The flavored quiver and its parity choice

Take one probe and retain the full compact gauge group $G = U(1)_1 \times U(1)_2$. The bifundamentals A_1, A_2 have charge $(1, -1)$ and B_1, B_2 have charge $(-1, 1)$. For each A_i, use the Abelian source labels, with p_i of charge $(0, 1)$ and q_i of charge $(-1, 0)$. The source's rank-one expression reads

$$W = A_1 B_1 A_2 B_2 - A_1 B_2 A_2 B_1 + p_1 A_1 q_1 + p_2 A_2 q_2, \qquad (k_1, k_2) = (0, 0). \quad \text{(VIII.8.8)}$$

The product is neutral term by term, since

$$q(p_i) + q(A_i) + q(q_i) = (0, 1) + (1, -1) + (-1, 0) = (0, 0). \quad \text{(VIII.8.9)}$$

When one restores nonabelian matrix order, the general indexed convention exchanges the names p and q relative to this Abelian display. Scalar commutativity makes the rank-one expression unambiguous; the matrix-order relabeling must not be skipped at larger rank.

In three dimensions a charged fermion changes the parity condition on a Chern–Simons coupling. It is not enough to inspect the diagonal levels separately when both gauge fields are dynamical. In the chosen spin-fermion prescription, form the half-matrix

$$P_{ab} = \frac{1}{2} \sum_{\psi} q_a(\psi) q_b(\psi), \qquad K_{\text{bare}} + P \in \text{Mat}_{2\times 2}(\mathbb{Z}) \quad \text{(VIII.8.10)}$$

for this gauge representation and basis. There are four bifundamental fermions and two

each of p and q. Their outer products give

$$\begin{aligned} P &= \frac{1}{2}\left[4\begin{pmatrix} 1 & -1 \\ -1 & 1 \end{pmatrix} + 2\begin{pmatrix} 0 & 0 \\ 0 & 1 \end{pmatrix} + 2\begin{pmatrix} 1 & 0 \\ 0 & 0 \end{pmatrix}\right] \\ &= \begin{pmatrix} 3 & -2 \\ -2 & 3 \end{pmatrix}. \end{aligned} \tag{VIII.8.11}$$

$$K_{\text{bare}} = \begin{pmatrix} 0 & 0 \\ 0 & 0 \end{pmatrix}, \qquad K_{\text{bare}} + P \in \mathrm{Mat}_{2\times 2}(\mathbb{Z}). \tag{VIII.8.12}$$

This checks the mixed dynamical gauge entry as well as the two diagonal entries for the declared model. It does not select a unique integer mixed counterterm or determine gauge-background flavor, R, or gravitational contacts. The choice of zero displayed levels is part of the specified theory.

The arithmetic can also be read node by node. Four fields of charges $\pm(1,-1)$ contribute 2 to each diagonal half-entry and -2 to the off-diagonal entry. The two p fermions add one to P_{22}; the two q fermions add one to P_{11}. The diagonal entries rise together from 2 to 3, while the mixed entry stays -2. Counting only arrows would miss the diagonal change caused by flavors. Counting only flavor fermions would miss the integer mixed contribution from the bifundamentals.

A one-flavor variant helps expose why this choice changes. Keep only the pair on A_1. Four bifundamentals and one p, q pair then give

$$P_{\text{one flavor}} = \begin{pmatrix} 5/2 & -2 \\ -2 & 5/2 \end{pmatrix}. \tag{VIII.8.13}$$

The source chooses opposite half-levels $(k_1, k_2) = (1/2, -1/2)$, which make both diagonal entries integral; the mixed entry is already integral. In the one-flavor theory the chosen bare matrix and corrected matrix are

$$K_{\text{one}} = \begin{pmatrix} 1/2 & 0 \\ 0 & -1/2 \end{pmatrix}, \qquad K_{\text{one}} + P_{\text{one}} = \begin{pmatrix} 3 & -2 \\ -2 & 2 \end{pmatrix}. \tag{VIII.8.14}$$

The diagonal half-integers are compensated by the bare terms, while the mixed contribution remains an integer. Moving a D6 along the real reduction line gives a signed real mass to its D2–D6 fermions and shifts effective levels in the source scheme. This geometric level jump is another way to see why a flavor addition changes the parity data. We will use the one-flavor model again after the monopole charge calculation, keeping its ring calculation deliberately small.

The displayed (k_1, k_2) are bare single-trace levels of the theory at the point under discussion. Integrating out a massive flavor pair defines effective levels in a chosen mass chamber. These effective levels can differ on the two sides of the D6 along r_0. The one-flavor half-levels should therefore be read with their retained fermion content and mass choice, rather than as a continuous change of an otherwise identical two-flavor theory.

VIII.8.3 What opposite monopoles know

The two-node theory has a full cocharacter lattice $\mathbb{Z}^2$. The diagonal flux $m = n(1,1)$ is therefore primitive at $n = \pm 1$; there is no further quotient of the diagonal gauge group. A monopole insertion creates magnetic flux through a small sphere around its position. In radial quantization the same operator is represented by a state on S^2 with

$$\frac{1}{2\pi}\int_{S^2} F_1 = \frac{1}{2\pi}\int_{S^2} F_2 = n \in \mathbb{Z}. \tag{VIII.8.15}$$

The integer follows from the compact $U(1)^2$ group, not just from its Lie algebra. A bare Chern–Simons term couples this flux to the temporal gauge field and supplies classical electric charge $n(k_1, k_2)$; charged fermion modes add the correction below. Let $T = T_{+1}$ and $\widetilde{T} = T_{-1}$ denote the two bare diagonal monopoles. The bifundamentals are neutral under this flux, but each flavor fermion has a nonzero pairing with it. In the source charge prescription the electric charge is

$$q(T_n) = K_{\text{bare}} m - \frac{1}{2}\sum_{\psi} |q(\psi)\cdot m| q(\psi). \tag{VIII.8.16}$$

This one-loop prescription is a physical input for the specified Abelian diagonal sector. It does not independently establish an exact infrared scaling dimension or a bare-operator BPS statement.

We can evaluate the sum without assigning a charge to a monopole by inspection. For either flavor pair and $m = n(1,1)$,

$$q(p_i)\cdot m = n, \qquad q(q_i)\cdot m = -n, \qquad q(p_i) + q(q_i) = (-1, 1). \tag{VIII.8.17}$$

Each pair contributes $|n|(1,-1)/2$ to the negative half-sum. With two pairs and diagonal bare levels, this becomes

$$q(T_n) = n(k_1, k_2) + |n|(1,-1). \tag{VIII.8.18}$$

Thus the zero-level theory has the initially surprising equality

$$q(T) = q(\widetilde{T}) = (1,-1), \qquad q(TB_j) = q(\widetilde{T}B_j) = (0,0). \tag{VIII.8.19}$$

Reversing flux reverses the classical nk contribution, but not the $|n|$ matter contribution. Treating the negative monopole as having electric charge $(-1, 1)$ would erase precisely the operators needed for the fourfold.

The bifundamentals do not contribute to this particular one-loop shift because their pairings with (n, n) vanish, although their electric charges are nonzero. If one chose flux $(n, 0)$ instead, the bifundamentals would contribute and the simple expression (VIII.8.18) would no longer follow. The primitive diagonal sector is therefore a scope condition, not a classification of all monopoles in the full $\mathbb{Z}^2$ lattice.

As a check on the absolute value, the same charge formula gives

$$q(T_{+2}) = 2(k_1, k_2) + 2(1,-1), \qquad q(T_{-2}) = -2(k_1, k_2) + 2(1,-1). \tag{VIII.8.20}$$

The matter term is identical for the two signs; the level term is opposite. This calculation uses the sourced diagonal charge prescription and makes no statement about a product relation for the nonprimitive operators.

The superpotential also constrains the possible R weights. On the geometric branch the source charge formula gives

$$R(T) = R(\widetilde{T}) = \frac{R(A_1) + R(A_2)}{2}, \qquad R(T\widetilde{T}) = R(A_1A_2). \tag{VIII.8.21}$$

The R result follows from the flavor superpotential rather than from assigning a guessed R charge to a monopole. At an infrared fixed point where each $p_iA_iq_i$ has superpotential R charge two,

$$R(p_i) + R(q_i) = 2 - R(A_i), \qquad R(\psi_{p_i}) + R(\psi_{q_i}) = -R(A_i). \tag{VIII.8.22}$$

Here a chiral fermion has R charge one less than its scalar. The negative half-sum of the flavor-fermion R charges then produces (VIII.8.21) for unit flux. This derivation inherits the same superpotential and charge prescription assumptions as the electric calculation.

Gauge and R charges are therefore compatible with $T\widetilde{T} = A_1A_2$. Compatibility is only a necessary condition. The operator product is conjectured in the source; its normalization is chosen so that the nonzero coefficient is one. The source further proposes that, after setting all $p_i = q_i = 0$, this relation together with the ordinary F equations is a complete presentation of the single-probe geometric branch, with no additional generators or relations there. We now adopt that entire proposed presentation as a physical premise:

$$\mathcal{R}_{\mathrm{geom}} = \left(\frac{\mathbb{C}[A_1, A_2, B_1, B_2, T, \widetilde{T}]}{(T\widetilde{T} - A_1A_2)} \right)^{U(1)_1 \times U(1)_2}, \qquad p_i = q_i = 0. \tag{VIII.8.23}$$

In the Abelian conifold superpotential the first two terms commute and cancel, so they impose no further F relation on A_i, B_j. The flavor F equations vanish on the chosen $p = q = 0$ branch. The resulting coordinate ring will be an exact algebraic consequence of the stated premise; the charge calculation alone does not prove the premise, nor does it describe flavor Higgs or mixed branches.

The one-flavor theory already tests the sign logic. At $(k_1, k_2) = (1/2, -1/2)$ the same formula, now with one flavor pair, gives

$$q(T) = (1, -1), \qquad q(\widetilde{T}) = (0, 0), \qquad T\widetilde{T} = A_1 \tag{VIII.8.24}$$

where the last relation is the source's one-flavor proposed OPE. On its $p = q = 0$ branch, five useful invariants are

$$u_j = TB_j, \quad v_j = A_2B_j \quad (j = 1, 2), \qquad s = \widetilde{T}, \qquad u_1v_2 - u_2v_1 = 0. \tag{VIII.8.25}$$

Hence its stated ring is the conifold ring in u_1, u_2, v_1, v_2 times the free line parametrized by s. This example tests a single flavor charge and one relation; it is not a second derivation of the two-flavor Cox construction.

VIII.8.4 From monopoles to six toric variables

The Q111 relation in (VIII.8.23) can be solved without introducing a square root. Use the six variables at the exact source points of (VIII.8.5) and set

$$\begin{aligned} A_1 &= a_{-1}a_0, \quad A_2 = c_0c_1, \quad B_1 = b_0, \quad B_2 = d_0, \\ T &= a_{-1}c_0, \quad \widetilde{T} = a_0c_1. \end{aligned} \tag{VIII.8.26}$$

Multiplication immediately gives

$$T\widetilde{T} = (a_{-1}c_0)(a_0c_1) = (a_{-1}a_0)(c_0c_1) = A_1A_2. \tag{VIII.8.27}$$

This map also gives an efficient gauge-invariance test in the original variables. For example TB_1 has charge $(1,-1)+(-1,1)=0$. In the six-variable description the same operator is $a_{-1}b_0c_0$. The first Q_B row gives $0-1+1=0$ and the second gives $-1+1=0$. The matching answers test two different descriptions of the same operator. The relation $T\widetilde{T}=A_1A_2$ is homogeneous under both descriptions, so it survives the gauge quotient.

The factorization makes the quantum relation polynomial and makes the two vertical columns visible. It also introduces two redundant rescalings. In the order $(a_0,b_0,c_0,d_0,a_{-1},c_1)$ their charge rows, and the separate global circle row, are

$$Q_B = \begin{pmatrix} 1 & -1 & 1 & -1 & 0 & 0 \\ 1 & 0 & 1 & 0 & -1 & -1 \end{pmatrix}, \qquad Q_M = (0,0,1,0,0,-1). \tag{VIII.8.28}$$

The rows act on the reconstructed original fields in a simple way:

	A_1	A_2	B_1	B_2	T	$\widetilde{T}$
Q_{B_1}	1	1	−1	−1	1	1
Q_{B_2}	0	0	0	0	0	0
Q_M	0	0	0	0	1	−1

. (VIII.8.29)

The second B row is invisible on the reconstructed original fields because it removes the redundancy introduced by their six factors. It is nevertheless essential when forming the Cox quotient: it prevents additional monomials in the factors from being mistaken for physical operators. The first row carries the effective relative gauge charge, while the M row distinguishes the two monopoles. This table also verifies the OPE's homogeneity under all three rows: $T\widetilde{T}$ and A_1A_2 have the same B charges and zero total M weight.

Only the two rows of Q_B are divided out. Their rank is two, so the generic toric quotient has complex dimension $6-2=4$. Gauging the third row instead would make a threefold and remove the physical circle action. Its different role is visible in the invariant operators below.

There is an independent lattice check on the factorization. Put the six homogeneous ray vectors from (VIII.8.5) into the columns of G, with first coordinate one:

$$G = \begin{pmatrix} 1 & 1 & 1 & 1 & 1 & 1 \\ 0 & 0 & 1 & 1 & 0 & 1 \\ 0 & 1 & 1 & 0 & 0 & 1 \\ 0 & 0 & 0 & 0 & -1 & 1 \end{pmatrix}. \tag{VIII.8.30}$$

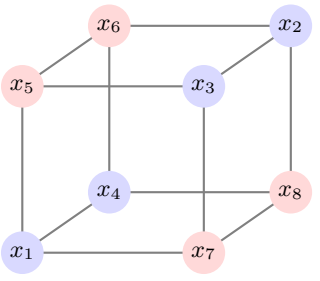


Figure VIII.8.3: The two quotient rows equate the total exponents in three pairs of Cox variables. Choosing one variable from each pair makes eight invariant triples. Four are ordinary conifold mesons and four contain a monopole; the diagram represents an operator ring, not an additional brane configuration.

Direct multiplication yields

$$Q_B G^{\mathsf{T}} = 0, \qquad Q_M G^{\mathsf{T}} = (0,0,0,-1). \tag{VIII.8.31}$$

For example the first quotient row states $v_{a_0} - v_{b_0} + v_{c_0} - v_{d_0} = 0$; the second states $v_{a_0} + v_{c_0} - v_{a_{-1}} - v_{c_1} = 0$. For the four columns a_0, b_0, c_0, a_{-1}, direct expansion along the last row gives

$$\det G_{(a_0,b_0,c_0,a_{-1})} = 1. \tag{VIII.8.32}$$

A unit minor means these four rays already span the ambient lattice integrally; an unnoticed common sublattice would change the toric global form. Thus the displayed four-dimensional ambient lattice is primitive. The second equation in (VIII.8.31) fixes the source-oriented generator $v_M = -e_z$. A positive Q_M charge therefore must not be read as positive plotted height.

The two unit vertical edges are now also differences of columns of G. Their projections recover the two corners found in the opening section. The planar conifold and the fourfold have the same projected square, but the z heights and global M action distinguish the lift. This is the toric counterpart of the extra charged monopoles.

VIII.8.5 Eight coordinates and the Segre cone

Why does the quotient have exactly eight basic invariant functions? For a monomial in the six Cox variables, let N_1, N_2, N_3 be its total exponents in the respective pairs

$$(a_0, c_0), \qquad (b_0, d_0), \qquad (a_{-1}, c_1). \tag{VIII.8.33}$$

The first Q_B row has weight $N_1 - N_2$ and the second has weight $N_1 - N_3$. Invariance is therefore equivalent to

$$N_1 = N_2 = N_3 = n, \qquad n \in \mathbb{Z}_{\geq 0}. \tag{VIII.8.34}$$

The equality can be made explicit before factoring. An invariant monomial of degree n has the form

$$a_0^r c_0^{n-r}\, b_0^s d_0^{n-s}\, a_{-1}^u c_1^{n-u}, \qquad 0 \le r, s, u \le n. \tag{VIII.8.35}$$

Its three exponents r, s, u are independent because the two charge equations constrain only the pair totals. Conversely, every choice in these bounded ranges satisfies both charge equations. This gives a constructive way to enumerate functions without first guessing the ring.

Every such monomial is a product of n triples, each containing one variable from each pair. This proves generation in all degrees, not just a list at low degree. The eight triples, in the source order, are

$$\begin{aligned} x_1 &= A_1B_1 = a_{-1}a_0b_0, & x_2 &= A_2B_2 = c_0c_1d_0,\\ x_3 &= A_2B_1 = b_0c_0c_1, & x_4 &= A_1B_2 = a_{-1}a_0d_0,\\ x_5 &= \widetilde{T}B_1 = a_0b_0c_1, & x_6 &= \widetilde{T}B_2 = a_0c_1d_0,\\ x_7 &= TB_1 = a_{-1}b_0c_0, & x_8 &= TB_2 = a_{-1}c_0d_0. \end{aligned} \tag{VIII.8.36}$$

The first four exist in the classical bifundamental quotient. The last four are gauge invariant only with the monopole charges derived in (VIII.8.19).

They are not algebraically independent. In terms of the x_i, the nine quadratic equations printed by the source can be arranged as

$$x_1x_2 = x_3x_4 = x_5x_8 = x_6x_7, \tag{VIII.8.37}$$

$$\begin{aligned} &x_1x_3 = x_5x_7, && x_1x_6 = x_4x_5, && x_1x_8 = x_4x_7,\\ &x_2x_4 = x_6x_8, && x_2x_5 = x_3x_6, && x_2x_7 = x_3x_8. \end{aligned} \tag{VIII.8.38}$$

The chain of four equal products supplies three equations; the next two lines supply six, hence nine independent quadrics in degree two. One can check a relation with the original fields before trusting a toric ideal calculation. For instance,

$$x_1x_3 = (A_1B_1)(A_2B_1) = A_1A_2B_1^2 = T\widetilde{T}B_1^2 = x_5x_7. \tag{VIII.8.39}$$

This relation shows exactly where the conjectured OPE enters the invariant ring. Replacing it by $T\widetilde{T} = A_1^2$ would retain the same gauge charge but spoil this equation.

The degree-two count predicts the number nine before checking any particular relation. A polynomial ring on eight degree-one generators has $\binom{8+1}{2} = 36$ quadratic monomials. The Cox description has $(2+1)^3 = 27$ independent degree-two invariant monomials. Their difference is nine. The equations above have rank nine in that vector space, so they span all degree-two relations. The remaining question is whether higher-degree relations require new generators; the exchange argument answers it.

Introduce binary labels $u_0 = a_0$, $u_1 = c_0$, $v_0 = b_0$, $v_1 = d_0$, $w_0 = a_{-1}$, and $w_1 = c_1$. Then each generator is $x_{ijk} = u_iv_jw_k$, with $x_{000} = x_1$, $x_{100} = x_7$, $x_{010} = x_4$, and $x_{110} = x_8$. One face of the resulting cube gives

$$x_{000}x_{110} - x_{100}x_{010} = x_1x_8 - x_7x_4 = 0. \tag{VIII.8.40}$$

The equality holds because both products contain one of each u, one of each v, and two w_0 factors. A second face can be obtained by fixing a different binary index. Relations

connecting opposite cube vertices, such as $x_1x_2 = x_6x_7$, are captured by the flattening minors as well. The picture in Figure VIII.8.3 records the choices, while the ideal calculation records all their dependencies.

The nine quadrics generate the entire kernel of the triple-monomial map. Arrange the eight variables as a $2 \times 2 \times 2$ array whose three indices select one member of each pair in (VIII.8.33). If two products of triples have identical Cox exponents, then in each pair they make the same number of either choice. Exchange one choice between two triples at a time. Each exchange is a 2×2 minor of a flattening of the array; repeated exchanges connect the products. The flattening minors therefore generate the monomial kernel. Direct substitution shows that the nine equations above vanish, and reducing every flattening minor by them gives zero. This identifies their ideal with the Segre ideal:

$$\mathcal{R}_{\mathrm{geom}} \simeq \frac{\mathbb{C}[x_1, \dots, x_8]}{I_9} \simeq \bigoplus_{n \geq 0} H^0\big((\mathbb{P}^1)^3, \mathcal{O}(n,n,n)\big). \tag{VIII.8.41}$$

An explicit degree-two example shows the exchange mechanism. The products x_1x_2 and x_3x_4 select different pairings of the six Cox factors, yet both equal $a_{-1}a_0b_0c_0c_1d_0$. Another pairing gives x_5x_8 and a third gives x_6x_7. A single orbit of four quadratic monomials therefore accounts for three of the nine independent relations. The other six equations swap one binary choice while keeping the remaining pair totals fixed. This is why counting eight generators alone would overstate the number of functions at the next degree.

The cone is a complex fourfold. Its seven-dimensional link is $Q^{1,1,1}$; $(\mathbb{P}^1)^3$ is the six-dimensional Segre base, not the link itself.

Give each invariant triple degree one. At degree n the exponents in each pair can be split in $n+1$ ways, independently for all three pairs. Hence

$$\dim_{\mathbb{C}}(\mathcal{R}_{\mathrm{geom}})_n = (n+1)^3, \tag{VIII.8.42}$$

$$H(t) = \sum_{n \geq 0} (n+1)^3 t^n = \frac{1 + 4t + t^2}{(1-t)^4} = 1 + 8t + 27t^2 + 64t^3 + 125t^4 + \cdots . \tag{VIII.8.43}$$

This integer triple degree counts functions in the chosen toric presentation. It is not a physical superconformal R assignment. The rational form can be obtained directly rather than inferred from the first few coefficients. Acting with $D = t\,d/dt$ on the geometric series gives

$$H(t) = (D+1)^3 \frac{1}{1-t} = \frac{1 + 4t + t^2}{(1-t)^4}. \tag{VIII.8.44}$$

The pole order at $t = 1$ is four, consistent with the four-complex-dimensional quotient. The numerator remembers the relations; a freely generated polynomial ring on eight variables would instead have $(1-t)^{-8}$ and would already disagree at degree two. Neither this formal degree nor the pole order fixes the actual conformal R symmetry.

Chapter 12 returns to the same $k = 0$, two-A-flavor model to compute R grading and volume with the required physical input. One must not insert the degree-one convention from this section as an IR R charge in that calculation.

VIII.8.6 Two fixed components and what the conifold misses

The global M row in (VIII.8.28) assigns weights

$$Q_M(x_1,\dots,x_8) = (0,0,0,0,-1,-1,1,1). \tag{VIII.8.45}$$

It distinguishes classical mesons from the two oppositely oriented monopole sectors without being part of the gauge quotient. To find the affine fixed locus of this circle, set the nonzero-weight coordinates x_5, x_6, x_7, x_8 to zero and retain the quadrics. They reduce to

$$I_{\text{fixed}} = (x_1x_2, x_1x_3, x_4x_2, x_4x_3) = (x_1, x_4) \cap (x_2, x_3). \tag{VIII.8.46}$$

The ideal identity can be checked directly. Every generator on the left contains one factor from (x_1, x_4) and one from (x_2, x_3), so it lies in their intersection. Conversely, a polynomial in both ideals has every monomial divisible by a variable from each pair; the four displayed cross-products generate all such monomials. Thus the ideal is radical and splits into the two coordinate planes, which intersect at the origin. The origin is shared by the components rather than counted as a third D6 divisor.

There are two irreducible $\mathbb{C}^2$ components. On one, $(x_1, x_4) = 0$ and (x_2, x_3) vary; on the other, $(x_2, x_3) = 0$ and (x_1, x_4) vary. Including the vanishing nonzero-weight coordinates, their ideals in the full ring are

$$\begin{aligned} J_a &= (x_1, x_4, x_5, x_6, x_7, x_8), \\ J_c &= (x_2, x_3, x_5, x_6, x_7, x_8). \end{aligned} \tag{VIII.8.47}$$

In the six-variable presentation the first branch is represented by $a_0 = a_{-1} = 0$, and the second by $c_0 = c_1 = 0$, as in the source's description. Their surviving invariants show the identification directly:

component	vanishing Cox pair	free invariant coordinates
J_a	(a_0, a_{-1})	(x_2, x_3)
J_c	(c_0, c_1)	(x_1, x_4).

(VIII.8.48)

The two affine planes meet at the cone origin. Their incidence, shown at the two marked corners in Figure VIII.8.1, cannot be read from the classical conifold equation alone without the M weights that singled out which coordinates had to vanish.

These are the two projected divisor corners of the primitive-circle construction. The algebra establishes two fixed components under the conditional ring presentation. Their D6 interpretation also uses the geometric fixed-locus and D2–D6 dictionary from the opening section.

The four classical mesons alone obey

$$x_1x_2 - x_3x_4 = 0. \tag{VIII.8.49}$$

Thus their ring is the conifold coordinate ring. It omits the four nonzero-M-weight coordinates, the two vertical unit intervals, and the monopole relation that ties them

to the mesons. The same planar diagram therefore does not determine the flavored fourfold lift.

The formal unflavored comparison can be written without mistaking it for the quantum vacuum of a different theory. If the flavor multiplicities and displayed levels are both set to zero in the source's proposed relation, then the algebraic relation becomes $T\widetilde{T} = 1$. Eliminating $\widetilde{T}$ makes T invertible:

$$\mathcal{R}_{\text{formal},0} = \frac{\mathbb{C}[A_i, B_j, T, \widetilde{T}]^{U(1)^2}}{(T\widetilde{T} - 1)} \simeq \mathcal{R}_{\text{conifold}} \otimes_{\mathbb{C}} \mathbb{C}[T, T^{-1}]. \tag{VIII.8.50}$$

This formal relation has no fixed point at $T = 0$ because T cannot vanish. It illustrates what the flavor factors change in the proposed product relation; it does not settle the physical zero-level vacuum, whose treatment would need additional input.

The one-flavor ring of (VIII.8.25) instead is conifold times $\mathbb{C}$ under its own proposed OPE. These three rings have different hypotheses; a smooth interpolation or identical infrared theory does not follow from the comparison.

The construction has three distinct outputs. Reduction geometry identifies the two D6 divisors, the field calculation fixes parity and diagonal monopole charges in the stated scheme, and the assumed geometric-branch presentation leads algebraically to the Segre cone. It does not determine a full nonabelian branch, a mixed-branch closure, background contact terms, or an exact infrared equivalence to the auxiliary toric quiver. Chapter 9 uses the same distinction between a divisor and a mass chamber when it studies deformations. The chapter's usable result is the conditional but explicit quantum-geometric dictionary: two vertical circle intervals become two flavor pairs, and their charged monopoles complete the fourfold coordinate ring missed by the conifold mesons.

Exercises

1. **Flavors and parity.** For the eight chiral fermions of (VIII.8.8), submit the 2×2 half-matrix P and the gauge charge of $p_i A_i q_i$. Explain why inspecting only P_{11} and P_{22} would miss a condition on a mixed gauge term.

2. **Opposite fluxes.** Use the complete field table and (VIII.8.16) at $k = (0, 0)$ to submit $q(T_{+1})$, $q(T_{-1})$, and the charge of $T_{+1}B_1$. State which term is even in the flux.

3. **Cox invariants.** Using the fixed matrix Q_B in (VIII.8.28), submit its rank, the charges of $a_{-1}a_0b_0$ and $a_0b_0c_1$, the quotient dimension, and $Q_M G^{\mathsf{T}}$. Explain the physical cost of gauging Q_M.

4. **Fixed locus and counting.** Under the stated geometric branch premise, set $x_5 = x_6 = x_7 = x_8 = 0$. Submit the four remaining monomial generators of the fixed ideal, its two component ideals in $\mathbb{C}[x_1, x_2, x_3, x_4]$, and the first four Hilbert coefficients in the selected triple degree. Explain why that degree cannot be used as an IR R charge without further input.

Status and sources

Sources by section. Source coordinates and scope qualifications follow.

§VIII.8.1. The calculation [GEO-E] uses the primitive regular circle and D6 fixed-locus premise (Benini et al. 2010, §§2.1–2.2).

§VIII.8.2. The calculation [GEO-E] is the D2–D6 flavor dictionary; C03 [ANOM] is the declared two-node parity choice (Benini et al. 2010, §§2.2–3 and 6.2.3; Benini et al. 2011, §6).

§VIII.8.3. The calculation [MATH] is primitive-flux arithmetic; C05–C06 [CONJ+] are the sourced monopole charge and OPE premises, conditional on the selected branch (Benini et al. 2010, equations (3.8)–(3.16), (6.27)).

§VIII.8.4. The calculation–C09 [MATH] are the one-flavor warmup and Cox quotient conditional on the complete proposed branch presentation (Benini et al. 2010, equations (6.18)–(6.21), (6.28)–(6.29)).

§VIII.8.5. The calculation–C11 [MATH] are the Segre ideal and Hilbert count conditional on that same presentation (Benini et al. 2010, equation (6.30)).

§VIII.8.6. The calculation–C13 [MATH] compare the invariant ring and two fixed components within the specified circle model (Benini et al. 2010, equations (6.31)–(6.32)).

The circle reduction and D2–D6 flavor dictionary are geometric and brane premises from Benini et al. (2010), Sections 2.1–2.2, Figure 1, equations (2.3)–(2.9), and Section 6.2.3, Figure 9. They require the specified primitive external vertical intervals and regular circle fixed loci. The parity choice and one-loop monopole charge prescription use its Sections 3–3.1, equations (3.3)–(3.16), and its Q111 model (6.25)–(6.27). The mixed dynamical gauge condition in the declared two-node representation also uses Benini et al. (2011), Section 6, equations (6.1) and (6.3)–(6.5). No background contact prescription is inferred.

The load-bearing physical premise is the complete proposed $p = q = 0$ geometric-branch presentation of Benini et al. (2010), equations (4.19)–(4.20), including its conjectured monopole OPE (3.15) specialized in (6.27), and absence of additional branch generators or relations. Conditional on that premise, the field-derived charge sum, exact Cox map (6.28), toric rows and rays (6.29), eight invariant operators and nine quadrics (6.30), all-degree Segre identification, Hilbert series, and two fixed components (6.31)–(6.32) are explicit algebraic deductions. The one-flavor comparison follows Section 6.2.1, equations (6.18)–(6.21), under its corresponding OPE. The specified flavored abelian branch uses the stated arrows, superpotential, levels and compact groups. No claim about a complete nonabelian moduli space, exact IR duality, or physical R grading is made here.

Evidence and assumptions. The circle fixed-locus and D2–D6 dictionary are [GEO-E] at their stated geometric and brane scope. The concrete two-node parity calculation is [ANOM]. The source monopole charge prescription and complete geometric-branch presentation, including the OPE, remain [CONJ+] physical inputs. The Cox quotient,

invariant semigroup, Segre ideal, Hilbert series, and fixed components are [MATH] conditional consequences. The chapter's exact checks cover the full 2×2 parity matrix, fluxes $n = -3, \ldots, 3$ in the declared diagonal sector, all eight invariant triples, all nine source quadrics and their Segre ideal, degrees 0 through 4 of the Hilbert count, and the two fixed-component ideals. Four bounded exercise submissions read their mathematical answers; written explanations remain for a reader or instructor.

References

Benini, F., C. Closset, and S. Cremonesi (2010). "Chiral flavors and M2-branes at toric CY4 singularities". In: *JHEP* 02, p. 036. DOI: 10.1007/JHEP02(2010)036. arXiv: 0911.4127 [hep-th].

Benini, F., C. Closset, and S. Cremonesi (2011). "Quantum moduli space of Chern-Simons quivers, wrapped D6-branes and AdS4/CFT3". In: *JHEP* 09, p. 005. DOI: 10.1007/JHEP09(2011)005. arXiv: 1105.2299 [hep-th].

Chapter VIII.9

Higgsing and mass deformations of membrane quivers

A membrane quiver can change in two physically different ways. A Fayet–Iliopoulos (FI) source can support a bifundamental expectation value, join two gauge nodes and move the probe into a different local region of its moduli space. A scalar mass changes the potential itself. It lifts commuting membrane positions, yet at nonabelian rank can leave isolated solutions made from matrices that do not commute. In this chapter we follow one five-field parent through two FI-supported Higgs vacua, then solve a separate mass-deformed ABJM vacuum equation in explicit square blocks. The comparison makes clear which data are read from a quotient, and which require the component potential.

The first calculation uses the equal-rank $U(N)^3$ phase of the cone over $Y^{1,2}(\mathbb{CP}^2)$ described by Benishti, He and Sparks. Its ordered bare levels are $(2,-1,-1)$. On the selected rank-one common-σ branch, the parent has five homogeneous coordinates and one continuous compact quotient. Turning on two different FI values opens local charts $\mathbb{C}^4$ and $\mathbb{C}^4/\mathbb{Z}_2$. At general rank the same vacua lock gauge nodes and pull the bare levels to $(1,-1)$ or $(2,-2)$. The second calculation starts from the mass-deformed ABJM component action of Gomis, Rodríguez-Gómez, Van Raamsdonk and Verlinde. Its square matrices solve the vacuum equations for every block size N and carry a spin-$(N-1)/2$ bilinear algebra. These are statements about the specified classical equations and local charts; quantum thresholds and a complete vacuum count require other data.

VIII.9.1 Two deformations, two questions

For one undeformed ABJM membrane, four complex scalar positions describe $\mathbb{C}^4/\mathbb{Z}_k$ after the compact gauge quotient. The quotient is a statement about zeros of a particular

potential and about the gauge transformations that identify them. An FI source shifts a moment map. At a nonzero bifundamental solution the unbroken gauge group acts on the fluctuations differently, so a new local geometry appears without adding a positive quadratic mass for every position. A mass instead changes the equations whose zeros we are finding. In the rank-one GRVV example the quadratic potential is

$$V_{N=1} = \mu^2 \sum_{I=1}^{4} |C^I|^2, \qquad [\mu] = 1, \quad [C^I] = \tfrac{1}{2}. \tag{VIII.9.1}$$

Here the brackets denote three-dimensional mass dimension. For $\mu \neq 0$ the only continuous scalar zero is the origin. At larger N there are noncommuting zeros because the cubic matrix interactions can balance the linear mass term. A diagram of toric vertices by itself cannot reveal these matrix solutions.

We will keep the examples on flat $\mathbb{R}^{2,1}$ and will use the full compact gauge groups. A supersymmetric squash of S^3 in Chapter 11 changes the background and the partition function; it is a different operation from either flat-space deformation considered here. The two calculations below share a question instead: what remains of a membrane's position data when a parameter changes the vacuum equations?

VIII.9.2 How a bifundamental vacuum joins gauge nodes

Start with an arrow $X_{ab} : a \to b$ in the tail-fundamental $(\mathbf{N}_a, \overline{\mathbf{N}}_b)$. We use Hermitian book connections and the covariant derivative

$$X_{ab} \longmapsto g_a X_{ab} g_b^{-1}, \qquad DX_{ab} = dX_{ab} + iA_a X_{ab} - iX_{ab} A_b. \tag{VIII.9.2}$$

A full-rank constant expectation value $X_{ab} = v\mathbf{1}_N$ is invariant precisely under $g_a = g_b$. Its kinetic term gives the relative connection a mass, while the diagonal one remains a connection of a full compact $U(N)$ rather than a separately rescaled Lie algebra:

$$\operatorname{Tr}(D_\nu X_{ab})^\dagger D^\nu X_{ab}\big|_{v\mathbf{1}_N} = |v|^2 \operatorname{Tr}(A_{a\nu} - A_{b\nu})^2. \tag{VIII.9.3}$$

The equality $A_a = A_b = A_D$ on the unbroken embedding specifies the surviving subgroup. In the low-energy theory, integrating out the heavy relative connection also produces derivative terms; setting it equal to zero is not an exact finite-momentum field equation.

For the book's bare fundamental-trace Chern–Simons (CS) form, write

$$\mathrm{CS}_{\mathrm{b}}(A) = \operatorname{Tr}\left(A\, dA + \frac{2i}{3} A^3 \right), \qquad S_{\mathrm{CS}} = \frac{1}{4\pi} \sum_i k_i \int \mathrm{CS}_{\mathrm{b}}(A_i). \tag{VIII.9.4}$$

Pulling this form back to the diagonal subgroup immediately adds the two levels:

$$\frac{k_a}{4\pi}\, \mathrm{CS}_{\mathrm{b}}(A_D) + \frac{k_b}{4\pi}\, \mathrm{CS}_{\mathrm{b}}(A_D) = \frac{k_a + k_b}{4\pi}\, \mathrm{CS}_{\mathrm{b}}(A_D). \tag{VIII.9.5}$$

This is an embedding calculation at the level of the bare action. It does not determine quantum parity or contact terms generated by massive fields. The distinction matters when an apparent ABJM-like two-node theory is inferred from a quiver diagram.

The Higgsing convention for this parent writes $D = d - iA_{\rm src}$. Our bosonic Hermitian convention matches it under $A_{\rm b} = -A_{\rm src}$. Substitution into the CS form checks that the quadratic coefficient is unchanged:

$$D_{\rm b} = d + iA_{\rm b} = d - iA_{\rm src}, \qquad \mathrm{CS}_{\rm b}(-A_{\rm src}) = \mathrm{Tr}\left(A_{\rm src}dA_{\rm src} - \frac{2i}{3}A_{\rm src}^3\right). \quad \text{(VIII.9.6)}$$

The map concerns these bosonic connections. We do not need a complete translation of fermions and auxiliary fields to read the following bare level pullbacks.

For the parent levels $k = (2, -1, -1)^T$, let the two columns of an embedding matrix say which original connections equal which daughter connection. The two choices relevant below are

$$E_A = \begin{pmatrix} 1 & 0 \\ 1 & 0 \\ 0 & 1 \end{pmatrix}, \qquad E_B = \begin{pmatrix} 1 & 0 \\ 0 & 1 \\ 0 & 1 \end{pmatrix}, \qquad A_{\rm parent} = E_X A_{\rm daughter}. \quad \text{(VIII.9.7)}$$

Both maps embed a full $U(N) \times U(N)$ in the same $U(N)^3$. Inserting them in the bare single-trace level matrix gives the worked level sums

$$E_A^T \,\mathrm{diag}(2, -1, -1)E_A = \mathrm{diag}(1, -1), \qquad E_B^T \,\mathrm{diag}(2, -1, -1)E_B = \mathrm{diag}(2, -2). \quad \text{(VIII.9.8)}$$

Thus condensing an arrow joining nodes 1 and 2 leaves level 1 on the joined node, while joining 2 and 3 leaves level -2 there. The two answers follow from the same parent and the same fundamental trace. Chapter 4's compact-level convention is essential here: replacing the diagonal compact connection by an arbitrary multiple would change the flux lattice and the local orbifold order. Figure VIII.9.1 will keep both embeddings attached to one parent quiver when the FI vacua are specified.

VIII.9.3 The five-field parent and its selected quotient

We now specify the parent so the geometric change can be calculated. All three gauge factors have rank N. Its five arrows are

$$A = X_{12}, \qquad B = X_{23}, \qquad D = X_{13}, \qquad C_1 = X_{31}^1, \quad C_2 = X_{31}^2; \qquad k = (2, -1, -1). \quad \text{(VIII.9.9)}$$

For noncommuting fields the order around a closed path is physical. Its superpotential is the difference of two ordered quintic traces:

$$W = h\,\mathrm{Tr}\big(C_1ABC_2D - C_2ABC_1D\big). \quad \text{(VIII.9.10)}$$

At $N = 1$ the fields commute and the two monomials cancel. At larger rank, every cyclic derivative at a configuration with only A or only B nonzero still contains an

uncondensed field. Those candidate vacua are therefore F-flat, but their D equations must still be solved.

It is useful to see one derivative before imposing a VEV. Varying C_1 inside a trace and moving the varied matrix to the front by cyclicity gives an ordered matrix equation. The two parent words contribute different paths from node 1 to node 3:

$$\frac{\partial W}{\partial C_1} = h\big(ABC_2D - DC_2AB\big). \tag{VIII.9.11}$$

If A alone is populated, each term still contains B, C_2, D; if B alone is populated, each still contains A, C_2, D. The other four cyclic derivatives have the same vanishing property because each parent monomial contains five distinct arrow occurrences. This argument uses cyclic derivatives of noncommuting traces, not the rank-one cancellation of the whole superpotential.

With tail-positive arrow charges, define $\mathfrak{m}_i$ as the Hermitian matter moment at node i. The full-rank matrix equations, including FI sources $\zeta_i \mathbf{1}_N$, are

$$\begin{aligned}
\mathfrak{m}_1 &= AA^\dagger + DD^\dagger - C_1^\dagger C_1 - C_2^\dagger C_2 = \frac{k_1}{2\pi}\sigma_1 + \zeta_1 \mathbf{1}_N, \\
\mathfrak{m}_2 &= BB^\dagger - A^\dagger A = \frac{k_2}{2\pi}\sigma_2 + \zeta_2 \mathbf{1}_N, \\
\mathfrak{m}_3 &= C_1C_1^\dagger + C_2C_2^\dagger - B^\dagger B - D^\dagger D = \frac{k_3}{2\pi}\sigma_3 + \zeta_3 \mathbf{1}_N.
\end{aligned} \tag{VIII.9.12}$$

Here each σ_i is the Hermitian real scalar of a vector multiplet, and $\sum_i \zeta_i = 0$ for the chosen FI family. A bifundamental zero of the positive intertwining terms also obeys

$$\sigma_a X_{ab} = X_{ab}\sigma_b \quad \text{for every populated arrow } a \to b. \tag{VIII.9.13}$$

These equations make the FI premise concrete. Set all fields except $A = v\mathbf{1}_N$ to zero and choose $\sigma_i = 0$. Then

$$(\mathfrak{m}_1, \mathfrak{m}_2, \mathfrak{m}_3) = |v|^2(1, -1, 0)\mathbf{1}_N, \qquad \zeta_A = |v|^2(1, -1, 0). \tag{VIII.9.14}$$

All three D equations and the intertwining condition hold. Repeating the calculation with only $B = v\mathbf{1}_N$ gives

$$(\mathfrak{m}_1, \mathfrak{m}_2, \mathfrak{m}_3) = |v|^2(0, 1, -1)\mathbf{1}_N, \qquad \zeta_B = |v|^2(0, 1, -1), \quad \sigma_i = 0. \tag{VIII.9.15}$$

For the fixed representatives, these are full equations, not merely projections along a charge vector. For example, adding tk to either FI vector changes the residual at fixed $\sigma = 0$; a common shift of σ can compensate that change. In the physical FI quotient the two directions are related by

$$\zeta_B = -2\zeta_A + |v|^2 k, \tag{VIII.9.16}$$

where the displayed relation uses the same $|v|$ for comparison. It does not make the two fixed-σ equations identical.

Neither nonzero single-field VEV is a vacuum of the diagonal-CS parent at zero FI. In the A case the moment equations alone would force $\sigma_1 = \pi|v|^2$ and $\sigma_2 = 2\pi|v|^2$, contradicting $\sigma_1 = \sigma_2$ required by the populated arrow. In the B case they would force $\sigma_2 = -2\pi|v|^2$ and $\sigma_3 = 2\pi|v|^2$, contradicting $\sigma_2 = \sigma_3$. Thus the FI source supports the actual node-locking vacuum; it is not just a label placed on a quiver mutation.

It is instructive to see why the zero-FI diagonal-CS equations naturally led to the common-σ branch before choosing the mixed completion. At rank one the sum of the three matter moments vanishes identically. With $\zeta = 0$, the sum of the right-hand sides of (VIII.9.12) is therefore

$$2\sigma_1 - \sigma_2 - \sigma_3 = 0. \tag{VIII.9.17}$$

Suppose $\sigma_2 \neq \sigma_3$. If all three values differ, the intertwining equations kill every arrow, and then each moment equation sets its σ_i to zero, a contradiction. If $\sigma_1 = \sigma_2 \neq \sigma_3$, only A can be populated; the two node equations give the inconsistent values

$$\sigma_1 = \pi|A|^2, \qquad \sigma_2 = 2\pi|A|^2, \tag{VIII.9.18}$$

unless $A = 0$. If $\sigma_1 = \sigma_3 \neq \sigma_2$, only D, C_1, C_2 can remain. Node 2 sets $\sigma_2 = 0$ and nodes 1 and 3 require opposite moments with incompatible level magnitudes:

$$\Delta := |D|^2 - |C_1|^2 - |C_2|^2 = \frac{\sigma_1}{\pi} = \frac{\sigma_3}{2\pi}. \tag{VIII.9.19}$$

Again $\sigma_1 = \sigma_3$ forces $\Delta = 0$. Thus the diagonal-only diagonal-CS equations at zero FI admit no unequal-σ solution of these types. This argument explains the selected common-σ stratum. It must not be promoted to a classification after adding Λ_H: the mixed term changes the moment equation precisely when σ has partially connected components.

The rank-one common-σ stratum at zero FI supplies a useful fourfold quotient. Remove the overall diagonal gauge phase and set $\theta_3 = 0$ for the two relative angles. The CS character is $2\theta_1 - \theta_2$; its connected compact kernel has primitive generator $(\theta_1, \theta_2, \theta_3) = t(1, 2, 0)$. The original character $(2, -1)$ is primitive, so there is no initial finite component hidden in this kernel. Acting on fields in the fixed order (A, C_1, D, C_2, B) gives

$$q = (-1, -1, 1, -1, 2). \tag{VIII.9.20}$$

For example, the physical phase of $A : 1 \to 2$ is $\theta_1 - \theta_2 = -t$, while the phase of $B : 2 \to 3$ is $\theta_2 - \theta_3 = 2t$. The two C arrows each have phase $\theta_3 - \theta_1 = -t$, and $D : 1 \to 3$ has phase $+t$. This direct incidence calculation fixes the sign and the factor of two in (VIII.9.20). Choosing a nonprimitive generator for the kernel would change the apparent residual finite group after Higgsing, even though the continuous quotient looked the same. The two signs in this vector allow generic closed orbits to meet a zero-moment representative. Since W vanishes for commuting scalars, the selected abelian geometric branch is the compactly specified quotient

$$\mathcal{M}^{\mathrm{sel}}_{\mathrm{geom}} = \mathbb{C}^5 /\!/ \mathbb{C}^*_{(-1,-1,1,-1,2)}, \qquad \dim_{\mathbb{C}} \mathcal{M}^{\mathrm{sel}}_{\mathrm{geom}} = 4. \tag{VIII.9.21}$$

The dimension is the five coordinates minus one continuous quotient, on the populated stratum. As in Chapter 7, a real moment equation selects representatives while the

complex quotient describes the affine coordinate ring. This calculation does not by itself classify all other σ strata after a parity completion.

To keep the integral geometry visible, choose a field-to-ray labeling compatible with the equal-weight columns of the toric diagram. In the same field order, a primitive ray matrix is

$$G = \begin{pmatrix} 1 & 1 & 1 & 1 & 1 \\ 0 & 1 & 0 & 1 & 1 \\ 0 & 1 & 1 & 0 & 0 \\ 0 & 0 & 1 & 1 & 0 \end{pmatrix}, \qquad Gq^T = 0. \tag{VIII.9.22}$$

The first row puts the rays at affine height one. The relation vanishes entry by entry; for example the second row yields $-1 - 1 + 2 = 0$. The maximal minors have greatest common divisor one, fixing the parent ray lattice primitively. Equal negative-weight fields can be relabeled among equal-weight source rays, so this displayed order is a declared coordinate choice rather than a uniquely inferred field/ray table.

There is a parity subtlety in treating this three-node theory as a compact spin gauge theory. For the rank-one parent we use the specific symmetric trace-product matrix

$$\Lambda_H = \begin{pmatrix} 0 & \frac{1}{2} & -\frac{1}{2} \\ \frac{1}{2} & -1 & \frac{1}{2} \\ -\frac{1}{2} & \frac{1}{2} & 0 \end{pmatrix}, \qquad S_{\text{mixed}} = \frac{1}{4\pi} \int \sum_{i,j} (\Lambda_H)_{ij} \operatorname{Tr}(A_i), d \operatorname{Tr}(A_j). \tag{VIII.9.23}$$

This is the selected combined fermion/CS parity prescription, in the framework of Benini, Closset and Cremonesi. It is a trace-product term, not a shift of the nonabelian fundamental-trace levels. In particular $\Lambda_H(1,1,1)^T = 0$: on the common-σ stratum the selected moments and primitive quotient above are unchanged. More strongly for our two bare Higgs embeddings,

$$E_A^T \Lambda_H E_A = 0, \qquad E_B^T \Lambda_H E_B = 0. \tag{VIII.9.24}$$

At the vacua in (VIII.9.14) and (VIII.9.15), $\sigma = 0$, so the same full moment residuals vanish with this completion. Row sums alone would be weaker: for $\sigma = (u, u, w)^T$,

$$\Lambda_H \sigma = \tfrac{1}{2}(u - w, w - u, 0)^T. \tag{VIII.9.25}$$

Thus a partially connected σ branch can change even though both selected bare pullbacks vanish. The completion is one allowed local choice, not a unique regulator selected by an M2 construction; its rank-one parity calculation does not settle general-N quantum dynamics.

For clarity, the rank-one parity arithmetic can be performed with the same arrow charges that produced the quotient. Arrange their three-node charge rows in the declared field order. The combined fermion shift of the compact Abelian CS matrix in this prescription is one half the Gram matrix:

$$\mathcal{Q} = \begin{pmatrix} 1 & -1 & 0 \\ -1 & 0 & 1 \\ 1 & 0 & -1 \\ -1 & 0 & 1 \\ 0 & 1 & -1 \end{pmatrix}, \qquad P = \tfrac{1}{2}\mathcal{Q}^T\mathcal{Q} = \begin{pmatrix} 2 & -\frac{1}{2} & -\frac{3}{2} \\ -\frac{1}{2} & 1 & -\frac{1}{2} \\ -\frac{3}{2} & -\frac{1}{2} & 2 \end{pmatrix}. \tag{VIII.9.26}$$

The chosen Λ_H cancels the fractional entries in the combined rank-one parity condition:

$$\operatorname{diag}(2,-1,-1)+\Lambda_H+P=\begin{pmatrix}4&0&-2\\0&-1&0\\-2&0&1\end{pmatrix}\in \mathrm{Mat}_{3\times 3}(\mathbb{Z}). \tag{VIII.9.27}$$

This integer test explains why a half-integral trace-product term can belong to a combined spin-theory prescription. It is not a license to use that term alone as an ordinary bosonic CS action. At equal rank N, the trace-product piece couples $\operatorname{Tr} A_i$ to $d \operatorname{Tr} A_j$; it must not be silently absorbed into a nonabelian shift of the fundamental-trace k_i.

VIII.9.4 Two Higgs routes from one parent

The two solutions above must be compared with the same initial ranks, levels and superpotential. Figure VIII.9.1 follows the parent through either VEV. Each condensed arrow is a full-rank identity, so the unbroken nodes really carry rank N; the diagrams do not infer a quantum flow from their shape.

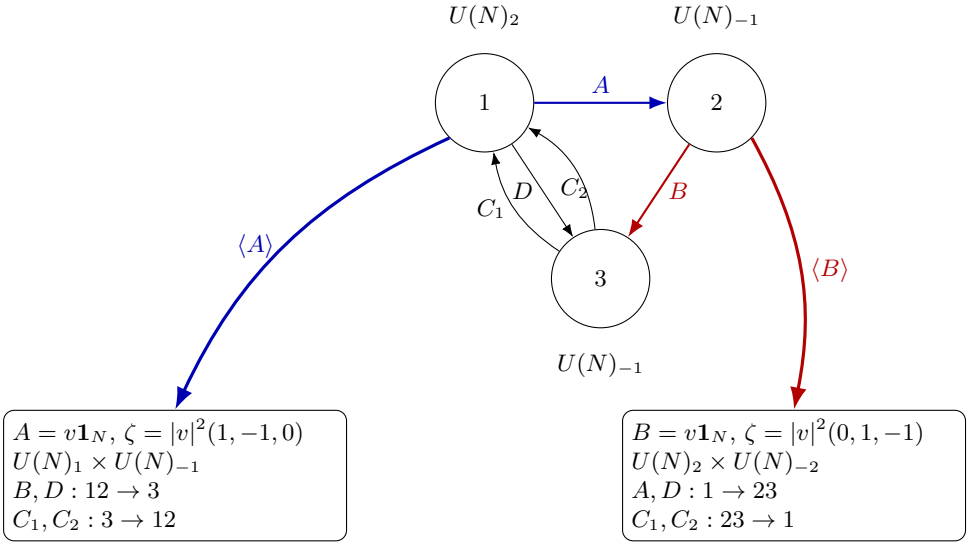


Figure VIII.9.1: One equal-rank five-arrow parent and two FI-supported full-rank Higgs vacua. The upper triangle always has levels $(2,-1,-1)$ and the ordered superpotential (VIII.9.10). The blue A VEV joins nodes $1,2$; the red B VEV joins nodes $2,3$. Each box lists the bare daughter levels and surviving arrow orientations. The picture does not include massive-field thresholds or assert an infrared equivalence.

First take $A = v\mathbf{1}_N$. The surviving arrow $B : 2 \to 3$ now runs from the joined node 12 to node 3, as does $D : 1 \to 3$. Both C arrows return from 3 to 12. Substitution into

the ordered parent word yields

$$W_A = hv\,\mathrm{Tr}\,(C_1BC_2D - C_2BC_1D)\,, \qquad (k_{12}, k_3) = (1, -1). \tag{VIII.9.28}$$

This is the alternating quartic pattern familiar from ABJM-like matter, but the statement derived here is its ordered field content, its bare levels and its local rank-one chart. The coupling hv has the appropriate changed dimension after inserting the VEV; interpreting all rank-N infrared interactions requires more than this substitution. The difference between the two trace words remains visible in a daughter F equation. For instance, cyclic differentiation with respect to C_1 gives

$$\frac{\partial W_A}{\partial C_1} = hv\big(BC_2D - DC_2B\big). \tag{VIII.9.29}$$

At rank one the right-hand side vanishes by commutativity; for a nonabelian fluctuation it is a genuine constraint. This is the local interaction inherited from the five-field parent rather than an independently postulated ABJM potential.

The second choice $B = v\mathbf{1}_N$ joins 2 and 3. Then $A, D : 1 \to 23$ and $C_1, C_2 : 23 \to 1$. Their ordered interaction is

$$W_B = hv\,\mathrm{Tr}\,(C_1AC_2D - C_2AC_1D)\,, \qquad (k_1, k_{23}) = (2, -2). \tag{VIII.9.30}$$

At rank one both quartic traces vanish by commutativity, but for nonabelian fields the ordering distinguishes the two terms. Canceling them before substitution would lose the daughter interaction. This is why the superpotential, not only the arrows and levels, has to be followed through a Higgs route. The corresponding sample derivative is

$$\frac{\partial W_B}{\partial C_1} = hv\big(AC_2D - DC_2A\big). \tag{VIII.9.31}$$

It has the same alternating form but a different arrow in the place vacated by the VEV. Comparing (VIII.9.29) and (VIII.9.31) is a simple way to check the ordered substitution. The two bare CS levels still differ, so even the classical daughter actions are not identified solely by relabeling these quartic words.

The local abelian geometry can be read directly from the primitive charge vector. A nonzero homogeneous coordinate of weight q_j fixes the continuous $\mathbb{C}^*$ action and leaves a finite stabilizer $\boldsymbol{\mu}_{|q_j|}$. In the A chart, $q_A = -1$, so the stabilizer is trivial. In the B chart, $q_B = 2$, so the element -1 remains. All four surviving weights are odd and it acts as inversion:

$$\begin{aligned} A \neq 0 :&\qquad (C_1, D, C_2, B) \in \mathbb{C}^4, \\ B \neq 0 :&\qquad (A, C_1, D, C_2) \sim -(A, C_1, D, C_2), \qquad \mathbb{C}^4/\mathbb{Z}_2. \end{aligned} \tag{VIII.9.32}$$

This explicit action matters: an index-two tetrahedron alone would not say which finite group acts on the four tangent coordinates. One can obtain the same charts by gauge fixing the homogeneous coordinate rather than starting from a toric diagram. Let $t \in \mathbb{C}^*$ act with weights q in (VIII.9.20). On $A \neq 0$, the condition $t^{-1}A = 1$ has one

solution for t and no residual finite root. The four gauge-invariant coordinates can be chosen as

$$(u_1, u_2, u_3, u_4) = \left(\frac{C_1}{A}, AD, \frac{C_2}{A}, A^2 B \right), \qquad A \neq 0. \tag{VIII.9.33}$$

Their powers cancel the respective weights $(-1, +1, -1, +2)$ against $q_A = -1$. They are algebraically independent because the rank-one F terms vanish, so this affine chart really has four free complex coordinates. It is the local chart containing the selected A vacuum, not a claim that the entire FI-resolved space is affine $\mathbb{C}^4$.

On $B \neq 0$, gauge fixing $t^2 B = 1$ requires a square root and leaves $t = -1$. We can work on the double cover with four coordinates

$$(z_1, z_2, z_3, z_4) = \left(A\sqrt{B}, C_1\sqrt{B}, \frac{D}{\sqrt{B}}, C_2\sqrt{B} \right), \qquad (z_1, z_2, z_3, z_4) \sim -(z_1, z_2, z_3, z_4). \tag{VIII.9.34}$$

The square-root notation describes the gauge slice, not a globally single-valued function on the quotient. Every invariant polynomial on this chart is even under the simultaneous sign, which recovers $\mathbb{C}^4/\mathbb{Z}_2$ with its specified action. This derivation also explains physically why the weight-two VEV leaves a discrete gauge transformation whereas the weight-one VEV does not.

The ray matrix provides an independent integral check. Remove the column whose coordinate is nonzero and take the determinant of the remaining 4×4 matrix. In the fixed column order of (VIII.9.22),

$$|\det G_{\widehat{A}}| = 1, \qquad |\det G_{\widehat{B}}| = 2. \tag{VIII.9.35}$$

The first cone is unimodular; the second has index two. The equality between these indices and $|q_A|, |q_B|$ is a consequence of the primitive one-relation presentation. Figure VIII.9.2 shows the same deletion on the five rays. It retains the selected field labels, because the three equal negative-weight rays otherwise admit arbitrary exchanges. The deletion determinants and finite stabilizers answer slightly different questions. The determinant measures the index of the four remaining rays in the parent lattice. The stabilizer calculation determines how a residual group acts on the actual fluctuation coordinates. Here they agree because the five-column presentation has one primitive relation and the four surviving B weights are all odd. In another quotient, a lattice index would not by itself name the representation of the finite group on matter.

The two routes make partial resolution a concrete operation: an FI value supports the full-rank VEV, a full compact diagonal subgroup survives, the ordered interaction shortens, and one homogeneous coordinate becomes nonzero. Benishti, He and Sparks relate these routes to the phase-Ib geometry. Other toric phases or torsion choices can have different physics even when a local toric diagram looks similar. The bare data and abelian tangent cones here are therefore the appropriate outputs of this calculation, not a universal duality among all phases. Chapter 7 supplies the toric lattice description used here; Chapter 4 explains why global compact data can still distinguish theories with similar local geometry.

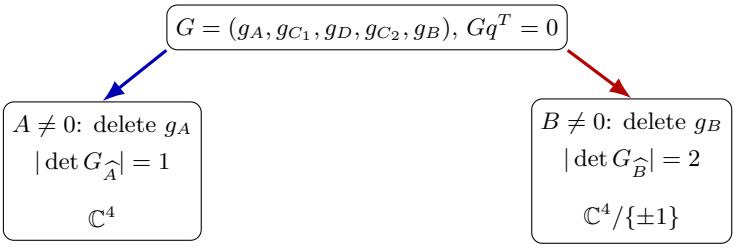


Figure VIII.9.2: Two local affine charts of the same primitive five-ray parent. Deleting the condensed coordinate gives the indicated lattice index. The weight calculation in (VIII.9.32) also fixes the $\mathbb{Z}_2$ action as simultaneous inversion. These are local abelian tangent cones around the chosen FI-supported vacua, rather than the entire resolved spaces or their metrics.

VIII.9.5 The component mass and the rank-one control

Higgsing changed the chosen vacuum inside a quiver with a fixed local interaction. To study a mass, we instead specify the altered potential. For flat-space $U(N)_k \times U(N)_{-k}$ ABJM at $k > 0$, use the GRVV component convention with matrices Q_α, R_α, $\alpha = 1, 2$, and real $\mu > 0$. Its positive scalar potential is

$$V = \sum_{\alpha=1}^{2} \left[\mathrm{Tr}(M_\alpha M_\alpha^\dagger) + \mathrm{Tr}(N_\alpha N_\alpha^\dagger) \right]. \tag{VIII.9.36}$$

The GRVV component action fixes the physical potential used here. We display all four matrix brackets because the mixed terms matter when we later combine different blocks. With $\beta = 1, 2$ summed, they are

$$\begin{aligned} M_\alpha = \mu Q_\alpha + \frac{2\pi}{k}\big(&Q_\alpha Q_\beta^\dagger Q_\beta - Q_\beta Q_\beta^\dagger Q_\alpha \\ &+ R_\beta R_\beta^\dagger Q_\alpha - Q_\alpha R_\beta^\dagger R_\beta + 2Q_\beta R_\beta^\dagger R_\alpha - 2R_\alpha R_\beta^\dagger Q_\beta\big), \\ N_\alpha = -\mu R_\alpha + \frac{2\pi}{k}\big(&R_\alpha R_\beta^\dagger R_\beta - R_\beta R_\beta^\dagger R_\alpha \\ &+ Q_\beta Q_\beta^\dagger R_\alpha - R_\alpha Q_\beta^\dagger Q_\beta + 2R_\beta Q_\beta^\dagger Q_\alpha - 2Q_\alpha Q_\beta^\dagger R_\beta\big). \end{aligned} \tag{VIII.9.37}$$

The opposite linear signs are part of this component convention. The positive quadratic potential alone would determine μ^2 but would not determine which sign appears in each first-order vacuum bracket. A sign change here changes the nonabelian solutions. Figure VIII.9.3 later depicts the scalar blocks and their bilinears after the branch equation has been derived.

To expose the roles of ordering and mixing, define left and right bilinears $L_Q = \sum Q_\beta Q_\beta^\dagger$, $R_Q = \sum Q_\beta^\dagger Q_\beta$ and similarly L_R, R_R. Also put $T = \sum Q_\beta R_\beta^\dagger$ and $U =$

$\sum R_\beta^\dagger Q_\beta$. The complete brackets regroup as

$$M_\alpha = \mu Q_\alpha + \frac{2\pi}{k}\big(Q_\alpha R_Q - L_Q Q_\alpha + L_R Q_\alpha - Q_\alpha R_R + 2T R_\alpha - 2R_\alpha U\big),$$
$$N_\alpha = -\mu R_\alpha + \frac{2\pi}{k}\big(R_\alpha R_R - L_R R_\alpha + L_Q R_\alpha - R_\alpha R_Q + 2T^\dagger Q_\alpha - 2Q_\alpha U^\dagger\big). \tag{VIII.9.38}$$

This is only an algebraic regrouping of (VIII.9.37); it provides a quick test for a candidate branch. When $Q = 0$, the four terms involving Q disappear and N_α depends on the difference of the two R bilinear actions. When $R = 0$, the analogous statement holds for M_α. For a mixed configuration, the T, U terms generally survive and must be checked rather than presumed zero. For instance, at $N = 2$ choose $Q_1 = E_{11}$ and $R_1 = E_{21}$, with $Q_2 = R_2 = 0$. Then

$$T = Q_1 R_1^\dagger = E_{12}, \qquad U = R_1^\dagger Q_1 = 0. \tag{VIII.9.39}$$

This off-shell example does not solve the vacuum equations. It demonstrates that a mixed Q, R ansatz can retain terms absent on either pure branch. The direct sum below works because its two species occupy orthogonal common blocks, not because the mixed terms of the action can be discarded in general.

At $N = 1$ all scalar products commute. The antisymmetric pairs cancel, as do both pairs of mixed products. Thus the brackets and the complete rank-one potential reduce to

$$M_\alpha = \mu Q_\alpha, \qquad N_\alpha = -\mu R_\alpha, \qquad V_{N=1} = \mu^2 \sum_{\alpha=1}^{2} (|Q_\alpha|^2 + |R_\alpha|^2). \tag{VIII.9.40}$$

Writing each complex field as $(x + iy)/\sqrt{2}$ with canonical kinetic term gives a Hessian μ^2 for each real component. Hence the origin is the only continuous rank-one scalar vacuum when $\mu \neq 0$. The massless limit removes the quadratic term; recovering the undeformed position quotient then still requires the compact gauge construction of Chapter 5. One cannot divide later branch equations by the scale c at $\mu = 0$ and read a massless classification from them. More explicitly, write $C^I = (x^I + iy^I)/\sqrt{2}$ for the four complex fields $C^I = (Q_1, Q_2, R_1, R_2)$ and use the canonical kinetic term $-\sum_I |D_\nu C^I|^2$. The quadratic form and its real Hessian are

$$V_{N=1} = \frac{\mu^2}{2} \sum_{I=1}^{4} \big[(x^I)^2 + (y^I)^2\big], \qquad \frac{\partial^2 V}{\partial x^I \partial x^J} = \frac{\partial^2 V}{\partial y^I \partial y^J} = \mu^2 \delta_{IJ}. \tag{VIII.9.41}$$

There are eight equal positive real mass squares. The statement concerns scalar directions, not the number of supersymmetric states of the residual topological sector. It also shows why merely quoting the positive potential is insufficient for the nonabelian problem: the Hessian remembers μ^2, whereas the first-order brackets remember the relative signs of μQ and $-\mu R$.

Noncommuting products can balance the linear term. On the $Q = 0$ branch, set $R^\alpha = cA_\alpha$; on the $R = 0$ branch set $Q^\alpha = cA_\alpha^\dagger$. The required dimensionful scale is

$$c^2 = \frac{\mu k}{2\pi}, \qquad [c] = \tfrac{1}{2}. \tag{VIII.9.42}$$

For example, the $Q = 0$ equation becomes

$$0 = -\mu c A_\alpha + \frac{2\pi c^3}{k}\left(A_\alpha S_R - S_L A_\alpha\right), \quad S_L = \sum_\beta A_\beta A_\beta^\dagger, \quad S_R = \sum_\beta A_\beta^\dagger A_\beta. \tag{VIII.9.43}$$

After using (VIII.9.42), both α equations take the dimensionless form

$$A_\alpha + S_L A_\alpha - A_\alpha S_R = 0, \qquad \alpha = 1, 2. \tag{VIII.9.44}$$

For $\alpha = 1$ the self-cubic terms cancel, leaving $A_1 + A_2 A_2^\dagger A_1 - A_1 A_2^\dagger A_2 = 0$; for $\alpha = 2$ one obtains $A_2 + A_1 A_1^\dagger A_2 - A_2 A_1^\dagger A_1 = 0$. The dagger in the Q branch is essential: substitution into M_α, with the same positive c, gives the adjoint of (VIII.9.44) in the correct order. Indeed, if $Q_\alpha = c A_\alpha^\dagger$ and $R = 0$, then $L_Q = c^2 S_R$ and $R_Q = c^2 S_L$. The first bracket is

$$M_\alpha = c\mu A_\alpha^\dagger + \frac{2\pi c^3}{k}\left(A_\alpha^\dagger S_L - S_R A_\alpha^\dagger\right) = c\mu\left(A_\alpha + S_L A_\alpha - A_\alpha S_R\right)^\dagger. \tag{VIII.9.45}$$

Thus the same dimensionless equation solves both branches, but their physical scalar matrices are related by Hermitian conjugation. Using $Q = cA$ without that dagger would test a different equation.

A first nontrivial check is the $N = 2$ pair

$$A_1 = \begin{pmatrix} 0 & 0 \\ 0 & 1 \end{pmatrix}, \qquad A_2 = \begin{pmatrix} 0 & 1 \\ 0 & 0 \end{pmatrix}, \qquad S_L = \mathbf{1}_2, \quad S_R = \mathrm{diag}(0, 2). \tag{VIII.9.46}$$

Both matrices obey $A_\alpha S_R = 2A_\alpha$, so $A_\alpha + S_L A_\alpha - A_\alpha S_R = 0$. Consequently $(Q, R) = (0, cA)$ and $(cA^\dagger, 0)$ each solve the complete GRVV brackets. This example already separates a mass-deformed matrix vacuum from a commuting membrane position: A_1 and A_2 do not commute. It also shows why the rank-one result cannot be extrapolated by simply replacing complex numbers with matrices.

VIII.9.6 Square blocks, bilinears and classical limits

The 2×2 solution suggests a controlled arbitrary-rank family. For one-based indices $i, j = 1, \ldots, N$, define square matrices

$$(A_1)_{ij} = \sqrt{i-1}\,\delta_{ij}, \qquad (A_2)_{ij} = \sqrt{N-i}\,\delta_{j,i+1}. \tag{VIII.9.47}$$

The entries follow the GRVV square-block convention; A_2 raises the column index by one and vanishes in its last row. Both matrices have a zero first column and each has rank $N - 1$ for $N > 1$. In particular, they are not full-rank Higgs VEVs of the preceding example. The familiar physical image is a finite collection of noncommuting scalar positions, not a node-locking identity matrix. The rank statement can be read without a determinant. On the subspace spanned by columns $2, \ldots, N$, the diagonal entries of A_1 are $1, \sqrt{2}, \ldots, \sqrt{N-1}$ and are nonzero. The same columns of A_2 map to

distinct rows $1, \dots, N-1$ with nonzero coefficients. Thus each map is injective on that $(N-1)$-dimensional subspace, while column 1 is in its kernel:

$$\ker A_1 = \ker A_2 = \operatorname{span}\{e_1\}, \qquad \operatorname{rank} A_1 = \operatorname{rank} A_2 = N-1 \quad (N \geq 2). \tag{VIII.9.48}$$

For $N = 1$ both ranks are zero. This is a useful contrast with $A = v\mathbf{1}_N$ in the Higgs example: the two objects are both matrix VEVs, but only the latter locks two full $U(N)$ nodes.

The proof of the branch equation needs only two matrix sums. At row i, the diagonal entries of $A_1 A_1^\dagger$ and $A_2 A_2^\dagger$ are $i-1$ and $N-i$. On the right, $A_1^\dagger A_1$ contributes $i-1$, while $A_2^\dagger A_2$ contributes $N-i+1$ for $i \geq 2$ and zero for $i = 1$. Therefore

$$S_L = \sum_\alpha A_\alpha A_\alpha^\dagger = (N-1)\mathbf{1}_N, \qquad S_R = \sum_\alpha A_\alpha^\dagger A_\alpha = \operatorname{diag}(0, N, \dots, N). \tag{VIII.9.49}$$

The first column of each A_α vanishes, hence multiplication by S_R gives $A_\alpha S_R = N A_\alpha$. Combining the two identities,

$$A_\alpha + S_L A_\alpha - A_\alpha S_R = A_\alpha + (N-1)A_\alpha - N A_\alpha = 0. \tag{VIII.9.50}$$

This analytic calculation proves both equations for every positive integer N. Checks on finitely many small matrices are useful for transcription but would not replace this argument. It also covers $N = 1$: both blocks vanish, in agreement with the isolated abelian origin at nonzero μ.

For a larger worked example, at $N = 3$ the matrices are

$$A_1 = \begin{pmatrix} 0 & 0 & 0 \\ 0 & 1 & 0 \\ 0 & 0 & \sqrt{2} \end{pmatrix}, \qquad A_2 = \begin{pmatrix} 0 & \sqrt{2} & 0 \\ 0 & 0 & 1 \\ 0 & 0 & 0 \end{pmatrix}, \qquad S_L = 2\mathbf{1}_3, \quad S_R = \operatorname{diag}(0, 3, 3). \tag{VIII.9.51}$$

One can see the left/right distinction without multiplying all cubic terms: S_L counts an equal weight on each row, while S_R singles out the unused first column. The difference is exactly one unit of A_α in (VIII.9.50).

The scalar matrices also produce a familiar finite-dimensional geometry through bilinears. Define

$$\begin{aligned} J_+ &= A_2 A_1^\dagger, \qquad J_- = J_+^\dagger, \\ J_3 &= A_2 A_2^\dagger - A_1 A_1^\dagger, \\ J_1 &= J_+ + J_-, \qquad J_2 = -i(J_+ - J_-). \end{aligned} \tag{VIII.9.52}$$

The entries are sparse enough to calculate the algebra directly:

$$(J_+)_{i,i+1} = \sqrt{i(N-i)}, \qquad (J_3)_{ii} = N + 1 - 2i. \tag{VIII.9.53}$$

For a nonzero entry of J_+, the adjacent diagonal entries of J_3 differ by two. Meanwhile the diagonal of $J_+ J_- - J_- J_+$ is $i(N-i) - (i-1)(N-i+1) = N + 1 - 2i$. Thus the two independent commutators are

$$[J_3, J_+] = 2J_+, \qquad [J_+, J_-] = J_3. \tag{VIII.9.54}$$

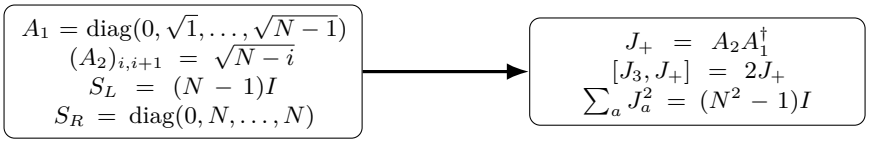


Figure VIII.9.3: A square GRVV scalar block and its spin bilinears. Each A_α has rank $N-1$, and the different left and right sums solve the first-order vacuum equation. The bilinears form spin $(N-1)/2$; this algebra does not itself construct a smooth three-sphere or a higher-dimensional brane worldvolume.

These are $su(2)$ generators in a normalization twice the usual spin operators. Since J_3 runs from $N-1$ down to $-(N-1)$ in steps of two, the representation has spin $j = (N-1)/2$. Its Casimir is obtained entry by entry rather than inferred from a continuum sphere. On the ith basis vector,

$$(J_+J_- + J_-J_+)_{ii} = i(N-i) + (i-1)(N-i+1), \tag{VIII.9.55}$$

while J_3^2 contributes $(N+1-2i)^2$. Since $J_1^2 + J_2^2 = 2(J_+J_- + J_-J_+)$, their sum is independent of i:

$$\frac{1}{4}\sum_{a=1}^{3} J_a^2 = j(j+1)\mathbf{1}_N, \qquad \sum_{a=1}^{3} J_a^2 = (N^2-1)\mathbf{1}_N. \tag{VIII.9.56}$$

For $N=3$, $J_3 = \mathrm{diag}(2,0,-2)$ and J_+ has upper entries $\sqrt{2}, \sqrt{2}$. The Casimir is $8\mathbf{1}_3$, the spin-one result in this normalization. Figure VIII.9.3 juxtaposes the scalar matrices with the bilinears: the former are the actual vacuum fields, while the latter give a useful algebraic picture of their noncommutativity.

A scalar-bilinear size can be defined without assigning a spacetime radius to the block. On the R branch, normalize by the matrix size:

$$\rho_R^2 := \frac{1}{N}\,\mathrm{Tr}\sum_\alpha R^\alpha R_\alpha^\dagger = c^2(N-1) = \frac{\mu k}{2\pi}(N-1). \tag{VIII.9.57}$$

The notation ρ_R^2 is a proxy for the squared scalar amplitude. Since $[R] = 1/2$, its physical dimension is mass, not geometric length squared. Turning it into a bulk radius requires a separate field/geometry conversion and dynamics. The Casimir similarly gives a two-sphere algebra of bilinears; it does not prove that the complete matrix vacuum is a smooth classical S^3.

Direct sums give further explicit classical solutions. Choose a 2×2 Q block, a 3×3 R block and a 1×1 zero block, all at the same positive k, μ. With $A^{(n)}$ denoting (VIII.9.47) at size n, set

$$Q^\alpha = \mathrm{diag}\big(c(A_\alpha^{(2)})^\dagger, 0_3, 0_1\big), \qquad R^\alpha = \mathrm{diag}\big(0_2, cA_\alpha^{(3)}, 0_1\big). \tag{VIII.9.58}$$

Every product in (VIII.9.37) remains block diagonal. Within the first block $R = 0$, within the second $Q = 0$, and in the third both vanish. Hence all mixed terms vanish blockwise and all four complete brackets are zero. More general common block-diagonal sums of these selected pieces work for the same reason. Off-block mixing would require a fresh solution of the coupled equations and is not licensed by the direct-sum argument. The common block decomposition is essential. If Q and R were diagonalized with incompatible projectors, the products T and U in (VIII.9.38) could be nonzero even though each field separately resembled a collection of familiar blocks. In the displayed $2Q \oplus 3R \oplus 1_0$ solution, the scalar matrices have total size six, with ranks $(1, 1)$ in the two Q fields and $(2, 2)$ in the two R fields. The zero block contributes a genuine extra gauge subspace but no scalar amplitude. These concrete ranks are useful checks on the placement of the blocks and daggers.

There are two useful limits to keep distinct. At $N = 1$ the square block is zero and the mass leaves only the continuous scalar origin. At $\mu = 0$ the scale in (VIII.9.42) vanishes, so the rescaling used to derive the dimensionless equation is no longer an invertible reparametrization of all massless vacua. The family above therefore exhibits classical nonabelian zeros at positive mass, but does not enumerate every classical solution, count quantum vacua, or establish M5-brane dynamics. GRVV itself discusses additional classical solutions. A protected quantum count would require the fermion spectrum, global compact data and the relevant index, not just a partition of these displayed blocks.

The two deformations now have concrete, different outputs. The FI-supported Higgs vacua change the local abelian chart and the bare two-node quiver through a full-rank node lock. The mass-deformed ABJM potential instead isolates the abelian position but admits selected rank-deficient nonabelian matrices whose bilinears form a finite spin algebra. In either case the physical interpretation rests on the stated equations; local quotient data and classical matrix algebra do not by themselves identify the complete infrared theory. These classical position and matrix data sharpen the probe question taken up in Chapter 10. Protected observables, studied in Chapter 11, require additional quantum input and cannot be replaced by counting the displayed blocks.

VIII.9.7 Exercises

See `benchmark/tasks.json` and `benchmark/PROTOCOL.md` for the public structured-answer format. Written explanations are separate from the exact algebraic fields.

1. **Two actual FI vacua.** Use $k = (2, -1, -1)$, $|v|^2 = 1$ and $\sigma = 0$. Submit the ordered moment vectors and the FI vectors needed for the pure $A = \mathbf{1}_N$ and $B = \mathbf{1}_N$ vacua, and the two 2×2 bare level pullbacks in (VIII.9.8). Explain why setting FI to zero would fail the intertwining equation.

2. **One parent, two local charts.** In the fixed (A, C_1, D, C_2, B) order, submit the primitive quotient charge vector, Gq^T, the absolute determinants after deleting A and B, and the nontrivial residual action on the four surviving B-chart coordinates. Explain why the action supplies information beyond the lattice index.

3. **A mass-deformed 2×2 block.** For $k = 2\pi$, $\mu = 1$ (so $c = 1$), submit A_1, A_2, S_L, S_R, the rank of each matrix, and the two residual matrices $A_\alpha + S_L A_\alpha - A_\alpha S_R$. State which dagger is needed when this block is placed in the Q branch.

4. **Spin and a mixed direct sum.** For $N = 3$, $k = 2\pi$, $\mu = 1$, submit J_3, the squares of the two upper entries of J_+, the three diagonal entries of $\sum_a J_a^2$, and the scalar-bilinear proxy ρ_R^2. Then give the total matrix size and the rank of each Q^α in its 2×2 block and each R^α in its 3×3 block for the $2Q \oplus 3R \oplus 1_0$ example. Explain why these data do not count quantum vacua.

Status and sources

The Higgs calculation fixes two FI-supported classical representatives, their bare diagonal embeddings, ordered daughter interactions and local abelian tangent cones. It uses the selected common-σ quotient and the chosen rank-one parity completion; it does not classify all branches of the completed theory or include quantum Higgs thresholds. The mass calculation solves the sourced GRVV classical brackets for displayed square blocks and their direct sums; it is not an exhaustive or quantum vacuum classification. No smooth S^3, M5 dynamics or universal toric phase duality follows from these calculations.

§VIII.9.1. The two questions concern classical FI Higgsing and the mass-deformed potential. The source premises are the Higgs setup of Benishti et al. 2010, arXiv:0909.4557v2, §3.3, printed pp. 11–12 / PDF pp. 12–13, and the component mass system of Gomis et al. 2008, arXiv:0807.1074v1 (2.5), printed p. 9 / PDF p. 10. superpotential normalization, Chern–Simons trace and levels, quiver gauge groups and Chern–Simons matter conventions and the classical FI and GRVV frame fix the restricted frames.

§VIII.9.2. The Higgsing calculation [**MATH**] gives the covariant-derivative mass and primitive bare-level pullbacks conditional on the full compact source action; it does not prove an infrared equivalence. Benishti et al. 2010, arXiv:0909.4557v2, §3.3, printed pp. 11–12 / PDF pp. 12–13; Chern–Simons trace and levels, quiver gauge groups and Chern–Simons matter conventions, the classical FI and GRVV frame.

§VIII.9.3. The FI-vacuum calculation [**MATH**] contains the two FI-supported representatives, full moment vectors, F equations and selected common-σ character quotient. Integrality of the chosen rank-one combined gauge-parity matrix is [**ANOM**]; its selection is a separate premise. Benishti et al. 2010, arXiv:0909.4557v2, §5.3.1, (5.10)–(5.13), Fig. 13, printed pp. 42–43 / PDF pp. 43–44; Benini et al. 2011, arXiv:1105.2299v2, §6, (6.1), (6.3)–(6.6); superpotential normalization, Chern–Simons trace and levels, quiver gauge groups and Chern–Simons matter conventions, the classical FI and GRVV frame and the classical tiling and gauge-parity frame.

§VIII.9.4. The daughter-action calculation [**MATH**] gives the ordered quartic daughter words and two local invariant charts under the specified VEVs and primitive gauge lattice. Their partial-resolution interpretation uses the sourced [**GEO-E**] dictionary, without a metric or infrared claim. Benishti et al. 2010, arXiv:0909.4557v2, §5.3.1,

(5.10)–(5.13), Fig. 13, printed pp. 42–43 / PDF pp. 43–44; superpotential normalization, Chern–Simons trace and levels, quiver gauge groups and Chern–Simons matter conventions, the classical FI and GRVV frame.

§VIII.9.5. The mass-deformation calculation [**MATH**] gives the rank-one Hessian, bracket substitutions and selected nonabelian zero conditional on the GRVV component potential. It does not count quantum vacua. Gomis et al. 2008, arXiv:0807.1074v1 (2.5), (3.1)–(3.5), printed pp. 9–11 / PDF pp. 10–12; superpotential normalization, Chern–Simons trace and levels and Chern–Simons matter conventions, the classical FI and GRVV frame and the mass and supersymmetric-sphere frame.

§VIII.9.6. The block calculation [**MATH**] gives the displayed square-block sums, bilinear commutators, Casimir and common direct sums within the sourced classical bracket system. It establishes neither exhaustiveness nor quantum multiplicities. Gomis et al. 2008, arXiv:0807.1074v1 (2.5), (3.1)–(3.5), printed pp. 9–11 / PDF pp. 10–12; superpotential normalization, Chern–Simons trace and levels and Chern–Simons matter conventions, the classical FI and GRVV frame and the mass and supersymmetric-sphere frame.

§VIII.9.7. The four exercises apply the Higgsing and massive-vacuum calculations under the same hypotheses.

Higgsing and the five-field parent. Benishti et al. (2010), §3.3 and §5.3.1, equations (5.10)–(5.13) and Fig. 13, gives the source phase, ordered superpotential and Higgs routes. The exact FI representatives, compact quotient charges, full-rank bare embeddings and residual finite action here are calculations at the stated source premises. The source's other phases and torsion possibilities are not identified by these local charts.

Parity convention. Benini et al. (2011), §6, equations (6.1) and (6.3)–(6.6), supplies the combined fermion and CS parity framework. The particular Λ_H in (VIII.9.23) is a selected compatible choice. Its row sums and two bare pullbacks are explicit calculations; the source does not select it from string theory or supply a complete general-rank quantum action for this parent.

Mass-deformed equations. Gomis et al. (2008), equations (2.5) and (3.1)–(3.5), supplies the component potential, branch equations and square-block family. The rank-one scalar mass, the all-N left/right-sum proof, bilinear commutators and direct-sum example follow from those equations. The source discusses classical solutions beyond this displayed family; quantum multiplicities require additional analysis.

References

Benini, F., C. Closset, and S. Cremonesi (2011). "Quantum moduli space of Chern-Simons quivers, wrapped D6-branes and AdS4/CFT3". In: *JHEP* 09, p. 005. DOI: 10.1007/JHEP09(2011)005. arXiv: 1105.2299 [hep-th].

Benishti, N., Y.-H. He, and J. Sparks (2010). "(Un)Higgsing the M2-brane". In: *JHEP* 01, p. 067. DOI: 10.1007/JHEP01(2010)067. arXiv: 0909.4557 [hep-th].

Gomis, J. et al. (2008). "A Massive Study of M2-brane Proposals". In: *JHEP* 09, p. 113. DOI: 10.1088/1126-6708/2008/09/113. arXiv: 0807.1074 [hep-th].

Chapter VIII.10

M2-branes at non-toric cones

VIII.10.1 The question posed by a quadric

The transverse positions of a single membrane can form a complex cone. In the ABJM example the cone is a finite quotient of $\mathbb{C}^4$, and four free complex coordinates remain visible before taking that quotient. A useful harder test starts with a cone that is neither $\mathbb{C}^4$ nor toric. Consider

$$X_2 = \left\{(z_0,\dots,z_4)\in\mathbb{C}^5 \;\middle|\; z_0^2+z_1^2+z_2^2+z_3^2+z_4^2=0\right\}. \tag{VIII.10.1}$$

The equation cuts out a complex fourfold with a single singular point at the origin. Its smooth radial link is the Stiefel manifold $V_{5,2}$. A proposed three-dimensional Chern–Simons quiver should pass a first test: one brane ought to move on $X_2/\mathbb{Z}_k$ for the stated compact gauge group. We shall derive that position space from the quiver, then ask what this test leaves undecided.

The target geometry already has two elementary checks. Write $F(z)=\sum_{a=0}^{4} z_a^2$. Its nonzero quadratic relation is irreducible and regular in the five-variable polynomial ring, so

$$\mathbb{C}[X_2]=\mathbb{C}[z_0,\dots,z_4]/(F), \qquad \dim_{\mathbb{C}} X_2 = 5-1=4. \tag{VIII.10.2}$$

The Jacobian gives the singular set without choosing a metric:

$$\nabla F = 2(z_0,z_1,z_2,z_3,z_4), \qquad \operatorname{Sing}(X_2)=\{z_0=\cdots=z_4=0\}. \tag{VIII.10.3}$$

Let $\mathfrak{m}=(z_0,\dots,z_4)$ be the maximal ideal at the origin. There the Zariski tangent space has all five ambient directions, one more than the dimension of the cone:

$$\dim_{\mathbb{C}} T_0X_2 = \dim_{\mathbb{C}} \mathfrak{m}/\mathfrak{m}^2 = 5 > 4. \tag{VIII.10.4}$$

These are algebraic properties that the quiver branch must reproduce. In particular, a dimension-four Hilbert series by itself will not distinguish this isolated singularity from a different quadratic hypersurface. We will later change one term in F to see the failure explicitly.

The calculation has an instructive second layer. The same superpotential that gives the quadric also leaves two nilpotent classes at its apex in the classical F-term scheme. These classes have no additional point-valued membrane positions. Consequently the geometric Hilbert series and the full classical F-term series differ. A quantum operator interpretation of the extra classes needs monopole and operator-product information beyond the polynomial calculation.

We use the fixed Martelli–Sparks candidate with two full compact $U(N)$ factors, bare levels $(+k, -k)$, positive integer k, and a nonzero cubic coefficient s. At one brane each original $U(1)$ has primitive $2\pi\mathbb{Z}$ flux; no common-center quotient is taken. This compact premise determines the finite group below. The identification of the candidate theory with membranes on the cone remains a proposed physical dictionary, even when its classical position-space test succeeds.

The three layers of the test can now be kept separate. The matrix F equations define an affine scheme. Its reduced component gives complex position coordinates. Compact gauge data then identify those coordinates by a residual finite action. The cone's Sasaki–Einstein metric and the infrared operator algebra require more than this polynomial and compact-gauge calculation. The quiver figure fixes the field content used in each step.

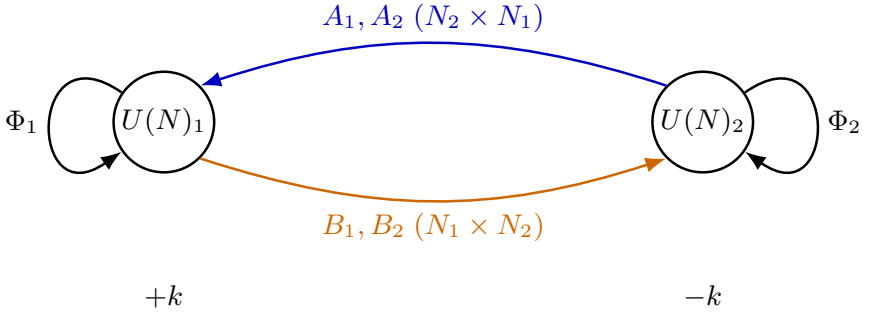


Figure VIII.10.1: The sourced two-node quiver in the book's fundamental-at-tail arrow convention. The ordered node ranks are (N, N) and the bare fundamental-trace levels are $(+k, -k)$. The upper arrows run $2 \to 1$ and the lower arrows $1 \to 2$; each node has one adjoint loop. The picture fixes representation types and trace order, not an infrared membrane duality.

VIII.10.2 From the source quiver to one-brane positions

Write A_i in $(\overline{N}_1, N_2)$ and B_i in $(N_1, \overline{N}_2)$, for $i = 1, 2$. The book arrow $i \to j$ carries an $N_i \times N_j$ matrix, with the fundamental at its tail. Thus A_i is $N_2 \times N_1$ and points $2 \to 1$, whereas B_i is $N_1 \times N_2$ and points $1 \to 2$. In particular, A_iB_i closes at node 2 and B_iA_i closes at node 1. This is visible even if the ranks differ: at $(N_1, N_2) = (2, 3)$, $\Phi_2 A_i B_i$ is a 3×3 product and $\Phi_1 B_i A_i$ a 2×2 product.

The matrix sizes determine which adjoint can multiply each path. In the example just given, the two closed products have types

$$A_iB_i:\ \mathbb{C}^3 \longrightarrow \mathbb{C}^3, \qquad B_iA_i:\ \mathbb{C}^2 \longrightarrow \mathbb{C}^2. \tag{VIII.10.5}$$

This check matters before differentiating a matrix superpotential: reversing the paths would make the interaction ill typed at unequal ranks. Equal ranks hide that mistake.

With one adjoint Φ_a at each node, the fixed source interaction is

$$W = \operatorname{Tr}\left[s(\Phi_1^3 + \Phi_2^3) + \Phi_2 \sum_{i=1}^{2} A_iB_i + \Phi_1 \sum_{i=1}^{2} B_iA_i \right], \qquad s \neq 0. \tag{VIII.10.6}$$

The two traces in this compact notation run over their respective node spaces. Cyclic differentiation gives

$$\delta_{A_i} W = \operatorname{Tr}_{N_2}[\delta A_i (B_i\Phi_2 + \Phi_1 B_i)], \qquad \delta_{B_i} W = \operatorname{Tr}_{N_1}[\delta B_i (\Phi_2 A_i + A_i \Phi_1)]. \tag{VIII.10.7}$$

The cyclic trace has moved each variation to the left without changing its node space. Consequently the four bifundamental equations and two adjoint equations are

$$\begin{aligned} F_{\Phi_1} &= 3s\Phi_1^2 + \sum_i B_iA_i, \quad F_{\Phi_2} = 3s\Phi_2^2 + \sum_i A_iB_i, \\ F_{A_i} &= B_i\Phi_2 + \Phi_1 B_i, \qquad F_{B_i} = \Phi_2 A_i + A_i \Phi_1. \end{aligned} \tag{VIII.10.8}$$

For $N = 1$, all six chiral fields commute. Put $p = \Phi_1$, $q = \Phi_2$, and $S = A_1B_1 + A_2B_2$. The matrix superpotential becomes $W = s(p^3 + q^3) + (p + q)S$, whose six ordinary derivatives are

$$W_{N=1} = s(p^3 + q^3) + (p + q)S, \qquad S = A_1B_1 + A_2B_2. \tag{VIII.10.9}$$

The path order has disappeared, but the relative coefficient between pS and qS has not. Differentiating gives

$$F_p = 3sp^2 + S, \quad F_q = 3sq^2 + S, \qquad F_{A_i} = (p + q)B_i, \quad F_{B_i} = (p + q)A_i \quad (i = 1, 2). \tag{VIII.10.10}$$

These equations make the geometric branch nearly visible. Let $u = p + q$. If at least one bifundamental is nonzero, the last four equations force $u = 0$. The two adjoint equations then coincide:

$$p = -q, \qquad 3sp^2 + S = 3sq^2 + S, \qquad 3sq^2 + S = 0. \tag{VIII.10.11}$$

Setting $\phi = q = -p$ leaves one equation in five variables. If instead all bifundamentals vanish, the first two equations force $p = q = 0$ as a point. This point lies in the closure of the open branch: the equation $3s\phi^2 + S = 0$ is homogeneous, and a nonzero point on it approaches the origin under common scaling. There is therefore one reduced point-set component, with ring

$$R_1^{\mathrm{geom}} = \frac{\mathbb{C}[\phi, A_1, A_2, B_1, B_2]}{(3s\phi^2 + A_1B_1 + A_2B_2)}. \tag{VIII.10.12}$$

Both cubic terms in (VIII.10.6) matter here. They fix the two adjoint equations that leave one ϕ direction. As a coefficient test, replace the cross coupling by $(p+\lambda q)S$ while retaining the cubics. Its relevant F equations are

$$3sp^2+S=0, \qquad 3sq^2+\lambda S=0, \qquad (p+\lambda q)A_i=(p+\lambda q)B_i=0. \tag{VIII.10.13}$$

On a branch with a nonzero bifundamental, $p=-\lambda q$, $S=-3s\lambda^2q^2$, and $\lambda S=-3sq^2$. Hence

$$3s(1-\lambda^3)q^2=0. \tag{VIII.10.14}$$

At $\lambda=1$ this is the fourfold above. At $\lambda=2$ it forces $p=q=0$ and $S=0$, leaving

$$R^{\mathrm{geom}}_{\lambda=2}=\mathbb{C}[A_1,A_2,B_1,B_2]/(A_1B_1+A_2B_2), \qquad \dim_{\mathbb{C}} R^{\mathrm{geom}}_{\lambda=2}=3. \tag{VIII.10.15}$$

The dimension change shows why the displayed coefficients are part of the construction rather than decoration. It also warns against inferring the fourfold from the quiver diagram alone.

Choose one square root of $3s$ and set

$$\begin{gathered} z_0=\sqrt{3s}\,\phi, \qquad (z_1,z_2)=\tfrac{1}{2}(A_1+B_1,\ i(A_1-B_1)),\\ (z_3,z_4)=\tfrac{1}{2}(A_2+B_2,\ i(A_2-B_2)). \end{gathered} \tag{VIII.10.16}$$

Since $z_1^2+z_2^2=A_1B_1$ and $z_3^2+z_4^2=A_2B_2$, equation (VIII.10.12) is precisely (VIII.10.1). This rescaling is a complex algebraic change of coordinates; it does not set a kinetic normalization. The nondegenerate quadratic equation is irreducible, so its hypersurface has complex dimension four. Its five partial derivatives vanish simultaneously only at the origin.

The inverse map makes clear that no coordinates were discarded:

$$A_1=z_1-iz_2, \quad B_1=z_1+iz_2, \qquad A_2=z_3-iz_4, \quad B_2=z_3+iz_4, \qquad \phi=z_0/\sqrt{3s}. \tag{VIII.10.17}$$

For $s\neq 0$ this is an invertible linear map. The Jacobian ideal of the transformed relation is (z_0,z_1,z_2,z_3,z_4), so the apex is the only singular point of the reduced covering cone.

The link has a simple topological description. Write $z=x+iy$ and intersect X_2 with $\sum_a |z_a|^2=1$. Taking real and imaginary parts gives

$$x\cdot x-y\cdot y=0, \qquad x\cdot y=0, \qquad |x|^2+|y|^2=1. \tag{VIII.10.18}$$

Thus $|x|=|y|=1/\sqrt{2}$, and $\sqrt{2}x$ and $\sqrt{2}y$ form an oriented orthonormal two-frame in $\mathbb{R}^5$. The link is $V_{5,2}=SO(5)/SO(3)$ as a manifold. The homogeneous Sasaki–Einstein metric used in the proposed M-theory background is an additional sourced geometric premise. The radial drawing in Figure VIII.10.2 and the ambient Euclidean metric do not derive it.

The calculation gives a precise local target for the quiver: its reduced branch has the same affine coordinate ring as the cone over this link. It uses neither a perfect-matching parametrization nor a toric diagram. Those tools are the subject of Chapters 7–9 and answer a different construction question. Here the superpotential fixes the quadratic relation directly. The $\lambda=2$ example shows how sensitive that relation is to the specified

interaction, while the next section shows why the same polynomial branch can still carry different compact quotients.

There is a limited many-brane check in the source construction. For equal ranks, choose a gauge in which every chiral matrix is diagonal and write its entries with a label $\alpha = 1, \ldots, N$:

$$(\Phi_1)_{\alpha\beta} = -\delta_{\alpha\beta}\phi_\alpha, \quad (\Phi_2)_{\alpha\beta} = \delta_{\alpha\beta}\phi_\alpha, \quad (A_i)_{\alpha\beta} = \delta_{\alpha\beta}a_{i\alpha}, \quad (B_i)_{\alpha\beta} = \delta_{\alpha\beta}b_{i\alpha}. \tag{VIII.10.19}$$

All products in the matrix F equations then stay diagonal. The αth diagonal entries obey their own copy of the one-brane relation:

$$3s\phi_\alpha^2 + a_{1\alpha}b_{1\alpha} + a_{2\alpha}b_{2\alpha} = 0 \qquad (\alpha = 1, \ldots, N). \tag{VIII.10.20}$$

The residual Weyl permutations exchange these copies. Including the corresponding compact abelian quotient on this separated diagonal locus gives the source's classical $\mathrm{Sym}^N(X_2/\mathbb{Z}_k)$ description. This is a locus produced by an ansatz, not a classification of all nonabelian vacua. At coincident eigenvalues, off-diagonal fields and quantum effects require separate analysis. The diagonal calculation is useful because it shows how the single-brane relation persists in one controlled sector without silently extending the one-brane proof to the complete rank-N theory.

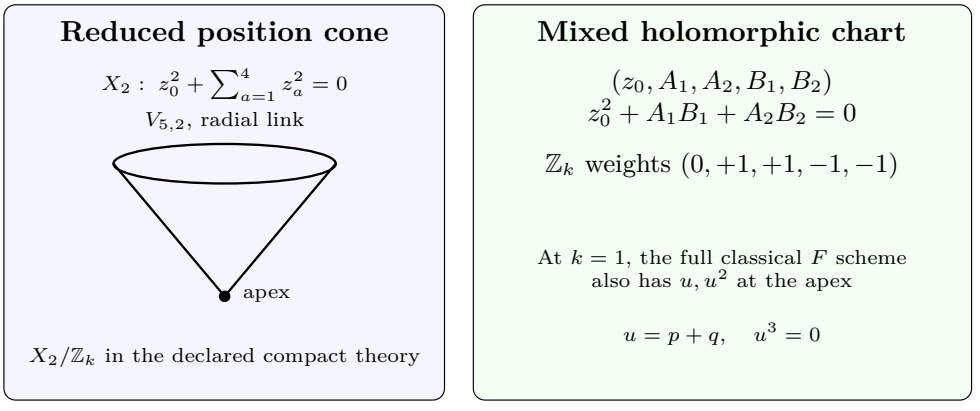


Figure VIII.10.2: A schematic radial slice of the reduced quadric and its separate mixed holomorphic chart. The five mixed coordinates carry the displayed $\mathbb{Z}_k$ weights; the sum-of-squares coordinates $z_1, \ldots, z_4$ mix under this action and do not carry those diagonal weights. At $k = 1$ the geometric quotient is trivial, while the fixed classical F-term scheme has origin-supported nilpotents. The opening toward large radius is schematic and does not determine the Sasaki–Einstein metric.

VIII.10.3 Why the compact gauge fields leave a finite quotient

A real moment-map equation must be handled before interpreting the complex branch as a vacuum space. Let $\mu = \sum_i |A_i|^2 - \sum_i |B_i|^2$. In the source-compatible sign convention, the abelian auxiliary terms are

$$\mu = |A_1|^2 + |A_2|^2 - |B_1|^2 - |B_2|^2, \qquad (\mu_1, \mu_2) = (-\mu, +\mu). \tag{VIII.10.21}$$

The adjoints have zero charge. With levels $(+k, -k)$, the relevant auxiliary Lagrangian is

$$L_D = \frac{k}{2\pi}(D_1\sigma_1 - D_2\sigma_2) + (D_2 - D_1)\mu. \tag{VIII.10.22}$$

Variation of D_1 and D_2 gives two equations rather than a single moment-map constraint:

$$\frac{\partial L_D}{\partial D_1} = \frac{k\sigma_1}{2\pi} - \mu = 0, \qquad \frac{\partial L_D}{\partial D_2} = -\frac{k\sigma_2}{2\pi} + \mu = 0. \tag{VIII.10.23}$$

In particular $\sigma_1 = \sigma_2 = \sigma$ and

$$\mu = \frac{k\sigma}{2\pi}. \tag{VIII.10.24}$$

The matter mass term $|\sigma_1 - \sigma_2|^2 \sum_i (|A_i|^2 + |B_i|^2)$ vanishes on this solution. Equation (VIII.10.24) solves for σ; it does not impose $\mu = 0$ and remove a complex coordinate. For instance $A_1 = 1$ with all other chirals zero has

$$\mu = 1, \qquad \sigma_1 = \sigma_2 = \frac{2\pi}{k}, \qquad \frac{\partial L_D}{\partial D_1} = \frac{\partial L_D}{\partial D_2} = 0. \tag{VIII.10.25}$$

At $A = B = 0$, $\mu = 0$ forces both σ_a to vanish, so this locus supplies no free real-scalar plane. Setting $\mu = 0$ at the outset would instead impose a false real constraint on the complex branch.

The diagonal compact connection acts trivially on matter but remains in the Chern–Simons term. Set $b = a_1 - a_2$ and $c = a_2$. The inverse integral change of basis is

$$\begin{pmatrix} a_1 \\ a_2 \end{pmatrix} = \begin{pmatrix} 1 & 1 \\ 0 & 1 \end{pmatrix} \begin{pmatrix} b \\ c \end{pmatrix}, \qquad \det \begin{pmatrix} 1 & 1 \\ 0 & 1 \end{pmatrix} = 1. \tag{VIII.10.26}$$

It preserves the primitive flux lattice. Substituting $a_1 = b + c$ and $a_2 = c$ into the diagonal Chern–Simons form gives, up to a total derivative,

$$S_{\mathrm{CS}} = \frac{k}{4\pi} \int b\, db + \frac{k}{2\pi} \int b\, dc, \qquad K_{bc} = \begin{pmatrix} k & k \\ k & 0 \end{pmatrix}. \tag{VIII.10.27}$$

The curvature $f = dc$ is primitive because both original fluxes have period 2π. Dualize f with a scalar $\tau \sim \tau + 2\pi$ by adding $(2\pi)^{-1} \int \tau\, df$. The terms containing f are

$$\frac{1}{2\pi} \int (kb - d\tau) \wedge f, \qquad kb = d\tau. \tag{VIII.10.28}$$

The second equation follows by varying f. Under $b \mapsto b - d\lambda$, consistency requires $\tau \mapsto \tau - k\lambda$. After fixing $\tau = 0$, the periodicity of τ allows precisely

$$\lambda = \frac{2\pi j}{k} \pmod{2\pi}, \qquad j = 0, \ldots, k-1. \tag{VIII.10.29}$$

Thus the quotient of complex vacuum coordinates is finite, $\mathbb{Z}_k$, rather than a continuous $\mathbb{C}^*$ quotient. The uncharged c field was essential to this conclusion.

Using the inverse generator to orient baryonic charge as in the source, the action in the mixed chart is

$$(z_0, A_1, A_2, B_1, B_2) \longmapsto (z_0, \omega A_1, \omega A_2, \omega^{-1} B_1, \omega^{-1} B_2), \qquad \omega = e^{2\pi i/k}. \tag{VIII.10.30}$$

The weights $(0, 1, 1, -1, -1)$ belong to this chart. Equation (VIII.10.16) combines A_i and B_i, so the same action is not diagonal with those weights on the sum-of-squares coordinates. The coordinate ring of the reduced geometric vacuum branch is

$$R_k^{\mathrm{geom}} = \left[\mathbb{C}[z_0, A_1, A_2, B_1, B_2]/(z_0^2 + A_1 B_1 + A_2 B_2)\right]^{\mathbb{Z}_k}. \tag{VIII.10.31}$$

A monomial survives when its total A exponent minus its total B exponent is divisible by k. At $k = 1$ the action is trivial and the five-coordinate quadric remains. For any k, a nonidentity element could fix a point only if every A_i and B_i vanished; the quadric then forces $z_0 = 0$. The group acts freely away from the apex, and the finite quotient retains complex dimension four. These statements use the declared full compact product and flux lattice. Different compact global forms or line sectors require their own analysis.

For a monomial $z_0^r A_1^{a_1} A_2^{a_2} B_1^{b_1} B_2^{b_2}$, the selection rule is

$$a_1 + a_2 - b_1 - b_2 \equiv 0 \pmod{k}. \tag{VIII.10.32}$$

At $k = 2$, A_1 fails this rule while $A_1 B_1$ and $A_1 A_2$ satisfy it. This concrete difference is what the Hilbert series in the next section must detect. A finite invariant subring has the same Krull dimension as the covering ring, so the four complex position directions survive even though their elementary coordinate names change.

The distinction between a real equation and a complex quotient is the same one encountered for ABJM in Chapter 3. If one were to impose $\mu = 0$ and then divide by the relative $\mathbb{C}^*$, the result would lose one complex dimension. The compact BF coupling instead turns the relative gauge action into the finite residual group. At $k = 1$ the group is the identity, yet the gauge fields have still done work: they have determined why the entire complex quadric survives. At $k = 2$ the quotient changes the available holomorphic coordinates, which will be visible already in degree one. The cone/ring drawing in Figure VIII.10.2 places the mixed weights beside the reduced geometry; neither that drawing nor an arbitrary choice of quotient weights can replace the primitive flux calculation.

VIII.10.4 Counting functions, and what they count

Grade each of the five geometric coordinates in (VIII.10.31) by one. This is polynomial degree in the fixed complex coordinates, not a claimed infrared R-charge. Let $P_5 =$

$\mathbb{C}[z_0, A_1, A_2, B_1, B_2]$ and $f = z_0^2 + A_1B_1 + A_2B_2$. Since P_5 is a domain and $f \neq 0$, multiplication by f is injective. Its graded exact sequence is

$$0 \longrightarrow P_5(-2) \xrightarrow{\times f} P_5 \longrightarrow R_1^{\mathrm{geom}} \longrightarrow 0. \tag{VIII.10.33}$$

The shift by two records the degree of f. Subtracting the Hilbert series of the first term from that of the middle term gives

$$H_{X_2}(t) = \frac{1-t^2}{(1-t)^5} = \frac{1+t}{(1-t)^4} = 1 + 5t + 14t^2 + 30t^3 + 55t^4 + \cdots . \tag{VIII.10.34}$$

Its pole has order four, as the coordinate-ring dimension requires. The first two coefficients can be checked without a generating function. There are five linear monomials and $\binom{6}{2} = 15$ quadratic monomials in five variables. The one independent degree-two relation removes one:

$$\dim(R_1^{\mathrm{geom}})_1 = 5, \qquad \dim(R_1^{\mathrm{geom}})_2 = \binom{6}{2} - 1 = 14. \tag{VIII.10.35}$$

This counts regular functions on the reduced cone. It has not counted monopole operators or the thickening studied below.

The finite action admits an equally explicit count. A group average projects each graded polynomial space onto its charge-zero part. The five coordinates have weights $(0, 1, 1, -1, -1)$, so the polynomial character at the jth group element is

$$\mathrm{Tr}_{P_5}(\omega^j; t) = \frac{1}{(1-t)(1-\omega^j t)^2(1-\omega^{-j}t)^2}. \tag{VIII.10.36}$$

The relation f is invariant and regular. Finite-group invariants are exact over $\mathbb{C}$, so the invariant exact sequence is obtained from (VIII.10.33). Averaging the character and multiplying by $1 - t^2$ gives

$$H_k^{\mathrm{geom}}(t) = \frac{1-t^2}{k} \sum_{j=0}^{k-1} \frac{1}{(1-t)(1-\omega^j t)^2(1-\omega^{-j}t)^2}. \tag{VIII.10.37}$$

The $k = 1$ term reproduces (VIII.10.34). For $k = 2$, the four bifundamentals change sign together. The polynomial invariants before imposing f are an arbitrary power of z_0 times an even polynomial in $x = (A_1, A_2, B_1, B_2)$. Thus

$$H_{P_5^{\mathbb{Z}_2}}(t) = \frac{1}{1-t} \sum_{m \geq 0} \binom{2m+3}{3} t^{2m}, \qquad H_2^{\mathrm{geom}}(t) = (1-t^2) H_{P_5^{\mathbb{Z}_2}}(t). \tag{VIII.10.38}$$

In degree one only z_0 survives. In degree two there are ten products $x_i x_j$ and z_0^2; the relation removes one. The result is

$$\dim(R_2^{\mathrm{geom}})_1 = 1, \qquad \dim(R_2^{\mathrm{geom}})_2 = (10+1) - 1 = 10,$$
$$H_2^{\mathrm{geom}}(t) = 1 + t + 10t^2 + 10t^3 + 35t^4 + \cdots . \tag{VIII.10.39}$$

The drop from five degree-one functions to one is a direct test that the finite quotient has been included. For degree four, the same sequence gives $(35+10+1)-(10+1)=35$, an independent check of the displayed coefficient.

The $k=2$ ring can also be seen without averaging. Set $Q_{ij}=x_ix_j=Q_{ji}$. All even monomials in x factor into these ten quadratics. Their symmetric 4×4 matrix has rank at most one. Every two by two minor therefore vanishes:

$$Q_{ij}Q_{\ell m}-Q_{i\ell}Q_{jm}=0 \quad \text{for all choices of indices for which these are minors.} \tag{VIII.10.40}$$

The invariant hypersurface equation gives the additional relation

$$z_0^2+Q_{13}+Q_{24}=0, \qquad Q_{11}Q_{33}-Q_{13}^2=0 \quad \text{as one representative minor.} \tag{VIII.10.41}$$

The full presentation uses all these minors, not merely the example displayed. To see that they generate the kernel, a monomial in the Q_{ij} encodes a pairing of a multiset of x indices. Any two pairings of the same multiset are connected by exchanges $Q_{ab}Q_{cd}=Q_{ac}Q_{bd}$, each a symmetric-matrix minor. Grouping polynomial terms by their image x-monomial therefore expresses every kernel element in the minor ideal. In degree two, ten Q_{ij} together with z_0^2 and one linear relation among them leave ten independent functions. Finite-group invariants preserve the exact quotient by the invariant quadric, which justifies this presentation. The Q_{ij} have degree two and z_0 degree one, so this is a weighted presentation of the same graded ring.

The degree-three coefficient can be counted in the same presentation. Before the quadric relation, the invariant monomials are z_0^3 and the ten products z_0Q_{ij}. Multiplying the degree-two relation by z_0 removes one linear combination. This leaves ten degree-three functions, in agreement with (VIII.10.39). The minors first constrain products of two Q's, in degree four. They do not change the preceding degree-two count. This ordering helps distinguish the hypersurface relation from the rank-one relations: both are needed for the ring, but they first appear at different degrees.

The selection rule also describes a generating set at general k. A monomial containing both A and B variables can be divided by some A_iB_j until only one sign of baryonic charge remains. The remaining charge is a multiple of k, so its variables can be grouped into blocks of k. Thus the invariant ring is generated by z_0, the four mesons and two families of pure-charge monomials:

$$M_{ij}=A_iB_j, \qquad U_r=A_1^{k-r}A_2^r, \qquad V_r=B_1^{k-r}B_2^r, \qquad 0\le r\le k. \tag{VIII.10.42}$$

This is a generating set, not a claim that the displayed symbols are algebraically independent. The geometric relation becomes $z_0^2+M_{11}+M_{22}=0$, and the mesons obey the rank-one relation $M_{11}M_{22}=M_{12}M_{21}$. Further relations involving the pure-charge generators depend on k.

$$z_0^2+M_{11}+M_{22}=0, \qquad M_{11}M_{22}-M_{12}M_{21}=0. \tag{VIII.10.43}$$

For $k\ge 3$, none of the pure-charge generators appears by degree two. There is one invariant in degree one and five polynomial invariants in degree two, namely z_0^2 and the four M_{ij}. The single quadratic equation leaves

$$\dim(R_k^{\mathrm{geom}})_1=1, \qquad \dim(R_k^{\mathrm{geom}})_2=5-1=4 \quad (k\ge 3). \tag{VIII.10.44}$$

The exceptional degree-two count at $k = 2$ comes from the additional pure-charge quadratics. The equality of all $k \geq 3$ counts through degree two does not make their higher-degree rings equal: the first pure-charge generators enter at degree k.

Hilbert series alone does not identify a singularity. Remove A_2B_2 from the five-variable relation while keeping all five variables. The altered equation $f' = z_0^2 + A_1B_1$ is still a regular quadratic polynomial, so it has exactly (VIII.10.34). Its Jacobian comparison is decisive:

$$\begin{aligned} &\mathrm{Jac}(f) = (2z_0, B_1, B_2, A_1, A_2), \quad &&\mathrm{Sing}(f) = \{0\}, \\ &\mathrm{Jac}(f') = (2z_0, B_1, 0, A_1, 0), &&\mathrm{Sing}(f') = \{z_0 = A_1 = B_1 = 0\} \simeq \mathbb{C}^2. \end{aligned} \tag{VIII.10.45}$$

The two free coordinates A_2, B_2 make the altered singular locus two-dimensional. The fixed nondegenerate quadric has only its isolated apex. A geometric check therefore needs the relation and its singular locus in addition to a coarse series. This also shows why the ring presentation is part of the answer to the position-space test, beyond a matching sequence of coefficients.

Chapter 12 will use a geometric volume comparison at large N, which probes a different feature of a proposed membrane dual. The unrefined polynomial Hilbert series here does not determine that volume, and its equality for f and f' does not make the two cones interchangeable. The altered Jacobian provides a particularly sharp warning: even the dimension and the full list of graded coefficients can agree while the singular set changes.

VIII.10.5 The thickened apex and the quantum question

Return to the fixed nonzero-cubic $k = 1$ action before taking a reduced point set. Work in $P = \mathbb{C}[p, q, A_1, A_2, B_1, B_2]$ and let I be the ideal of all six equations (VIII.10.10). A point-valued solution sends every nilpotent polynomial to zero. A ring can still retain such polynomials, so the ideal itself must be compared with the reduced branch ideal. Define

$$\begin{aligned} &J = (p + q,\ 3sq^2 + S), \\ &Q = (A_1, A_2, B_1, B_2, p^2, q^2). \end{aligned} \qquad I = J \cap Q, \quad \sqrt{I} = J. \tag{VIII.10.46}$$

Here J is the reduced quadric component. The second ideal has support only at the origin. To see the thickening directly, set $u = p + q$. The four bifundamental equations and the difference of the two adjoint equations yield, modulo I,

$$uA_i = uB_i = 0, \qquad p^2 - q^2 = u(p - q) = 0, \qquad q^2 = -S/(3s). \tag{VIII.10.47}$$

Since $uS = 0$, the last relation gives $uq^2 = 0$. Also $u(p - q) = 0$ implies $up = uq$, and therefore

$$u^2 = u(p + q) = 2uq, \qquad u^3 = 2u^2q = 4uq^2 = 0. \tag{VIII.10.48}$$

Yet u and u^2 survive. Their images in $P/Q = \mathbb{C}[p,q]/(p^2,q^2)$ are $p+q$ and $2pq$, both nonzero. They vanish in P/J. Since $J = (u, F_q)$ and $F_q \in I$, the kernel of $P/I \to P/J$ is generated by u. Every multiple of u reduces to a linear combination of u and u^2 by (VIII.10.47)–(VIII.10.48). Their independent images in P/Q show that this kernel meets Q/I trivially. Thus $I = J \cap Q$: the intersection has exactly the same image in the reduced branch and the origin-supported quotient as I. Taking radicals gives $\sqrt{I} = J$, because the support of Q is the origin already contained in the quadric.

The intersection exact sequence makes the count transparent:

$$0 \longrightarrow P/I \longrightarrow P/J \oplus P/Q \longrightarrow P/(J+Q) \longrightarrow 0. \tag{VIII.10.49}$$

Here P/Q has basis $1, p, q, pq$, whereas $P/(J+Q) \simeq \mathbb{C}[q]/(q^2)$ has basis $1, q$. Their series are $(1+t)^2$ and $1+t$. Subtracting the overlap gives

$$H_{P/I}(t) = H_{P/J}(t) + (1+t)^2 - (1+t) = H_{X_2}(t) + t + t^2. \tag{VIII.10.50}$$

In particular, the fixed classical F-term scheme has six degree-one classes and fifteen degree-two classes, whereas the reduced position cone has five and fourteen:

$$H_{P/I}(t) = 1 + 6t + 15t^2 + 30t^3 + \cdots, \qquad H_{R_1^{\mathrm{geom}}}(t) = 1 + 5t + 14t^2 + 30t^3 + \cdots. \tag{VIII.10.51}$$

The two extra classes are represented by u and u^2, in degrees one and two. Since $u^3 = 0$, they do not represent a second family of point-valued vacua. They are nilpotent functions supported at the existing apex.

A gauge-invariant quantum chiral ring is a further object. The source analysis of this model finds an analogous $t+t^2$ correction for its $k=1$ total abelian operator count, using dressed monopoles, their charges and operator-product relations. Our polynomial ideal proof neither derives those operator relations nor decides the infrared fate of the nilpotents. In particular, a modified superpotential in that analysis drops a cubic in $p+q$ and changes the extra component; it is not the fixed interaction (VIII.10.6). The distinction can be read directly from the maps

$$P/I \longrightarrow P/J = R_1^{\mathrm{geom}}, \qquad \ker(P/I \to P/J) = \langle u, u^2 \rangle_{\mathbb{C}}. \tag{VIII.10.52}$$

The target describes reduced positions. The source is the fixed classical F scheme. A quantum operator ring requires its own monopole and operator-product premises; equality of two short series does not provide them.

Chapter 8 already makes monopole operators indispensable in a flavored toric example. The present calculation does not import that chapter's operator relations into this different theory. It only identifies the precise classical ambiguity that a quantum analysis would have to resolve. The correction is concentrated at the apex: away from $A_i = B_i = 0$, one bifundamental becomes invertible locally, its F equation sets $u = 0$, and the thickening disappears. At the origin, every complex point still evaluates u and u^2 to zero. This explains how the function count can change without adding a geometric branch or changing the dimension of the cone.

VIII.10.6 Geometry and the edge of the method

Why is this example more than a complicated way to write a quadric? A toric complex fourfold would admit an effective four-dimensional algebraic torus with a dense orbit. The quadric X_2 cannot. Its unique singular apex forces every algebraic torus action to fix that point, where the tangent representation must preserve the nondegenerate quadratic initial relation up to scale. The following rank count makes the obstruction visible. It concerns algebraic torus actions, not the cone metric.

To see the rank without relying on the name of the group, make a complex linear change of variables that writes the same nondegenerate quadratic form as

$$F = w_0^2 + u_1 v_1 + u_2 v_2. \tag{VIII.10.53}$$

A diagonal torus preserving F up to an overall factor acts with one common scale c and two reciprocal ratios t_1, t_2:

$$(w_0, u_1, v_1, u_2, v_2) \mapsto (cw_0, ct_1 u_1, ct_1^{-1} v_1, ct_2 u_2, ct_2^{-1} v_2). \tag{VIII.10.54}$$

The square of c is the similitude factor. Every algebraic torus in the orthogonal similitude group lies in a maximal torus, and this one already has three independent parameters. The apex is fixed because it is the unique singular point. If an element acted identically on its tangent space, torus semisimplicity would make it act identically on every graded piece of the completed local ring, and then on the affine ring itself. Thus the tangent-rank bound also bounds a faithful torus action on the whole cone.

$$\operatorname{gr}_{\mathfrak{m}} \mathbb{C}[X_2] \simeq \mathbb{C}[z_0, \dots, z_4]/(F). \tag{VIII.10.55}$$

Because the relation is homogeneous, the tangent generators determine this associated graded ring. A torus element trivial on the generators is trivial on every graded piece; its semisimple action cannot acquire a hidden unipotent term in the completion.

$$T \hookrightarrow \operatorname{Aut}(\mathfrak{m}/\mathfrak{m}^2, [F]) \subseteq GO(5, \mathbb{C}), \qquad \mathfrak{m} = (z_0, \dots, z_4). \tag{VIII.10.56}$$

Here $[F]$ is the quadratic initial relation. The injection is the step that turns a bound on linear transformations into a statement about the affine fourfold.

The rank obstruction can be made concrete. A maximal diagonal torus preserving a nondegenerate quadratic form on five coordinates has two independent reciprocal pairs of eigenvalues and one common scale. Hence

$$\operatorname{rank} GO(5, \mathbb{C}) = 2 + 1 = 3 < \dim_{\mathbb{C}} X_2 = 4. \tag{VIII.10.57}$$

This excludes the dense four-torus required by a toric fourfold. It does not exclude a lower-rank torus action or a useful brane description.

The source construction proposes an M2-brane theory for this $V_{5,2}/\mathbb{Z}_k$ geometry. Its homogeneous Sasaki–Einstein metric and cone description supply the geometric background premise. Its type IIA discussion reduces along an M-circle to D2 and fractional D4 data with RR F_2 inducing the Chern–Simons levels; its type IIB discussion uses a related T-dual suspended-D3 and curved-fivebrane picture. These constructions

explain why the quiver is a physically motivated candidate. They share parent and lift assumptions, and the one-brane calculation here tests the local positions only. Establishing an exact infrared QFT duality would additionally require the decoupling, quantum and global data that this calculation has not supplied.

The contrast with crystal models is instructive. Chapters 7–9 develop the toric fourfold construction and its deformations. The original M-theory crystal proposal starts from toric Calabi–Yau fourfold information and seeks a crystal description through special Lagrangian data. Its inverse step was incomplete even within that toric setting. Familiar toric contexts include $\mathbb{C}^4$ and cones over $Q^{1,1,1}$; the present non-toric quadric is outside the original input class. Neither the successful quiver calculation above nor a crystal diagram supplies an inverse procedure that assigns a unique theory to an arbitrary Calabi–Yau fourfold.

Chapter 12 will compare large-N free energy with a geometric volume in examples where the required hypotheses and normalizations can be controlled. That is a different test from the one-brane coordinate ring derived here: a position-space match fixes neither a large-N coefficient nor the homogeneous Sasaki–Einstein metric. Full nonabelian and quantum moduli, alternative compact global forms and line operators, and monopole operator products also remain separate tasks. The local position-space agreement is valuable precisely because its algebra and its physical premise can be stated independently.

VIII.10.7 Exercises

1. **VIII.10.E1: A coefficient that changes dimension.** At $N = 1$ and $s = 1$, take $W_\lambda = p^3+q^3+(p+\lambda q)(A_1B_1+A_2B_2)$ for $\lambda = 1, 2$. Submit all six F derivatives at each value, the reduced ideal on the branch with a nonzero bifundamental, its five-coordinate ring at $\lambda = 1$, and the corresponding ring and complex dimension at $\lambda = 2$. Explain why the origin does not identify the reduced ring with the entire chiral ring. The polynomial and dimension answers can be checked from the fixed model; the quantum interpretation requires more information.

2. **VIII.10.E2: The same series, a different cone.** In $\mathbb{C}[z_0, A_1, A_2, B_1, B_2]$ compare $q = z_0^2 + A_1B_1 + A_2B_2$ with $q' = z_0^2 + A_1B_1$. Submit both Hilbert series and pole orders, then compute each Jacobian ideal and the dimension of its singular locus. State separately the $k = 1$ source-reported total-ring correction. The geometric series and Jacobian are algebraic; relating the correction to a quantum operator ring requires the source's monopole and OPE premises.

3. **VIII.10.E3: What compactness leaves behind.** For the declared full $U(1)_k \times U(1)_{-k}$ product at $k = 1, 2$, submit the primitive (b, c) basis, its Chern–Simons matrix, the dual-scalar gauge shift, the signs in (VIII.10.22), and the residual orders. Give the mixed-chart weights, the $k = 1$ relation, and at $k = 2$ the ten Q_{ij} generators, their rank-one-minor family and one explicit minor. Submit the degree-one and degree-two geometric Hilbert coefficients for both levels. Prove the complete minor presentation by even-monomial factorization and pairing exchanges.

Take-home message of this chapter

For the fixed compact quiver and nonzero cubic coupling, its one-brane reduced vacuum coordinates form the finite quotient $X_2/\mathbb{Z}_k$ of the quadric X_2. The compact BF term is what leaves the finite quotient; the F equations give the quadric. At $k = 1$ the classical F scheme also has two nilpotent classes at the apex, so counting geometric functions is not the same as counting every classical F-term class. The proposed membrane interpretation rests on additional physical premises beyond these algebraic results.

Status and sources

Sources by section. Source coordinates and scope qualifications follow.

§VIII.10.1. The quadric target and link metric are sourced physical proposals [GEO-E], not an exact IR identification (Martelli and Sparks 2009, §§2.1 and 3.1).

§VIII.10.2. For the fixed $s \neq 0$ source action, its F equations and one-brane classical branch are conditional [MATH] (Martelli and Sparks 2009, §§2.1–2.2; arrow orientation, superpotential normalization and Chern–Simons trace and levels).

§VIII.10.3. The primitive compact quotient and residual group are conditional [MATH] under the stated full gauge product and the primitive compact flux and dual-scalar convention (Martelli and Sparks 2008, §3; Martelli and Sparks 2009, §2.2).

§VIII.10.4. The geometric Hilbert count is conditional [MATH] for the stated polynomial grading; it does not assign the exact infrared R charge (Martelli and Sparks 2009, §2.2).

§VIII.10.5. The fixed-action thickened ideal is conditional [MATH]; physical monopole operators and OPEs remain separate sourced premises (Cremonesi et al. 2016, §6.2.4).

§VIII.10.6. The rank-five quadric torus-action obstruction is [MATH] at its stated algebraic scope; the inverse-crystal question remains open (Lee et al. 2007, §§1–2.1 and 6).

§VIII.10.7. Three bounded submissions reuse the preceding conditional [MATH] algebra, (Martelli and Sparks 2009, §2.2; Cremonesi et al. 2016, §6.2.4; superpotential normalization, Chern–Simons trace and levels and Chern–Simons matter conventions). The physical interpretation and complete minor-ideal reasoning remain written tasks.

The source action, representations, levels and proposed membrane geometry are inputs from Martelli and Sparks 2009, arXiv:0909.2036v1, §2.1, Figure 1 and equations (2.2)–(2.8), physical PDF pp. 5–7; the abelian branch and quotient are in §2.2, equations (2.9)–(2.10), physical p. 8. The separate diagonal nonabelian ansatz and its classical symmetric-product locus are equation (2.11) and following discussion, physical p. 9; this is not a full nonabelian-moduli classification. The link and its homogeneous metric premise occur in §3.1, equations (3.19)–(3.25), pp. 15–16. The IIA and IIB source context is in §3.5 and §§4.1–4.2, pp. 25–34. The named M2/QFT identification is a **[GEO-E]** proposal. Neither those two related engineering descriptions nor the local

branch calculation earns a [**GEO-X**], [**DUAL**], or [**DEC**] transfer. G-006 concerns the ABJM $\mathbb{C}^4/\mathbb{Z}_k$ case only.

The opening target checks and equations (VIII.10.8)–(VIII.10.18) are conditional [**MATH**] statements for the fixed $s \neq 0$ source action. Equations (VIII.10.46)–(VIII.10.52) concern its classical F scheme. The point-set description in Martelli and Sparks 2009, §2.2, does not by itself count the nilpotents. The independently derived fixed-action classical ideal has $I = J \cap Q$ and contribution $t + t^2$. The source's distinct gauge-invariant operator treatment is Cremonesi et al. 2016, arXiv:1607.05728v1, §6.2.4, equations (6.61)–(6.73), physical pp. 69–70; its altered superpotential is equation (6.87), pp. 71–73. Monopole dressing, OPE relations and infrared identification are source premises, not consequences of the polynomial ideal.

The auxiliary-field and compact quotient method follows Martelli and Sparks 2008, arXiv:0808.0912v3, §3, equations (3.3)–(3.17), physical pp. 6–8, and (3.18)–(3.35), pp. 9–11. Equations (VIII.10.21)–(VIII.10.32) are conditional [**MATH**] for the full primitive-flux compact product. The BF algebra is reused in the restricted scope of the primitive compact flux and dual-scalar convention under the separately declared Martelli–Sparks group premise. The arrows carry fundamentals at the tail, with the superpotential and levels as stated in the source action. A different common-center quotient can alter the residual group and is outside this result. The geometric Hilbert, invariant-ring and Jacobian calculations in (VIII.10.33)–(VIII.10.45) are likewise [**MATH**], with polynomial degree rather than an asserted exact infrared R-charge.

The bounded non-toric argument in §VIII.10.6 is [**MATH**] for algebraic torus actions on the rank-five quadric. The original crystal domain and incomplete special-Lagrangian inverse step are sourced to Lee et al. 2007, arXiv:hep-th/0702120v1, §§1–2.1 and §6, physical pp. 2–4 and 22. S-051 records the open general Calabi–Yau fourfold inverse construction, nonabelian/quantum ring and crystal frontier; S-036 records the additional monopole/OPE machinery. Three bounded submitted-answer exercises test stated classical fields only; their written physical explanations and the full $k = 2$ minor ideal require separate reasoning.

References

Cremonesi, S., N. Mekareeya, and A. Zaffaroni (2016). "The moduli spaces of 3d $\mathcal{N} \geq 2$ Chern-Simons gauge theories and their Hilbert series". In: *JHEP* 10, p. 046. DOI: 10.1007/JHEP10(2016)046. arXiv: 1607.05728 [hep-th].

Lee, S., S. Lee, and J. Park (2007). "Toric AdS4/CFT3 duals and M-theory Crystals". In: *JHEP* 05, p. 004. DOI: 10.1088/1126-6708/2007/05/004. arXiv: hep-th/0702120.

Martelli, D. and J. Sparks (2008). "Moduli spaces of Chern-Simons quiver gauge theories and AdS(4)/CFT(3)". In: *Phys. Rev. D* 78, p. 126005. DOI: 10.1103/PhysRevD.78.126005. arXiv: 0808.0912 [hep-th].

Martelli, D. and J. Sparks (2009). "AdS(4)/CFT(3) duals from M2-branes at hypersurface singularities and their deformations". In: *JHEP* 12, p. 017. DOI: 10.1088/1126-6708/2009/12/017. arXiv: 0909.2036 [hep-th].

Chapter VIII.11

Localization and the physical R charge

The ABJM construction supplies a Lagrangian description of membranes on a cone. Its scalar moduli space records possible positions, but it does not by itself determine a sphere partition function. On a supersymmetric sphere the functional integral reduces, under a specified localization prescription, to an integral over constant Cartan scalars. This integral retains information about the interacting theory that is invisible in the classical vacuum variety. It also supplies a way to test a trial R symmetry.

The question throughout this chapter is concrete. For the full compact $U(N)_k \times U(N)_{-k}$ theory with equal ranks and positive integer k, what normalization and which R-charge combinations are measured by the sphere integral? At rank one we obtain $Z_{1,k} = 1/(4k)$ with a stated oscillatory prescription. At large N, a sourced trial function has an interior maximum at four physical charges equal to $1/2$. The coefficient of that function is derived from an eigenvalue saddle in Chapter 12. Here we determine its charge dependence and explain why one direction in the bare assignment is redundant. We then change the sphere shape together with its supersymmetric background fields and follow the leading free energy.

Unless a section says otherwise, real flavor masses, physical FI sources and the flat-space GRVV mass vanish. We use $F = -\log|Z|$; a source-dependent phase is removed by the modulus. Localization, the relevant integration cycle and physical selection of a large-N saddle are inputs from the cited constructions. Our calculations test their normalized consequences.

VIII.11.1 A supersymmetric deformation of the sphere integral

Why can a field theory on a curved 3D space become a finite integral? Let Φ stand for fields, $S[\Phi]$ for the even Euclidean action, and Q for an odd supersymmetry of that action. Choose an odd functional V so that $Q^2V = 0$. The parameter $t \geq 0$ multiplies

a Q-exact term,

$$Z(t) = \int_{\mathcal{C}} D\Phi\, e^{-S-tQV}, \qquad QS = 0, \qquad Q^2 V = 0. \tag{VIII.11.1}$$

Here $\mathcal{C}$ is the integration cycle, which includes any contour prescription for bosonic zero modes. The measure and the cycle must be Q invariant. These are physical premises, rather than consequences of writing Q in an equation.

Differentiating the integral exposes exactly where the invariance is used. Since V is odd, the graded product rule gives

$$Q\big(Ve^{-S-tQV}\big) = (QV + VQS)e^{-S-tQV}, \tag{VIII.11.2}$$

$$\frac{dZ}{dt} = -\int_{\mathcal{C}} D\Phi\, Q\big(Ve^{-S-tQV}\big) + \int_{\mathcal{C}} D\Phi\, V(QS)e^{-S-tQV}. \tag{VIII.11.3}$$

The second term vanishes by $QS = 0$. The first vanishes when integration of a Q variation produces no boundary or anomaly term and differentiation under the integral is valid. Thus $dZ/dt = 0$ under these hypotheses. If $QS \neq 0$, the displayed second term remains. If the cycle has a boundary contribution, the first term remains. These two failures have distinct origins and cannot be repaired by taking t large. For example, if the action varies as $QS = \eta\mathcal{O}$ for a fixed insertion $\mathcal{O}$ and a formal parameter η, even a closed cycle leaves

$$\frac{dZ}{dt} = \eta \int_{\mathcal{C}} D\Phi\, V\mathcal{O}\, e^{-S-tQV}. \tag{VIII.11.4}$$

The right-hand side need not vanish. This shows why the invariance of the original action is a separate input to the deformation argument.

At large t, a suitable positive bosonic part of QV suppresses field configurations away from its zero locus. For the chosen round-sphere supersymmetry, the sourced localization construction leaves constant real Cartan variables and their one-loop fluctuations. One can view the calculation as the sequence in Figure VIII.11.1. The Q-exact parameter changes the computational representation of the same observable. Changing a physical coupling, a real mass, or the supersymmetric background need not leave it invariant. In particular, the choice of Q here does not assign a Wilson-line BPS fraction to the partition function. A line projector is an extra operator condition. Chapter 3 introduced protected local operators; the sphere integral uses the same idea of a selected supercharge for a different observable.

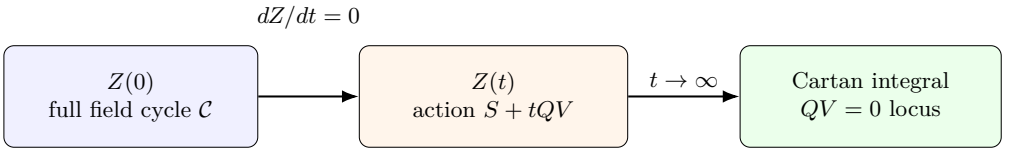


Figure VIII.11.1: The Ward step preserves the sphere integral only under its stated measure and cycle hypotheses. The large-t step uses the sourced localization locus and fluctuation determinants. The arrows do not represent an RG flow or a change of physical mass.

VIII.11.2 The determinant fixes an absolute normalization

How do the surviving Cartan variables acquire a measure? Write the physical real scalar in a vector multiplet as σ, and let $\widehat{\sigma} = r\sigma$ on a round sphere of radius r. It is $\widehat{\sigma}$, not σ, that enters the dimensionless one-loop functions. The DMP matrix variable used below is

$$\lambda = 2\pi\widehat{\sigma}, \qquad \frac{d\lambda}{2\pi} = d\widehat{\sigma}, \qquad e^{ik\lambda^2/(4\pi)} = e^{i\pi k\widehat{\sigma}^2}. \tag{VIII.11.5}$$

The last equality is for one $U(1)_k$ Cartan direction. It makes the source-to-book conversion of both phase and measure visible. A convention that conjugates the Chern–Simons phase yields the same positive rank-one answer with the regulator used in the next section.

For a chiral multiplet with trial R charge Δ and gauge weight ρ, the sourced round-sphere determinant is

$$Z_{\text{chiral}}(\Delta, \rho) = \exp[\ell(1 - \Delta + i\rho(\widehat{\sigma}))]\,, \qquad \ell'(z) = -\pi z\cot(\pi z), \qquad \ell(1/2) = -\frac{1}{2}\log 2. \tag{VIII.11.6}$$

The final value is the zeta-normalized integration constant. A derivative of $\log Z_{\text{chiral}}$ determines its dependence on the Cartan scalar, but cannot determine Z at zero. The absolute sphere free energy needs that constant. For one ungauged charge-1/2 chiral at zero mass, $Z = 2^{-1/2}$, so $F = (\log 2)/2$.

The simplest weight calculation uses two chirals of opposite weights $+1$ and -1, each at $\Delta = 1/2$. Put $g(x) = \ell(1/2 + ix) + \ell(1/2 - ix)$. The identity $\cot(\pi/2 + iy) = -i\tanh(\pi y)$ gives

$$g'(x) = i\ell'(1/2 + ix) - i\ell'(1/2 - ix) = -\pi\tanh(\pi x), \tag{VIII.11.7}$$

$$g(0) = 2\ell(1/2) = -\log 2, \qquad e^{g(x)} = \frac{1}{2\cosh(\pi x)}. \tag{VIII.11.8}$$

For the ABJM bifundamental weight $x = x_i - y_j$ there are two such opposite-weight pairs. Their combined factor is $[2\cosh\pi(x_i - y_j)]^{-2}$. At $x = 0$ it is $1/4$, rather than 1. This one number will survive every other simplification of the rank-one integral. Figure VIII.11.2 shows the distinction between one pair and the two-pair ABJM factor.

The full compact equal-rank model has Cartan variables $\mu_i = 2\pi x_i$ and $\nu_i = 2\pi y_i$. Its sourced round prescription, with vanishing real masses and FI sources, reads

$$Z^{\rm loc}_{N,k} = \frac{1}{(N!)^2}\int_{\mathbb{R}^{2N}} \prod_{i=1}^{N} \frac{d\mu_i}{2\pi}\frac{d\nu_i}{2\pi} \exp\left[\frac{ik}{4\pi}\sum_i(\mu_i^2 - \nu_i^2)\right] \times \frac{\prod_{i<j}[2\sinh((\mu_i-\mu_j)/2)]^2[2\sinh((\nu_i-\nu_j)/2)]^2}{\prod_{i,j}[2\cosh((\mu_i-\nu_j)/2)]^2}. \tag{VIII.11.9}$$

The two factorials divide by the two Weyl permutation groups. The numerator comes from roots of the two vector multiplets. The denominator comes from their bifundamental weights and the two opposite pairs just calculated. A root product or a Weyl divisor must be changed when the gauge group changes. This is one reason the full $U(N) \times U(N)$ model is kept explicit rather than silently replaced by an SU quotient.

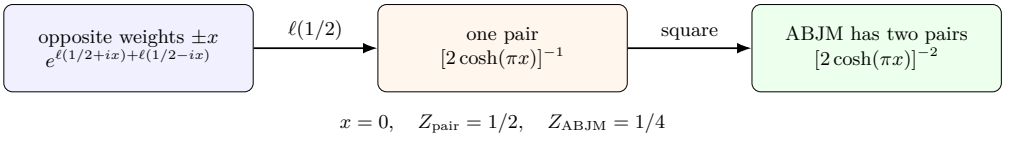


Figure VIII.11.2: The zero-weight value fixes the constant lost by integrating ℓ'. A single opposite-weight pair gives $1/2$ at $x = 0$, and the two ABJM pairs give $1/4$. The diagram concerns the matter determinant only; roots, Weyl factors and the integration cycle enter separately.

VIII.11.3 One membrane and the regulated Fourier integral

Can the normalized integral be evaluated without a large-N limit? At $N = 1$ the root products are empty and both Weyl factorials equal one. In the x, y variables of the preceding section, the phase-conjugate version of the same rank-one prescription is

$$Z_{1,k} = \int_{\mathbb{R}^2} dx\, dy\, \frac{e^{-i\pi k(x^2-y^2)}}{[2\cosh\pi(x-y)]^2}. \tag{VIII.11.10}$$

The measure is $dx\,dy$ because $d\mu\,d\nu/(2\pi)^2 = dx\,dy$. The integrand is not absolutely integrable along the common eigenvalue direction. An integration order without a regulator would therefore leave the answer undefined.

Choose relative and common coordinates

$$u = x - y, \qquad v = \frac{x+y}{2}, \qquad x = v + \frac{u}{2}, \quad y = v - \frac{u}{2}, \quad \left|\frac{\partial(x,y)}{\partial(u,v)}\right| = 1, \quad x^2 - y^2 = 2uv. \tag{VIII.11.11}$$

The unit Jacobian is easy to miss. It ensures that the eventual factor $1/k$ comes only from the Fourier direction. Multiply the integrand by $e^{-\epsilon v^2}$ with $\epsilon > 0$. The Gaussian Fourier transform then gives

$$Z_{1,k}(\epsilon) = \int_{\mathbb{R}^2} du\, dv\, \frac{e^{-\epsilon v^2 - 2\pi i k u v}}{[2\cosh(\pi u)]^2} \tag{VIII.11.12}$$

$$= \sqrt{\frac{\pi}{\epsilon}} \int_{\mathbb{R}} du\, \frac{e^{-\pi^2 k^2 u^2/\epsilon}}{[2\cosh(\pi u)]^2}. \tag{VIII.11.13}$$

With $t = \pi k u/\sqrt{\epsilon}$ and $k > 0$, this becomes

$$Z_{1,k}(\epsilon) = \frac{1}{k\sqrt{\pi}} \int_{\mathbb{R}} dt\, \frac{e^{-t^2}}{[2\cosh(\sqrt{\epsilon}\, t/k)]^2}. \tag{VIII.11.14}$$

The final integrand is bounded by $e^{-t^2}/4$, independently of ϵ. Dominated convergence gives a precise limit rather than an informal delta-function substitution. Equivalently, the Gaussian kernel in the u integral has area $1/k$ and tends to $\delta(u)/k$. Hence

$$Z_{1,k} = \frac{1}{4k}, \qquad F_{1,k} = \log(4k), \qquad (Z_{1,1}, Z_{1,2}, Z_{1,3}) = \left(\frac{1}{4}, \frac{1}{8}, \frac{1}{12}\right). \tag{VIII.11.15}$$

The three examples show both the k^{-1} Fourier scaling and the $1/4$ matter normalization. Dropping the 2 from each cosh would instead produce $1/k$, a fourfold error in the absolute answer.

A second representation of the same localized integral is useful because it is positive. The sourced Fermi-gas form has the diagonal one-particle kernel $\rho(q,q) = [4\pi k]^{-1}[2\cosh(q/2)]^{-1}$. At rank one,

$$Z_{1,k} = \operatorname{Tr}\rho = \frac{1}{4\pi k} \int_{-\infty}^{\infty} \frac{dq}{2\cosh(q/2)}, \tag{VIII.11.16}$$

$$\int_{-\infty}^{\infty} \frac{dq}{2\cosh(q/2)} = \int_{-1}^{1} \frac{ds}{\sqrt{1-s^2}} = \pi, \qquad s = \tanh(q/2). \tag{VIII.11.17}$$

This recovers $1/(4k)$ without an oscillatory integral. It checks the Fermi representation against the regulated Fourier calculation; both represent the same localized theory and share its physical localization premise. Chapter 12 uses the Fermi description in a different limit, where N grows at fixed k.

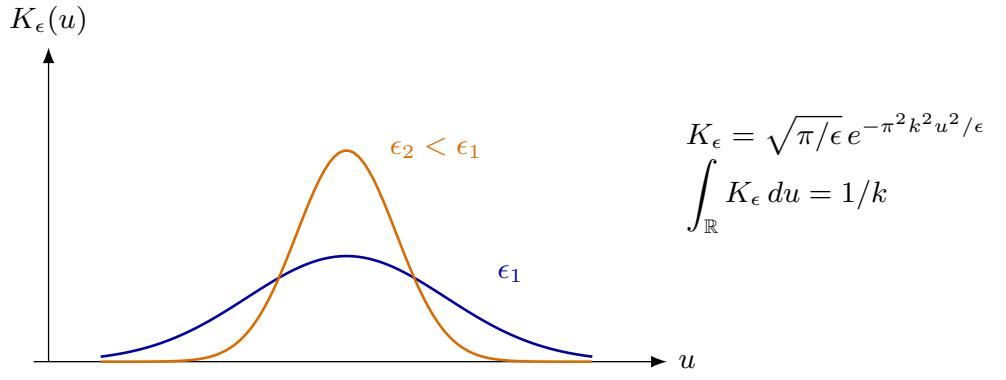


Figure VIII.11.3: Schematic narrowing of the regulated Fourier kernel for fixed $k > 0$. The vertical scale illustrates a fixed area $1/k$; the exact Gaussian is specified in the label. The plotted window omits its tails. The area and the value of the matter factor at $u = 0$ give $Z_{1,k} = 1/(4k)$.

VIII.11.4 A trial R charge is a measurable variable

The sphere integral can also depend on a candidate R charge. Write the trial generator as $R_{\mathrm{tr}} = R_0 + \sum_j t_j F_j$, where each F_j is a flavor generator that may mix with R. This is a physical variation only when the symmetry really exists and the curved-space coupling follows the specified supersymmetric prescription. The sourced stationarity statement for the superconformal R symmetry assumes that no accidental symmetry has been omitted. It does not establish a global maximum for an arbitrary trial family.

One free chiral at zero real mass is an exact elementary example. With $0 < \Delta < 1$ and the determinant of (VIII.11.6), its real sphere free energy is

$$F_{\mathrm{ch}}(\Delta) = -\ell(1-\Delta). \tag{VIII.11.18}$$

Differentiation gives a nontrivial curvature test,

$$F'_{\mathrm{ch}}(\Delta) = \pi(1-\Delta)\cot(\pi\Delta), \tag{VIII.11.19}$$

$$F''_{\mathrm{ch}}(\Delta) = -\pi\cot(\pi\Delta) - \pi^2(1-\Delta)\csc^2(\pi\Delta). \tag{VIII.11.20}$$

The only stationary point in $0 < \Delta < 1$ is $\Delta = 1/2$. At that point the cotangent term vanishes and

$$F_{\mathrm{ch}}(1/2) = \frac{\log 2}{2}, \qquad F''_{\mathrm{ch}}(1/2) = -\frac{\pi^2}{2} < 0. \tag{VIII.11.21}$$

Thus this particular trial direction has a strict local maximum. The calculation is a useful sign test for any proposed extremization rule. It also repeats the absolute determinant constant in an observable form. A derivation using only ℓ' could locate the stationary point, but would miss $F_{\mathrm{ch}}(1/2)$.

The source frame introduces a second kind of trial coordinate for a $U(N)$ node. In the JKPS prescription the matrix coordinate called σ there is our dimensionless λ, and a node insertion has the form $e^{-m_a\lambda_a}$. The parameter m_a records trial mixing with a topological current through bare monopole charges. Its source definition is

$$m = \sum_a m_a = \frac{R(T) - R(\widetilde{T})}{2}, \qquad e^{-m_a\lambda_a}, \qquad \lambda_a = 2\pi\widehat{\sigma}_a. \tag{VIII.11.22}$$

At the same real eigenvalue, the Jafferis baryonic parameter obeys $\Delta_B = -m_a$. That baryonic insertion was stated conjecturally in its original presentation; we adopt the JKPS matrix prescription for this chapter. The symbol m_a is a trial R-mixing coordinate. It is neither GNO magnetic flux nor a switched-on physical real FI parameter. The distinction matters in Chapter 8, where actual monopole sectors and flavor charges enter the vacuum ring.

The matrix prescription can be written schematically for a gauge group with nodes a and matter multiplets I as

$$Z_{S^3}(\Delta, m) = \frac{1}{|W|}\int \prod_a \frac{d\lambda_a}{2\pi} e^{\sum_a ik_a\lambda_a^2/(4\pi) - \sum_a m_a\lambda_a} Z_{\rm vec}(\lambda) \prod_I e^{\ell(1-\Delta_I + i\rho_I(\lambda)/(2\pi))}. \tag{VIII.11.23}$$

The product notation suppresses multiple Cartan variables and their weights; the precise ABJM product was displayed in (VIII.11.9). Equation (VIII.11.23) states the adopted source scheme and its 2π conversion. It is not a derivation of a general localization theorem or of monopole OPE coefficients.

VIII.11.5 Extremizing physical charges in ABJM

What should be varied in the constructed four-field theory? Let $a_i = R(A_i)$ and $b_i = R(B_i)$ for $i = 1, 2$, in a trial assignment. The quartic superpotential requires

$$a_1 + a_2 + b_1 + b_2 = 2. \tag{VIII.11.24}$$

For the full $U(N)_k \times U(N)_{-k}$ theory, the sourced large-N trial function also depends on the monopole-mixing coordinate m of (VIII.11.22). At fixed positive integer k and within the common-real-part $N^{1/2}$ saddle, the source gives

$$\frac{F_{\rm tr}}{N^{3/2}} = \frac{4\sqrt{2}\pi}{3k^{3/2}}\sqrt{(ka_1 - m)(ka_2 - m)(kb_1 + m)(kb_2 + m)}. \tag{VIII.11.25}$$

This full trial function is a sourced saddle result. Its physical identification requires localization, an admissible positive-charge branch and selection of the relevant saddle. Chapter 12 derives the symmetric $m = 0$ coefficient by an eigenvalue calculation. We can extract the extremum and its charge geometry directly from (VIII.11.25).

Define four dressed combinations

$$h_{A_i} = a_i - \frac{m}{k}, \qquad h_{B_i} = b_i + \frac{m}{k}, \qquad h_{A_1} + h_{A_2} + h_{B_1} + h_{B_2} = 2. \tag{VIII.11.26}$$

The two minus signs and two plus signs cancel in the sum. They also identify a null direction in the original five trial symbols,

$$a_i \mapsto a_i + d, \qquad b_i \mapsto b_i - d, \qquad m \mapsto m + kd \quad \Longrightarrow \quad h_{A_i}, h_{B_i} \text{ unchanged.} \tag{VIII.11.27}$$

The transformation preserves the quartic constraint and the entire trial function. It is a redundancy in assignments to gauge-charged letters. A genuine flavor variation changes at least one h and cannot be removed by this shift. Schematic dressed operators such as $\widetilde{T}A_i^k$ and TB_i^k motivate these combinations; that notation alone does not establish a finite-N color contraction.

Inside the positive domain $h_I > 0$, the function reduces to

$$\frac{F_{\text{tr}}}{N^{3/2}} = \frac{4\sqrt{2k}\pi}{3}\sqrt{h_1 h_2 h_3 h_4}, \qquad \sum_{I=1}^{4} h_I = 2. \tag{VIII.11.28}$$

The arithmetic-geometric mean inequality, applied only on this physical simplex, gives

$$\prod_{I=1}^{4} h_I \le \left(\frac{1}{2}\right)^4, \qquad h_I = \frac{1}{2}\ (I = 1, 2, 3, 4), \qquad F_* = \frac{\pi\sqrt{2k}}{3}N^{3/2}. \tag{VIII.11.29}$$

This is a global maximum of the displayed positive product on its specified simplex. It is not a claim about every saddle or every possible accidental mixing in the complete quantum theory. A bare assignment with $m = 0$ and $a_i = b_i = 1/2$ is one convenient representative. The entire family related by (VIII.11.27) gives the same physical answer.

The local curvature makes the difference between physical and redundant directions explicit. Put $h_4 = 2 - h_1 - h_2 - h_3$. Then

$$\log F_{\text{tr}} = \text{constant} + \frac{1}{2}\left(\sum_{i=1}^{3} \log h_i + \log h_4\right), \tag{VIII.11.30}$$

$$\left.\frac{\partial^2 \log F_{\text{tr}}}{\partial h_i \partial h_j}\right|_{h_I = 1/2} = -2(\delta_{ij} + 1), \qquad \text{spec} = (-8, -2, -2). \tag{VIII.11.31}$$

All three physical directions curve downward. The unquotiented trial assignment has, in addition, the flat direction (VIII.11.27); calling its full Hessian negative definite would be false. As a diagnostic, replacing the minus sign in $h_A = a - m/k$ by a plus sign would make the simultaneous shift change h_A by $2d$, so it would erase this required null direction. The example connects an extremization calculation to the gauge quotient that already mattered for the moduli space in Chapter 3.

VIII.11.6 Squashing with its supersymmetric background

A shape change of the sphere poses a different question from the Q-exact deformation of Section VIII.11.1. The supersymmetric ellipsoid changes both its metric and an R

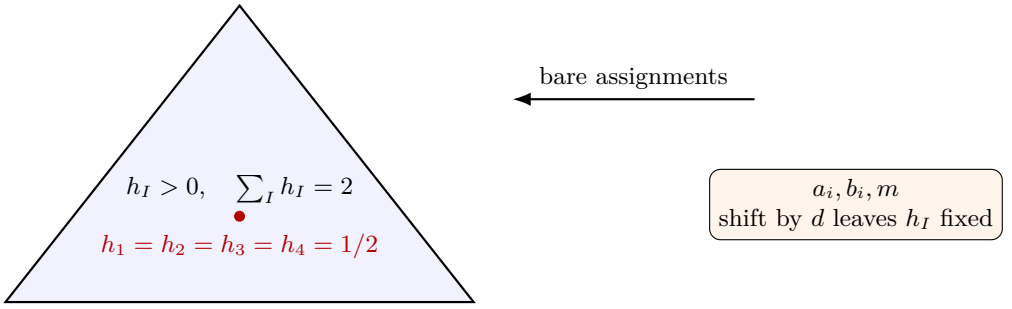


Figure VIII.11.4: A simplex slice represents the positive physical charge domain; the full four-charge simplex has one additional independent coordinate. Its symmetric point maximizes the sourced product. The separate arrow indicates that many bare assignments map to the same h_I, so the extra d direction is not a physical curvature direction.

connection. Use angles $0 \le \theta \le \pi/2$ and periodic ϕ, χ with positive length scales $\ell, \widetilde{\ell}$. In the HHL frame,

$$ds^2 = f(\theta)^2 d\theta^2 + \ell^2 \cos^2\theta \, d\phi^2 + \widetilde{\ell}^2 \sin^2\theta \, d\chi^2, \qquad f^2 = \ell^2 \sin^2\theta + \widetilde{\ell}^2 \cos^2\theta. \tag{VIII.11.32}$$

The relevant dimensionless variables are

$$b = \sqrt{\frac{\widetilde{\ell}}{\ell}}, \qquad Q_b = b + b^{-1}, \qquad \widehat{\sigma} = \sqrt{\ell\widetilde{\ell}}\,\sigma. \tag{VIII.11.33}$$

Here Q_b is a shape combination; it is not the supercharge Q of the Ward identity. At $\ell = \widetilde{\ell} = r$ one has $b = 1$ and $\widehat{\sigma} = r\sigma$, consistent with the round convention above.

The metric alone does not preserve the chosen supercharge. One HHL choice of charged spinor uses an R connection

$$V_R^{(st)} = \frac{t}{2}\left(1 - \frac{\ell}{f}\right) d\phi + \frac{s}{2}\left(1 - \frac{\widetilde{\ell}}{f}\right) d\chi, \qquad s, t \in \{+1, -1\}, \tag{VIII.11.34}$$

with the matching curved Killing-spinor equation. For example, choose $s = +1, t = -1$. At $\theta = 0$, $f = \widetilde{\ell}$ and the source spinor obeys $\partial_\phi \psi_{st} = it\psi_{st}/2$ and $\gamma_\phi \psi_{st} = -s\ell\psi_{st}$. The ϕ component then gives

$$(\nabla_\phi - iV_{R,\phi}^{(st)})\psi_{st} = \frac{it\ell}{2\widetilde{\ell}}\psi_{st} = -\frac{ist}{2\widetilde{\ell}}\gamma_\phi\psi_{st}. \tag{VIII.11.35}$$

Dropping V_R leaves $it\psi_{st}/2$ on the left and fails this component when $\ell \neq \widetilde{\ell}$. This is a useful local test of why the geometry and R field must move together. It is not a derivation of the full curved-background construction.

For an R-charge-q chiral of weight ρ, the sourced ellipsoid one-loop factor is

$$s_b\left(\frac{iQ_b(1-q)}{2} - \rho(\widehat{\sigma})\right). \tag{VIII.11.36}$$

At $b = 1$ and $q = 1/2$, two opposite weights reproduce the normalized round pair,

$$s_1\left(\frac{i}{2} - x\right) s_1\left(\frac{i}{2} + x\right) = \frac{1}{2\cosh(\pi x)}, \qquad x = \rho(\widehat{\sigma}). \tag{VIII.11.37}$$

This is a local determinant consistency test, not a determination of the full finite-rank contour or contact phase. In particular, a physical flat-space GRVV mass cannot be identified with $\widehat{\sigma}$ or with the shape b.

The leading large-N relation has a useful source-frame subtlety. The MPS shape parameter β is inverse to our b, $\beta = b^{-1}$, while its symmetric Q_b agrees. Its eigenvalue coordinate is written $\lambda^I(x) = N^{1/2}x + iy^I(x)$ and $\rho(x)$ is a normalized density. For the zero-mass, nonchiral, common-real-part $N^{3/2}$ saddle, define

$$c = \frac{\beta Q_b}{2} = \frac{Q_b}{2b}, \qquad x = cx_0, \qquad \rho(x) = \frac{\rho_0(x_0)}{c}, \qquad \widehat{y}^I = \frac{y^I}{c}. \tag{VIII.11.38}$$

The density normalization survives, since $\int dx\, \rho(x) = \int dx_0\, \rho_0(x_0) = 1$. The source functional in these variables separates into a classical term $\mathcal{C}$, linear in x, and a one-loop term $\mathcal{L}$, quadratic in the density,

$$\frac{F_b^{(0)}}{N^{3/2}} = \frac{bQ_b}{2}\,\mathcal{C}[x, \rho, \widehat{y}] + \frac{Q_b^3}{8b}\,\mathcal{L}[\rho, \widehat{y}]. \tag{VIII.11.39}$$

More explicitly, the sourced class has $\mathcal{C} = \int dx\, \rho x \sum_I k_I \widehat{y}^I/(2\pi)$ and $\mathcal{L} = \int dx\, \rho^2 \mathcal{P}(\widehat{y}^I - \widehat{y}^J; \Delta)$, with the same matter polynomial $\mathcal{P}$ and trial charges fixed. Under (VIII.11.38), $\mathcal{C}$ gains c and $\mathcal{L}$ gains $1/c$. Both prefactors therefore become

$$\frac{bQ_b}{2}c = \frac{Q_b^2}{4}, \qquad \frac{Q_b^3}{8b}\frac{1}{c} = \frac{Q_b^2}{4}. \tag{VIII.11.40}$$

The two terms scale together. If the corresponding nonchiral saddle exists, remains admissible and dominates the localized integral, this change of variables yields

$$F_b^{(0)} = \frac{Q_b^2}{4} F_1^{(0)}, \qquad Q_b = b + b^{-1}. \tag{VIII.11.41}$$

The superscript denotes the leading $N^{3/2}$ term at fixed levels and charges. It is not an identity for the full finite-N free energy, nor a response to an arbitrary metric deformation. Chapter 12 supplies $F_1^{(0)}$ for the symmetric round ABJM saddle.

The round point and an asymmetric shape provide immediate checks. At $b = 2$, $Q_b = 5/2$ and $F_2^{(0)}/F_1^{(0)} = 25/16$. With $b = e^t$,

$$\frac{Q_b^2}{4} = \cosh^2 t = 1 + t^2 + O(t^4), \qquad \partial_b F_b^{(0)}\Big|_{b=1} = 0, \qquad \partial_b^2 F_b^{(0)}\Big|_{b=1} = 2F_1^{(0)}. \tag{VIII.11.42}$$

The zero first derivative reflects the leading $b \leftrightarrow b^{-1}$ symmetry. Subleading terms and contact choices need separate treatment. Figure VIII.11.5 depicts the background change without confusing it with the flat-space mass deformation of Chapter 9.

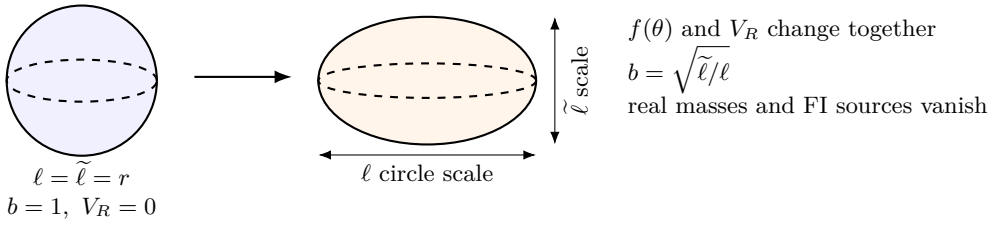


Figure VIII.11.5: The two supersymmetric backgrounds. The ellipses indicate unequal circle scales; the actual metric and R connection are (VIII.11.32) and (VIII.11.34). Shape variation changes the observable, whereas the Q-exact deformation in Figure VIII.11.1 preserves its value under the Ward hypotheses.

VIII.11.7 Exercises

See `benchmark/tasks.json` and `benchmark/PROTOCOL.md` for the public structured-answer format. Exact rational coefficients multiply the explicitly named powers of π and $\log 2$; written solutions should also show the derivations.

E1. For the normalized $U(1)_k \times U(1)_{-k}$ round integral at $k = 1, 2, 3$, submit the three values of $Z_{1,k}$ and the integer arguments of $F_{1,k} = \log(4k)$, the three products $kZ_{1,k}$, and the Fourier-kernel area at $k = 2$. Show the unit Jacobian of $u = x - y$, $v = (x + y)/2$ and explain which integral requires a regulator. State how omitting both factors of 2 in the matter denominator changes the answer.

E2. For a free chiral with $0 < \Delta < 1$ and zero real mass, calculate the stationary charge, free energy and second derivative of $F_{\mathrm{ch}}(\Delta)$. Then evaluate the opposite-weight pair at $x = 0$. Explain which of these values would be lost if only ℓ' were known.

E3. In the sourced positive-charge ABJM trial function, set $k = 2$, $a_1 = a_2 = b_1 = b_2 = 1/2$ and $m = 0$. Submit the four dressed charges, the coefficient $F/N^{3/2}$, the three physical eigenvalues of $\mathrm{Hess}(\log F)$ and the shifted bare assignment for $d = 1/4$. Explain why the latter has the same free energy and why a physical flavor direction is different.

E4. For the supersymmetric ellipsoid at $b = 2$, submit Q_b, the leading ratio $F_b^{(0)}/F_1^{(0)}$, the ratio at inverse shape, and the first two b derivatives divided by $F_1^{(0)}$ at the round point. State the background and dominant-saddle conditions under which these numbers describe the physical leading observable.

Take-home message of this chapter

A normalized localization prescription turns the round ABJM sphere integral into a matrix model whose rank-one answer is $1/(4k)$. The zeta determinant fixes its absolute factor. Trial R extremization acts on dressed physical charge combinations, not on a redundant bare gauge assignment. A supersymmetric ellipsoid changes the metric and R connection together; its leading $Q_b^2/4$ relation holds for the specified nonchiral dominant saddle.

Status and sources

Sources by section. Source coordinates and scope qualifications follow.

§VIII.11.1. The calculation [MATH] is conditional on $QS = 0$, an invariant measure and cycle, and no boundary terms; the physical localization step is sourced (Kapustin et al. 2010, §3.1).

§VIII.11.2. The calculation [MATH] fixes the determinant constant within the sourced compact ABJM localization prescription (Drukker et al. 2011, Appendix A; Jafferis 2012, §3).

§VIII.11.3. The calculation [MATH] is the regulated rank-one Fourier evaluation for that same matrix integral; contour choice remains sourced (Marino and Putrov 2012, §3).

§VIII.11.4. The calculation [MATH] covers the free-chiral derivatives under the sourced trial-charge prescription; global R selection needs its physical hypotheses (Jafferis 2012, equations (1.1)–(1.3), §5).

§VIII.11.5. The calculation [MATH] gives the constrained algebraic extremum conditional on the sourced large-N trial function and physical charge domain (Jafferis et al. 2011, equations (5.7)–(5.8)).

§VIII.11.6. The calculation [MATH] gives the change of variables conditional on a dominating common-real-part saddle; the background and density functional are sourced (Hama et al. 2011, §§2,5; Martelli et al. 2012, equations (3.26), (3.36)–(3.38)).

§VIII.11.7. The exercises reuse the preceding conditional [MATH] calculations under the localization, trial-charge and volume frame and Chern–Simons trace and levels, quiver gauge groups and Chern–Simons matter conventions (Jafferis 2012, §3; Jafferis et al. 2011, equations (5.7)–(5.8); Martelli et al. 2012, equations (3.26), (3.36)–(3.38)).

The Ward calculation is conditional on $QS = 0$, a Q-invariant measure and cycle, valid differentiation and absence of boundary or anomaly terms. The physical localization map, integration contour and general contact phase are sourced premises. The determinant and rank-one normalization are for the full compact equal-rank ABJM model on a round sphere at positive integer k with zero real masses and FI sources. The trial ABJM function and ellipsoid relation require their stated large-N saddle domains. None of these formulas determines a universal finite-N squashing law or a general global R maximum.

Round localization and normalization. The Ward deformation follows Kapustin et al. 2010, v4, §3.1, equations (3.1)–(3.2). The normalized ABJM matrix integral and zeta constant follow Drukker et al. 2011, v4, equation (2.1) and Appendix A, equations (A.1)–(A.7). The Fermi diagonal kernel and trace are in Marino and Putrov 2012, §3, equations (3.3)–(3.5). Equations (VIII.11.11)–(VIII.11.15) spell out the regulated Fourier evaluation. Both evaluations use the same localized model.

Trial charges. The chiral ℓ function, free-chiral example and stationarity conditions follow Jafferis 2012, v2, equations (1.1)–(1.3) and (3.4)–(3.5), printed pp. 13–14, and §5. Its baryonic insertion in §4, printed p. 16, is conjectural. We adopt the matrix prescription and monopole-mixing coordinates of Jafferis et al. 2011, v2, equations (2.1)–(2.3), and its full ABJM trial function in equations (5.7)–(5.8). The free-chiral curvature, dressed-charge invariance, product maximum and constrained Hessian are the algebra displayed here. The sourced large-N function is an input, not a consequence of those algebraic steps.

Ellipsoid. The metric, R connection and one-loop double sine follow Hama et al. 2011, v1, §2 and §5, equations (2.15)–(2.23) and (5.19)–(5.22). The inverse shape coordinate and leading density functional follow Martelli et al. 2012, v3, equations (1.1), (3.26) and (3.36)–(3.38). The change of variables in (VIII.11.38)–(VIII.11.40) shows the stated leading relation when the common-real-part nonchiral saddle exists and dominates. Exact finite-rank contour and phase questions, accidental R mixing and saddle selection remain open here.

References

Drukker, N., M. Marino, and P. Putrov (2011). "From weak to strong coupling in ABJM theory". In: *Commun. Math. Phys.* 306, pp. 511–563. DOI: 10.1007/s00220-011-1253-6. arXiv: 1007.3837 [hep-th].

Hama, N., K. Hosomichi, and S. Lee (2011). "SUSY Gauge Theories on Squashed Three-Spheres". In: *JHEP* 05, p. 014. DOI: 10.1007/JHEP05(2011)014. arXiv: 1102.4716 [hep-th].

Jafferis, D. L. (2012). "The Exact Superconformal R-Symmetry Extremizes Z". In: *JHEP* 05, p. 159. DOI: 10.1007/JHEP05(2012)159. arXiv: 1012.3210 [hep-th].

Jafferis, D. L. et al. (2011). "Towards the F-Theorem: N=2 Field Theories on the Three-Sphere". In: *JHEP* 06, p. 102. DOI: 10.1007/JHEP06(2011)102. arXiv: 1103.1181 [hep-th].

Kapustin, A., B. Willett, and I. Yaakov (2010). "Exact Results for Wilson Loops in Superconformal Chern-Simons Theories with Matter". In: *JHEP* 03, p. 089. DOI: 10.1007/JHEP03(2010)089. arXiv: 0909.4559 [hep-th].

Marino, M. and P. Putrov (2012). "ABJM theory as a Fermi gas". In: *J. Stat. Mech.* 1203, P03001. DOI: 10.1088/1742-5468/2012/03/P03001. arXiv: 1110.4066 [hep-th].

Martelli, D., A. Passias, and J. Sparks (2012). "The gravity dual of supersymmetric gauge theories on a squashed three-sphere". In: *Nucl. Phys. B* 864, pp. 840–868. DOI: 10.1016/j.nuclphysb.2012.07.019. arXiv: 1110.6400 [hep-th].

Chapter VIII.12

Large-N free energy and geometric volume

A stack of M2-branes has a curious number of degrees of freedom. The free energy on a round three-sphere grows as $N^{3/2}$ in its M-theory regime, rather than as the N^2 suggested by a weakly coupled matrix of fields. ABJM theory lets us find both the exponent and its coefficient in a localized gauge-theory integral. A second question is more demanding. If a different quiver describes M2-branes at a different cone, can its free energy be compared with a volume calculated from that cone itself?

We begin with the symmetric ABJM eigenvalue continuum. The Fermi-gas description and the Freund–Rubin geometry then give two ways to read the same leading coefficient. Our non-ABJM example is the full $U(N) \times U(N)$, zero-level quiver with one flavor pair on each of the two A arrows of Chapter 8. Its proposed single-probe ring is the Segre cone with link $Q^{1,1,1}$. For this same theory we calculate a piecewise large-N density and independently count the graded holomorphic functions that determine a trial Sasakian volume. The comparison will hold on the positive trial-charge interval, subject to the localization, geometric-branch and selected-saddle premises stated below.

VIII.12.1 A continuum of ABJM eigenvalues

How can a finite-dimensional matrix integral produce $N^{3/2}$? In the round-sphere integral of Chapter 11, take the full compact $U(N)_k \times U(N)_{-k}$ theory, equal ranks, integer $k > 0$, four bifundamentals of charge $1/2$, and vanishing real masses and trial topological mixing. Write $F = -\log |Z_{S^3}|$. The complex eigenvalues of the selected large-N saddle have a common real coordinate x and imaginary coordinates y_1, y_2,

$$\lambda_i^{(a)} = N^{1/2} x_i + i y_a(x_i), \qquad \rho(x) = \frac{1}{N} \sum_i \delta(x - x_i), \qquad \int_{\mathbb{R}} \rho(x)\, dx = 1. \quad \text{(VIII.12.1)}$$

Here ρ is the real-eigenvalue density, not a Fermi-gas state density. Define $\delta y = y_1 - y_2$. Cancellation of the long-range forces in the sourced saddle reduction leaves a local

functional at order $N^{3/2}$. The general bifundamental polynomial of the source is especially easy to specialize. If $\Delta_{A_i}, \Delta_{B_i}$ are the four trial charges, set

$$A = \Delta_{A_1}\Delta_{A_2} - \Delta_{B_1}\Delta_{B_2}, \tag{VIII.12.2}$$

$$B = \Delta_{A_1}\Delta_{A_2}(\Delta_{B_1} + \Delta_{B_2}) + \Delta_{B_1}\Delta_{B_2}(\Delta_{A_1} + \Delta_{A_2}), \tag{VIII.12.3}$$

$$\mathcal{P}(\delta y) = -\delta y^2 - 2\pi A\delta y + 2\pi^2 B. \tag{VIII.12.4}$$

At four charges $1/2$, one has $A = 0$ and $B = 1/2$. The local matter term is therefore $\rho^2\mathcal{P} = \rho^2(\pi^2 - \delta y^2)$. The two opposite Chern–Simons levels supply the remaining term, so

$$f[\rho, \delta y] := \frac{F}{N^{3/2}} = \int dx \left\{ \frac{kx\rho\,\delta y}{2\pi} + \rho^2(\pi^2 - \delta y^2) \right\}, \qquad -\pi \le \delta y \le \pi. \tag{VIII.12.5}$$

The polynomial form applies on the displayed determinant branch. It is a source-dependent large-N reduction of the normalized localized integral, not an identity for arbitrary complex eigenvalue distributions. We use $\Lambda = \mu_{\mathrm{JKPS}}/(2\pi)$ for the multiplier imposing $\int \rho = 1$. This Λ is unrelated to the bulk radius L, the Fermi chemical potential μ_F, or the mass in Chapter 9.

In the interior, vary $f - \Lambda(\int \rho - 1)$ in both functions. The two equations are

$$0 = \frac{kx\rho}{2\pi} - 2\rho^2\delta y, \qquad \delta y = \frac{kx}{4\pi\rho}, \tag{VIII.12.6}$$

$$\Lambda = \frac{kx\delta y}{2\pi} + 2\rho(\pi^2 - \delta y^2), \qquad \rho = \frac{\Lambda}{2\pi^2}. \tag{VIII.12.7}$$

The cancellation of the x^2 terms in the second equation explains the constant density. The imaginary separation is linear,

$$\delta y(x) = \frac{k\pi x}{2\Lambda}, \qquad |x| \le x_* := \frac{2\Lambda}{k}. \tag{VIII.12.8}$$

The support ends when $|\delta y| = \pi$. Its density remains finite at the ends; setting $\rho(x_*) = 0$ would solve a different endpoint problem. Normalization now fixes every constant,

$$1 = \frac{\Lambda}{2\pi^2}\frac{4\Lambda}{k} = \frac{2\Lambda^2}{\pi^2 k}, \quad \Lambda = \pi\sqrt{\frac{k}{2}}, \quad x_* = \pi\sqrt{\frac{2}{k}}, \quad \rho = \frac{\sqrt{k}}{2\sqrt{2}\pi}. \tag{VIII.12.9}$$

Substitution into the two terms of (VIII.12.5) gives equal contributions. For example, the Chern–Simons term is

$$\int_{-x_*}^{x_*} dx\, \frac{kx\rho\delta y}{2\pi} = \frac{k^2}{4\Lambda}\rho\frac{2x_*^3}{3} = \frac{\Lambda}{3}, \qquad \int_{-x_*}^{x_*} dx\, \rho^2(\pi^2 - \delta y^2) = \frac{\Lambda}{3}. \tag{VIII.12.10}$$

Thus the selected saddle has

$$F^{(0)}_{\mathrm{ABJM}} = \frac{2\Lambda}{3}N^{3/2} = \frac{\pi\sqrt{2k}}{3}N^{3/2}. \tag{VIII.12.11}$$

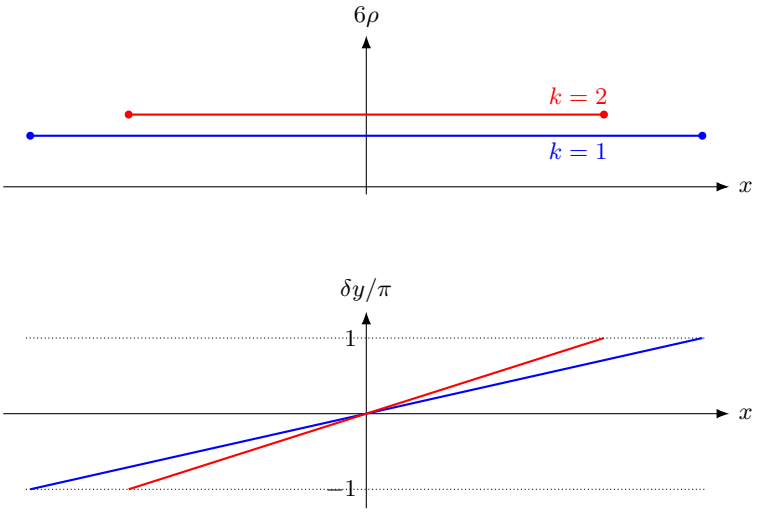


Figure VIII.12.1: Computed symmetric ABJM saddle at $k = 1$ and $k = 2$. The horizontal coordinate is the real eigenvalue x. The density is constant and nonzero at each support edge; the imaginary separation reaches $\pm\pi$ there. Only the branch $|\delta y| \le \pi$ enters the functional.

At $k = 1$, the density is $1/(2\sqrt{2}\pi)$ on $[-\pi\sqrt{2}, \pi\sqrt{2}]$; at $k = 2$ it is $1/(2\pi)$ on $[-\pi, \pi]$. The interval contracts while its height grows, preserving unit area. The support and δy profiles are plotted from these equations in Figure VIII.12.1.

The balance in (VIII.12.10) is the mechanism behind the coefficient. The calculation finds a stationary distribution within the sourced ansatz and determinant branch. It does not establish that no other complex saddle dominates. Chapter 11 supplies the normalized localization starting point; we now recast that same starting point as a fermion problem.

VIII.12.2 Counting fermion states instead

The ABJM integral can be transformed into an ideal Fermi gas. The sourced one-particle kernel can be written in position space as

$$\mathcal{K}(q, q') = \frac{1}{2\pi k} \frac{1}{\sqrt{2\cosh(q/2)}} \frac{1}{2\cosh[(q - q')/(2k)]} \frac{1}{\sqrt{2\cosh(q'/2)}}. \tag{VIII.12.12}$$

The square roots make the position and momentum factors symmetric. Indeed, with $\hbar = 2\pi k$ its leading Weyl symbol has Hamiltonian

$$H_{\mathrm{cl}}(q, p) = \log[2\cosh(q/2)] + \log[2\cosh(p/2)] \sim \frac{|q| + |p|}{2} \quad (|q| + |p| \gg 1). \tag{VIII.12.13}$$

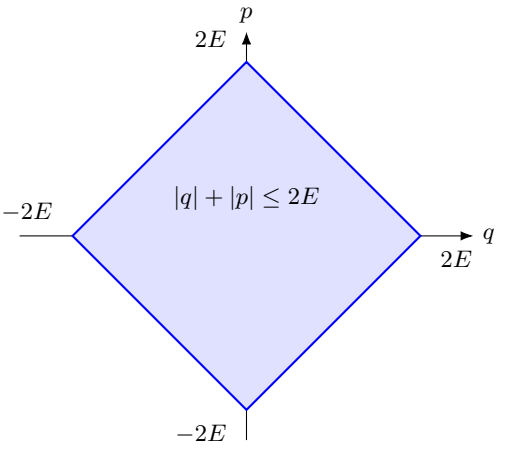


Figure VIII.12.2: The high-energy Fermi region in canonical (q, p) coordinates. Its four intercepts are $\pm 2E$ and its area is $8E^2$. One quantum state occupies leading phase-space area $2\pi\hbar = 4\pi^2 k$.

This is a change of variables in the same localized integral. At high one-particle energy E, a classical Hamiltonian has an accessible region that approaches a diamond,

$$\mathcal{D}_E = \{(q,p) : |q| + |p| \le 2E\}, \qquad \text{Area}(\mathcal{D}_E) = \frac{(4E)(4E)}{2} = 8E^2. \tag{VIII.12.14}$$

Figure VIII.12.2 displays the axes and intercepts. Dividing by one quantum cell $2\pi\hbar = 4\pi^2 k$ gives the leading integrated state count

$$n(E) \sim \frac{8E^2}{4\pi^2 k} = CE^2, \qquad C = \frac{2}{\pi^2 k}. \tag{VIII.12.15}$$

For $k = 1$ and 2, the same diamond contains respectively $2E^2/\pi^2$ and E^2/π^2 leading states. The phase-space picture shows the coefficient geometrically. The fixed-k spectral asymptotic of the quantum operator, including the fact that quantum corrections do not alter this leading coefficient, is a separate sourced input.

Let μ_F denote the Fermi chemical potential and $\Xi(\mu_F) = \sum_{N\ge 0} e^{N\mu_F} Z_{N,k}$ the grand partition function. Its logarithm $J = \log \Xi$ obeys

$$J(\mu_F) = \int_0^\infty dE\, n(E) \frac{1}{1 + e^{E-\mu_F}} \sim \int_0^{\mu_F} CE^2\, dE = \frac{C}{3}\mu_F^3, \tag{VIII.12.16}$$

$$N = \frac{\partial J}{\partial \mu_F} \sim C\mu_F^2, \qquad \mu_F \sim \sqrt{\frac{N}{C}}. \tag{VIII.12.17}$$

Here the first equality follows by integrating the one-particle Fermi occupation by parts. The inverse Laplace saddle gives $\log Z_N \sim J - N\mu_F$, hence

$$F_N \sim N\mu_F - J = \frac{2}{3} C^{-1/2} N^{3/2} = \frac{\pi\sqrt{2k}}{3} N^{3/2}. \tag{VIII.12.18}$$

This route makes the exponent transparent. Quadratic growth of the number of one-particle states gives $N \sim \mu_F^2$, and its Legendre transform gives $N^{3/2}$. Both field-theory routes consume the same localized matrix model and determinant normalization. Their agreement checks two calculations of that model; it is not a second physical derivation of localization. The geometric calculation below supplies a different description under the M2-brane duality premise.

VIII.12.3 The gravity coefficient and its normalization

For a Freund–Rubin background $AdS_4 \times Y_7$, normalize the Einstein metric on the seven-dimensional link by $\mathrm{Ric}(Y) = 6g_Y$. The cone is Ricci-flat; the link is positively curved. Write L for the metric radius multiplying Y, so the AdS_4 radius is $a = L/2$, and $V_Y = \mathrm{Vol}(Y)$ in this unit-radius convention. At leading zero-torsion charge, flux quantization and dimensional reduction give

$$L^6 = \frac{(2\pi\ell_p)^6 N}{6V_Y}, \qquad G_{11} = 16\pi^7\ell_p^9, \qquad \frac{1}{G_4} = \frac{L^7 V_Y}{G_{11}}. \tag{VIII.12.19}$$

These relations fix the units that a schematic volume argument cannot fix. The renormalized Euclidean action for a round S^3 boundary is $I_{\mathrm{ren}} = \pi a^2/(2G_4)$. Substituting the actual AdS radius gives

$$F^{(0)}_{\mathrm{grav}} = \frac{\pi L^9 V_Y}{8G_{11}} = \frac{\pi V_Y}{128\pi^7\ell_p^9}\left[\frac{(2\pi\ell_p)^6 N}{6V_Y}\right]^{3/2} = N^{3/2}\sqrt{\frac{2\pi^6}{27V_Y}}. \tag{VIII.12.20}$$

The two geometric factors of V_Y have different origins. The Kaluza–Klein reduction multiplies G_4^{-1} by V_Y, while holding the integer flux N fixed makes L^6 inversely proportional to V_Y. Since the on-shell action contains L^9, the net dependence is $V_Y^{-1/2}$. This dimensional argument predicts the direction of the volume dependence, but only the coefficients in (VIII.12.19) and the renormalized action fix its absolute normalization.

It is useful to make the flux relation itself visible as a comparison between two links. If Y and Y' carry the same leading charge N, their radii and free energies satisfy

$$\frac{L_Y^6}{L_{Y'}^6} = \frac{V_{Y'}}{V_Y}, \qquad \frac{F_Y^{(0)}}{F_{Y'}^{(0)}} = \sqrt{\frac{V_{Y'}}{V_Y}}. \tag{VIII.12.21}$$

The radius ratio is meaningful only after both unit link metrics use $\mathrm{Ric} = 6g$ and both charges use the same leading flux convention. A trial Reeb deformation off the Einstein point does not give a new Freund–Rubin solution to insert into this equation. For $Y = S^7/\mathbb{Z}_k$ with $V_Y = \pi^4/(3k)$, the result becomes

$$L^6 = 32\pi^2 k N \ell_p^6, \qquad F^{(0)}_{\mathrm{grav}} = \frac{\pi\sqrt{2k}}{3}N^{3/2}. \tag{VIII.12.22}$$

Using L instead of $L/2$ in the action would multiply the answer by four. The agreement with (VIII.12.11) therefore tests an absolute coefficient, not only a power of N.

The comparison uses the proposed field-theory/gravity identification, leading flux charge and the classical renormalized action. Torsion, charge shifts, loops and exact finite-N equality are outside this calculation. For the non-ABJM cone below, the same formula turns an independently computed link volume into a predicted leading free energy. In particular, a link volume $\pi^4/8$ would yield

$$\frac{F^{(0)}_{\rm grav}}{N^{3/2}} = \sqrt{\frac{2\pi^6}{27(\pi^4/8)}} = \frac{4\pi}{3\sqrt{3}}. \tag{VIII.12.23}$$

We will compute that volume from the $Q^{1,1,1}$ ring, without using the field-theory free energy to determine it. This gives the next calculation a definite target while preserving the distinction between geometry input and a result extracted from the gauge theory.

VIII.12.4 A flavored Q111 saddle

We now change the actual theory. Set the displayed Chern–Simons levels to zero in the full $U(N)\times U(N)$ product and place n flavor pairs on each of A_1, A_2, with none on B_1, B_2. The worked $n=1$ model is exactly the two-A-flavor construction of Chapter 8. The positive integer n family is a sourced extension of that model, not unflavored ABJM with $k=n$. Assign $R_A=\Delta$, $R_B=1-\Delta$ with $0<\Delta<1$, and let $m=\Delta_m$ be trial topological R mixing. In the source monopole dictionary, the two opposite diagonal monopoles have $R(T_\pm)=n\Delta\pm m$. Thus m is half their trial-R difference; it is neither GNO flux nor a physical FI coupling.

The eigenvalue real coordinate and density retain the meanings of (VIII.12.1). Define a shifted imaginary difference $z=\delta y+\pi(2\Delta-1)$. The sourced local functional and its determinant branch are

$$f=\int dx\left[\rho^2(\pi^2-z^2)+\rho\left(\frac{n|x|}{2}+\frac{n|x|z}{2\pi}+mx\right)\right], \qquad -\pi\le z\le\pi. \tag{VIII.12.24}$$

The flavor term is sensitive to the number and placement of the pairs. In particular, dropping its factor $1/2$ changes the extremum. Vary $f-\Lambda(\int\rho-1)$ in the interior. First varying z and then ρ yields

$$0=-2\rho^2 z+\frac{n|x|\rho}{2\pi}, \qquad z=\frac{n|x|}{4\pi\rho}, \tag{VIII.12.25}$$

$$\Lambda=2\rho(\pi^2-z^2)+\frac{n|x|}{2}+\frac{n|x|z}{2\pi}+mx, \qquad \rho=\frac{\Lambda-n|x|/2-mx}{2\pi^2}. \tag{VIII.12.26}$$

The z^2 terms cancel in the density equation. Consequently the density is affine on each side of the origin. With $u=|x|\ge 0$,

$$\rho_+(u)=\frac{\Lambda-(n/2+m)u}{2\pi^2}, \quad \rho_-(-u)=\frac{\Lambda-(n/2-m)u}{2\pi^2}, \quad z_\pm(u)=\frac{n\pi u}{2\Lambda-(n\pm 2m)u}. \tag{VIII.12.27}$$

The sign on m changes across the origin. On the positive side, $z'_+(u)=2\pi n\Lambda/[2\Lambda-(n+2m)u]^2>0$; the negative side has the corresponding expression with $m\mapsto -m$.

Thus the origin has $z = 0$ and each side first reaches the branch edge $z = \pi$ at its support endpoint. For $|m| < n$,

$$x_+ = \frac{\Lambda}{n+m}, \qquad x_- = -\frac{\Lambda}{n-m}, \qquad \rho(x_\pm) = \frac{n\Lambda}{4\pi^2(n \pm m)} > 0. \tag{VIII.12.28}$$

Here the lower sign in the last expression uses $n - m$. Since each piece is affine between two positive values, ρ remains positive throughout. At $z = \pi$, the ρ equation reduces to $n|x| + mx = \Lambda$. It holds only at these endpoints, so there is no finite saturated plateau appended to the linear solution.

The support lengths differ when $m \neq 0$. Normalization must be done before comparing free energies. Integrating the two affine pieces gives

$$I_+ := \int_0^{x_+} \rho_+(x)\,dx = \frac{\Lambda^2(3n+2m)}{8\pi^2(n+m)^2}, \qquad I_- := \int_{x_-}^0 \rho_-(x)\,dx = \frac{\Lambda^2(3n-2m)}{8\pi^2(n-m)^2}, \tag{VIII.12.29}$$

$$1 = \int_{x_-}^0 \rho_- dx + \int_0^{x_+} \rho_+ dx = \frac{\Lambda^2 n(3n^2-m^2)}{4\pi^2(n^2-m^2)^2}, \tag{VIII.12.30}$$

$$\Lambda = \frac{2\pi(n^2-m^2)}{\sqrt{n(3n^2-m^2)}}. \tag{VIII.12.31}$$

Directly integrating (VIII.12.24) on this support gives the same virial split as in ABJM,

$$\int \rho^2(\pi^2 - z^2)\,dx = \frac{\Lambda}{3}, \qquad \int \rho\left(\frac{n|x|}{2} + \frac{n|x|z}{2\pi} + mx\right)dx = \frac{\Lambda}{3}. \tag{VIII.12.32}$$

The leading answer of this sourced stationary family is therefore

$$\frac{F_n(m)}{N^{3/2}} = \frac{2\Lambda}{3} = \frac{4\pi(n^2-m^2)}{3\sqrt{n}\sqrt{3n^2-m^2}}, \qquad |m| < n. \tag{VIII.12.33}$$

The domain is part of the result. Continuing the closed expression beyond $|m| = n$ does not continue this positive-support saddle.

For the $Q^{1,1,1}$ case $n = 1$, $m = 0$ gives $\Lambda = 2\pi/\sqrt{3}$, support $[-2\pi/\sqrt{3}, 2\pi/\sqrt{3}]$, central density $1/(\pi\sqrt{3})$ and endpoint density $1/(2\pi\sqrt{3})$. At $m = 1/2$, $\Lambda = 3\pi/\sqrt{11}$ and the support is $[-6\pi/\sqrt{11}, 2\pi/\sqrt{11}]$; its central density is $3/(2\pi\sqrt{11})$, while the negative and positive endpoint densities are respectively $3/(2\pi\sqrt{11})$ and $1/(2\pi\sqrt{11})$. Replacing m by $-m$ reflects the profile. The sourced extension with $n = 2$ supplies a second scale comparison. At $m = 0$ it has

$$\Lambda = \frac{4\pi}{\sqrt{6}}, \qquad x_\pm = \pm\frac{2\pi}{\sqrt{6}}, \qquad \rho(0) = \frac{2}{\pi\sqrt{6}}, \qquad \rho(x_\pm) = \frac{1}{\pi\sqrt{6}}, \qquad \frac{F_2(0)}{N^{3/2}} = \frac{8\pi}{3\sqrt{6}}. \tag{VIII.12.34}$$

Compared with $n = 1, m = 0$, the greater flavor force contracts the support by $1/\sqrt{2}$ and raises the density by $\sqrt{2}$ while preserving unit area. The free-energy coefficient grows by $\sqrt{2}$. This comparison changes the number of flavor pairs; it is not a comparison

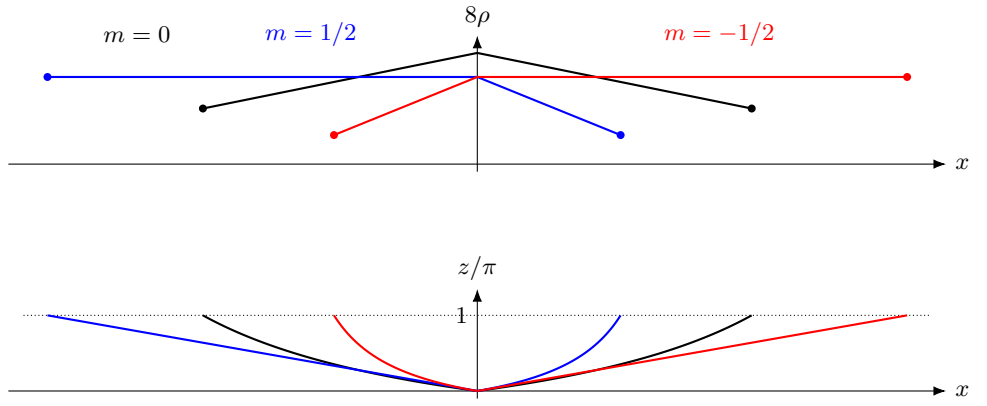


Figure VIII.12.3: The $n = 1$ flavored density and shifted imaginary difference for $m = 0, 1/2, -1/2$. Each curve uses its own normalized Λ. The asymmetry at nonzero m changes the two support lengths, while z reaches π only at the finite-density ends. The $m \mapsto -m$ profiles are reflections, as required by the piecewise equations.

between two Chern–Simons levels of the same ABJM model. Figure VIII.12.3 plots the $n = 1$ pieces, including their finite ends and the branch-boundary values of z.

There is an apparent charge ambiguity that must be read with the gauge group. The shift of Δ changes z through the definition above but leaves (VIII.12.33) unchanged in the full product of unitary groups. This is a gauge-flat R assignment, not an additional physical maximization direction. In the distinct $SU(N) \times SU(N) \times U(1)$ construction of the source, an extra condition $\int \rho\, \delta y\, dx = 0$ is imposed. For this solution,

$$\int \rho\, z\, dx = \frac{4\pi n^2}{3n^2 - m^2} - \pi, \qquad \int \rho\, \delta y\, dx = \pi \left(\frac{4n^2}{3n^2 - m^2} - 2\Delta \right). \tag{VIII.12.35}$$

At $m = 0$ the extra condition selects $\Delta = 2/3$. Imposing it on the full $U(N) \times U(N)$ example would silently change the theory. The saddle construction here also does not prove dominance among every allowed complex eigenvalue configuration.

VIII.12.5 Volume from holomorphic functions

The free energy has so far used a gauge-theory saddle. To calculate a geometric volume without feeding that answer back into geometry, use the conditional single-probe ring of Chapter 8. Its Cox coordinates form three pairs, (a_0, c_0), (b_0, d_0) and (a_{-1}, c_1), whose gauge-invariant triples generate the Segre ring. At formal triple degree d, each pair has total exponent d. If p counts the c_0 exponent and q the c_1 exponent, the global monopole charge is $M = p - q$. The middle pair has $d + 1$ choices. Therefore the refined degree-d character is

$$\chi_d(w) = (d+1) \sum_{p,q=0}^{d} w^{p-q} = \sum_{M=-d}^{d} (d+1)(d+1-|M|) w^M. \tag{VIII.12.36}$$

For $d = 1$ the multiplicities are $2, 4, 2$ at charges $-1, 0, 1$. These are the eight invariant generators. The coefficient at $w = 1$ is $(d + 1)^3$, but the unrefined series alone loses the physical mixing parameter m.

Sum all degrees. For $M \geq 0$, write $d = M + r$. The charge-M coefficient at degree d is $(r + 1)(M + r + 1)$. Its geometric series, including both positive and negative charges and subtracting the common $M = 0$ term, gives the exact rational identity

$$\sum_{r\geq 0}(r + 1)(M + r + 1)t^r = \frac{M + 1}{(1 - t)^2} + \frac{2t}{(1 - t)^3}. \tag{VIII.12.37}$$

Summing this expression against $(tw)^M$ for $M \geq 0$ produces the first term $C(t, w)$ below. The analogous sum with w^{-1} counts negative charges. Both include $M = 0$, whose generating series is $(1 + t)/(1 - t)^3$. Therefore

$$C(t, w) = \frac{1}{(1 - t)^2(1 - tw)^2} + \frac{2t}{(1 - t)^3(1 - tw)}, \tag{VIII.12.38}$$

$$H(t, w) = C(t, w) + C(t, w^{-1}) - \frac{1 + t}{(1 - t)^3}. \tag{VIII.12.39}$$

The subtraction is necessary because zero-charge monomials occur in both half-sums. Equivalently, summing the p, q series directly yields

$$H(t, w) = \frac{1}{(1 - w)(1 - w^{-1})}\left[\frac{2}{(1 - t)^2} - \frac{w}{(1 - tw)^2} - \frac{w^{-1}}{(1 - t/w)^2}\right], \tag{VIII.12.40}$$

$$H(t, 1) = \frac{1 + 4t + t^2}{(1 - t)^4}. \tag{VIII.12.41}$$

The two rational forms agree at every degree. This all-degree identity matters because a finite list of invariant generators or low-degree coefficients would not by itself fix a Reeb-volume pole.

The formal variable t in (VIII.12.39) counts triple degree, not physical R charge. In the monopole dictionary of Chapter 8, an invariant of degree d and charge M has trial $R = d + mM$. The geometric Reeb vector $\boldsymbol{b}$ acts with weight $2R$ in this Calabi–Yau fourfold convention, and the holomorphic top-form has weight four. Therefore set

$$t = e^{-2s}, \qquad w = e^{-2sm}, \qquad t^d w^M = e^{-s(2d+2mM)}, \qquad |m| < 1. \tag{VIII.12.42}$$

The positivity interval is visible already on the degree-one generators of weights $2(1+m)$, 2 and $2(1 - m)$. A generic m in this interval defines a Sasakian trial Reeb metric on the fixed cone. Only the volume-critical member is the Sasaki–Einstein metric in this family; calling every trial metric Einstein would erase the extremization question.

The cone-volume theorem identifies the fourth-order character pole with the volume normalized to the round seven-sphere,

$$\frac{V(m)}{\mathrm{Vol}(S^7)} = \lim_{s\to 0^+} s^4 H(e^{-2s}, e^{-2sm}), \qquad \mathrm{Vol}(S^7) = \frac{\pi^4}{3}. \tag{VIII.12.43}$$

The factor two in the exponent is fixed by the physical Reeb/R map. For the flat cone $\mathbb{C}^4$, four fields of $R = 1/2$ have Reeb weight one, so $H = (1 - e^{-s})^{-4}$ and the limit is one. Using R instead of $2R$ would give $H = (1 - e^{-s/2})^{-4}$ and an erroneous factor sixteen.

For the Segre cone, the pole can be evaluated from the lattice itself. Put $u = sd$, $P = sp$, $Q = sq$ in the all-degree sum. The middle-pair factor $d + 1$ supplies u, and the other two sums become integrals,

$$\lim_{s\to 0^+} s^4 H = \int_0^\infty du\, ue^{-2u} \int_0^u dP\, e^{-2mP} \int_0^u dQ\, e^{2mQ} \tag{VIII.12.44}$$

$$= \frac{3 - m^2}{8(1 - m^2)^2}. \tag{VIII.12.45}$$

To evaluate the displayed integral without inserting the free-energy answer, first perform the P and Q integrals. Their product is

$$\left(\int_0^u e^{-2mP}\, dP\right)\left(\int_0^u e^{2mQ}\, dQ\right) = \frac{\sinh^2(mu)}{m^2}, \qquad \lim_{m\to 0} \frac{\sinh^2(mu)}{m^2} = u^2. \tag{VIII.12.46}$$

Using $\sinh^2(mu) = [\cosh(2mu) - 1]/2$ and $\int_0^\infty ue^{-au}du = a^{-2}$ gives

$$\int_0^\infty du\, ue^{-2u} \frac{\sinh^2(mu)}{m^2} = \frac{(1 - m)^{-2} + (1 + m)^{-2} - 2}{16m^2} = \frac{3 - m^2}{8(1 - m^2)^2}. \tag{VIII.12.47}$$

Consequently

$$V_{Q^{1,1,1}}(m) = \frac{\pi^4(3 - m^2)}{24(1 - m^2)^2}, \quad V(0) = \frac{\pi^4}{8}, \quad V(1/2) = \frac{11\pi^4}{54}. \tag{VIII.12.48}$$

The density of lattice points and the steepening volume curve are shown in Figure VIII.12.4. This is a direct ring calculation for $n = 1$ under the proposed complete geometric-branch presentation. The general-n expression

$$V_n(m) = \frac{n\pi^4(3n^2 - m^2)}{24(n^2 - m^2)^2} \tag{VIII.12.49}$$

is supplied by the cited geometry analysis; we have not derived a general-n quantum ring. Neither calculation replaces the distinct Calabi–Yau threefold Reeb normalization used in Volume VI.

VIII.12.6 Extrema and the reach of the comparison

The sourced flavored saddle and the independently counted $n = 1$ ring now give a continuous test rather than one fitted number. First take $n = 1$ in (VIII.12.33). Its trial free energy and the ring volume are

$$f_1(m) = \frac{4\pi(1 - m^2)}{3\sqrt{3 - m^2}}, \qquad V_1(m) = \frac{\pi^4(3 - m^2)}{24(1 - m^2)^2}, \qquad |m| < 1. \tag{VIII.12.50}$$

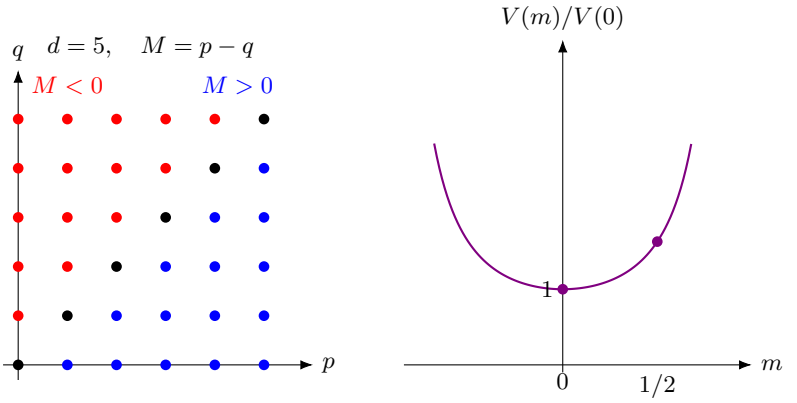


Figure VIII.12.4: Left, the lattice of (p, q) at Segre degree $d = 5$, colored by $M = p - q$. Each point has six choices in the middle Cox pair. Right, the computed normalized trial volume $V(m)/V(0)$ on the positive interval. The marked values at $m = 0$ and $m = 1/2$ follow from the fourth-order Reeb pole, not from a fitted free energy.

Their opposite trends have an elementary algebraic origin. On the stated interval,

$$\frac{d}{dm}\log f_n(m) = \frac{m(m^2 - 5n^2)}{(n^2 - m^2)(3n^2 - m^2)}, \tag{VIII.12.51}$$

$$\frac{d^2}{dm^2}\log f_n\Big|_{m=0} = -\frac{5}{3n^2}, \qquad \frac{d}{dm}\log V_n = -2\frac{d}{dm}\log f_n. \tag{VIII.12.52}$$

The even f_n has its unique maximum at $m = 0$ within $|m| < n$; V_n has its corresponding minimum. Its logarithmic curvature is

$$\frac{d^2}{dm^2}\log V_n\Big|_{m=0} = \frac{10}{3n^2} > 0. \tag{VIII.12.53}$$

The positive curvature gives a local geometric stability statement on this one-parameter Reeb slice. It does not by itself examine all possible Reeb directions. For $n = 1$ the critical values are

$$f_1(0) = \frac{4\pi}{3\sqrt{3}}, \qquad V_1(0) = \frac{\pi^4}{8}, \qquad f_1(1/2) = \frac{2\pi}{\sqrt{11}}. \tag{VIII.12.54}$$

At $m = 1/2$, the separately calculated volume is $11\pi^4/54$, giving the same product as at the extremum,

$$f_1(1/2)^2 V_1(1/2) = \left(\frac{2\pi}{\sqrt{11}}\right)^2 \frac{11\pi^4}{54} = \frac{2\pi^6}{27}. \tag{VIII.12.55}$$

Indeed, throughout the trial interval,

$$\frac{F_n(m)^2 V_n(m)}{N^3} = \frac{16\pi^2(n^2 - m^2)^2}{9n(3n^2 - m^2)} \frac{n\pi^4(3n^2 - m^2)}{24(n^2 - m^2)^2} = \frac{2\pi^6}{27}. \tag{VIII.12.56}$$

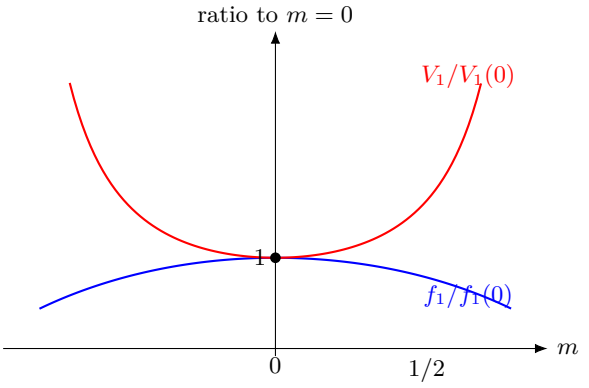


Figure VIII.12.5: The $n = 1$ trial functions, each divided by its value at $m = 0$. The free energy falls and the volume rises as $|m|$ increases. Their product satisfies $[f_1(m)/f_1(0)]^2[V_1(m)/V_1(0)] = 1$ throughout the computed positive interval. Values off $m = 0$ describe trial Sasakian Reeb metrics, not additional Einstein links.

For $n = 1$ both sides of this comparison have been obtained here from their own inputs. For general n, the geometry expression remains a source premise. Figure VIII.12.5 shows the paired curves and their shared stationary point.

Equation (VIII.12.56) reproduces the gravity coefficient (VIII.12.20) along a trial family, provided one uses the sourced continuum functional, the $Q^{1,1,1}$ ring premise and the classical gravity dictionary in their respective domains. At the critical point it compares the candidate conformal theory with the Sasaki–Einstein link. Away from it, the functional and the volume are trial quantities; the associated Sasakian metrics need not solve the Einstein equations. The flat Δ assignment of the full unitary gauge theory is separate from this physical m direction.

The result gives a more discriminating lesson than the bare $N^{3/2}$ law. Flavor changes both the eigenvalue support and the link volume, yet their normalizations match over the allowed trial family. This does not establish a universal F-maximization theorem for all toric quivers, settle alternative chiral saddles, prove the monopole OPE, or make the leading Freund–Rubin action exact at finite N. It gives a concrete bridge from the quantum ring of Chapter 8 and the localized observable of Chapter 11 to the model comparisons of Chapter 13.

VIII.12.7 Exercises

See `benchmark/tasks.json` and `benchmark/PROTOCOL.md` for the public structured-answer format. The first two problems use Λ/π, x/π, $\pi\rho$ and $F/(\pi N^{3/2})$; the fourth uses $C\pi^2$ and $F/(\pi N^{3/2})$. A scalar triple $[a, b, c]$ denotes $a\sqrt{c}/b$, with integer $|a| \leq 100$ and $1 \leq b, c \leq 100$. The volume answers are normalized by $\mathrm{Vol}(S^7)$. Physical explanations and derivations remain written work.

1. **ABJM support.** Set $k = 2$ in the symmetric continuum functional. Submit Λ,

x_*, the constant density, and the coefficient $F/N^{3/2}$. Explain why the support ends while the density is nonzero.

2. **A signed flavored saddle.** In the $n = 1$, $m = 1/2$ flavored theory, submit Λ, both support endpoints, central and endpoint densities, and $F/N^{3/2}$. Explain how $m \mapsto -m$ changes the profile.

3. **A refined lattice count.** At triple degree $d = 2$, submit the multiplicities for charges $M = -2, -1, 0, 1, 2$ and the unrefined total. Then use the physical Reeb weight $2R$ to submit the normalized volume coefficient at $m = 0$ and $m = 1/2$. Explain the factor of sixteen from using R in place of $2R$.

4. **The two Legendre coefficients.** For $k = 1, 2$, use the Fermi state count $n(E) \sim CE^2$ to submit C and the leading $F/N^{3/2}$. Explain why the phase-space diamond alone does not prove the fixed-k spectral statement.

Status and sources

Sources by section. Source coordinates and scope qualifications follow.

§VIII.12.1. The calculation [MATH] is the stationary continuum solution conditional on the sourced localized functional; dominance is a separate physical premise (Jafferis et al. 2011, equations (5.3)–(5.4)).

§VIII.12.2. The calculation [MATH] covers the stated phase-space and Legendre algebra conditional on the sourced fixed-k Fermi-gas operator (Marino and Putrov 2012, §§4.2,5.3).

§VIII.12.3. VIIIr13.12-The classical zero-torsion flux and renormalized gravity coefficient are [SUGRA]; coefficient comparison is conditional on the sourced M2 dictionary (Drukker et al. 2011, §5.4).

§VIII.12.4. The calculation [MATH] gives a stationary piecewise flavored saddle conditional on the source functional and support ansatz; no global dominance follows (Jafferis et al. 2011, §§6.2–6.3).

§VIII.12.5. The calculation [MATH] gives the $n = 1$ character and Reeb pole conditional on the complete proposed ring of Chapter VIII.8; general-n volume remains sourced [GEO-E] input (Benini et al. 2010, §6.2.3; Martelli et al. 2008, equations (1.17), (5.25), (6.10)).

§VIII.12.6. The calculation [MATH] gives derivatives and the stated trial-family ratio conditional on the saddle and positive Reeb domain; physical agreement retains the sourced gravity and localization premises (Jafferis et al. 2011, §7.3.4).

§VIII.12.7. Exercises reuse the conditional [MATH] above. Inherited conventions: Chern–Simons trace and levels, quiver gauge groups and Chern–Simons matter conventions, the localization, trial-charge and volume frame; Jafferis et al. 2011, §§5, 6.2–6.3, 7.3.4; Marino and Putrov 2012, §§4.2,5.3. Explanations remain written work.

The normalized ABJM integral and the sourced large-N local functional are taken from Jafferis et al. (2011), Sections 2 and 5, especially equations (5.3)–(5.4). The flavor content, trial monopole assignment, piecewise saddle and general-n geometry expression use its Sections 6.2–6.3 and 7.3.4. The physical localization prescription and the selected large-N ansatz are source premises. The variations, support proof, normalization, direct integrals and derivatives displayed here are conditional mathematical consequences. No global saddle dominance or exact finite-N statement follows from them.

The exact model identification and the complete proposed geometric-branch ring for $n = 1$, including its monopole OPE and absence of additional relations, use Benini et al. (2010), Sections 4 and 6.2.3, at the restricted Chapter VIII.8 scope. The all-degree refined character and its Reeb pole are [MATH] conditional on that ring. The conversion from the fourth-order pole to Sasakian volume uses the positive-Reeb theorem of Martelli et al. (2008), equations (1.17), (5.25), (6.10), and the Calabi–Yau fourfold R/Reeb normalization of Lee et al. (2007), Section 2.1. Only $n = 1$ has a direct ring count in this chapter; the general-n volume is [GEO-E] source input.

The Fermi-gas operator, fixed-k leading spectral coefficient and grand-potential relation are from Marino and Putrov (2012), Sections 4.2 and 5.3. They reuse the same localized model [LOC] as the continuum calculation. Leading zero-torsion flux, Newton reduction and the renormalized AdS_4 action use Drukker et al. (2011), Section 5.4, and the leading M2 dictionary of Chapters VIII.1–VIII.2. The gravity comparison is [GRAV] at classical Freund–Rubin order. The trial-charge and volume calculations use the specified supersymmetric-sphere and Reeb normalizations. The source algebra checks for this chapter cover the ABJM and flavored stationarity equations, normalizations and endpoints, the all-degree character identity, the Reeb pole and factor-sixteen control, and the trial-family product. Four bounded exercise submissions are checked on their numerical or algebraic answers. The physical interpretation is a written exercise.

References

Benini, F., C. Closset, and S. Cremonesi (2010). "Chiral flavors and M2-branes at toric CY4 singularities". In: *JHEP* 02, p. 036. DOI: 10.1007/JHEP02(2010)036. arXiv: 0911.4127 [hep-th].

Drukker, N., M. Marino, and P. Putrov (2011). "From weak to strong coupling in ABJM theory". In: *Commun. Math. Phys.* 306, pp. 511–563. DOI: 10.1007/s00220-011-1253-6. arXiv: 1007.3837 [hep-th].

Jafferis, D. L. et al. (2011). "Towards the F-Theorem: N=2 Field Theories on the Three-Sphere". In: *JHEP* 06, p. 102. DOI: 10.1007/JHEP06(2011)102. arXiv: 1103.1181 [hep-th].

Lee, S., S. Lee, and J. Park (2007). "Toric AdS4/CFT3 duals and M-theory Crystals". In: *JHEP* 05, p. 004. DOI: 10.1088/1126-6708/2007/05/004. arXiv: hep-th/0702120.

Marino, M. and P. Putrov (2012). "ABJM theory as a Fermi gas". In: *J. Stat. Mech.* 1203, P03001. DOI: 10.1088/1742-5468/2012/03/P03001. arXiv: 1110.4066 [hep-th].

Martelli, D., J. Sparks, and S.-T. Yau (2008). "Sasaki-Einstein manifolds and volume minimisation". In: *Commun. Math. Phys.* 280, pp. 611–673. DOI: 10.1007/s00220-008-0479-4. arXiv: hep-th/0603021.

Chapter VIII.13

An atlas of M2-brane constructions

A membrane can move on a cone, but the cone does not by itself specify the compact gauge group, its Chern–Simons levels, or the operators that survive quantization. In the simplest ABJM example, four complex position fields become a point of $\mathbb{C}^4/\mathbb{Z}_k$ only after a compact gauge quotient. An M-theory circle provides another route to the level k; a tiling provides a toric presentation; a flavored quiver can require monopole operators before its cone appears. These routes answer related questions, but each carries a different physical premise.

This chapter collects the constructions of Chapters 1–12 into a working atlas. A reader may start from a compact quiver, a specified circle, a vacuum deformation, or an observable. The tables give the theory and the object that can actually be extracted. Two arrows in the atlas are genuine Higgs vacua of one parent. A final comparison tests what a common free-energy and volume normalization can say about two distinct theories.

VIII.13.1 From a question to a construction

The first question is what is being constructed. A worldvolume proposal fixes fields, gauge group and interactions. A rank-one moduli calculation then asks which scalar vacua remain after compact identifications. A partition function probes the quantum theory under a chosen background. A large-N gravity comparison also needs a flux and radius dictionary. Agreement at one stage does not by itself provide the next one.

For an abelian quiver with arrows X_e from tail $t(e)$ to head $h(e)$, our charge convention is $q_{ie} = \delta_{i,t(e)} - \delta_{i,h(e)}$. The scalar quotient is controlled by F equations, moment maps, a common σ stratum and the compact gauge lattice. For the examples with a diagonal branch, the selected level vector sums to zero. This is a property of those examples, not a general classification. A toric diagram or a chiral ring may describe one component of this quotient. To identify a quantum operator ring one must also know monopole sectors and their products.

The atlas therefore follows a useful route. First identify the full compact product and ordered bare levels. Next specify the matter and the physical domain. Then ask whether the displayed geometry is a classical position quotient, a conditional operator presentation, or a sourced geometric input. The remaining sections put this route to work.

VIII.13.2 Compact groups and probe geometries

Which compact theory gives the advertised cone? Table VIII.13.1 keeps the gauge group beside its levels because the Lie algebra alone cannot determine the flux lattice. The A_4 BLG model uses a selected $SU(2) \times SU(2)$ global form at levels $(2, -2)$ and eight real bifundamental scalar fields subject to the A_4 reality condition. ABJM at rank one uses the full $U(1) \times U(1)$ product and four complex bifundamentals. Their local algebras can be compared, but the selected BLG global form is an independent part of the question.

Theory, compact group, bare levels	Matter	Selected object
BLG A_4 $SU(2) \times SU(2)$ $(2, -2)$	eight real A_4 bifundamental scalars	local three-bracket; selected global form
ABJM rank one $U(1) \times U(1)$ $(2, -2)$	four complex bifundamentals	$\mathbb{C}^4/\mathbb{Z}_2$ position quotient
ABJM flux $U(2) \subset U(2) \times U(2)$ $(2, -2)$	bifundamentals	primitive cocharacter; central flux $1/2$
$V_{5,2}$ example $U(1) \times U(1)$ $(1, -1)$	four bifundamentals, two adjoints	reduced quadric branch
$M^{1,1,1}$ tiling $U(1)^3$ $(1, 1, -2)$	nine U_i, V_i, W_i arrows	coherent toric cone; compact finite action
flavored $Q^{1,1,1}$ $U(1) \times U(1)$ $(0, 0)$	four A_i, B_i arrows; two flavor pairs	conditional Segre cone; $Q^{1,1,1}$ link

Table VIII.13.1: Selected compact constructions. Levels are bare, ordered by the factors displayed. The BLG row has eight real fields with its A_4 reality condition. The $M^{1,1,1}$ row is a coherent classical branch and the flavored $Q^{1,1,1}$ ring is conditional on its monopole presentation.

For the rank-one ABJM position branch, the compact dual scalar and primitive flux leave a finite identification. At $k = 2$ it acts by $C^I \mapsto -C^I$ on all four complex

positions, so

$$U(1)_2 \times U(1)_{-2} \quad \rightsquigarrow \quad \mathcal{M}_{\rm pos} = \mathbb{C}^4/\mathbb{Z}_2. \tag{VIII.13.1}$$

This is a position-space statement. It does not by itself settle an identification of all line operators or the full quantum action. The $U(2)$ flux entry gives a compact reminder. A primitive diagonal cocharacter has trace flux one and central flux $1/2$ in that factor; the fractional center value is tied to the nonabelian bundle rather than an independent pure-center flux.

Two other rows show why one cannot classify every Calabi–Yau fourfold from a single recipe. The $V_{5,2}$ example of Chapter 10 has four bifundamentals, two adjoints and a fixed nonzero cubic coupling. Its reduced quadric branch differs from its classical nonreduced F-term scheme. The $M^{1,1,1}$ tiling of Chapter 7 instead starts with nine arrows of a three-node $U(1)^3$ quiver at $(1,1,-2)$. On the coherent common-σ branch, its forward matching map is

$$U_i = p_i q_1, \qquad V_i = p_i q_2, \qquad W_i = p_i q_3, \qquad Q_F = (-1,-1,-1,1,1,1). \tag{VIII.13.2}$$

Let d be the head-positive edge incidence and let P be the nine-by-six exponent matrix of the matching map in Chapter 7. The actual nine-edge flow $n = (-1,0,0,-2,0,0,0,0,0)$ gives $dn = (1,1,-2)$ in the displayed arrow order. Its compact baryonic lift is

$$Q_D = (0,0,0,2,-1,-1), \qquad Q_D P^T = (2,2,2,-1,-1,-1,-1,-1,-1), \tag{VIII.13.3}$$

where P is the matching map in (VIII.13.2). Together with Q_F, the charge lattice is primitive and saturated. The fixed-label height calculation, followed by an integral shear and reflection, yields five external rays and one internal matching. At doubled levels the finite generator sends $(U,V,W) \mapsto (-U,V,-W)$; it cannot be replaced by a universal "divide the Hilbert series by two" rule. For this selected component the invariant counts at formal p-degrees $0,3,6,9,12$ are respectively $1,10,84,165,455$. Other σ strata and a complete quantum operator ring are outside this result.

The flavored $Q^{1,1,1}$ row is different again. It uses full $U(1)^2$, zero bare levels and a chosen zero mixed gauge term, with two A-arrow flavor pairs. If the proposed branch monopole OPE $T\widetilde{T} = A_1 A_2$ and the completeness of that presentation hold, its gauge-invariant Cox monomials have equal degree d in each of three pairs. Thus

$$h_d = (d+1)^3, \qquad H(t) = \sum_{d\geq 0} (d+1)^3 t^d = \frac{1+4t+t^2}{(1-t)^4}. \tag{VIII.13.4}$$

This is the affine Segre cone over $(\mathbb{P}^1)^3$. Its seven-dimensional link is $Q^{1,1,1}$; the six-dimensional base is not the link. The two gauged Cox rows and the additional global row are

$$Q_B = \begin{pmatrix} 1 & -1 & 1 & -1 & 0 & 0 \\ 1 & 0 & 1 & 0 & -1 & -1 \end{pmatrix}, \qquad Q_M = (0,0,1,0,0,-1), \tag{VIII.13.5}$$

in the ordered variables $(a_0, b_0, c_0, d_0, a_{-1}, c_1)$. The first two rows are gauged; Q_M grades a global M circle in the negative z direction of the chosen toric frame. Gauging it would change the dimension and the invariant ring. The ring statement retains the proposed OPE premise, so it does not establish an exact infrared equivalence.

VIII.13.3 Choosing a circle and a toric description

How does a chosen geometric direction enter a quiver? A free circle in an appropriate chamber reduces M-theory to type IIA, where its first Chern class becomes F_2 flux. Fractional D-branes pair with that flux through Wess–Zumino couplings. For the oriented conifold choice of Chapter 5, the declared curve has period $-k$ and the two fractional curve coefficients are $(-1, +1)$. With the stated orientation, the ordered Chern–Simons levels are

$$\int_{\mathbb{P}^1} c_1 = -k, \qquad (-1, +1)(-k) = (k, -k). \tag{VIII.13.6}$$

This calculation specifies a circle and a regular free-orbit chamber. The level vector alone does not extend the circle construction through all singular chambers.

Theory, compact group, bare levels	Matter	Selected object
conifold circle $U(1) \times U(1)$ $(k, -k)$	fractional D4 classes; A_i, B_j	specified circle and F_2 periods
SPP flux $U(1)^3$ $(k, -k, 0)$	three fractional classes	supplied F_2 periods only
$Y^{1,2}$ parent $U(N)^3$ $(2, -1, -1)$	five arrows A, C_1, D, C_2, B	FI-supported local charts
A Higgs chart $U(N) \times U(N)$ $(1, -1)$	four remaining bifundamentals	local $\mathbb{C}^4$
B Higgs chart $U(N) \times U(N)$ $(2, -2)$	four remaining bifundamentals	local $\mathbb{C}^4/\mathbb{Z}_2$
GRVV blocks $U(N) \times U(N)$ $(k, -k)$	Q^α, R^α bifundamentals	selected rank-$(N-1)$ blocks

Table VIII.13.2: Specified geometric routes and changes of vacuum. The SPP periods are supplied; both Higgs rows descend from the same five-field $Y^{1,2}$ parent at distinct FI values. The local chart labels refer to rank one.

The suspended pinch point provides a useful limit of the same language. A supplied oriented F_2 class has periods $(k, -k)$ on the two chosen curves. For the selected fractional charge rows, the pairing is

$$\begin{pmatrix} 1 & 0 \\ 0 & 1 \\ -1 & -1 \end{pmatrix} \begin{pmatrix} k \\ -k \end{pmatrix} = \begin{pmatrix} k \\ -k \\ 0 \end{pmatrix}. \tag{VIII.13.7}$$

This is a Wess–Zumino level calculation from a supplied class. The supplied periods and fractional charge rows determine this pairing, but do not determine an oriented circle action and its base. It would be wrong to read the SPP row as a completed lift solely because the numbers resemble a Chern–Simons quiver.

A tiling answers a complementary question. Its directed arrows and perfect matchings build an integral toric diagram from a forward quiver construction. In the $M^{1,1,1}$ example, the actual edge flow becomes matching heights $(-3,0,0,-1,-2,0)$ before a fixed shear and reflection put the rays in the Chapter 7 frame. The geometry is the coherent component under the stated quotient and finite action. This is a forward computation for a specified phase. It is not an inverse algorithm that chooses a unique quiver for every fourfold. Crystal models and the D1-brick constructions discussed in Chapter 7 use other combinatorial objects; their presence does not turn a matching map into an independent duality proof.

The flavored route needs still another input. In Chapter 8 the two ordinary gauge charges of the $Q^{1,1,1}$ Cox presentation impose the equal-degree condition in (VIII.13.4), while the global M-circle charge grades the surviving operators. Monopole OPE data are needed to connect these coordinates to the quiver. The same cone can therefore appear in a toric quotient and in a conditional quantum presentation without making their starting theories identical.

VIII.13.4 Changing a vacuum or changing a theory

A deformation can move the probe within one theory, alter the potential, or change the compact theory being defined. The distinction is sharp in the five-field $U(N)^3$ parent of Chapter 9. Its ordered bare levels are $(2,-1,-1)$, its arrows are $(A,C_1,D,C_2,B) = (12,31,13,31,23)$, and its noncommuting superpotential is

$$W = h\,\mathrm{Tr}(C_1ABC_2D - C_2ABC_1D). \tag{VIII.13.8}$$

Both local daughter charts below use this same parent action.

At $\sigma = 0$, a full-rank $A = v\mathbf{1}_N$ solution requires $\zeta_A = |v|^2(1,-1,0)$; a full-rank $B = v\mathbf{1}_N$ solution requires $\zeta_B = |v|^2(0,1,-1)$. The unbroken primitive embeddings are

$$E_A = \begin{pmatrix} 1 & 0 \\ 1 & 0 \\ 0 & 1 \end{pmatrix}, \qquad E_A^T\,\mathrm{diag}(k)E_A = \mathrm{diag}(1,-1). \tag{VIII.13.9}$$

$$E_B = \begin{pmatrix} 1 & 0 \\ 0 & 1 \\ 0 & 1 \end{pmatrix}, \qquad E_B^T\,\mathrm{diag}(k)E_B = \mathrm{diag}(2,-2). \tag{VIII.13.10}$$

Each embedding annihilates its condensed arrow charge before the bare-level pullback.

The selected mixed gauge-parity completion is

$$\Lambda_H = \begin{pmatrix} 0 & \frac{1}{2} & -\frac{1}{2} \\ \frac{1}{2} & -1 & \frac{1}{2} \\ -\frac{1}{2} & \frac{1}{2} & 0 \end{pmatrix}, \qquad \Lambda_H\mathbf{1} = 0, \qquad E_A^T\Lambda_H E_A = E_B^T\Lambda_H E_B = 0. \tag{VIII.13.11}$$

The matrix has zero row sums and vanishes on both surviving compact subgroups. It is the chosen rank-one combined-fermion prescription, not an arbitrary-rank quantum completion.

The FI moments cancel the corresponding D equations, and every cyclic F derivative contains an uncondensed field. At zero FI these representatives fail the fixed-$\sigma = 0$ D equations. After substitution, the signed quartic interactions retain the order of the four remaining matrices. They are

$$W_A = hv\,\mathrm{Tr}(C_1BC_2D - C_2BC_1D), \tag{VIII.13.12}$$
$$W_B = hv\,\mathrm{Tr}(C_1AC_2D - C_2AC_1D). \tag{VIII.13.13}$$

At rank one the ordered words commute, but they must be kept at general rank. The nonzero-A chart has trivial finite stabilizer and is locally $\mathbb{C}^4$. The nonzero-B chart retains an inversion on all four coordinates and is locally $\mathbb{C}^4/\mathbb{Z}_2$. These are neighborhoods of the chosen vacua, not a global metric.

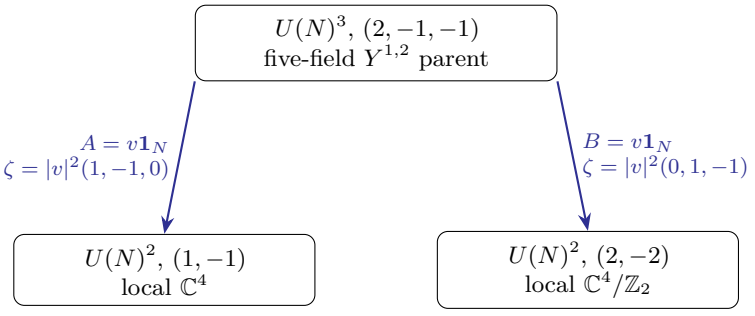


Figure VIII.13.1: Two FI-supported arrows from the same full $U(N)^3$ parent. The displayed levels are ordered bare levels. Each arrow fixes $\sigma = 0$ and a nonzero full-rank VEV, with the indicated node-moment vector. The endpoints name local rank-one nonzero-field charts; the figure does not assert a complete resolved metric or threshold-corrected infrared action.

A scalar mass makes a different change. In the flat-space GRVV component potential, selected square blocks have scale $c = \sqrt{\mu k/(2\pi)}$ for $k, \mu > 0$. Their matrices satisfy $A^\alpha + S_L A^\alpha - A^\alpha S_R = 0$, with $S_L = (N-1)\mathbf{1}_N$ and $S_R = \mathrm{diag}(0, N, \ldots, N)$. These rank-$(N-1)$ blocks solve the chosen classical vacuum equations, while the rank-one scalar mass lifts continuous position zeros. Their scalar bilinear has mass dimension one; it is not a geometric radius squared. No count of all quantum vacua follows.

A supersymmetric deformation of the sphere in Chapter 11 changes the background for a partition function, not the same flat-space potential. Changing $SU(2) \times SU(2)$ to a quotient global group changes the compact flux and line sectors even if a local Lie algebra stays fixed. The atlas keeps these operations separate because they ask different questions of the theory.

VIII.13.5 Observables and what agreement tests

Can a free energy and a link volume identify a theory? We can answer by comparing two concrete models whose leading numbers are both known. Let $F = -\log|Z_{S^3}|$ and write its leading fixed-level coefficient as $F = fN^{3/2} + o(N^{3/2})$. Let $v = \mathrm{Vol}(Y)$ for the seven-dimensional link, normalized with $\mathrm{Vol}(S^7) = \pi^4/3$. In the flavored model the physical Reeb weight is $2R$, and positive trial charges require $|m| < 1$. These definitions fix the units before any comparison.

Theory, compact group, bare levels	Matter	Selected object
ABJ charge frame $U(10) \times U(11)$ $(3, -3)$	bifundamentals	Page and Maxwell charge frames
GRVV rank one $U(1) \times U(1)$ $(2, -2)$	mass-deformed ABJM scalars	scalar Hessian at origin
ABJM ellipsoid $U(N) \times U(N)$ $(k, -k)$	balanced bifundamentals	leading shape factor
ABJM rank-one Z $U(1) \times U(1)$ $(k, -k)$	four complex bifundamentals	round-sphere partition function
ABJM leading F $U(N) \times U(N)$ $(2, -2)$	four complex bifundamentals	fixed-k $N^{3/2}$ coefficient
ABJM / $Q^{1,1,1}$ two $U(N) \times U(N)$ theories $(2, -2)$ / $(0, 0)$	four bifundamentals / two A flavor pairs	separate F and link volumes

Table VIII.13.3: Selected deformation and observable entries. Page and Maxwell charges, a scalar Hessian, a sphere partition function and a leading free-energy coefficient are different quantities. The last row compares distinct theories.

For equal-rank ABJM at $k = 2$, the leading localization saddle and classical zero-torsion gravity comparison of Chapter 12 give

$$f_A = \frac{2\pi}{3}, \qquad v_A = \frac{\pi^4}{6}. \tag{VIII.13.14}$$

The v_A entry is the volume of $S^7/\mathbb{Z}_2$ in this leading comparison. The matrix-model statement uses the selected physical localization and saddle premises; the gravity volume uses the leading flux-radius relation. Neither is a finite-N identity.

For the different full $U(N) \times U(N)$ flavored theory with one pair on each A arrow,

the selected $m = 0$ saddle and the conditional Segre character instead give

$$f_Q = \frac{4\pi}{3\sqrt{3}}, \qquad v_Q = \frac{\pi^4}{8}. \tag{VIII.13.15}$$

The ring volume uses the complete proposed monopole presentation of Chapter 8. The free energy uses the chosen large-N saddle of Chapter 12. These are independent assumptions about the same flavored model, so their agreement is informative within that model.

Divide like by like. The two ratios are not one,

$$\frac{f_Q}{f_A} = \frac{2}{\sqrt{3}}, \qquad \frac{v_Q}{v_A} = \frac{3}{4}. \tag{VIII.13.16}$$

Their inverse-square relation is exactly what the leading Freund–Rubin normalization predicts for a fixed M2 charge convention. Indeed, multiplication gives a common value,

$$f_A^2 v_A = \left(\frac{2\pi}{3}\right)^2 \frac{\pi^4}{6} = \frac{2\pi^6}{27}, \tag{VIII.13.17}$$

$$f_Q^2 v_Q = \left(\frac{4\pi}{3\sqrt{3}}\right)^2 \frac{\pi^4}{8} = \frac{2\pi^6}{27}. \tag{VIII.13.18}$$

This equality tests the normalization of two separate leading field-theory/geometry comparisons. It cannot identify the ABJM and flavored quivers. Their bare levels, matter, monopole sector and links are different, as the earlier tables make explicit.

The distinction survives a continuous trial test. For the selected $Q^{1,1,1}$ family on $|m| < 1$, the saddle of Chapter 12 and conditional character volume are respectively

$$f_Q(m) = \frac{4\pi(1-m^2)}{3\sqrt{3-m^2}}, \qquad v_Q(m) = \frac{\pi^4(3-m^2)}{24(1-m^2)^2}. \tag{VIII.13.19}$$

The character counts three pairs of Cox variables with equal degree. Its leading Laplace pole, using weight $2R$, has coefficient $(3-m^2)/[8(1-m^2)^2]$ relative to S^7. Multiplying the two expressions in (VIII.13.19) gives

$$f_Q(m)^2 v_Q(m) = \frac{2\pi^6}{27}, \qquad |m| < 1. \tag{VIII.13.20}$$

The cancellation is an exact algebraic consequence of the two displayed functions. It does not test global saddle dominance or all monopole branches. Taking m to the boundary would violate the positive-Reeb premise rather than extend the comparison.

The earlier atlas also contains ABJ Page/Maxwell charge frames, an ellipsoid shape factor, and rank-one ABJM sphere integrals. They are useful observables of different sorts; none is a replacement for the leading f used above. In particular, no $M^{1,1,1}$ or $V_{5,2}$ free-energy coefficient has been computed in this atlas. Leaving those entries open is part of reading the table correctly.

VIII.13.6 Beyond brane probes

The probe constructions of Volumes VI, VII and VIII begin with branes and ask for their worldvolume theories, vacua and selected observables. The next parts of the monograph pose a different engineering question. In XI, singular Calabi–Yau geometry and wrapped branes lead toward four-dimensional $\mathcal{N} = 2$ systems. In XIII, canonical singularities and their resolutions organize five-dimensional engineering. The compact group, chamber, charge lattice and observable still have to be stated in each setting. The membrane atlas provides a habit for doing so; it does not transfer an M2 quotient calculation into a new dimension.

Take-home message

A geometry enters a membrane theory through a specified construction and a specified domain. Compact levels and matter fix the quiver; a circle, matching map or monopole presentation supplies further information. FI vacua, scalar masses and background changes act on different objects. A common leading $f^2\,\mathrm{Vol}(Y)$ normalization is a useful consistency test, while the theories compared may remain distinct.

VIII.13.7 Exercises

Each structured answer is one JSON object containing exactly the named fields below; it has no additional `task` or `domain` field. See `benchmark/tasks.json` and `benchmark/PROTOCOL.md` for the public structured-answer format. The checker grades algebraic entries; explanations are separate written work.

1. **Two leading observables.** Use ABJM at $k = 2$ and the $n = 1, m = 0$ flavored $Q^{1,1,1}$ model. In exact units, submit the coefficients f_A/π, f_Q/π, v_A/π^4, v_Q/π^4, f_Q/f_A, v_Q/v_A, and each $f^2 v/\pi^6$. Write a separate explanation of why the common product does not identify the theories. Use the keys `f_A_over_pi`, `f_Q_over_pi`, `v_A_over_pi4`, `v_Q_over_pi4`, `f_Q_over_f_A`, `v_Q_over_v_A`, `f_A2v_A_over_pi6` and `f_Q2v_Q_over_pi6`, in that correspondence. Each value is an integer triple $[a, b, c]$ meaning $a\sqrt{c}/b$, with $|a| \le 100$ and $1 \le b, c \le 100$. For example, $[1, 2, 3]$ represents $\sqrt{3}/2$; equivalent triples are allowed.

2. **Inherited construction or deformation.** Start from the five-field $U(N)^3$ parent with ordered levels $(2, -1, -1)$. Choose $A = v\mathbf{1}_N$ at $\sigma = 0$ and submit the required FI vector in units of $|v|^2$, the ordered daughter levels, and the residual local finite-group order at rank one. Then decide whether this operation is an FI-supported vacuum, a scalar-mass deformation, or a change of compact global form. Explain separately whether the supplied SPP level vector $(k, -k, 0)$ determines an oriented circle/base map, and justify your answer. Use `fi_over_abs_v2` for the three ordered FI integers, `daughter_levels` for the two ordered levels, `residual_order` for the group order, and `category` for the operation. Array entries obey $|a| \le 10$; the order is an integer from 1 to 10. The category is one of `fi_vacuum`, `scalar_mass` or `global_form_change`.

Status and sources

Sources by section. The following tags attach to the specific constructions and calculations, with their conditions.

§VIII.13.1. The opening distinguishes worldvolume proposal, classical quotient, localized observable and leading gravity comparison. Each comparison uses the branch, compact group and normalization stated in its example.

§VIII.13.2. The table collects selected compact groups and position branches. BLG A_4 uses eight real scalar fields with its reality condition as a sourced premise; Bagger and Lambert 2008, (41), (42), (45), and Chapter 3 calculations. ABJM rank-one quotient and compact flux use Chapters 3–4 calculations and the stated compact membrane conventions. The $M^{1,1,1}$ matching, finite action and coherent cone are [MATH] on the selected coherent branch; Hanany, Vegh, et al. 2009, §5.5.1 (5.48)–(5.53), and Hanany and Zaffaroni 2008, §6, with Chapter 7 calculations §§3–7. The flavored $Q^{1,1,1}$ Segre ring is [MATH] conditional on the complete proposed monopole OPE; Benini et al. 2010, §6.2.3 (6.25)–(6.32), and Benini et al. 2011, §6, with Chapter 8 calculations §§2–3 and the specified flavored abelian branch. The $V_{5,2}$ reduced quadric and classical scheme are separate Chapter 10 results.

§VIII.13.3. The conifold-circle calculation [MATH] uses the specified oriented conifold circle and fractional-brane F_2 pairing. The suspended-pinch-point flux calculation [MATH] gives the level pairing conditional on supplied oriented periods. Its physical input is source-only; the source-angle circle and base map is outside the calculation. Aganagic 2010, §4 and §6.1; Chapter 5 calculations and its local IIA circle and flux-to-level map. The forward toric route is Chapter 7's actual nine-edge calculation under the selected coherent-branch conventions, and the conditional monopole route is Chapter 8 under the specified flavored abelian branch. Chern–Simons trace and levels, quiver gauge groups and Chern–Simons matter conventions control arrows, levels and compact flux.

§VIII.13.4. The table records two FI-supported classical vacua [MATH] of the same $Y^{1,2}(\mathbb{CP}^2)$ phase Ib source parent, their primitive embeddings, bare-level pullbacks, ordered daughter actions and local rank-one charts. Selected combined gauge-parity is [ANOM] only at the stated rank-one/equal-rank scope; no quantum threshold is supplied. Benishti et al. 2010, §3.3 printed pp. 11–12 / PDF pp. 12–13, §5.3.1 (5.10)–(5.13), Fig. 13 printed pp. 42–43 / PDF pp. 43–44; Benini et al. 2011, §6; Chapter 9 calculations §§A–D, the classical tiling and gauge-parity frame and the classical FI and GRVV frame. The GRVV calculation [MATH] covers selected square blocks for the sourced classical component potential; Gomis et al. 2008, (2.5), (3.1)–(3.5), printed pp. 9–11 / PDF pp. 10–12; Chapter 9 calculations §E and the stated massive potential. The fields and bare levels use the stated classical normalizations.

§VIII.13.5. The free-energy and volume comparison [MATH] uses the exact ratios and products of separately sourced leading coefficients. ABJM and flavored $Q^{1,1,1}$ free energies use the selected localized saddles of Jafferis et al. 2011, (5.3)–(5.8), (6.14)–(6.17), (7.23); Chapter 12 calculations and the localization, trial-charge and volume

frame. The conditional $Q^{1,1,1}$ character uses Benini et al. 2010, §6.2.3 and the specified flavored abelian branch of Chapter 8. Positive-Reeb volume conversion uses Martelli et al. 2008, (1.17), (5.25), (6.10), and Lee et al. 2007, §2.1. Gravity normalization is leading zero-torsion [SUGRA], not finite-N equality. The stated trial-charge and gravity conventions fix m, $2R$, and $\mathrm{Vol}(S^7)$. $M^{1,1,1}$ and $V_{5,2}$ free energies remain uncomputed here.

§VIII.13.6. This bridge makes a route to Volumes XI and XIII, with no imported calculation or duality claim. The present atlas does not classify all Calabi–Yau fourfolds.

§VIII.13.7. Two bounded exercises test exact comparison and the A-vacuum's inherited construction. Their structured entries are machine graded; written explanations remain for human assessment. The source premises and conditions are those of the sections above.

References

Aganagic, M. (2010). "A Stringy Origin of M2 Brane Chern-Simons Theories". In: *Nucl. Phys. B* 835, pp. 1–28. DOI: 10.1016/j.nuclphysb.2010.01.007. arXiv: 0905.3415 [hep-th].

Bagger, J. and N. Lambert (2008). "Gauge symmetry and supersymmetry of multiple M2-branes". In: *Phys. Rev. D* 77, p. 065008. DOI: 10.1103/PhysRevD.77.065008. arXiv: 0711.0955 [hep-th].

Benini, F., C. Closset, and S. Cremonesi (2010). "Chiral flavors and M2-branes at toric CY4 singularities". In: *JHEP* 02, p. 036. DOI: 10.1007/JHEP02(2010)036. arXiv: 0911.4127 [hep-th].

Benini, F., C. Closset, and S. Cremonesi (2011). "Quantum moduli space of Chern-Simons quivers, wrapped D6-branes and AdS4/CFT3". In: *JHEP* 09, p. 005. DOI: 10.1007/JHEP09(2011)005. arXiv: 1105.2299 [hep-th].

Benishti, N., Y.-H. He, and J. Sparks (2010). "(Un)Higgsing the M2-brane". In: *JHEP* 01, p. 067. DOI: 10.1007/JHEP01(2010)067. arXiv: 0909.4557 [hep-th].

Gomis, J. et al. (2008). "A Massive Study of M2-brane Proposals". In: *JHEP* 09, p. 113. DOI: 10.1088/1126-6708/2008/09/113. arXiv: 0807.1074 [hep-th].

Hanany, A., D. Vegh, and A. Zaffaroni (2009). "Brane Tilings and M2 Branes". In: *JHEP* 03, p. 012. DOI: 10.1088/1126-6708/2009/03/012. arXiv: 0809.1440 [hep-th].

Hanany, A. and A. Zaffaroni (2008). "Tilings, Chern-Simons Theories and M2 Branes". In: *JHEP* 10, p. 111. DOI: 10.1088/1126-6708/2008/10/111. arXiv: 0808.1244 [hep-th].

Jafferis, D. L. et al. (2011). "Towards the F-Theorem: N=2 Field Theories on the Three-Sphere". In: *JHEP* 06, p. 102. DOI: 10.1007/JHEP06(2011)102. arXiv: 1103.1181 [hep-th].

Lee, S., S. Lee, and J. Park (2007). "Toric AdS4/CFT3 duals and M-theory Crystals". In: *JHEP* 05, p. 004. DOI: 10.1088/1126-6708/2007/05/004. arXiv: hep-th/0702120.

Martelli, D., J. Sparks, and S.-T. Yau (2008). "Sasaki-Einstein manifolds and volume minimisation". In: *Commun. Math. Phys.* 280, pp. 611–673. DOI: 10.1007/s00220-008-0479-4. arXiv: hep-th/0603021.